Printing Bone

The application of 3D fiber deposition for bone tissue engineering

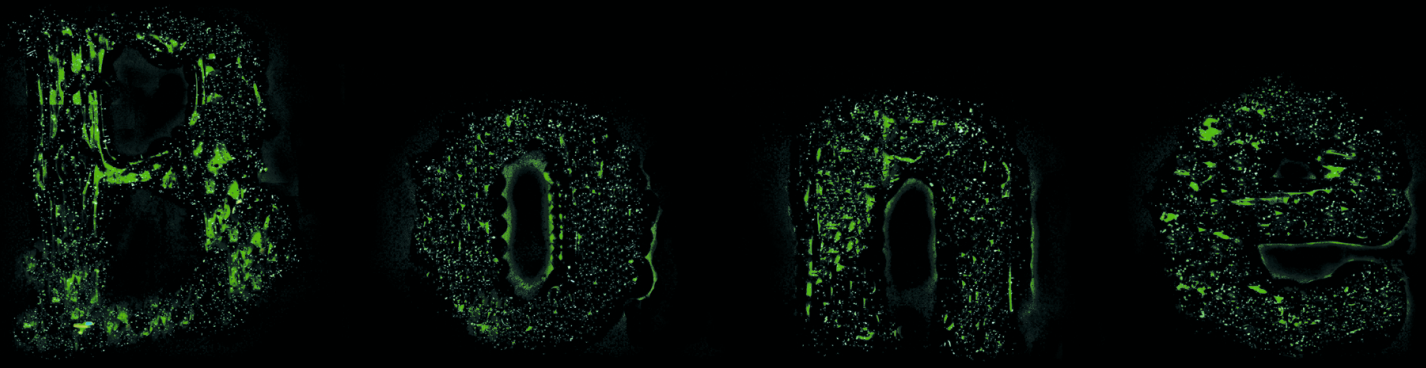

Natalja Leeuwis Fedorovich

Printing bone

The application of 3D fiber deposition for bone tissue engineering

Het printen van botweefsel

Toepassing van 3D fiber deposition voor bot tissue engineering

Natalja E. Leeuwis Fedorovich

Orthopaedie
UMC Utrecht

Printing bone
The application of 3D fiber deposition for bone tissue engineering

N.E. Leeuwis Fedorovich

ISBN: 978-90-39355633
Cover by Vladimir Khristov
Design and layout by Natalja Leeuwis Fedorovich
Press by GVO drukkers & vormgevers B.V. | Ponsen en Looijen

The research described in this thesis was performed at the Department of Orthopaedics of the University Medical Center Utrecht, Utrecht, The Netherlands. This research was supported by the Netherlands Organisation for Scientific Research (NWO) under project number: 017.001.181

Financial support for the reproduction of this thesis was generously provided by the following institutions and companies:

UMC Utrecht
J. E. Jurriaanse Stichting
Stichting Anna Fonds
DSM Biomedical
GlaxoSmithKline B.V.
Nederlandse vereniging voor Biomaterialen en Tissue Engineering
XPand Biotech B.V.
George In der Maur orthopedische schoentechniek
BD Biosciences
Synthes B.V.
Propath N.V.
Arthrex Nederland B.V.
A.Menarini Diagnostics Benelux

Printing bone
The application of 3D fiber deposition for bone tissue engineering

Het printen van botweefsel
Toepassing van 3D fiber deposition voor bot tissue engineering

(met een samenvatting in het Nederlands)

Proefschrift

ter verkrijging van de graad van doctor aan de Universiteit Utrecht
op gezag van de rector magnificus, prof.dr. G.J. van der Zwaan,
ingevolge het besluit van het college voor promoties
in het openbaar te verdedigen op donderdag 23 juni 2011 des middags te 12.45 uur.

door

Natalja Evgenjevna Fedorovich
geboren op 5 juli 1979 te Leningrad, Rusland

Promotoren:	Prof. dr. W.J.A. Dhert Prof. dr. C.A. van Blitterswijk
Co-promotor:	Dr. J. Alblas

Aan mamma

Table of contents

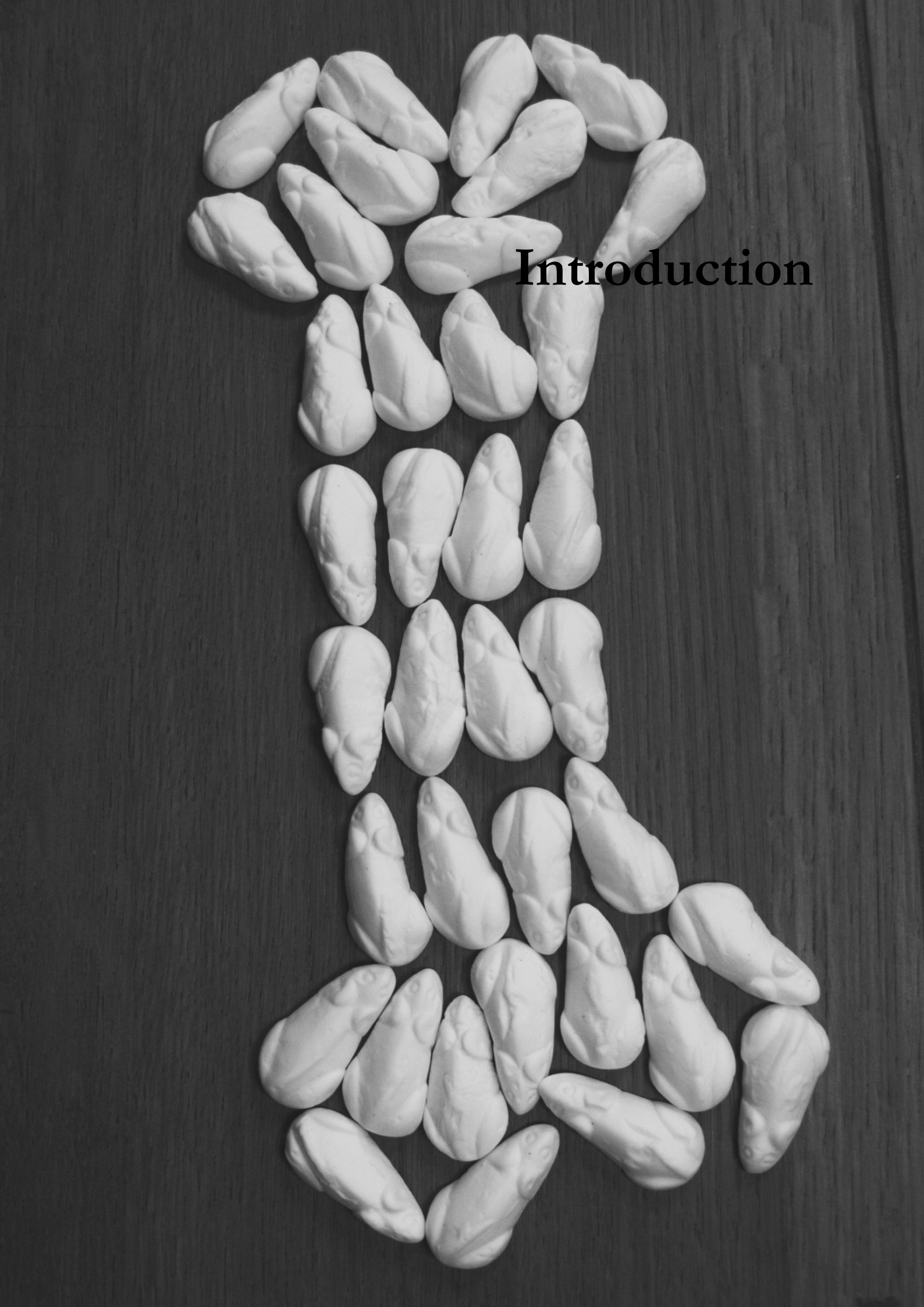

Introduction

Chapter 1

General background, aims and outline of the thesis

General background

Bone grafting is used to provide stability after spinal surgery and to augment critical size bone defects, in which the bone is not able to bridge the existing lesion.[1] Autologous bone is the gold standard for bone grafting, and refers to bone taken from one anatomic site and transplanted to another site in the same individual. Autologous transplants combine (stem) cells and growth factors and do not induce immunological rejection. Upon transplantation, the mineralized collagen matrix of an autograft provides the initial scaffolding. Strength further increases as additional new bone is deposited onto the osteoconductive matrix of hydroxyapatite and collagen. Osteogenic cells and osteoinductive growth factors such as bone morphogenetic proteins (BMPs) contribute to the bone formation process. Viable and functional osteogenic cells are a basic requirement for bone formation. The local environment of the graft, including vasculature and extracellular matrix, is critically important in this process. Adequate supply of nutrients, including oxygen, by surrounding blood vessels is one of the prerequisites for successful bone formation, while the adjacent tissue also presents the cells with vital intercellular and mechanical and biochemical cues.

Regretfully, autologous bone is limited in quantity, while harvest of autologous bone grafts is associated with increased surgical time and donor-site morbidity.[2-4] Furthermore, non-unions are a common complication: when autograft is used in long bone reconstruction or in spinal fusion surgery, pseudoarthrosis is reported to reach from 13 to 44%,[5,6] limiting the success rate of the autograft approach. Alternatives to autologous bone graft include the use of recombinant growth factors and biomaterials, such as ceramics.[7] Allograft bone can be used as a substitute when a large quantity of bone graft is required, and autologous bone marrow aspirates are optional sources of osteoprogenitor cells.[8,9] None of the presently available approaches achieves the performance of autologous bone graft, rendered by its superior characteristics of osteogenicity and lack of tissue response.[10] Alternative strategies such as tissue engineering (TE) allow combining elements such as biomaterials, cells and growth factors, which cumulatively yield a so-called hybrid graft.

In bone TE, osteogenic stem cells are commonly combined with osteoconductive materials and osteoinductive bioactive molecules in an effort to replace and regenerate bone and make current bone repair and reconstruction with metal implants redundant. Osteogenic stem cells are usually isolated from bone marrow of the recipient, but allogeneic sources are currently under investigation as well, due to for intrance their immunomodulatory properties, or their supposed production of trophic factors that stimulate bone formation.[11] Among biomaterials used as scaffold for stem cells or bone marrow, are polymers and calcium phosphate ceramics.[12] Polymers used for scaffolding either include stiff thermoplastics for cell-seeding or hydrogel-forming polymer chains for cell-encapsulation. Calcium phosphate ceramics can combine osteoconductive and osteoinductive properties. Bioactive cues to induce bone formation include the use of proteins or coding sequences to growth factors from the BMP-family.[13] Delivery of osteoinductive growth factors together with proangiogenic molecules, either simultaneously or sequentially, has proven to result in synergistic effects on tissue formation.[14] Current focus in this research therefore lies in combined application of osteoinductive growth factors with

proangiogenic cues and investigation of delivery strategies and adequate dosage of administered proteins *in vivo*.

In recent years, bone TE has made a step from preclinical studies in large animal models to the application in clinical trials. Large bone defects in humans can be regenerated using autologous *in vitro* expanded pluripotent mesenchymal cells associated to a porous ceramic, and BMP-related proteins are administered in clinical trials for spinal arthrodesis.[15] The concept of regenerative medicine is being implemented in orthopaedic clinical practice also for regeneration of other tissues, illustrated by successful technique such as (matrix assisted) autologous chondrocyte implantation (M)ACI, in which isolated chondrocytes are culture-expanded *ex-vivo* and transplanted back into the patient by seeding on a supportive matrix. However relevant progress of regenerative medicine in terms of clinical realization is limited.[16] Chondrocyte grafting techniques can suffer from poor integration and quality of newly formed tissue, at the same time as in bone tissue engineering current effect of cellular grafts at orthotopic location is moderate and possibly even irrelevant at long-term implantation.[17]

The limited success of cell-based grafts has been attributed to several factors. One of the issues is the survival of transplanted cells. Viability of osteoprogenitors is crucial for bone formation at ectopic locations,[18] and is in part compromised due to interrupted nutrients and oxygen supply associated with implantation. Vascularization from the host takes a couple of weeks to develop and permeate the graft, which means that nutrient supply in the core of the implant is restricted during this first period after the implantation.[19] The transplanted cells therefore often lose function or die after delivery to the recipient.[20] This constraint will be especially important in large grafts of clinically relevant size (cm-scale). Prevascularization of the grafts with endothelial cells is one of the possible solutions to surpass the vascularisation delay, while porous constructs are highly important to enable fast tissue infiltration from the host.[21] The fate of surviving, transplanted cells,[22,23] regarding their retention and differentiation, remains unclear as illustrated by studies describing the loss of most transplanted osteogenic progenitors after implantation.[24] Another issue to consider is the location of implanted graft. While many of the feasibility studies on engineered grafts have been conducted at ectopic locations, an orthotopic environment presents crucially different cues and requirements to the graft, associated with elaborate hematoma formation, bone microenvironment and mechanical stimulation.[25] Finally, the matter of tissue complexity has so far been scarcely addressed by current TE applications. Commonly, a singular cell type is seeded on one type of biomaterial, in contrast to microenviroment of native tissues that presents the residing variety of different cell types with a rich assortment of matrix- and other cues. Studies that have investigated various combinations of cells or growth factors for skeletal tissue engineering report on positive effects of intercellular contact[26] and synergistic effects of growth factors on differentiation and tissue formation.[14] Anatomically designed layered cell-laden matrices demonstrate marked increase in biosynthetic activity of embedded cells according to the 3D arrangement.[27]

For above reasons, it is attractive to take a step back from the clinical application of skeletal grafts and start looking at the anatomical structure of connective tissues and investigate whether introduction of complex 3D organization into tissue-engineered grafts may help develop functional implants. Organ- or tissue printing (OP) is a new technology in regenerative

medicine,[28] that enables mimicking anatomical organization of tissues by using coculture of different cell-types and by tailored spatiotemporal release of growth-factor combinations. It can help developing structured multimaterial scaffolds and can help investigating whether the imposed organization is actually necessary for obtaining fully functional newly formed tissues. OP integrates cell-laden hydrogels with the so-called rapid prototyping technology (RP), which is based on computer-assisted design and manufacturing of layered structures.[29] Hereby a model of the implant is created on a computer, the dispensing material is loaded into the 3-axis robot arm and material is extruded layer-by-layer enabling formation of 3D structures of defined external shape and internal morphology. In organ printing, the extrudate consists of a (cell-laden) hydrogel (Figure 1.1). By exchanging the printing syringe during the deposition process multiple cells types can be incorporated at predefined locations in one construct. This way intricate structures mimicking the original cell organization can be built. By combining osteogenic progenitors with endothelial cells, prevascularization of the graft can potentially be addressed. Integrated pores in printed constructs enable nutrient delivery to seeded cells and facilitate ingrowth of blood vessels after implantation.
3D fiber deposition (3DF) is an OP technique based on extrusion of cell-laden hydrogel fibers on a stationary stage, yielding layered 3D structures.[30] In this thesis we characterized the use of 3D fiber deposition technology for development of bone tissue equivalents. Specifically, we determined the critical values of printing parameters in development of viable cell-laden constructs and assessed the performance of printed, multicellular constructs *in vitro* and *in vivo*.

Thesis aims and outline

The central aim of this thesis is to study the application of organ printing with 3D fiber deposition technique for development of viable printed bone tissue equivalents. It is hypothesized that by organizing the cells and matrix in a way that mimics the anatomical distribution of these components in natural tissues, one can enhance the functionality of tissue-engineered grafts. First, in **Chapter 2** we describe the rationale behind the use of organ printing technique as a tool to study the role of anatomical organization and for development of 3D structured tissues.

Specific aims of this thesis

I: Defining minimal requirements for 3DF printing of bone tissue equivalents

Components that are involved in 3DF printing of viable structured tissue equivalents include scaffold design, hydrogels and cells. So far, 3DF was mainly used for deposition of thermoplastic materials such as polycaprolactone and polylactid acid, at high temperatures ranging from 120 to 250 °C. However, using lower temperatures, cell-laden hydrogels can also be processed with this dispensing system. To apply 3DF for printing of cell-laden hydrogel structures for bone tissue engineering, it is important to determine the conditions that result in adequate tissue formation. Therefore the goal of the investigations presented in the first part of the thesis is to define conditions suitable for osteogenesis in printed gels. In **Chapter 3** we review hydrogel materials applicable for encapsulation of cells for skeletal tissue engineering. We describe various hydrogel systems that can present biochemical and physical stimuli to guide cellular processes such as migration, proliferation, and differentiation and could be used for organ printing. In **Chapter 4** we characterize the feasibility of using 3DF for printing of porous hydrogel constructs laden with

osteogenic progenitors. Specifically, we assess the viability of printed multipotent stromal cells in time, in several hydrogels, extruded from needles with different diameters, as well as the ability of the cells to differentiate along osteogenic lineage after printing. Some of the hydrogels are formed by photosensitive polymers. These materials undergo crosslinking in the presence of UV-light and photoinitiator molecules. The effect of photopolymerization on functionality of osteogenic progenitors embedded in such hydrogels is described in **Chapter 5.** Subsequently, the application of photocrosslinked Lutrol hydrogel for encapsulation of osteogenic progenitors and printing of patterned hydrogel structures with 3DF is addressed in **Chapter 6**. 3DF allows easy patterning of hydrogel constructs, making it possible to introduce various degrees of porosity into the scaffolds. Scaffold design and resultant architecture are important printing parameters, which impact on tissue development. We address these factors in **Chapter 7** by assessing the influence of scaffold porosity on oxygenation and functioning of embedded osteogenic progenitors *in vitro* and upon subcutaneous implantation in immunodeficient mice. Unmodified hydrogels used in organ printing often lack the appropriate stimuli to direct osteogenic differentiation of embedded multipotent stromal cells. This results in limited bone formation in these matrices *in vivo* and addition of calcium phosphate particles to the printing mixture is hypothesized to overcome this drawback. To this end, in **Chapter 8** we assess the addition of biphasic calcium phosphate microparticles and apatitic nanoparticles to printable cell-laden Matrigel constructs and compare the osteoinductive potential of calcium phosphate-substituted composites against cell-laden Matrigel constructs *in vivo*.

Questions addressed:

1. *Can 3D fiber deposition tool be used for processing of osteoprogenitor cells?*
2. *Which hydrogel materials are suitable for printing of viable bone tissue equivalents?*
3. *How do printing characteristics affect construct properties?*
4. *How does construct porosity affect functionality of embedded cells?*
5. *Does addition of calcium phosphate micro- and nanoparticles to cell-laden hydrogels lead to enhanced bone formation in vivo?*

II: Development of printed multicellular grafts and validation of heterogeneous tissue formation

Multiple cell types are present in native bone tissue. Endothelial cells and chondrocytes are important cell populations that coexist next to osteogenic cells and their progenitors during bone tissue development and in fracture healing, and in the setting of tissue engineering can greatly impact on osteogenesis. In the second part of the thesis we present studies with a common goal to develop multicellular grafts, as well as to test whether cellular organization introduced by printing is retained and translated to heterogeneous organization of extracellular matrix. For this, (stem) cells are included at predetermined locations in designed patterned constructs and the formation of extracellular matrix is studied both *in vitro* and *in vivo*. **Chapter 9** describes the isolation and characterization of goat endothelial progenitor cells, and their subsequent application as a potent source of endothelial cells for coimplantation with goat multipotent stromal cells. In **Chapters 10 and 11** we describe *in vitro* and *in vivo* extracellular matrix formation in printed composite grafts. Two models were tested: endothelial progenitors combined with multipotent stromal cells for vascularized bone grafts (**Chapter 10**) and chondrocytes combined with osteogenic progenitors for development of osteochondral grafts (**Chapter 11**).

Questions addressed:

1. *What are the characteristics of goat endothelial progenitor cells isolated from bone marrow and peripheral blood, and do they form blood vessels in vivo?*
2. *Can we use endothelial progenitors to enhance osteogenic differentiation in vitro and bone formation in vivo?*
3. *Do printed heterogeneous constructs demonstrate osteogenesis in vitro and form heterogeneous tissues, including bone, in vivo?*

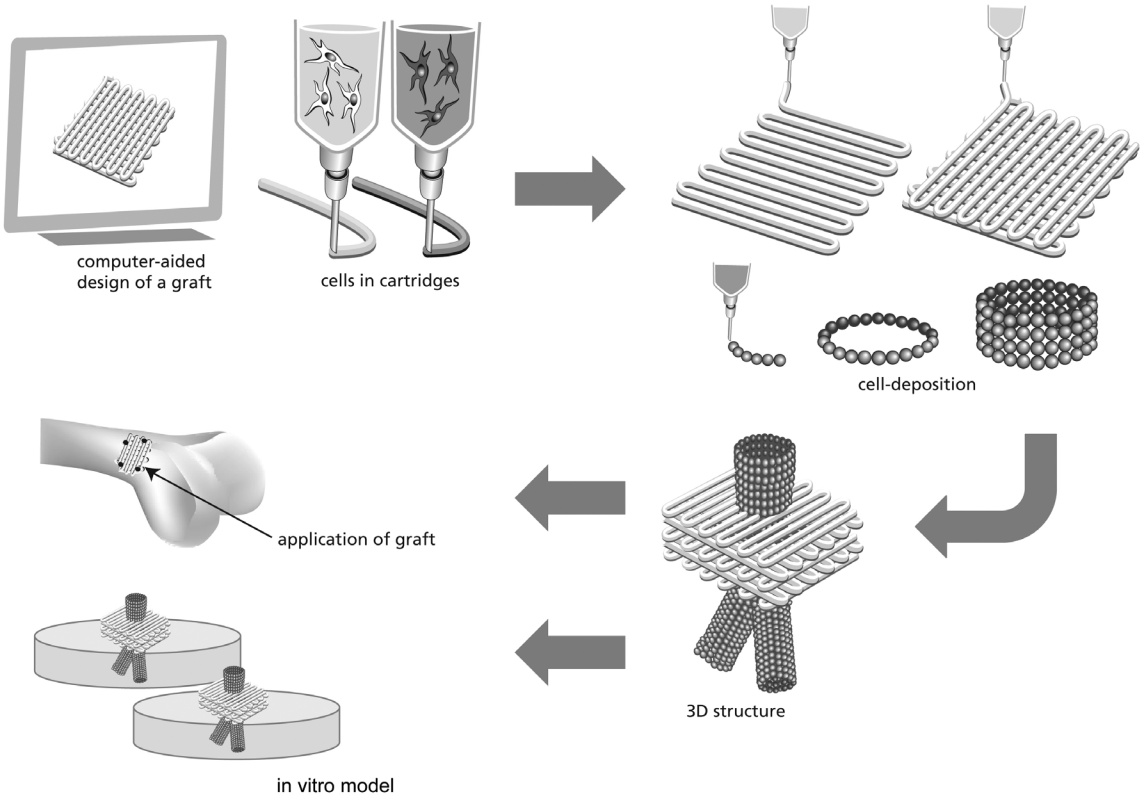

Figure 1.1: Organ printing. Computer-assisted design of the implant is translated by the organ printing machine into layered, cell-laden hydrogel structure with defined external shape and internal morphology, for use as *in vitro* model or for *in vivo* grafting.

Chapter 2

Development of organized skeletal tissues; is there a role for organ printing?

Fedorovich NE[1], Malda J[1,2], van Blitterswijk CA[3], Alblas J[1], Dhert WJA[1,4]

Manuscript in preparation

[1]*Department of Orthopaedics, University Medical Center Utrecht, Utrecht, The Netherlands*
[2]*Institute of Health and Biomedical Innovation, Queensland University of Technology, Queensland, Australia*
[3]*Department of Tissue Regeneration, University of Twente, Enschede, The Netherlands*
[4]*Faculty of Veterinary Medicine, Utrecht University, Utrecht, The Netherlands*

Abstract

The introduction of organ/tissue printing technology in 2003 has paved the road for the development of novel approaches to design organized tissue grafts for *in vitro* and *in vivo* applications. The directed placement of biomaterials, bioactive components and cells, together with biomimicking as a guiding principle, investigates the most optimal route to tissue formation, -integration and/or -remodeling. The resulting three-dimensional (micro)organization of cells has direct consequences for cell functioning. For connective tissues like bone and cartilage it is known that temporo-spatial presentation of environmental factors and mechanical cues regulate their growth and differentiation. The required level of complexity of printed tissues is, however, still unclear, as self-organization may concurrently influence tissue performance, and the question arises whether tissue mimicry should be all that accurate in order to achieve formation of functional tissues. Organ/tissue printing is the technology of choice to help answer these questions. The design of printable, tailored support-matrices of high shape-fidelity that drive cellular responses is crucial in the further refinement of a number of organ printing technologies and their development towards clinical application.

Rationale for building organized anatomical-like structures

Regenerative Medicine (RM) aims at developing implants to replace damaged tissues and to restore lost tissue function, by integrating engineering design with the ability of the body to heal itself. A considerable interest lies in the application of cell-based strategies, whereby (stem)cells are combined with scaffolding biomaterials and/or growth factors, yielding so-called hybrid grafts for implantation. Organs and tissues under close investigation by tissue engineers are blood vessels, liver, myocardium, kidney and skeletal tissues, including bone and cartilage. Current cell-based approaches focusing on regeneration of skeletal tissues produce inferior grafts that often lack organization and durability.[31,32] The generation of grafts of clinically relevant size that readily integrate and remodel is an additional challenge. Limited clinical success of tissue-engineered grafts has prompted an increasing awareness of the need to step away from a (relatively) simplistic approach of combining one cell type with one type of scaffolding matrix. Most tissues in the body possess a naturally occurring 3D structure with its own composition of cells, bioactive molecules and matrix components, driving tissue development and regulating its function. An alternative to develop more sophisticated skeletal grafts could therefore lie in imitating the anatomical organization of connective tissues (Information box 2.1), either by following the sequential steps during morphogenesis or regeneration by for example mimicking endochondral bone formation,[33] or by building tissues that mimic native cell- and matrix structure,[34] as described further below.

Initial attempts to copy nature's design in skeletal tissue engineering have focused on anatomically shaped implants and composite scaffolds with variable (chemical) composition, stiffness, porosity and degradability. Examples of such approaches include anatomically shaped cartilage implants,[35-37] as well as implants for intravertebral discs,[38] osteochondral[39,40] and bone defects.[41,42] The variable presence of adhesive ligands and temporo-spatial presentation of growth factors,[43] by combined or sequential delivery, are additional regulating parameters for directing tissue organization. Sophisticated growth factor delivery by independent release of two or more molecule types that mimic the endogenous spatial and temporal distribution of native growth factors is a particularly successful approach applied in bone and cartilage tissue engineering (Information box 2.2). For bone formation at ectopic location, sequential delivery of vascular endothelial growth factor (VEGF) in combination with local sustained BMP-2 release significantly enhances the amount of newly formed bone, compared to BMP-2 alone.[14] For therapeutic angiogenesis, combined delivery of platelet derived growth factor (PDGF) and VEGF from a polymer scaffold results in the formation of more mature blood vessels than monotherapy with either factor.[44] The concept of the use of a single growth factor, randomly delivered to promote vascular network formation, has even been called "somewhat naive and even misguided".[45] Others have focused their efforts on development of heterogeneous cellular grafts, including vascularized bone grafts and zonal cartilage implants.[27,46] Bilayered gel constructs formed from a layer of deep- and a layer of superficial chondrocytes demonstrate better mechanical properties that gels from randomly mixed cells.[47] Another example of anatomical design in skeletal tissue engineering is the development of osteochondral grafts.[39] Such grafts consist of a superficial cartilaginous layer and an underlying calcified tissue on top of subchondral bone. The use of composite matrices in osteochondral tissue engineering is inspired on the compositional properties of native tissue, yielding heterogeneous grafts.[39,48] The challenges associated with such hybrid osteochondral grafts are matching topology of the grafts with the

injured site, controlling tissue formation in respective layers and achieving adequate integration at cartilage- and bone interface.[49,50]
Organization of engineered tissue has a profound influence on the outcome thereof (see Information box 2.2). In the 3D environment many parameters including mechanical cues, cell density, matrix binding and nutrient diffusion must be taken into account. Predictive computational modeling that accounts for all these input parameters may be very useful in gaining additional insight in the design parameters necessary for complex engineered tissues. For example, validated computational models are now providing evidence that bone and cartilage formation are best achieved under diverse mechanical strain regimes.[51,52] Given the significant influence of 3D organization on tissue formation, mechanical signals should not be overlooked in the design of 3D constructs either for use as *in vitro* model systems or as *in vivo* grafts. In order to understand the challenges associated with design of structured 3D constructs we first discuss the capability of cells to self-organize into relevant structures and subsequently address how novel rapid prototyping technologies can additionally dictate organization. Finally we indicate how these two routes can synergize.

Cellular self-organization and organization by heterogeneous differentiation

Tissue fusion and cell sorting are fundamental principles during tissue development.[53-55] Tissue fusion refers to a morphogenic process whereby two or more cell types interact to generate a single tissue. This process may be guided by internal factors such as microtissue maturity, external factors such as the presence of ECM interactions, growth factors and nutrients, or can occur as self-assembly of for instance cell-aggregates or cells deposited with inkjet printing.[56,57]
Cell sorting, on the other hand, refers to the ability of multiple cells types to sort themselves on the basis of shared characteristics, e.g. surface marker expression. Levels of cell surface adhesion proteins such as cadherins and cytoskeletal-mediated tension, drive cell sorting in a process described by the differential adhesion hypothesis.[58-60] This theory describes cells behaving like immiscible fluids due to differences in cell adhesion and cohesion, so that when two types of monodispersed cells expressing different levels of adhesion molecules are mixed, they may self-organize into a 3D microtissue where one cell forms the inner core and the other the outer coating.[58] Maturation of cell-to-cell contacts, the presence of extracellular matrix and cell-to-extracellular matrix contact and differences in cell motility, additionally influence cell sorting. Integrin-mediated binding to extracellular matrix and cadherin expression levels may vary from cell to cell.[61] While epithelial tissues depend on cadherin adhesion molecules for adhesive stability, mesenchymal tissues are more reliant on adhesive interactions with extracellular matrix elements, such as fibronectin, laminin and collagen.[62-64]
It has been demonstrated that after tissue spheroids fuse to form microtissues,[55,58]cells sort in a heterogeneous fashion forming (luminal) structures with distinct cell layers. These structures range from large vascular spheroids and tubular rods to complex 3D patterned shapes.[54,65] Also cells employed for skeletal tissue engineering tend to spontaneously reorganize in heterogeneous fashion when combined in cocultures. These are for instance coculture spheroids of osteoblasts and endothelial cells into an osteoblast core and a surface layer of endothelial cells within four days of culture.[66,67] Comparable effects are seen for cocultures of endothelial cells and smooth muscle cells.[68] High-density culture of immature primary chondrocytes on porous filter membranes resulted in formation of hyaline cartilage, which spontaneously exhibited some features of the zonal stratified cartilage, characterized by columnar organization of cells.[69]

To date there is, however, little understanding of the underlying mechanisms when multiple microtissues undergo tissue fusion.[54] Therefore, the explanation of how self-organization of skeletal cells is achieved remains elusive. Apart from the influence of differential adhesion between different cell types, cells divide or differentiate according to their potential and the influence of local environment. While cellular self-organization can additionally be driven by cell adhesion to extracellular matrix,[63,70] organization can also be achieved by differential maturation of (stem) cells induced by spatial differences in mechanical loading, by gradients in available nutrients or by differential response to chemotactic gradients when different cell types affect the organization of each other through secretion of growth factors.[71] Stratification of cartilage for example, possibly arises from metabolic gradients occurring in the developing tissue,[69] while oxygen tension might play an important regulatory role during cartilage and bone tissue development.[72] Above factors can explain the occurrence of organized differentiation in the following study whereby upon long-term *in vivo* implantation, polymers seeded with chondrocytes and wrapped with periosteum exhibited appearance of a putative growth plate in the cartilaginous regions of the bone constructs, with cells arranged in columnar fashion at specific zones of cartilage without prior mechanical induction.[73] A similar trend of growth-plate organization was observed for chondrocytes and osteoblasts homogeneously encapsulated in alginate after subcutaneous implantation in mice.[70]

Self-organization potential is different for different tissues, and is quite robust in processes occurring in organization of skin, bladder lining, and blood-vessel formation. [74] Until now, strong evidence that skeletal cells can spontaneously form organized tissues is not available. We expect that in part (self)-organization principles described above will also be applicable to tissue engineered bone and cartilage, and in part additional structure can be introduced in these tissues by organ printing technologies. When using a bioprinting approach the final structure of the engineered tissue-equivalent will be the resultant of the structure introduced by the printing process and intrinsic organization ability of cells and/or the surrounding host tissue.

Adding structure by printing technologies

Rapid-prototyping (RP) technologies provide additional means of achieving organized structures. Various RP-based techniques allow mimicking of anatomic geometries, building constructs with a customized architecture and defined compositional variation. RP-based approaches that enable layer-by-layer deposition of cells or cell-laden hydrogels are collectively called tissue- or organ printing technologies, and present a novel tool to mimic intra-tissue cell distribution.[28] Information box 2.3 and Figure 2.2 present an overview of organ printing techniques, describing their resolution, advantages and drawbacks.

Several papers have reviewed the capability of RP technologies to build acellular scaffolds for tissue engineering.[29,75-78] All these systems are based on computer-aided design of 3D constructs with high reproducible architecture (size, shape, porosity, interconnectivity, pore-geometry and orientation) and compositional variation.[75] Anatomically organized, custom-shaped grafts can be manufactured based on magnetic resonance imaging or computerized tomography scans.[29,48,79] Such grafts are especially relevant when the defect is unconfined,[39] surpassing the use of molds.[40,80] Composition or pore structure at specific regions of a printed scaffold can be varied providing cues for adhesion and growth of specific cell types in defined patterns. Further, RP can optimally match the mechanical properties of the specific application being considered, depending on materials used.[29,81,82] Amongst other RP approaches, 3D fiber deposition has been

investigated to modulate mechanical properties of cartilage tissue engineering scaffolds[30,82,83] by varying fiber geometries and pore-size gradients, introducing inhomogeneous pore-size gradients to mimic anatomic matrix spacing.[84]

Control over bioactive factors in 2D is provided by a number of RP-based patterning techniques, including photolithography, soft lithography and microcontact printing, which spatially control the surface chemistry and topography at micrometer level. By introducing spatial concentration gradients of adhesive molecules followed by cell seeding, one can affect cell alignment, morphology and motility.[85-87] Cell function not only depends on the concentration of adhesive molecules, but also on composition[88] and geometry of adhesive micropatterned islands.[89,90] Patterning of adhesive molecules and the use of nanotopographies can be used to modulate MSC differentiation.[91,92] Considering that several RP techniques can process (hydrogel) materials under non-denaturing conditions, growth factors can be easily incorporated into the process of deposition without loss of their bioactivity. Experimental approaches to assess cellular responses to printed gradients of soluble hormones range from *in vitro* organization of pro-osteoblastic cells[93] to driving cell differentiation responses *in vitro*[94] and spatial control of bone formation *in vivo*.[95] Although RP patterning techniques can be used to drive cellular responses and achieve tissue regeneration *in vivo,*[96] they are particularly useful for *in vitro* applications such as screening studies as they provide a means to study the effects of multiple biomaterials and patterned bioactive molecules on cells.

When considering organ- and tissue printing techniques, the most important factor is the incorporation of viable cells into the deposition process, either for 2D or 3D applications.[97] In 2D, laser-directed writing of cells[98] allows manipulating individual cells by trapping the cells in a laser beam, while laser-induced forward transfer (LIFT) possesses the capability to print cell suspensions using a wide range of gel viscosities and at high cell densities.[99-102] Soft lithographic techniques including microcontact printing and microfluidic patterning[103] make it possible to sequentially pattern multiple cell types.[104] Multimask photolithographic patterning enhances these possibilities by patterning large surfaces with distinct surface chemistries enabling extensive coculture studies.[105] Such cellular patterning techniques can easily control the degree of interaction between two cells types and allow studying cellular interactions at different ratios. Subsequent stacking or micromolding of cell-laden patterns makes it possible to design 3D structures.[106,107] Another direct cell-patterning approach is based on organizing the cells by dielectrophoretic forces and subsequent entrapment in a UV-sensitive hydrogel,[108,109] fabricating layered 3D matrices with variable cell organization. Using this technique local cell density can be uncoupled from cell organization, and as a result of that changes in extracellular matrix formation can be attributed to differences in cellular organization.[109]

Organ/tissue printing can also result in direct deposition of viable 3D structured constructs. Simultaneous printing of cells and biomaterials in 3D is possible with LIFT,[100-102,110] ink-jet based printing[28,57,111-113] and dispensing techniques.[114-117] Laser-based techniques print multiple cell populations in 3D, and printed cells retain differentiated phenotype.[100,101] Ink-jet printing of cells uses a modified commercial version of bubble jet or piezoelectric methods to deposit cells in suspension. Dispensing-based techniques process a broad range of (cell-laden) hydrogel mixtures of various viscosities. Multi-nozzle deposition of hydrogel matrices allows constructing scaffolds with heterogeneous localization of multiple cell types.[117] A recent application includes printing of stratified skin layers (fibroblasts and keratinocytes) via 3D robotic cell printing tool also on non-planar surfaces.[118] The cells, deposited in separate layers by interlayered crosslinking, retain the

printed architecture.[118] Recently printing systems have also demonstrated the potential of direct *in vivo* application.[113] *In vivo* ink-jet printing of cells combined with gene transfection is a promising new approach to enhance tissue formation.[113]
In conclusion, RP-based technologies enable the production of constructs with spatial variations along multiple axes with high geometric complexity and can be used to aid in fabrication of arbitrary shaped tissues with complex geometries and heterogeneous growth factor- and cell distribution in tissue- or organ printing.[28]

What are the challenges?

Specific examples of heterogeneous anatomical design in skeletal tissue engineering that might profit from additional structuring include the creation of (vascularized) bone grafts, formation of osteochondral implants and design of stratified cartilage.[119] The development of printed tissues is expected to help differentiating between different effects that modulate tissue formation and function, provide a valuable tool to study the effect of anatomy on graft performance and to increase functionality of current engineered implants.[91,120] The practice is however elusive. While many exciting data on cell pattering are available, data supporting the formation of functional extracellular matrix *in vitro* and retention of organization *in vivo* are limited, and actual functional printed tissues are not available yet.
Clearly, patterned cells do not equal a functional tissue. In some cases layered cartilage populations have demonstrated inferior mechanical properties when compared to randomly mixed cells, despite exhibiting adequate depth-dependent mechanical profile resembling that of native cartilage.[32] Furthermore, disruption of imposed stratification in zonal cartilage implants was already seen after one week of *in vivo* implantation.[31] Both studies suffered from compromised retention of synthesized matrix, providing a possible explanation for limited mechanical properties of the anatomically organized constructs *in vitro* and rapid loss of imposed stratification *in vivo*. Tailoring the scaffold properties to sustain the phenotype of the embedded cells could potentially improve the quality and retention of the synthesized ECM. Scaffold properties tailored with tissue printing techniques, could lead to further development of these cartilaginous grafts. Another example is directed self-organization of endothelial cell-aggregates by ink-jet printing. Although studies demonstrate the organization of cell-aggregates into tubular structures upon printing in[55,121] or sustained by[122] hydrogel matrices, the functionality of the newly formed tissues[56] is questionable. Recent application of this self-organization concept using microtissue building blocks[123] to produce small diameters blood vessels with spheroid myofibroblast/endothelial cells microtissues did not yield functional tissue. Myofibroblast spheroids seeded with a layer of endothelial cells were impacted in a tubular fashion yielding homogeneous association of the microtissues and cellular reorganization of fibroblasts lining the luminal part after flow and mechanical stimulation. However, endothelial cells were not detected on the luminal surface of the mechanically stimulated constructs and were distributed throughout the vessel wall, possibly as a result of limited migration potential of cells or VEGF in the microspheres. This finding underscores the necessity of additive organization of self-assembling spheroids by for example printing technologies to improve tissue structure by introducing porosity in the construct.
The question arises how much effort should be put in trying to design structures that more and more closely mimic the native skeletal tissue organization. Other challenges of cell-based skeletal

tissue printing research include finding the appropriate material properties to guide tissue formation and a way to validate the functionality of printed tissues, both *in vitro* and *in vivo* setting.

The size and resolution of printed tissues

The degree of intricacy of printed tissue-equivalents is determined by the balance between organization imposed by the printed tissue design and self-organization potential of the cells, and will be different for different tissues. Also the envisioned application of the printed tissues determines the desired resolution. Printed tissue-equivalents to be used as *in vitro* models in a number of applications such as pharmacokinetic studies, to understand the effects of mechanical or genetic manipulations, to determine the effect of 3D organization on tissue formation or as model systems for skeletal diseases,[103,124,125] could require a higher level of complexity than constructs used for tissue regeneration that can be more simplistic relying on the organization capacity of the body (remodeling).

Different RP technologies attain different scale of resolution (Information box 2.3). Despite the fact that tissues built by precise micro-scale patterning techniques are much too small to ultimately function as tissue equivalents for *in vivo* implantation, these micropatterned structures can be used as *in vitro* models that capture more of the relevant tissue complexity than current tissue engineering approaches.[126,127] Micropatterning of cells has been used to study diverse aspects of cell physiology, including the effect of spatial control on cell attachment, spreading and outgrowth of blood vessels.[90] Other RP techniques such as 3D ink-jet printing and dispensing, that may be too crude for facilitating the small scale cell organization for the *in vitro* tissue models,[126] can in turn enable fast and efficient cell-laden scaffold formation for construction of grafts for *in vivo* application. An important aspect hereby is the ultimate clinical application of the grafts.[128] Resolution and size constraints of available printing technologies play a significant role in time- and cost-efficient production of clinically relevant sized grafts.

The role of the printed matrix

Another important parameter in printed tissues is the composition of the coprinted hydrogel matrix. Obviously this material should be at least printable, cytocompatible and biodegradable. Moreover, the matrix should be stiff enough to allow fiber stacking and sustain forces associated with implantation. For this, the mechanical properties of the hydrogels currently employed for organ printing need further optimization to ensure formation of structures with sufficient mechanical properties for development of fully porous scaffolds that can endure weight baring. In addition, the printed matrix should promote adequate differentiation of encapsulated cells, and hence facilitate the tissue formation *in vivo,* in particular the development of instructive hydrogel matrices containing adhesive, degradable and differentiation-inducing sequences can contribute to further development of printed tissues. [129]

Additional focus to stimulate tissue formation can include mechanical modulation of the designed scaffolds prior to the implantation,[130-132] or induction of oxygen tension gradients to promote heterogeneous differentiation profile of printed progenitors. In both of these, computational modeling[52] can play a role for prediction of the effect of scaffold properties on tissue function.

Validate the performance of printed tissues

The functionality of printed tissues, both *in vitro* and *in vivo*, needs validation as current progress in the field is mostly limited to short-term evaluation of *in vitro* deposited cells.[100,118,133] *In vitro* models can be designed by modulating composition of printed matrices, by using cell types with various degrees of differentiation and by comparing different cell ratios, in order to analyze the effect of these different modulators on ECM formation and function. Relevant readouts include retention of phenotype in culture and organization after printing, composition and amount of formed ECM and mechanical properties. To assess the degree of capillary formation by endothelial cells, the amount and degree of branching of the newly formed vessels and possibly connection to the host vasculature are assessed (by injection of radioopaque polymer or fluorescent label).[14,134,135] An important question is how different cell arrangements are retained *in vivo,* which is most obviously studied by histology. The contribution of host cells including immunological responses to tissue formation is probably a good indicator of implant success.

Conclusion

The introduction of organ printing has resulted in development of novel approaches to generate organized engineered tissues. Printed constructs await a wide range of potential applications including the use for *in vivo* implantation and as *in vitro* models in pharmacokinetic studies, to determine the effect of 3D organization on tissue formation or to study skeletal diseases. The question arises how precise native tissue organization should be recapitulated and how far developmental morphogenesis should be imitated. If we aim to achieve not just patterning cells, but developing functional 3D tissues, technologies that enable fast, cost-efficient multicellular approach are preferred. Moreover, many relevant parameters for deposition of viable, heterogeneous, multicellular structures need to be defined. These include the resolution and cytocompatibility of the deposition process and the required printing matrix. The development of instructive matrices that add structure to available self-organization processes of cells are thus a necessity.

Acknowledgements

We thank Tijmen van Blijswijk for his contribution to this overview. We acknowledge the financial support by the Netherlands Organisation for Scientific Research to NF (NWO; grant number: 017.001.181) and the Smart Mix Program of the Netherlands Ministry of Economic Affairs and the Netherlands Ministry of Education, Culture and Science.

Information box 2.1: 3D structure of bone and cartilage

Bone

Bone is a rigid tissue that gives structure to the body, supports and protects various organs, produces blood cells and stores minerals. Bone consists of cancellous and compact bone tissue[136],[137] in which the different bone forming/regulating cells (osteoblasts, osteocytes) and bone resorbing cells (osteoclasts) are located (Figure 2.1A,B). Hierarchy of bone structure comprises distinct levels starting from hydroxyapatite crystals organized within collagen fibrils and parallel organization of collagen fibrils within lamellae, progressing to concentrically arranged lamellae that form osteons, towards trabecular or compact arrangement of osteons to form cancellous and compact bone respectively.[138]

Bone is both vascular and innervated tissue that contains the bone marrow, an important source of multipotent stromal cells (MSCs, the progenitors of bone and cartilage) and hematopoietic stem cells (HSC, the progenitors of blood cells).[139] There is a high level of interaction between the cells present in bone (Figure 2.1C), exemplified in the osteogenesis-angiogenesis coupling, which ensures a dense vascular network.[140,141] Vascular endothelial growth factor (VEGF) and bone morphogenetic proteins (BMPs) are the most well-known players in this system. During embryonic development and fracture healing, endochondral bone is formed from a cartilage matrix, and blood vessel invasion is essential for coupling resorption of cartilage with bone formation.[142] Bone formation involves a large number of hormones, cytokines and growth factors and their receptors, each showing distinct spatial organization and temporal expression.[43,143-148] Together, they contribute to bone's unique regenerative capacity of scarfree healing.

Cartilage

Cartilage is an avascular, aneural tissue that contains relatively few cells (chondrocytes), and abundant collagen, proteoglycans (PG) and other proteins and glycoproteins. A network of fibrillar collagen provides form and a framework that immobilizes PGs and swells with water.[149] The mature cartilage is both structurally and functionally heterogeneous, both at different topographical locations in jointsand throughout the tissue.[69,150] Articular cartilage tissue consists of four distinct zones: superficial, middle, deep and a zone of calcified cartilage. Each of these zones differs in chondrocyte morphology, biosynthetic activity, metabolic needs, gene expression, biochemical composition, and collagen fiber organization.[47,150,151] Collectively, all of these factors allow cartilage tissue to withstand the biomechanical load and contribute to good joint articulation.

Information box 2.2: The contribution of biomimicking to function of engineered tissues

Parameters mostly being mimicked in tissue engineering are heterogeneous matrix organization and composition, as well as the distribution of multiple cell types and growth factors in native tissues. Several findings described below indicate that certain biomimicking strategies have a positive effect on cell performance *in vitro* and tissue formation *in vivo.*

Matrices used as scaffold material can be designed with graded chemical composition.[129,152,153] In bone tissue engineering, polymeric scaffolds or composite grafts, consisting of a ceramic and matrix phase,[12] can be designed with organized structure with defined external shape and graded porosity.[81] Anisotropic porous scaffolds for bone tissue engineering[154,155] devised by electrospinning and centrifugation techniques demonstrate graded tissue formation throughout the construct.

Growth factor delivery that mimic their (combined) endogenous spatial and temporal distribution efficiently guide bone formation and cartilage development.[43,156-158] Blood vessel tissue engineering has also highly profited from a combined application of multiple growth factors, overcoming formation of immature and unstable vessels,[159,160] when monotherapies are employed. Cocktails of growth factors have additive and in some cases synergistic effects on the performance of osteoblasts *in vitro* and bone formation and fixation strength *in vivo*, as compared to the use of a single growth factor.[161-163] The delivery of angiogenic factors along with osteoinductive growth factors is a widely used biomimicking approach to enable reconstitution of higher amount of vascularized bone, compared to the use of osteoinductive factors only.[14,143,164,165]

Heterotypic cell interactions are powerful biomimetic cues driving differential organization in skeletal tissue-engineered constructs. Addition of endothelial cells to osteoblasts or their progenitors promotes osteogenic differentiation and bone formation.[26,71,166,167] This effect is partly based on direct cellular interactions mediated by a gap junction protein connexin 43,[168] and partly on reciprocal growth factor production and receptor interactions. For formation of adequate blood vessels, coexistence of endothelial cells and smooth muscle cells[67,169] are indispensable, ensuring long-term stabilization by association of the two cell types.[134,170] Design of osteochondral grafts is an excellent illustration of anatomical cellular gradients in skeletal tissue engineering.[39] Combining chondrocytes with osteoblasts supports the integration between bone and cartilage layers,[73,80,171-173] and produces well-organized osteochondral tissue upon *in vivo* implantation. Underscoring the importance of zonal organization for the normal function of articular cartilage, cartilage matrix formation is greatly affected by coculture of chondrocytes from different zones in monolayer[174] and stratified organized in a bilayered photosensitive hydrogel.[27]

Information box 2.3: Organ printing techniques

Laser-induced optical forces can be used for non-contact manipulation of particles of 100 nm to 10 mm in diameter and include laser-directed cell writing[98] and laser-induced forward transfer (LIFT) or laser-printing (LP) of cells.[99,100,175] Laser-directed cell writing allows manipulating individual cells in suspension but is limited to processing of low cell numbers. The laser-printing technique is an orifice free technique based on the instant focus of a high-energy laser to the focal spot above a cell-laden substrate and subsequent dispensing of the cells under the evaporated focal point. LIFT prints organic and inorganic material, single to tens of cells simultaneously without any damage to pheno -or genotype,[101,176,177] easily attains microscale organization of deposited cells,[110] but cannot reach high-throughput rate with continuous dispensing of cells due to the need of cell-laden strips used in the deposition and is limited to printing fluids of relatively low viscosity.[110] [178] Soft lithographic techniques including microcontact printing,[179,180] microfluidic patterning[103] and multimask photolithographic patterning[105] enable patterning of multiple cell types with a minimum feature size of ten micrometer.[104] Such cellular patterning techniques can easily control the degree of interaction between the two cell populations and allow studying cellular interactions of different ratios.[120] Organizing the cells by dielectrophoretic forces and subsequent entrapment in a UV-sensitive hydrogel, makes it possible to directly fabricate layered 3D matrices with variable cell organization.[108,109]

Ink-jet printing of cells uses a modified commercial version of thermal or piezoelectric methods to dispense cells in suspension. Some disadvantages of ink-jet printing are nozzle clogging, the loss of cells during printing and a limited number of suitable materials to process. The inkjet printing fluids must have a relatively low viscosity, which forms a severe restriction.

Dispensing-based techniques process a broad range of (cell-laden) hydrogel mixtures of various viscosities, and make cm-scale structures at 100-200 micrometer resolution, with controllable porosity Transverse pores are difficult to control, which sometimes limits the constructs to several layers due to diffusion restrictions.[118] Use of predictable cell densities is challenging for some dispensing tools due to clogging or sedimentation and aggregation of cells occurring between the time of cell preparation and actual printing procedure.

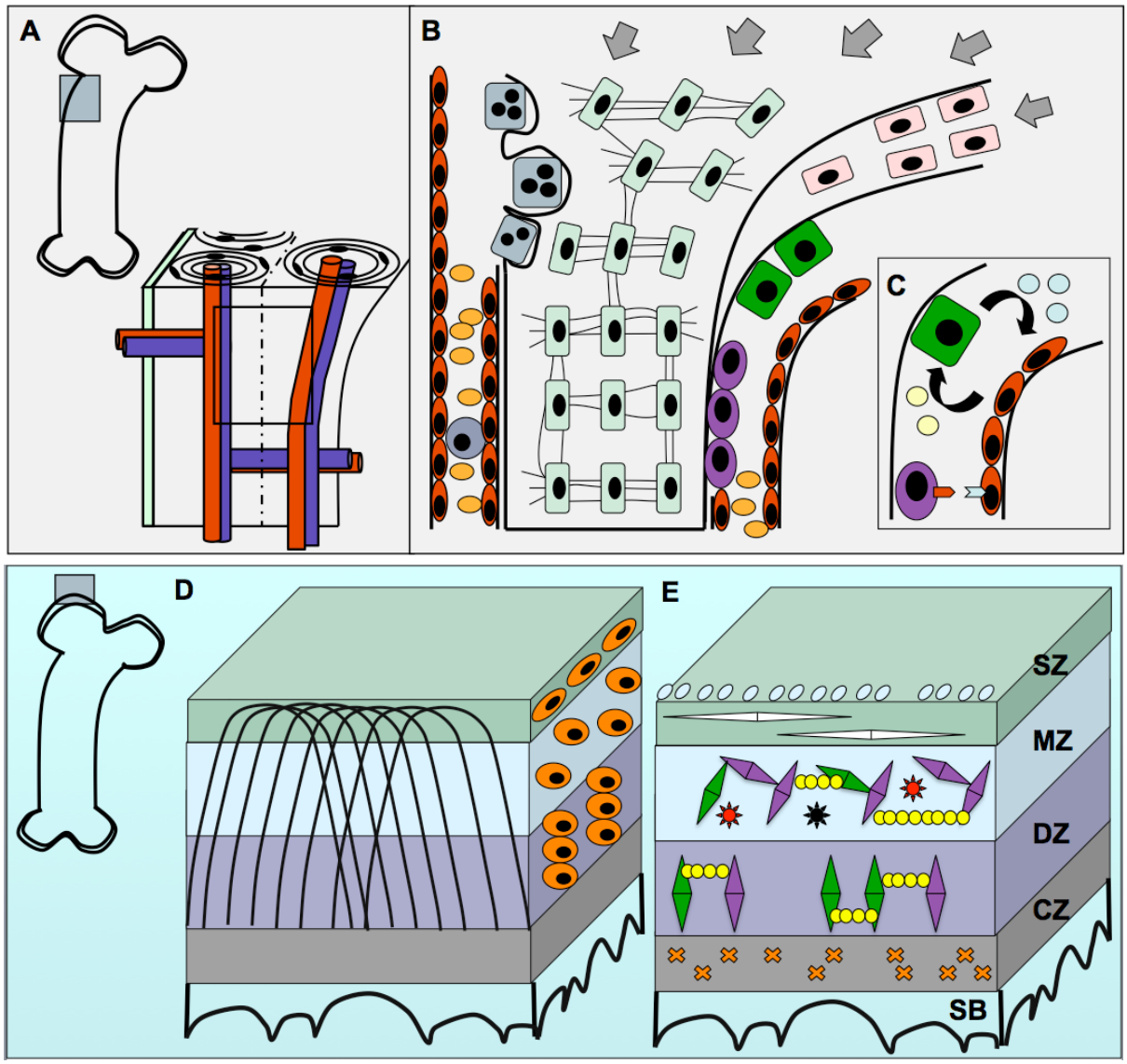

Figure 2.1: Natural organization of bone and cartilage. A-C: Bone tissue organization; A: Compact bone consists of osteons: concentrically arranged layers of osteocytes (lamellae) around the central canal containing vessels and nerves (Haversian channel); B: Bone cells include mesenchymal stem cells (MSCs) from the blood, MSCs differentiate into osteoblasts that synthesize bone matrix and become embedded within it, hereafter they are called osteocytes. Osteocytes sense the stimuli from outside (for example mechanical forces (grey arrows)) and communicate these via cytoplasmatic processes called canaliculi. When bone matrix is no longer required at certain places, bone-specific multinucleated macrophages called osteoclasts, derived from hematopoietic stem cells, resorb the matrix; C: Angiogenesis-osteogenesis coupling refers to (HIF-mediated) VEGF release by osteoblasts which leads to blood vessel formation, supplying the MSCs by oxygen and nutrients, with endothelial cells and their progenitors stimulating osteogensis either by direct cell-cell interactions or indirectly by production of BMPs; D,E: Cartilage organization, adapted from[69]; D: Orientation of collagen fibers and cell morphology in different cartilage zones; E: Biochemical composition of the matrix in the zones. In the superficial zone (SZ) the chondrocytes are flat and fibers are organized horizontally to the surface, matrix contains collagen type I and superficial zone proteins. In the middle zone (MZ)

the chondrocytes are round and dispersed through the matrix containing heterogeneously arranged collagen type II en VI, aggrecans, cartilage oligomeric matrix proteins and cartilage intermediate zone matrix proteins. In de deep zone (DZ) the chondrocytes are stacked between vertically arranged collagen fibrils of collagen II en VI, and aggrecans. In the calcified zone (CZ) the cells are sparse, lying between fibers of collagen type X.

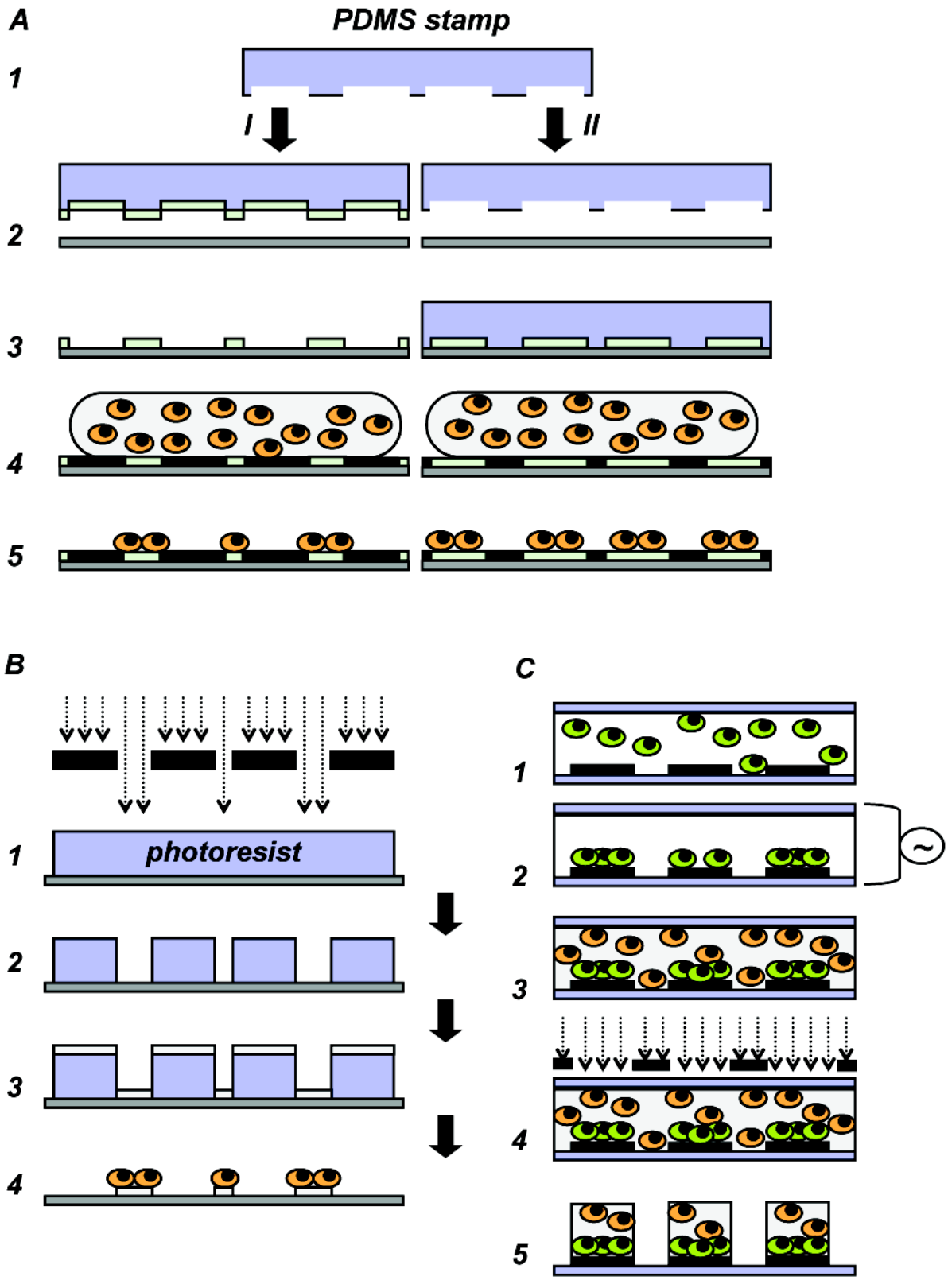
A
PDMS stamp
1
I
II
2
3
4
5
B
1
photoresist
2
3
4
C
1
2
3
4
5

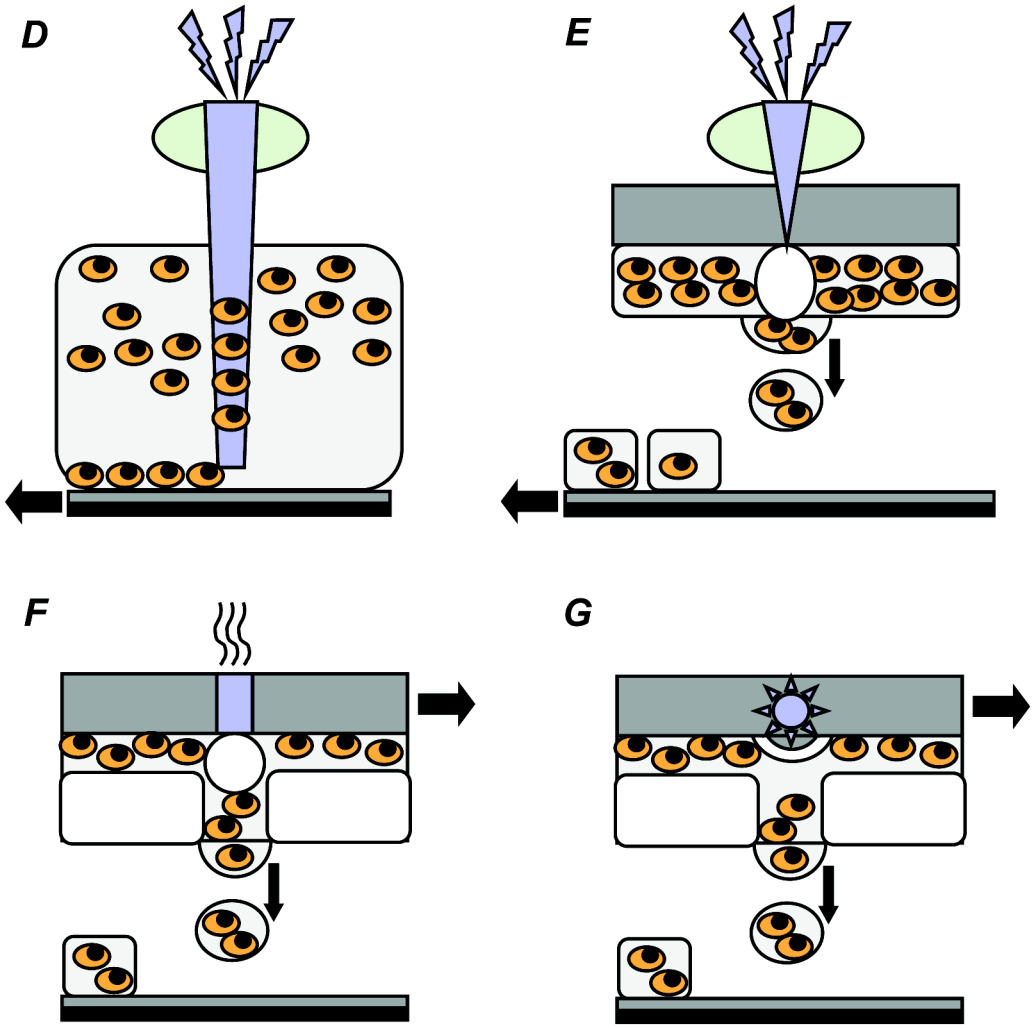
D
E
F
G

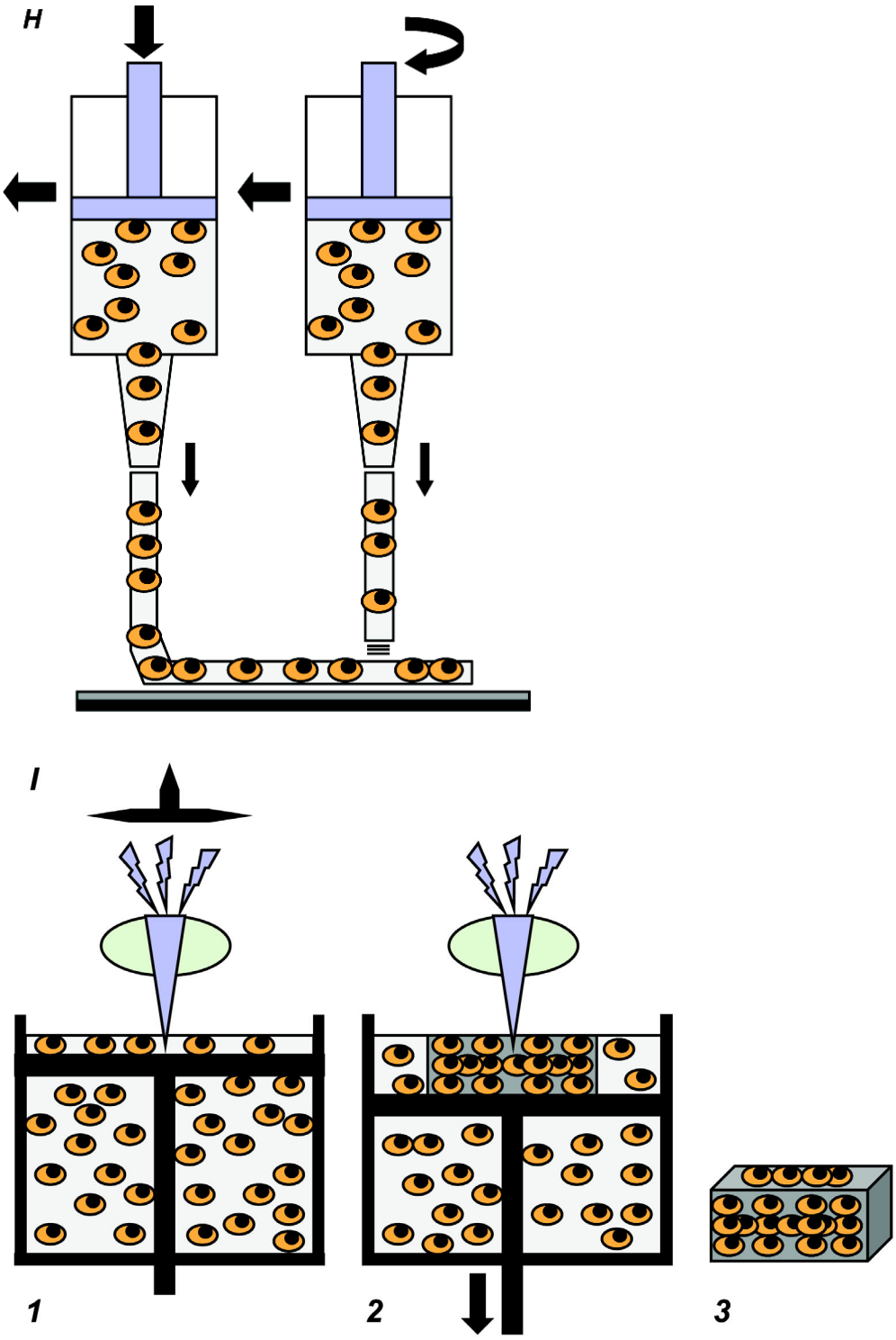

Figure 2.2: Cell patterning and organ printing techniques. A: Cell patterning by microcontact printing (I) and microfluidic patterning (II). Polydimethylsiloxane (PDMS) stamp (1) is prepared by casting and curing of the DMS polymer on a master (commonly a silicon wafer patterned by photolithography). In I the stamp is coated with a solution containing the bioactive molecules (2) and transferred onto a substrate (3). The empty spaces are filled with a passivating solution to limit the biofunctionalisation to the printed areas only, hereafter the surface is incubated with the cells (4) that get restricted to the printed area (5). In II the PDMS stamp is

brought in direct contact with the substrate (2) and the resulting channels are filled with the patterning solution (3). Following the backfilling step with the passivating solution, the surface is incubated with the cells (4) that get restricted to the biofunctionalised area (5).
B: Cell patterning by photolithography. Photoresist layer is exposed to UV light passing through a mask (1), yielding a pattern (2). The surface is coated with a solution containing the bioactive molecules (3), hereafter the photoresist is removed uncovering the patterned area whereto the cells adhere (4).
C: Patterning of (encapsulated) cells by combining photolithography and electropatterning. First, one cell population (1) is organized by the dielectroforetic forces (2). Subsequently a second population of cells mixed with a UV-sensitive hydrogel is added (3) and the gel is exposed to UV-light passing through a mask (4), yielding patterned multicellular cell-hydrogel constructs (5).
D: Cell patterning by laser guided direct writing. Hereby a laser beam scatters photons off the surface of the cell, and when the refraction index of the cell is larger than that of the surrounding medium, the cell experiences both a radial force pulling it towards the center of laser beam and an axial force pushing the cell in the propagation direction of the light. The cells are then guided onto the substrate by optical force momentum.
E: Cell manipulation by laser-induced forward transfer, and derived techniques such as laser-printing (BioLP) and matrix-assisted pulsed-laser evaporation direct-write (MAPLE DW), involve a laser that is focused onto the thin coating of matrix-embedded cells causing the formation of vapor at the coating-donor substrate interface and the ejection of a portion of the coating as a high speed jet. The droplet of material is ejected onto the receiving substrate.
F,G: Ink-jet printing of cells, by using a thermal (F) of piezoelectric (G) delivery of the material. In an inkjet system the printhead contains a cartridge/reservoir filled with cells (mixed with a hydrogel): i.e. the bio-ink. Pressure is generated in the cartridge, and the bio-ink is expelled by thermal (a heating pulse leads to a bubble formation, F) or piezoelectric (a voltage pulse deforms a diaphragm pushing out a drop of bio-ink, G) forces. A cell droplet forms and is ejected through an orifice, hereafter the droplet lands on a receiving substrate.
H: Robotic dispensing of cell/hydrogel mixtures. In this set-up the cell/hydrogel mixtures are contained in a dispensing syringe, and the plunger is displaced either by pneumatic pressure or volumetrically pushing out a strand of cell-laden hydrogel on a stage. Layer-by-layer deposition of strands yields porous 3D structures. By simultaneous use of several syringes for the deposition, multiple cells types and matrices can be combined in one construct.
I: Stereolithography for building of cell/hydrogel constructs. The principle is based on spatially controlled solidification/gel formation of a liquid resin (cells in a UV-sensitive hydrogel-forming polymer) by photopolymerization. It is a layer-by-layer form of photolithography, where the pattern is created by the use of a computer-driven laser beam. The pattern is projected on the surface of a resin, exposed parts polymerize forming a gel. After photopolymerization of each layer, the supporting platform is moved away from the surface and the built layer is recoated with liquid resin. A pattern is then cured in this second layer. Adherence to the preceding layer is ensured by modulating the depth of curing by UV-light intensity and exposure time.

Part I: Defining critical parameters in 3DF printing

We shall not fail or falter; we shall not weaken or tire…
Give us the tools and we will finish the job.
Sir Winston Churchill

Chapter 3

Hydrogels as extracellular matrices for skeletal tissue engineering: state-of-the-art and novel application in organ printing

Fedorovich NE[1], Alblas A[1], de Wijn JR[2], Hennink WE[3], Verbout AJ[1], Dhert WJA[1]

Tissue Engineering. 2007, 13(8):1905-25

[1]Department of Orthopaedics, University Medical Center Utrecht, Utrecht, The Netherlands
[2]Institute for BioMedical Technology, University of Twente, Enschede, The Netherlands
[3]Department of Pharmaceutics, Utrecht Institute for Pharmaceutical Sciences, Utrecht University, Utrecht, The Netherlands

Abstract

Organ printing, a novel approach in tissue engineering, applies layered computer-driven deposition of cells and gels to create complex 3-dimensional cell-laden structures. It shows great promise in regenerative medicine, because it may help to solve the problem of limited donor grafts for tissue and organ repair. The technique enables anatomical cell arrangement using incorporation of cells and growth factors at predefined locations in the printed hydrogel scaffolds. This way, 3-dimensional biological structures, such as blood vessels, are already constructed. Organ printing is developing fast, and there are exciting new possibilities in this area. Hydrogels are highly hydrated polymer networks used as scaffolding materials in organ printing. These hydrogel matrices are natural or synthetic polymers that provide a supportive environment for cells to attach to and proliferate and differentiate in. Successful cell embedding requires hydrogels that are complemented with biomimetic and extracellular matrix components, to provide biological cues to illicit specific cellular responses and direct new tissue formation. This review surveys the use of hydrogels in organ printing and provides an evaluation of the recent advances in the development of hydrogels that are promising for use in skeletal regenerative medicine. Special emphasis is put on survival, proliferation and differentiation of skeletal connective tissue cells inside various hydrogel matrices.

Introduction

It is hoped that regeneration of cartilage, bone, tendons, and intervertebral discs using tissue engineering (TE) will offer a source for the increasing demand for these tissues in an aging population. In a classic cell-based TE approach, cells, supportive structures, and molecular signals (growth factors) are combined to form hybrid constructs. Bone hybrid grafts can be used in a clinical setting for spinal fusion, fracture healing in non-unions, and critical-sized defects, whereas tissue-engineered cartilage grafts can ensure tissue formation in otherwise non-healing articular defects. Defined macrostructure and cell localization, together with vascularization of these constructs, are regarded to be key issues in the success of skeletal cell-based TE. Recent advances in biomedical engineering have led to the development of the concept of tissue or organ printing.[28] Layered deposition of cells and cell aggregates using various rapid prototyping (RP) techniques confers reproducible control over cell placement, surpassing uneven, random, and slow cell distribution within the scaffold, and yields a defined scaffold structure with regard to external shape and internal morphology.

Organ printing – a new development in tissue engineering

To increase the functionality of tissue-engineered constructs, research in recent years has turned toward the creation of cell-seeded implants that mimic native tissues with respect to anatomical geometry,[84] cell placement,[70] and the microenvironment of the cells. The success of such engineered structures will depend on scaffold properties, which should ensure sufficient transport of nutrients, possibly by containing structures suitable for integration with the systemic circulation, provide adequate mechanical support, and allow for incorporation of multiple cell types. Traditionally, three-dimensional (3D) constructs are created by seeding cells onto preshaped porous polymer scaffolds or by casting a cell-seeded hydrogel into a mold. The resulting constructs have a complex geometry but lack a defined cell distribution. Seeding of different cell types onto solid, usually porous, scaffolds makes placement at specific locations technically difficult. Furthermore, static cell seeding of scaffolds is inefficient and leads to a heterogeneous cell distribution, in particular when perfusion systems are not used for seeding.

To achieve zonal distribution of multiple cell types, researchers have combined cells with photosensitive polymers that could be injected and gelled *in situ* or photopolymerized in layers, reproducing the structures of articular cartilage and osteochondral tissues.[27,34,171] Recently, embryonic stem cells have also been encapsulated in an effort to accomplish simultaneous osteogenic and chondrogenic differentiation and formation of discrete osteochondral tissue layers.[181] Layered cellular assembly has also been proposed as an option to construct 3D tissues.[182] Assembling layers of cardiomyocyte sheets cultured on temperature-responsive hydrogel culture surfaces created *in vitro* myocardial tissue constructs.[183] Cultured cell layers have also been used in vascular TE by rolling sheets of fibroblasts and smooth muscle cells into a cylindrical shape and seeding endothelial cells within the lumen.[184]

In organ printing, designing scaffolds using RP[185] is combined with cell-based TE to produce complex cell-laden hydrogel scaffolds with customized external shape and reproducible internal morphology (Figure 3.1).[28] This technique would enable fabrication of vascular beds and thus make survival of larger tissue constructs after implantation possible. Moreover, by mimicking the microenvironment of the cells, printed tissues can be used as a tool to study cell–cell and cell–matrix interactions in pharmacological or development studies. Elaborate reviews of rapid

prototyping techniques have compared their resolution and utility for TE research.[29,76,106] Table 3.1 lists 3D tissue fabrication techniques that can deposit hydrogels or hydrogels together with cells.

Several RP techniques, with a relatively low resolution (in the range of 200–1000 μm), have been used to construct 3D hydrogel scaffolds in which biomolecules may be incorporated.[186-188] In general, inclusion of cells during the deposition process was limited because of harsh postprocessing procedures, the use of high temperatures, or acidic conditions during processing. In particular, reactive plotting of the gels is demanding, because it entails precise control of material and medium properties. The first experiments in cell deposition were conducted with a laser-guided machine, which placed individual cells on a glass,[175] and later a hydrogel surface,[189] using optical trapping forces to guide the cells. Scaling up of this technique is challenging, because cells are processed one by one. Converted ink-jet printers can dispense cell solutions onto hydrogels according to a computer-generated template to produce viable 2D and 3D tissue constructs.[111,112,190] This technique allows for precise cell(aggregate) placement and is dependent on subsequent self-assembly. Laser forward transfer technology[178] (matrix-assisted pulsed laser evaporation—direct write) and biological laser printing[176] are used to create patterns of functional cells on a micron scale. This is done using focused laser pulses that transfer cells, along with a gel matrix, onto a substrate. Furthermore, mammalian cells can be patterned in 2D and 3D using photo- and soft lithographic techniques. Topographically patterned hydrogel stamps and channels are designed using soft lithography,[191] whereas photolithographic techniques use ultraviolet (UV) light to cure photopolymerizable hydrogels with the help of patterned transparency masks.[86,108] In addition, electropatterning is an option.[109] Although photopatterning can construct (layered) patterns of cell-laden hydrogels,[192] the procedure is partially hand-operated and time consuming and requires prefabricated masks for each layer of polymerization. Stereolithography overcomes these drawbacks and is used to create hydrogel scaffolds with seeded or encapsulated cells[193,194] by generating a spot of UV light that selectively polymerizes a liquid photosensitive material layer by layer. Laser micro-stereolithography (μSL),[195] which achieves high degrees of resolution and is used for fabrication of precise, spatially distributed microenvironments, has recently been modified to allow high-throughput, layer-by-layer manufacturing of cell-laden structures.[196] Microfluidic technology is used to build a heterogeneous multilayer tissue structure inside microchannels.[197] More complex, porous 3D architectures are, however, difficult to realize because of restriction of this system to the 2D channel network.

Dispensing systems, such as the BioAssembly Tool[198] and RP cell assembling technique,[133] use pneumatic or volumetrically driven displacement pens for the fast deposition of a mix of cells and hydrogel in a controlled, complex, 3D pattern, tubular structures included. A volumetrically controlled deposition tool has recently demonstrated that cells could be printed in an anatomical shape, according to computed tomography data.[115] Dispensing systems allow for fast and efficient processing of cell-laden gels, although they currently suffer from low resolution.

In all of the above systems that may be used for organ printing, hydrogels are used as support matrices. Hydrogels not only allow for easy processing with various RP techniques, most of them are also suitable for entrapping living cells and therefore are popular as TE matrices. For embedded cells, they provide a highly hydrated microenvironment that is amenable to nutrient diffusion and can present biochemical, cellular, and physical stimuli that guide cellular processes such as migration, proliferation, and differentiation. Depending on their functional requirements,

various types of gels can be used. In subsequent sections, we present an overview of hydrogels, their use in skeletal TE, and their potential in organ printing.

Hydrogels

Hydrogel-forming polymers

Hydrogels are polymeric materials that swell in water, maintaining a distinct 3D network structure by virtue of crosslinks.[199] Hydrogels typically contain between 1% and 20% of dry mass. Their structural integrity depends on crosslinks between polymer chains that are covalent bonds or physical interactions.[200]

Stimulus-responsive hydrogels lend themselves to rapid prototyping applications, because gel formation can be controlled during and after the printing process. These types of polymers commonly crosslink in response to changes in their environment, which transforms their aqueous solutions or dispersions into a hydrogel network. Crosslinking can be initiated using physical stimuli such as changes in temperature, pH, ionic environment, and shear stress or can be chemically induced via a crosslinking agent, enzymatic reaction, or exposure to light (photopolymerization). Of all crosslinking mechanisms to obtain hydrogels, phototopolymerization[201] and temperature-responsive hydrogel formation[202] have been explored most extensively in TE.

Hydrogels and cell encapsulation

Current design and fabrication of organic scaffolds in skeletal TE involves a range of various materials: proteinbased polymers (collagen, fibrin, gelatin, and synthetic polypeptides), carbohydrate-based natural polymers (agarose, alginate, hyaluronate, chitosan, dextran), fully synthetic polymers (polylactic acid, polyglycolic acid, and their copolymers: Polyactive, Dacron, Teflon, polyester urethane), and composite materials of hydrogels and inorganic compounds. As a result of this, scaffolds can take on various forms—from porous solid meshes to hydrogel networks. Although solid scaffolds provide a mechanically strong substrate for seeded cells, hydrogel scaffolds that can physically entrap the cells are becoming increasingly popular as TE matrices.[199,201,203] Hydrogels have already been used independently as injectable *in situ* gelling networks and in cell-sheet engineering[182] or for wound healing and cellular patterning using spray deposition.[204,205] For load-bearing applications, they are often combined with solid, mechanically strong scaffolds, such as polyesters or ceramics.[206-209] With the development of RP, hydrogels can be used in a new application of organ printing (Figure 3.2).

In general, hydrogels have good biocompatibility. They can homogeneously incorporate and suspend cells, growth factors, and other bioactive compounds while allowing rapid diffusion of hydrophilic nutrients and metabolites of incorporated cells. They can be processed under mild conditions or even be formed *in situ*. Hydrogels generally contain low amounts of dry mass, causing little irritation and a low quantity of degradation products. Hydrogels based on extracellular matrix (ECM) polymers provide an adhesive surface for the cells, but their composition is variable, and their mechanical properties and degradation rates are difficult to control. Synthetic hydrogels are appealing materials for TE because they offer a higher lot-to-lot uniformity with a more controllable and reproducible scaffold structure, gel formation dynamics, degradation rates and mechanical properties.

A major disadvantage of hydrogels is their low mechanical strength, which makes handling and *in vivo* application difficult. In line with their low mechanical stability, the use of hydrogels is limited for load-bearing implants. Furthermore, many hydrogels may not provide an ideal environment for anchorage-dependent cells such as osteoblasts, because they lack suitable binding sites. ECM proteins such as laminin, fibronectin, and vitronectin typically do not adsorb to a gel surface because of its hydrophilic nature. Several modifications have been applied to overcome these drawbacks (Table 3.2).

Hydrogel modifications to improve cell performance

Physical properties of hydrogels such as their mechanical properties, gel formation, and degradation, together with diffusion through the gel and biological interactions, influence material choice for TE applications.[210] Incorporation of growth factors and other biological cues, ranging from inorganic minerals such as calcium phosphate to specific adhesive or degradable sequences in hydrogels, can modulate cell function and material degradation. The so-called bioactive hydrogel materials can alter proliferation or matrix organization while matching the gel's degradation rate with the deposition of new tissue.[129,211] Many modified hydrogels that provide an "instruction" for embedded cells are used for skeletal TE.

Adhesive peptides

To promote adhesion, migration, and proliferation of cells within a gel, covalent immobilization of ECM molecules or peptides containing the adhesion domains of ECM proteins is often applied.[70,212,213] The ligand studied mostly, arginine-glycine- aspartic acid (RGD) is an integrin-binding peptide. RGD molecules stimulate the differentiation of skeletal cells and mineralization in a dose-dependent manner[213-215] until saturation occurs. The presence of a covalently bound RGD sequence significantly increases the amount of formed bone in an alginate scaffold.[216] Nanoscale clustering of RGD promotes cellular migration.[217] The amount of adhesive ligands should be chosen carefully, because high concentrations stimulate adhesion but block migration. Intermediate adhesion is required for optimal cell migration,[218-220] that is especially important for angiogenesis and tissue formation during bone regeneration.

Other ECM molecules or peptide sequences used to enhance cell performance in hydrogels are fibronectin,[215,221,222] glycosaminoglycans (GAGs)[223] and heparin-binding domains.[224] In cartilage TE, attachment of collagen mimetic peptides to polymer chains of hydrogel scaffolds was applied to render materials more adhesive and to increase ECM production inside the gels.[225] Heparin-functionalized gels have been shown to promote human mesenchymal stem cell (hMSC) adhesion and osteogenic differentiation.[226]

Degradable linkages and phosphate groups

Hydrogel degradability affects tissue development in skeletal TE.[227-229] The gel forms a temporary mechanical support for the cells that the natural ECM eventually replaces. Ideally, hydrogel degradation should keep pace with ECM production. The addition of biodegradable units to the biomaterials that increases the mesh size over time allows more homogenous ECM formation and ingrowth of cells. The introduction of degradable linkages such as hydrolysable poly(a-hydroxy esters)[230] and protease-sensitive substrates[231] inside poly(ethylene) glycol-based hydrogels with photoencapsulated chondrocytes affects ECM distribution and enhances transcription of major cartilage matrix proteins. Mineralization by embedded osteoblasts is enhanced in

biodegradable hydrogels.[229] Phosphate groups promote cellular viability and osteogenesis,[232,233] possibly because negatively charged phosphate groups (or phosphoric acid produced by degrading phosphoester-containing hydrogels) attract positively charged free calcium ions from the medium, thus facilitating mineralization. Subsequently, osteopontin is adsorbed to the mineralized regions and enhances cell adhesion and viability because of improved cell–matrix interactions.

Growth factors

Another important way to regulate cell behavior and enhance the functionality of skeletal tissue constructs is the incorporation of growth factors. Adequate signaling relies on timing of their release and their spatial distribution.[234] Growth factors involved in chondrogenesis, osteogenesis, and vascularization have successfully been incorporated in various hydrogels, as reviewed elsewhere.[235] Depending on the degradability of a gel, these may even be covalently bound proteins or peptides.[236] An immobilized bone morphogenetic protein (BMP)-2-derived synthetic oligopeptide was found to promote ectopic bone formation *in vivo*.[237] Release of growth factors can occur by diffusion, cell-mediated proteolysis of the hydrogel matrix,[238] or in response to mechanical stimuli (e.g. by mechanical compression).[239] To further prolong the action of growth factors, plasmid deoxyribonucleic acid coding for growth factors can be included.[240-242] Simultaneous delivery of multiple growth factors[243] was found to be a powerful stimulus promoting chondrogenesis inside poly(ethylene) glycol (PEG)[244] and enhancing bone tissue formation[163] and angiogenesis[245] in alginate gels. These cellular stimuli will ultimately prove to be indispensable for successful bone or cartilage engineering.

Other soluble bioactive molecules that have been incorporated into hydrogels, to promote skeletal tissue regeneration, include glucosamine in PEG gels for enhanced ECM production in cartilage TE[246,247] and covalently linked dexamethasone, continuously released from PEG gels, for bone TE.[248]

Enhancing mechanical properties of the gels

Ideally, a hydrogel scaffold should provide a stable structure for cell adhesion and tissue formation, maintain its volume, withstand manipulations associated with handling and implantation, and resist the forces associated with *in vivo* existence. However, the challenge of tissue-engineered grafts is to also match the mechanical properties of native bone or cartilage tissue.[249] For example, in tissue-engineered cartilage grafts, mechanical properties remain inferior to natural tissue, reaching a maximum of 10% to 20% for natural hydrogels,[250,251] 20% to 40% for polyesters,[252,253] and approximately 50% for photopolymerized PEG hydrogels,[230] based on compression modulus. A number of measures have been found to enhance mechanical properties of hydrogel constructs:[254] introduction of covalent crosslinks, increase in crosslinking density, increase of monomer content and monomer molecular weight, addition of fillers and biodegradable fibers, and preculturing to allow embedded cells to generate functional tissue before implantation. A simple change consists of altering the composition of the co-monomers used for preparing the hydrogel. Increasing the amount of physically stronger components will lead to an increase in the mechanical strength of the final product, for example, by replacing acrylates with methacrylates. Increase of the content of more hydrophilic monomers will lead to a greater degree of swelling for the resulting hydrogel, leading to a decrease in the mechanical strength of the polymer gel. Because the mechanical strength of a hydrogel is dependent on the

crosslinks in the system, particularly in the swollen state, strength of the hydrogel increases dramatically with increasing crosslinking density.
The application of chemical crosslinking and high polymer concentrations only partly solves the problem; although the hydrogels obtain a higher mechanical stability, crosslinking agents are often toxic and can affect the integrity of the entrapped substances, whereas high polymer concentration can impair nutrient diffusion. As stated above, despite the modifications, mechanical properties of the gels remain low. Hydrogels are therefore not suitable for load-bearing applications.

Hydrogels for skeletal cell encapsulation

Hydrogels that are used for entrapment of skeletal cells are listed in Table 3.3. These stimuli-sensitive hydrogel-forming polymers allow for processing with RP, and their way of polymerization defines the type technique to be used in organ printing.

Thermosensitive hydrogels

Aqueous solutions of some polymers undergo a sol-to-gel transition in response to a temperature change. This mechanism provides little control over the gelation process; once crosslinking is induced, the process cannot be altered or stopped. Thermosensitive polymers such as gelatin and agarose form gels when the temperature is lowered. At high temperatures, these polymers exhibit a random coil formation and start to form helices that aggregate as the temperature is lowered (Figure 3.3A). This process is usually reversible. Inverse thermosensitive materials, on the other hand, are liquid below room temperature and gel at 37 °C. Such polymers precipitate in solution and form gels at the socalled lower critical solution temperature (LCST) because of the balance of intermolecular forces between polymer-polymer and polymer-solvent.
Agarose is a galactose polymer extracted from red seaweed that gels by virtue of hydrogen bond formation. Agarose is mechanically stabile, non-toxic, and well suited for 3D cell encapsulation, especially of chondrocytes.[255-258] Embedded chondrocytes remain differentiated and functional *in vitro* and *in vivo*, whereas agarose stimulates re-expression of the original phenotype by dedifferentiated cells. Chondrogenesis studies[259,260] have showed that agarose facilitates differentiation along the chondrogenic lineage and also redirects osteoblasts to become chondrocytes.[261] Despite the fact that agarose strength initially falls 25% after cell incorporation,[262] chondrocytes form mechanically functional ECM in one month (*in vitro*).[256] BMP-2-transduced MSCs form more cartilage-like tissue in agarose gels than in other matrices,[209] such as collagen or alginate. This indicates that the agarose gel, in addition to its tendency to resist blood vessel invasion (resulting in low oxygen tension), is especially suited for cartilage TE and can also be used for encapsulation of intervertebral disc cells (IVDCs)[263,264] that were shown to produce high levels of proteoglycans inside agarose. For bone TE, agarose per se lacks rigidity and durability and needs stabilization from other, more rigid, materials. Although agarose has successfully been processed using Bioplotter technology and yielded well-defined 3D scaffolds, cells have not yet been included in the deposition process because of the high temperature of agarose during dispensing.[187,265]
Collagen is a fibrous protein with a triple-helix structure and is a main component of the connective tissue ECM. Physically formed collagen gels are thermally reversible, mechanically weak matrices that provide good cell adhesion and are degraded by cells. Collagen gels, and the stiffer, chemically crosslinked collagen sponges, have been used for entrapment of various cell

types, including MSCs, that retain their pluripotency.[266] In addition, chondrocytes,[267-272] IVDCs,[273,274] and osteoblasts[275-279] maintain their differentiated phenotype and produce ECM in collagen gels and sponges. Comparison of collagen type I and II matrices indicated greater chondrogenic activity of the cells in collagen type II gels.[280-283] MSCs suspended in collagen I gels and then implanted *in vivo* showed better biomechanical properties in tendon TE[284] and good regeneration of intervertebral disc,[274] bone formation in femoral segment defect[277] and spinal fusion models.[278] However, the use of collagen gels remains limited because of qualitative batch variations and loss of shape and consistency through shrinkage.[285] In organ printing, collagen gels have been used as easily processed, mechanically weak substrates for ink-jet printing of cells and cell aggregates,[57,190] laser-guided direct writing of cells,[189] and construction of layered anatomical shapes.[198]

The easily gelling gelatin is derived from denatured collagen. Although used successfully as a cell vehicle in chondrogenesis studies[260,286] and in bone TE,[287] gelatin hydrogels are weak at physiological temperature,[187] limiting their use in TE to combinations with stiffer solid scaffolds. Because of their unstable nature as matrices for cells in organ printing, cell-laden gelatin scaffolds have been crosslinked after the deposition and yielded defined, stable 3D structures.[133]

Matrigel is a reconstituted basement membrane matrix, a mixture of mainly type IV collagen and laminin, which is liquid at 4 °C and becomes a gel at room temperature. Matrigel supports the osteogenic phenotype *in vitro*,[288,289] *in vivo* in subcutaneous implants,[290] and in spinal fusion.[291] Matrigel is used extensively as a substrate for cell deposition in laser-guided direct writing[189] and biological laser printing,[176] although no porous, defined 3D structures have been produced with this costly gel yet.

Poly (N-isopropylacrylamide)–(pNiPAAm), a derivative of poly (acrylic acid), exhibits phase transition behavior above its LCST of approximately 32 °C. Copolymerization of NiPAAm with hydrophilic monomers such as acrylic acid (pNiPAAm-co-AAc) results in an increase in LCST. PNiPAAm-co-AAc gels at 37 °C or above and becomes liquid at lower temperatures. Thermoresponsive, low-toxic[292] pNiPAAm and its copolymers have been used for entrapment of cells in cell patterning and cell-sheet harvesting with pNiPAAm-grafted culture surfaces.[182,293] Materials obtained using copolymerization of pNiPAAm with hyaluronate and PEG retain pNiPAAm's thermosensitive properties.[294,295] PNiPAAm-based gels support the chondrocyte phenotype *in vitro*[296,297] and have been patented for this application. To provide attachment for cells, pNiPAAm has been modified with RGD sequences[298,299] and grafted on gelatin molecules.[300] Degradable crosslinks were introduced in pNiPAAm gels to surpass the non-degradable nature of pNiPAAm gels.[301,302] Despite the advantages of pNiPAAm, the poorly understood metabolism of pNiPAAm, together with suggestions that acrylamide-based polymers activate platelets in blood, makes pNiPAAm gel less popular for *in vivo* applications.[303] In organ printing, these gels have been used as substrates for cell deposition with ink-jet technology.[57]

Aqueous solutions of some triblock copolymers of poly(ethylene oxide) (PEO) and poly(propylene oxide), generically called poloxamers and commercially known as Pluronics, exhibit sol-to-gel phase transition at physiological temperatures because of an equilibrium shift from unimers to spherical micelles and subsequent micelle packing. Depending on polymer composition and concentration, Pluronics remain in gel phase between the two critical transition temperatures (Figure 3.3C,D). Poloxamer 407 (Pluronic F-127) is a material approved by the Food and Drug Administration (FDA) that forms gels at 37 °C in solutions above 20 wt% of polymer. Membrane-stabilizing agents can be added to Pluronic to enhance cell survival *in vitro*.[304]

Pluronic F-127 loaded with chondrocytes led to the formation of cartilage with good histological properties after subcutaneous injection[305,306] and in composite scaffolds *in vitro*[307] and full-thickness defects *in vivo*.[206] However, Pluronic provided poor conditions for encapsulated MSCs *in vitro* and failed to induce bone formation *in vivo*.[209] In a recent application, a mixture of Pluronic and chondrocytes has been applied as a "painted" cartilage lining on a tissue-engineered osseous surface, eventually resulting in a bone–cartilage interface.[42] Physical and chemical mechanisms to crosslink poloxamers have been combined to promote gel stability.[308] Although Pluronics have successfully been applied for controlled deposition of cell-laden tubular structures with a BioAssemly Tool, these gels dissolve quickly in medium during culture, resulting in loss of the construct.[198]

PEG and PEO are polyethers with identical structures and variable chain length and end groups. Both are prepared using polymerization of ethylene oxide. PEG is a lowmolecular- weight polymer, whereas PEO has a higher molecular weight. PEG and PEO polymers are biocompatible and have been approved by FDA for many medical applications. Inverse thermosensitive PEG-based materials are promising as matrices for cell encapsulation.[309,310] The *in situ* gelling, non-toxic, biodegradable copolymers of PEG and poly(ethylene glycol-b-(DL-lactic acid-co-glycolic acid)-b-ethylene glycol) (PLGA) exhibit sol-to-gel temperature transition, possibly due to micelle expansion and an increase in polymer–polymer attraction with increasing temperature (Figure 3.3D). Changing PEG length and composition controls their transition temperature. The limitation in molecular weight of these copolymers led to the development of thermosensitive graft-copolymers of PLGA-g-PEG and PEG-g-PLGA. By varying the composition of the two moieties, the durability of the gels can be tailored.[311] However, the need for high polymer concentrations and high injection temperature restricts the use of this system for cell delivery.

Poly(propylene fumarate-co-ethylene glycol) (PPF-co-EG) is a block copolymer of a hydrophobic polyester PPF and hydrophilic PEG[312] and forms a gel when exposed to 37 °C, by the association of the copolymer chains. Cell viability inside this biocompatible material increases with higher PEG concentrations.[313] PPF-co-EG gels support chondrocyte survival and ECM production *in vitro*.[314] PPF–tricalcium phosphate composites and fully crosslinked PPF-co-EG hydrogels are good substrates for proliferation and differentiation of seeded osteoblasts.[315,316] Because rat bone marrow osteoblasts incorporated directly into PPF do not survive, they have to be temporarily encapsulated in crosslinked gelatin microparticles.[317]

Chitosan is a pH-sensitive, biodegradable glucosamine polymer obtained using de-acetylation of chitin, which is present in the exoskeletons of arthropods and insects. Chitosan-glycerol-phosphate and hydroxybutyl chitosan hydrogels exhibit inverse thermogelling properties, gelling at 37°C. A higher degree of de-acetylation of the chitin chain promotes the biocompatibility of these hydrogels.[318] A chitosan molecule contains structural features also found in GAGs and has been crosslinked with GAGs to promote chondrogenesis.[223] Chitosan-based gels support the chondrogenic and osteogenic phenotype *in vitro*[319-321] and can be used for encapsulation of IVDC.[322,323] These gels have a promising applicability for skeletal TE because of chitosan's ability to bind ECM components and growth factors, its potential to enhance osteogenesis, and possible mineral deposition, as well as its intrinsic antibacterial activity.[324]

pH-sensitive polymers

Methylcellulose is a methylether of cellulose - a longchain polymeric polysaccharide carbohydrate and a primary structural component of green plants. Non-ionic cellulose ether polymers, combined with phosphate granules, are used in bone TE as carriers for BMP[325] and as injectable bone substitute.[326] In cartilage TE, methylcellulose hydrogels have also been used to control proliferation and clonal growth of chondrocytes. Patented pH-sensitive silated hydroxypropylmethylcellulose hydrogels support embedded osteoblasts[327] and the proliferation of differentiated chondrocytes.[328]

Hydrogels obtained by ionic crosslinking

Alginate is a non-biodegradable polysaccharide, with mannuronic and guluronic acid repeating units, derived from brown seaweed and bacteria. Monovalent alginic salts form an ionic network in the presence of multivalent cations (e.g., calcium). Alginate hydrogels are advantageous because of their biocompatibility, low toxicity, and low cost. Alginate gels have been mostly used for drug delivery and cell entrapment,[329] as (injectable) matrices for TE, and for treatment of vesicoureteral reflux.[330]

In skeletal TE applications, alginate gels and beads support chondrocyte function *in vitro*[268,331-334] and (inside shaped cartilage implants) *in vivo*.[335,336] Similar to agarose, alginate stimulates differentiation of marrow- and fat-derived stromal cells toward a chondrogenic phenotype,[260,337,338] possibly due to the lack of cellular interactions or limited oxygen and nutrient supply inside alginate hydrogels. Bone ECM formation inside alginates, demonstrated *in vitro*,[339,340] subcutaneously,[70,228] and in cranial bone defects,[341] occurred by enchondral ossification. An alginate-based hydrogel, with improved mechanical stability and degradation properties — derived from a portion of the alginate molecule, poly(aldehyde guluronate) — has been used for encapsulation of osteogenic cells *in vivo*.[342] Alginate beads have also been used for culture of functional IVDCs[343] and stimulated MSCs toward a nucleus pulposus-like phenotype.[344] In organ printing, alginate has provided a stable, cell-compatible matrix for deposition of cells, yielding tubular structures,[111] and for dispensing of cell-laden gels in anatomic shapes.[115]

Alginates quickly lose their mechanical properties *in vitro* (approximately 40% within 9 days), presumably due to an outward flux of ions into the surrounding medium,[262] a process also responsible for slow, uncontrolled dissolution of the gels over time. Increasing the proportion of guluronic monomers and covalent linkages improves the mechanical properties of alginate hydrogels.[250,345,346] Alginate chains have been truncated using partial oxidation[347] and gamma-irradiation[228] in an effort to promote degradation. However, unpredictable degradation and purity remain problematic. Finally, it should be noted that human and animal cells behave differently on alginate surfaces.[348]

Photopolymerizable hydrogels

Hydrogels can also be obtained using polymerization of (di)acrylate or methacrylate endcapped water-soluble polymers *in vitro* and *in vivo* using visible or UV light. Light interacts with added light-sensitive compounds (photoinitiators) to create free radicals that initiate crosslinking (Figure 3.3B). Photopolymerization has become popular because it offers spatial and temporal control over polymerization, showing high curing rates (seconds to minutes) at physiological temperatures with minimal heat production. Photopolymerizable hydrogels with encapsulated cells can be injected and subsequently crosslinked *in situ* using UV light. Low photo-initiator

concentrations and low-intensity UV light should be used to minimize possible adverse side effects on the cells caused by the release of free radicals.

Apart from their application as thermosensitive materials, PEG hydrogels can also be synthesized through UV photopolymerization, when modified with photosensitive groups, and used for photo-encapsulation of chondrocytes, osteoblasts, and MSCs. Cytocompatibility of several photoinitiating systems for cell encapsulation[349,350] in PEG has been compared, and most cells tolerate the photo-initiator Darocure 2959 best. Mechanically functional cartilage-like tissue was engineered *in vitro*[351-353] and *in vivo*, using transdermal photopolymerization,[354] inside PEG gels. In contrast, lack of cell adhesion to PEG hydrogels forms a major drawback for bone TE, leading to decreased survival of embedded osteoblasts[212] and hMSCs.[355] Although MSCs are able to undergo osteogenic differentiation in regular PEG hydrogels, modification of PEG with adhesive and degradable sequences not only increases cell viability,[232] but also enhances mineralized ECM formation.[213] PEG hydrogels have been used extensively as mechanically strong, cytocompatible matrices deposited with a variety of photopatterning and stereolithographic techniques.[76,86,109,194]

Poly(vinyl alcohol) (PVA) hydrogels have been employed in various biomedical applications, including contact lenses, drug delivery systems,[356] and cartilage[357] and tendon repair.[358] PVA hydrogels are mostly crosslinked using non-cytocompatible freeze-thaw processes and chemical crosslinking with aldehydes. Photopolymerizable biocompatible PVA gels, grafted with a photosensitive group,[359,360] have been used for encapsulation of skeletal cells.[361] Degradation and mechanical properties of PVA can be tailored by grafting hydrolyzable PLA side chains onto the PVA backbone and varying crosslinking density of the gels.[360,362]

Hyaluronan (HA) gels are obtained using esterification of biocompatible and biodegradable hyaluronate, which forms one of the GAG components in the ECM. A commercially available HA is produced in various 3D configurations, including sponges (Hyaff 11 and ACP), which are used as carriers of growth factors and seeded cells in tissue engineered repair of bone, cartilage, and ligament.[363-366] Photopolymerizable HA-(meth)acrylate hydrogels can entrap cells[367] and stimulate angiogenesis,[368] making hyaluronate gels appealing materials for skeletal TE. However, the gels often contain impurities and remain mechanically weak, despite the introduced crosslinks, compromising their use in skeletal TE.

Other gels for cellular encapsulation

Fibrin hydrogels, formed using enzyme-catalyzed crosslinking of fibrinogen at room temperature in the presence of thrombin, calcium chloride, and factor XIIIa, are readily available from patient's blood and have been approved for clinical use. Human chondrocytes embedded in fibrin hydrogels and beads produce tissue with high GAG content.[369-372] To overcome fast cellular disintegration of fibrin, addition of proteinase inhibitors stabilized fibrin for up to 4 weeks *in vitro*,[373] whereas embedded cells formed adequate ECM *in vivo*.[374] The major drawback of fibrin gels is their low mechanical quality, limiting their role in load-bearing *in vivo* applications to a cell-carrier function, usually in combination with stiff polymer or ceramic scaffolds.[207,208,375]

Hydrogels prepared through radical polymerization of oligo(poly(ethylene glycol) fumarate) (OFP) are currently evaluated as injectable carriers for MSCs.[376] OFP is a biodegradable linear macromer comprising two repeating units of PEG and fumaric acid. High-molecular weight OFP hydrogels promote MSC differentiation and formation of calcified ECM throughout the gel. OFP hydrogels of low molecular weight PEG perform better with regard to cell survival and tissue reactivity.[377]

Physical crosslinking of self-assembling (supramolecular) hydrogels[378,379] theoretically provides a cell-friendly encapsulation process, and therefore these gels may prove to be suitable matrices for skeletal cells. Self-assembling polypeptides are a new, exciting class of biomaterials under investigation for application in TE. Self-complementary oligopeptide matrices, consisting of alternating hydrophilic and hydrophobic amino acids, assemble in the presence of monovalent salts. They form large, regular microscopic structures that provide a matrix for encapsulation of skeletal cells.[380,381]

Some other potential self-assembling materials for cytocompatible encapsulation are degradable, dextran-modified hydrogels of poly(2-hydroxyethylmethacrylate). Dextran gels can be formed without chemical reagents, by mixing positively and negatively charged poly (2-hydroxyethylmethacrylate) microspheres[382] or by physical crosslinking by virtue of stereocomplexation.[383] When gels composed of oppositely charged microspheres are exposed to shear stress and deformation, such as inside a needle, the network is broken, and the hydrogel becomes liquid, gelling again when shear stress is removed.

Matching hydrogels to target tissues

Several studies have compared the effectiveness of hydrogels as matrices for skeletal TE. Initial differences in performance of alginate, collagen, and agarose with respect to cartilage formation tend to decrease over time,[258,260,285] with agarose performing particularly well. In alginate, embedded chondrocytes synthesize ECM with a high GAG content,[268] although sporadic tissue formation was suboptimal.[258,307] Cells imbedded in collagen I matrices exhibit high proliferative potential[384] and ECM formation despite the sometimes observed fibroblastic morphology.[258,260] Methylcellulose and Pluronics perform equally well in stimulating chondrocyte proliferation and regeneration.[307] *In vitro* and *in vivo* bone formation using BMP-transduced and regular MSCs embedded in hydrogels and loaded on a ceramic scaffold was optimal when collagen gels were used.[209,385] Fibrin gels performed well *in vitro* but failed to induce bone formation *in vivo*. However, using BMP-7-transduced fibroblasts, collagen I, Pluronic F-127, and Matrigel induced bone formation *in vivo* equally well.[386] For *in vitro* encapsulation of human IVDCs, collagen I gels and sponges provided the best environment for proliferation, ECM production and gene expression.[264,273] The same cells embedded in agarose showed high ECM production and low cell proliferation. Alginate and fibrin environments were inferior, with spindle-shaped cells uncharacteristic of IVDC phenotype. These cells formed little to no ECM in fibrin hydrogels.

No studies have compared tissue formation in thermosensitive hydrogels with that in photopolymerizable hydrogel-forming materials, possibly because the latter polymers are often custom made with specific modifications. It is to be expected that the use of these mechanically strong, tailored hydrogels results in high-quality tissue formation by the embedded cells in cartilage and bone TE applications.

Conclusion

Organ printing is a new concept for engineering of tissues, which extends the application of currently available hydrogels. Cells inside hydrogels can survive the printing process and retain their potential to differentiate, and although hydrogels themselves are mechanically weak, hydrogel remodeling and matrix formation *in vivo* are expected to provide the mechanical strength needed in the newly formed tissue.

When making a choice between various polymer hydrogels, the main concerns are their mechanical properties, biodegradability and induction of tissue formation. The choice of hydrogel also depends on the target tissue, because different cell types behave differently in gel polymers. Although natural materials offer the advantage of cell compatibility, synthetic polymers are more reliable in terms of tailored mechanical and degradation properties, together with uniformity. Of all synthetic hydrogels, photopolymerizable PEG-based systems are currently the most promising materials for skeletal TE. These gels have adequate mechanical properties and have been widely investigated with regard to incorporation of degradative and adhesive linkages to promote tissue formation. Photopolymerizable gels are suitable for stereolithography, and thermosensitive hydrogels are more useful for 3D ink-jet printing or robotic dispensing systems. New self-assembling systems that gel under mild cytocompatible conditions are currently being evaluated for cellular encapsulation, with self-assembling peptide nanofibers showing potential for embedding of skeletal cells and growth factors.[242,381]

The future directions of organ printing with hydrogels include the development of better hydrogels, with emphasis on mechanical properties and degradation rates. In addition, so-called instructive scaffolds will tightly control cell function. In particular, the addition of ECM molecules or growth factors during printing can control diverse cell types at the proper location with respect to adhesion/migration and growth/differentiation. In regulating differentiation, matrix elasticity is also a determining factor, as recently shown in an important paper by Engler et al.[387] In addition, the development of micro-printing will facilitate the incorporation of channels as a basis for vascularization. Another interesting development is the use of printed tissues and organs for pharmacological drug testing or as a disease model.[388]

Because of the complexity of native tissues, actual printing of organs may be a remote goal. However, printing of ordered, layered tissue structures will lead to development of better, more-functional tissue-engineered grafts for clinical applications. Scaffold optimization by creation of biomimetic hydrogels with tailored biological properties and knowledge of cell–hydrogel interactions will provide a vital contribution to this development.

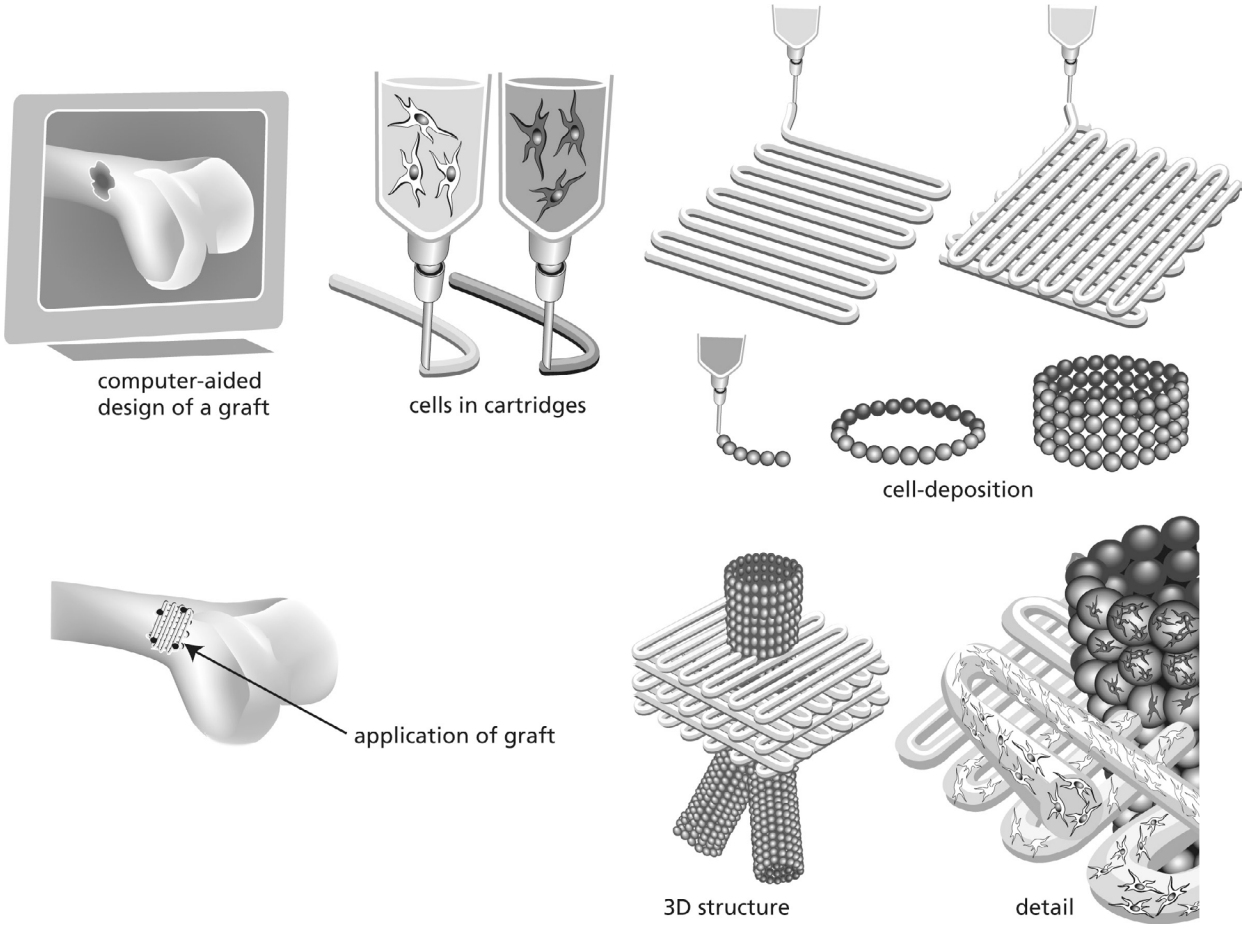

Figure 3.1: Concept of organ printing.

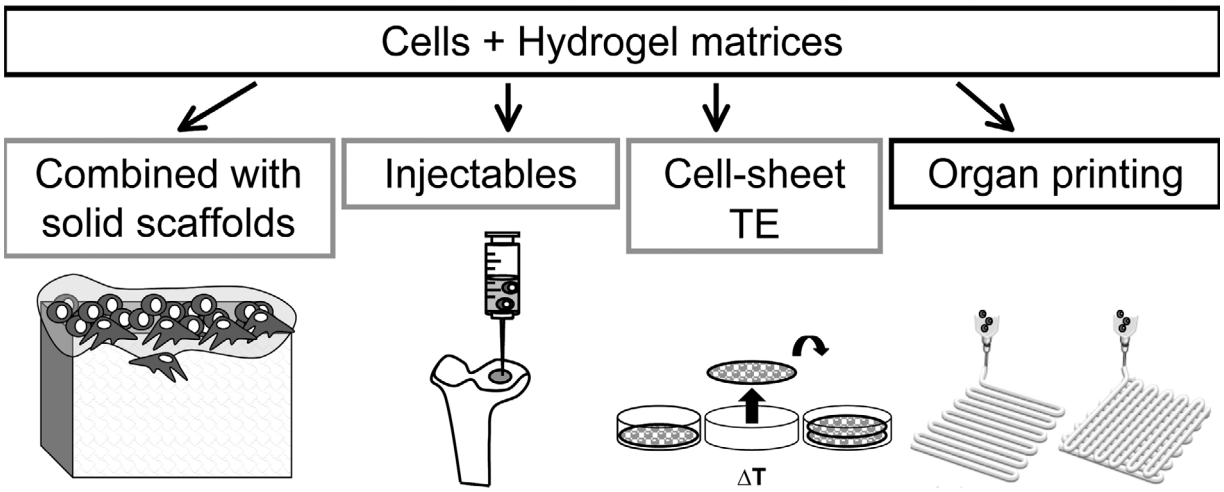

Figure 3.2: Applications of cell-encapsulating gels in tissue engineering (TE).

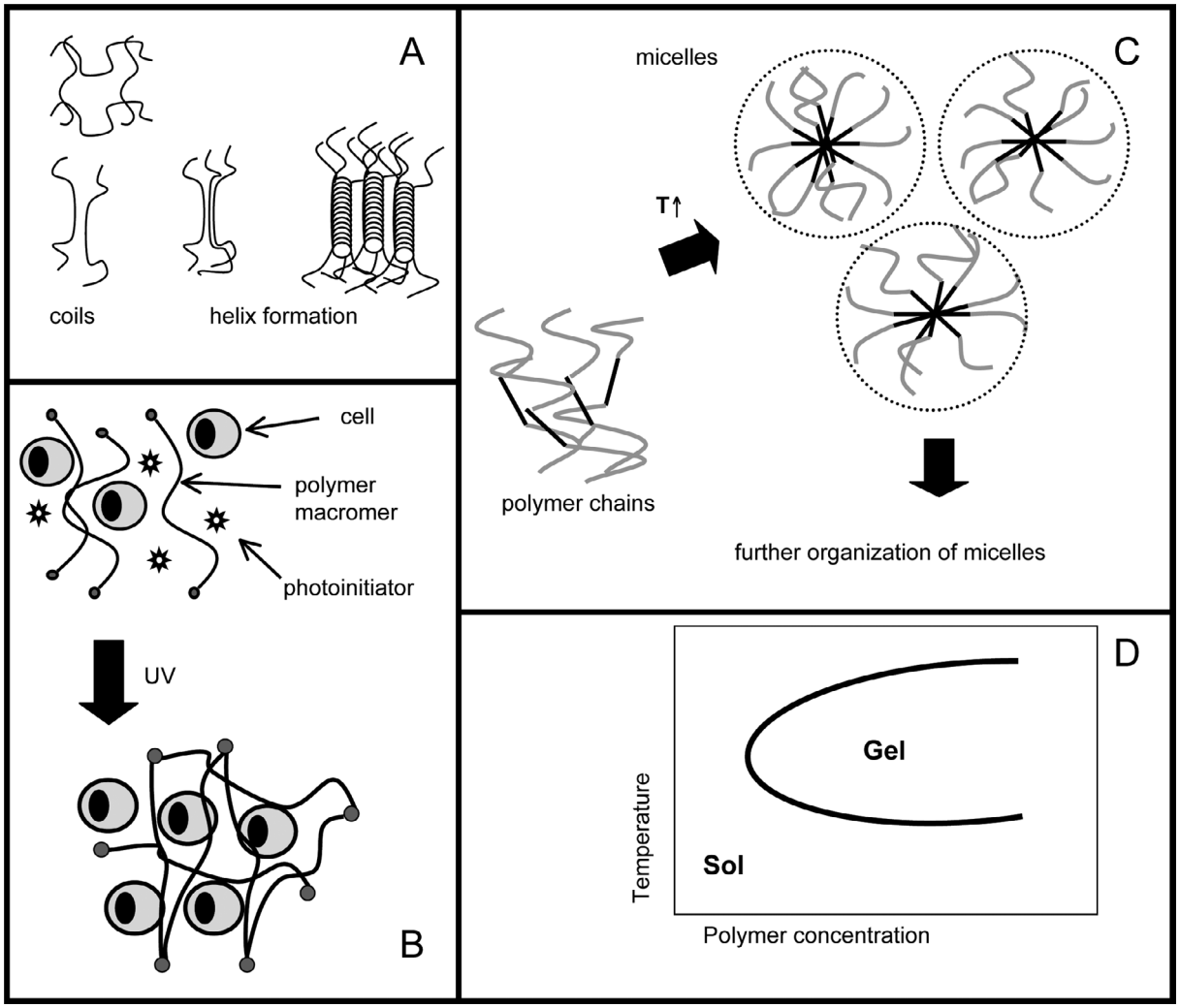

Figure 3.3: Hydrogel polymerization properties. (A) Physical crosslinking of regular thermosensitive gels, (B) covalent crosslinking using photopolymerization, (C) polymerization of Pluronic, and (D) phase transition diagram of thermosensitive triblock polymers. UV, ultraviolet.

TABLE 3.1 CELL DEPOSITION TECHNIQUES

Technology		Cell type	Hydrogel	Structure	Outcome/Cell-survival	Ref
Hydrogel deposition	3D printing	-	Pluronic; starch/dextran/gelatin	2D/3D	Use of organic solvent; post-processing required	186,389
	3D plotting	-	Agarose, gelatin; alginate-fibrin	3D	Heated (90°C) gels; reactive plotting	187,265
	RP Robotic dispensing	-	Chitosan	3D	Plotting in NaOH/ethanol	188
Combined hydrogel/cell deposition	Laser-guided direct writing	Embryonic spinal cord, E	Matrigel, collagen	2D/ML	89% [2]	175,189
	Ink-jet printing	E, SMC	Matrigel, collagen	2D	75% [3]	190
		CHO, Motoneuron	Agar, collagen	2D	>90% [1]	111
		E	pNiPAA-based gel, collagen	ML	Viable, % not reported	57
		E, SMC, CHO, OB	Alginate	3D tubes	Viable, % not reported	112
	Laser-forward transfer MAPLE-DW	OB, EC, Neuroblasts	Matrigel	2D	100% [3]	178
	Biological laser printing	Osteosarcoma, E	Matrigel	2D/ML	100% [3]	99,176
	Photolithography/ Electropatterning	Hepatocytes, Fibroblasts, Chondrocytes	PEGDA	2D/ML	94% dependant on photoinit. % [2] 80%[3]	76,108,109
	(Micro)stereolithography	CHO; MSC line	PEO/PEGDM; PEGDA	3D	65% [2]; viable, % not reported	194,196
	BioAssembly Tool	Fibroblasts	Pluronic F-127	3D tubes	60% [1]	198
		E	Collagen	3D layers	Up to 86% [2]	198
	RP deposition tool	Hepatocytes	Gelatin	3D	98% [1], 93% after 3 months	133
	Volumetrical deposition tool	Chondrocytes	Alginate	3D	94% [1]	115

Table 3.1: Cell deposition techniques. 3D: 3-dimensional; RP: rapid prototyping; MAPLE-DW: matrix-assisted pulsed laser evaporation-direct write; E: endothelial cells; SMC: smooth muscle cell; CHO: Chinese hamster ovary cells; OB: osteoblasts; EC: embryonic carcinoma; MSC: mesenchymal stem cell; pNiPAA: poly (N-isopropylacrylamide); PEGDA: poly(ethylene glycol diacrylate); PEGDM: poly(ethylene glycol dimethacrylate); PEO: poly(ethylene oxide); ML: multilayer; NaOH: sodium hydroxide.

[1]viability directly after cell deposition.

[2]viability after 1–2 days.

[3]viability after 3 days.

TABLE 3.2 HYDROGEL PROPERTIES

Type	Hydrogel	Origin	Properties	Modifications	References
Thermo-sensitive	Agarose	N	low cost; dubious biodegradability; low physical qualities; resistant to protein adsorption		256,257
	Collagen	N	adhesive ECM component; shrinkage; batch variance; coll II>I for chondrogenesis	GAG	280,390
	Gelatin	N	weak at physiological temp; limited to combined use/chemical crosslinking	gpNiPAAm	133,187,300
	Matrigel	S	commercially available; expensive		176,290
	pNiPAAm	S	non-degradable; activation platelets?	RGD; HDL; PDL: MMP13; combined	294,298-303
	Pluronics	S	fast dissolution; induction of hyperlipidemia in rats; inverse thermosensitive	covalent crosslinks	308
	PEG triblocks	S	FDA approved; inverse thermosensitive		310
	PPF-co-EG	S	higher PEG concentrations support cell viability	RGD	316
	Chitosan	N	structurally similar to GAG; intrinsically antibacterial	combined, GAG	223,324
pH sensitive	HPMC	S	patent on silated gels		327
Ionic crosslinking	Alginate	N	FDA approved; low cost; loss mechanical qualities overtime; non-biodegradable; resistant to protein adsorption; performance depends on purity	RGD; γ-irradiation; oxidation; combined	70,228,342,345-347
Photo-polymerizable	PEG-based	S	resistant to protein adsorption; non-biodegradable	RGD; collagen mimetic peptide; phosphate; HDL; PDL; MMP/plasmin/elastase; glucosamine	152,212,213,220,222,225,231,232,359,391-396
	PVA	S	sites for bioactive molecules; amount of crosslinks is variable; non-biodegradable	RGD; fibronectin; HDL	221,360,362
	Hyaluronic acid	N	biodegradable; purity is important	RGD	367
Enzymatic	Fibrin	N	FDA approved; blood-derived; facilitates tissue healing, weak	Protease inhibitors	374
Other	OFP	S		RGD; osteopontin derived peptide	215,397
	(Dex)-HEMA	S	self-assembling: opposite charge interactions; stereocomplexes	+/- charged groups; D/L-lactic acid	382,383
	Polypeptides	S	self-assembling; intrinsically biodegradable	RGD	380,381

Table 3.2: Hydrogel properties. Combined: with other hydrogel-forming polymers; ECM: extracellular matrix; FDA: Food and Drug Administration; g: grafted onto a polymer chain; GAG: glycosaminoglycans; HDL: hydrolytically degradable linkages; (dex)-HEMA: poly(2-hydroxyethyl methacrylate); MMP: matrix metalloproteinase; N: natural; OFP: oligo(poly(ethylene glycol) fumarate); PDL: proteolytically degradable linkages; PEG: poly(ethylene glycol); pNiPAAm: poly (N-isopropylacrylamide); PPF-co-EG: poly(propylenefumarate-co-ethyleneglycol); RGD: arginine-glycine-aspartic acid; S: synthetic.

TABLE 3.3 HYDROGELS FOR SKELETAL CELL ENCAPSULATION

TE	Hydrogel	Cell type	Studies	Cell performance	Conclusions	References
Cartilage	Agarose	CH, hMSC, hADAS	#	diff+rediff; chondrogenesis; mechanically functional ECM	1	255-260
			♥ FTD	cartilage formation, merging with surrounding defect in 25%	1	
	Collagen	hCH, MSC	#	diff + ECM; occasionally observed dediff + fibroblastic morphology	1/4	267-269,272
			♥ FTD	hyaline cartilage (precultured gels); sporadically fibrotic cartilage	1/4	270,271
	Gelatin -sponges -gPNiPAAm gels	CH, hADAS, hMSC	#	chondrogenesis of seeded cells; ECM	1	260,286
			#/ ♥	gels: surface deformation, cartilage formation in precultured samples	1/4	300
	pNiPAAm	CH	#	support chondrogenic phenotype	1/4	296,297
	Pluronics	CH	# C	ECM	4	42,206,305-307
			♥ GEC/FTD	cartilage formation	1	
	PEG	CH	♥ SC	cartilage formation	1/4	309
	PPF-co-EG	CH	#	ECM	4	314
	Chitosan	CH	#	ECM	4	223,319
			♥ SC/FTD	ECM, gel persists in osteochondral defects > 1 wk	4	320
	HPMC (silated)	CH	#	support growth and GAG formation	4	328
	Alginate	(h)CH, MSC, ADAS	#	diff+rediff; chondrogenesis; ECM	1	268,331-334
			♥ SC/FTD	formation cartilaginous tissue/shaped implants, sporadic fibrotic cartilage	1/4	260,285,335-338
	Polypeptides	CH	#	ECM	1	380
	PEG	CH, MSC	#	chondrogenesis, ECM	1	352,353
			♥ TDPP	cartilage formation	1	354
	PVA	CH	#	ECM	1/4	253
	Fibrin	CH	#/♥ SC	ECM/cartilage formation, also in shaped precultured constructs	1	369,372,398,399
			♥ FTD	cartilage formation, no biomechanical support in load application	5/4	

TE	Hydrogel	Cell type	Studies	Cell performance	Conclusion	References
Bone	Agarose	pOB, MSC	#/♥	chondrogenesis/ formation hyaline cartilage	5	209,261
	Collagen	pOB, MSC	#/♥ CSD/SF	bone like ECM/ bone formation with ce;;-transduced MSCs	1/2	275-279
	Gelatin	OB	#	survival inside crosslinked gelatin as protection in hostile environment	4	287
	Matrigel	Osteogenic	#/♥ SC/SF	support osteogenic phenotype/ bone formation	1	288-291
	pNiPAAm	OB	#	support adhesion/diff of seeded cells; proliferation in RGD modified gels	4	298,301
	Pluronics	MSC	#/♥	poor conditions for cells/ little to no bone formation	5/4	209
	Thermo PEG	MSC	♥	ECM formation	1/4	310
	PPF-co-EG	OB	#	good surface for seeded cells; incorporated cells die	5/4	316
	Chitosan	MSC	#	support diff + ECM formation	1/4	321
	HPMC(silated)	Osteogenic	#	ECM formation	1/4	327
	Alginate	OB, MSC	#/♥ SC/defects	chondrogenic and osteogenic phenotype/bone formation	1/4	70,228,339-341
	Photo PEG	OB, hMSC	#	survival, ECM in modified gels; osteogenesis	1	212,213,232,233,355
	Fibrin	hMSC, pOB	# C scaf	osteogenic diff	2	208,400
			♥ C scaf/SC/defects	bone formation	2	207,375
	OFP	MSC	#	calcified ECM	1/4	401
IVD	Agarose	IVDC	#	multicelled colonies, low proliferation; high PG content	1/4	381
	Collagen	IVDC, MSC	#/♥	proliferation/regeneration IVD	1/4	263,264
	Chitosan	MSC, IVDC	#	variable survival annulus fibrosus cells; ECM production	1/4	322,323
	Alginate	IVDC, MSC	#	nucleus pulposus phenotype	1/4	343,344
	Fibrin	NPC	#/♥	spindle shaped cells/ ECM production when combined with hyaluronate	5	273,402
Tendon	Collagen	MSC	♥	improved biomechanics; unchanged microstructure	1	284,403

Table 3.3 Cartilage, bone, intervertebral disc (IVD), and tendon TE. ADAS: adipose tissue derived adult stem cells; C: composite scaffold of gel and solid material; CH: chondrocytes; CSD: critical size defects; ECM: extracellular matrix; FTD: full-thickness defects; GAG: glycosaminoglycans; GEC: graft elastic cartilage; h: human; HPMC: Hydroxypropylmethylcellulose; IVDC: intervertebral disc cell; MSC: mesenchymal stem cell; NPC: nucleus pulposus cell; OB: osteoblast; OFP: oligo(poly(ethylene glycol) fumarate); p: periosteal; PEG: poly(ethylene glycol); pNiPAAm: poly (N-isopropylacrylamide); PPF-co-EG: poly(propylenefumarate-co-ethyleneglycol); PVA: poly(vinyl alcohol); SC: subcutaneous implants; SF: spinal fusion; TDPP: transdermal photopolymerization; #: *in vitro* studies; ♥: *in vivo* studies; 1: suitable for this application; 2: applicable in composite scaffolds; 3: applicable *in vivo* after preculture; 4: further evaluation needed; 5: not (yet) suitable.

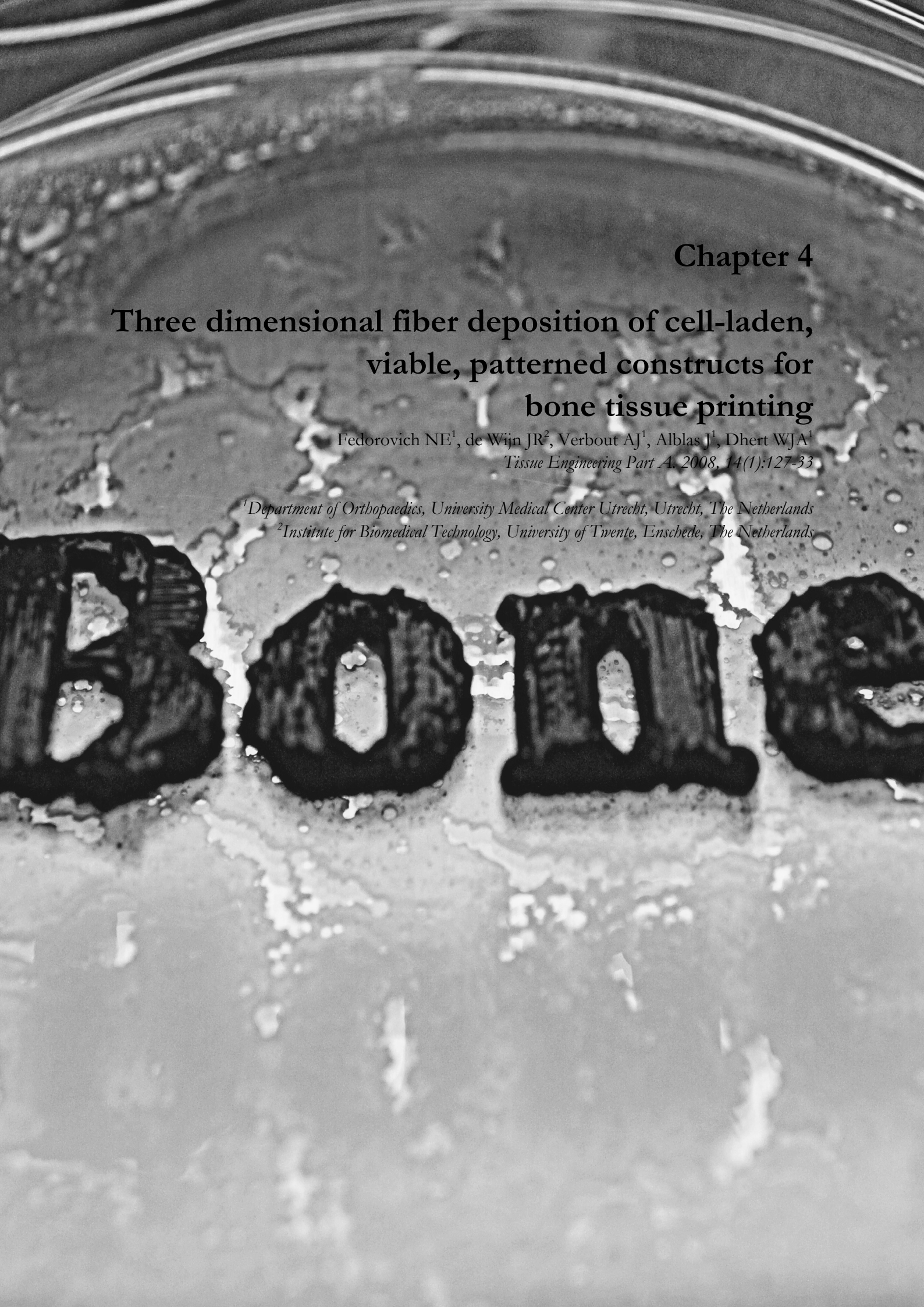

Chapter 4

Three dimensional fiber deposition of cell-laden, viable, patterned constructs for bone tissue printing

Fedorovich NE[1], de Wijn JR[2], Verbout AJ[1], Alblas J[1], Dhert WJA[1]

Tissue Engineering Part A. 2008, 14(1):127-33

[1]*Department of Orthopaedics, University Medical Center Utrecht, Utrecht, The Netherlands*
[2]*Institute for Biomedical Technology, University of Twente, Enschede, The Netherlands*

Abstract

Organ or tissue printing, a novel approach in tissue engineering, creates layered, cell-laden hydrogel scaffolds with a defined three-dimensional (3D) structure and organized cell placement. In applying the concept of tissue printing for the development of vascularized bone grafts, the primary focus lies on combining endothelial progenitors and bone marrow stromal cells (BMSCs). Here we characterize the applicability of 3D fiber deposition with a plotting device, Bioplotter, for the fabrication of spatially organized, cell-laden hydrogel constructs. The viability of printed BMSCs was studied in time, in several hydrogels, and extruded from different needle diameters. Our findings indicate that cells survive the extrusion and that their subsequent viability was not different from that of unprinted cells. The applied extrusion conditions did not affect cell survival, and BMSCs could subsequently differentiate along the osteoblast lineage. Furthermore, we were able to combine two distinct cell populations within a single scaffold by exchanging the printing syringe during deposition, indicating that this 3D fiber deposition system is suited for the development of bone grafts containing multiple cell types.

Introduction

Regenerative medicine is an interdisciplinary field that integrates the principles of engineering and life sciences to create constructs capable of restoring or reinforcing tissue function. In cell-based bone tissue engineering, osteoprogenitor cells, scaffolds, and growth factors can be combined to create so-called hybrid constructs. These constructs can be used as bone grafts *in vivo*. Small grafts have been successfully applied in small-animal models (e.g. rodents), but upscaling to clinically relevant-sized grafts remains challenging. It is now widely recognized that methods to improve diffusion of nutrients and enhanced vascularization of the tissue-engineered bone grafts may be essential for the development of larger grafts.[249] Also, spatial organization of engineered (skeletal) tissue is important in further directing its biological function.[30,48,404,405] Therefore, scaffold design with controlled architecture, organized placement of cells, and the use of cell types that enhance vascularization are considered critical to the success of cell-based bone tissue engineering.[29,76]

Application of a rapid prototyping approach in cell-based tissue engineering has led to the development of a novel concept, termed organ or tissue printing, in which cells and hydrogel matrices are spatially organized into layered hybrid constructs, with controlled architecture and defined cellular placement.[28] Creation of cell-seeded implants that mimic native tissues with respect to anatomical geometry, spatial organization, and the microenvironment of the cells[190] could ultimately accelerate and improve the assembly and functionality of tissue-engineered constructs.[406] By incorporating several cell types at predetermined locations, specifically osteoprogenitors and endothelial progenitors, we strive for fabrication of vascular bed structures suitable for integration with the systemic circulation, thus permitting survival of large tissue constructs after implantation.

Viable two-dimensional (2D) and layered 3D cell-laden constructs have already been manufactured with the use of modified ink-jet printers,[111,112] laser-assisted transfer techniques,[99,178] and various dispensing technologies.[115,133,198] The application of such dispensing machines as the BioAssembly tool,[198] rapid prototyping tool,[133] and volumetrically controlled deposition tool[115] have resulted in printed tubular, vascular-like structures with endothelial cells and viable, spatially organized constructs with hepatocytes or chondrocytes embedded in gelatin or alginate matrices. Hydrogels provide the embedded cells with a support matrix and a highly hydrated microenvironment that is amenable to nutrient and waste diffusion. Various hydrogel systems are currently being developed that can present biochemical and physical stimuli to guide cellular processes such as migration, proliferation, and differentiation and could be used for organ printing.[407]

To apply the concept of organ or tissue printing for development of vascularized bone grafts, we characterized layered 3D fiber deposition of osteoprogenitor cells in hydrogels using a pneumatic dispensing system. To test the ability of the system to print hydrogel scaffolds, four different hydrogels were deposited alone. Two of these gels were subsequently printed with cells. The viability of embedded cells was compared in printed and unprinted (cast) samples at several time points. The effect of needle diameter on cell survival was compared in several hydrogel systems for up to 3 days. We investigated whether multiple cell populations could be incorporated within one scaffold by printing two differently labeled cell populations during the same printing session by exchanging the printing syringe. In addition, the ability of printed osteoprogenitor cells to

differentiate was studied 2 weeks after the deposition, using histological analysis of alkaline phosphatase activity.

Materials and methods

3D fiber deposition system (Bioplotter) presets

The Bioplotter pneumatic dispensing system (Envisiontec GmbH, Gladbeck, Germany) was used for 3D fiber deposition (3DF). This system was previously employed for extrusion of hydrogels alone and has been described in more detail elsewhere.[187] Briefly, the Bioplotter is a three-axis dispensing machine that builds up 3D constructs by coordinating the motion of a pneumatic syringe dispenser to deposit extrudate on a stationary platform. The extrudate consists of a hydrogel of a suitable polymer, with or without cells. Computer models of the scaffolds are loaded via the Bioplotter computer-aided design–computer-aided manufacturing software, which translates this information for layer-by-layer fiber deposition by the Bioplotter. In the current study, the speed of deposition varied from 1 to 30 mm/s, and the pneumatic pressure that was applied to the dispensing syringe varied from 0.5 to 3.0 bar. Pressure was set to yield uniform, continuous extrusion of fibers. The fiber diameter varied with the inner nozzle diameter (100–450 μm) and the deposition speed. Rectangular 3D scaffolds of 20x20 mm with spacing between fibers of 300 μm and a layer thickness of 150 μm were constructed in a sterile Petri dish. Two different configurations of deposited fibers (0/90 and 0/45:0/90 configuration) were tested for Lutrol F127. The number of layers varied according to the experiment.

Hydrogels

High-viscosity non-medical-grade alginate (Sigma, Zwyndrecht, The Netherlands) was dissolved at a concentration of 20 mg/ml in standard culture medium and passed through a 0.22 μm filter. During the deposition, alginate was printed or pipetted into a Petri dish containing 100 mM of autoclaved calcium chloride supplemented with 10 mM of 4-(2-hydroxyethyl)-1-piperazineethane sulfonic acid pH 7.4 (Gibco, Glasgow, Scotland), which resulted in gel formation. Other hydrogels included Lutrol F127, a PEO-PPO-PEO block copolymer (Poloxamer 407, BASF ExAct, Ludwigshafen, Germany) used at 25% (w/v) in culture medium, Matrigel (BD Biosciences, Erembodegem, Belgium), agarose MP (Sigma) 1–5% (w/v), and methylcellulose (Sigma) 4% (w/v), the last two in culture medium.

Cell isolation and culture

Bone marrow stromal cells (BMSCs) were obtained from iliac bone marrow aspirates of two Dutch milk goats, each two years old. The plastic adherent fraction was culture-expanded according to previously described methods[18] in alpha minimum essential medium (Gibco) and 15% (v/v) fetal bovine serum (Cambrex, Verviers, Belgium) and supplemented with antibiotics (100 U/ml penicillin, 100 μm/ml streptomycin) and 2 mM L-glutamine (Gibco). The cells were cultured at 37 °C and 5% carbon dioxide (CO_2). BMSCs between passages 4 and 6 were used in the experiments.

Preparing hydrogel–cell constructs

Cells were detached from culture plastic and mixed with the hydrogel solutions at $2.5x10^5$ cells/ml. The hydrogel–cell mixtures were kept on ice in the case of Lutrol F127 and Matrigel samples, whereas the alginate and methylcellulose mixtures were processed at room temperature

and agarose at 40 °C. The hydrogel–cell mixtures were put into a syringe and loaded into the Bioplotter. The mixture was extruded into a Petri dish at room temperature and various speeds and air pressures, depending on the needle diameter (Figure 4.1).
Four-layer constructs were created and then cultured in standard culture medium for cell viability studies or in osteogenic medium, consisting of standard culture medium supplemented with 0.1 mM ascorbic acid (Sigma), 10 nM dexamethasone (Sigma), and 10 mM β-glycerophosphate (Sigma) to study the differentiation potential of the embedded BMSCs. The cell–hydrogel constructs were cultured at 37 °C and 5% CO_2.

Sterility

Because the Bioplotter is also used for processing of other materials such as polyesters, placement in a flow cabinet was not possible; therefore, specific measures against bacterial contamination were taken. To minimize the risk of scaffold contamination during the deposition, hydrogels were passed through a 0.22-μm filter, and all of the other materials in direct contact with the cells were autoclaved before processing. Constructs were printed in sterile Petri dishes or 12-well plates. To test the effectiveness of these precautions, four printed scaffolds and the surrounding culture media were plated onto sheep-blood-agar plates and cultured at 37 °C. No outgrowth of fungi or bacteria from the hydrogel samples was observed for up to 10 days after printing of the cell-laden Lutrol F127 hydrogels.

Analysis of cell survival after printing

A LIVE/DEAD viability assay was performed to assess the viability of cells after printing as a function of time after printing and as a function of the needle diameter used for printing. The printed constructs studied were 20x20x2-mm cell-laden ($2.5x10^5$ cells/ml) scaffolds printed in 12-well plates. The viability of cells as a function of time after printing was analyzed using a 210-μm-diameter needle to print alginate (η=11 Pas, 2% w/v, 23°C) and Lutrol F127 (η=3600 Pas, 25% w/v, 23 °C). Triplicate samples of each hydrogel were evaluated at three follow-up times (5 hours, 1 day, 3 days). The effect of needle diameter (150 μm, 180 μm, 210 μm, 420 μm, 610 μm) on cell survival was analyzed using Lutrol F127 scaffolds at 5 hours after the deposition in triplicate.
The LIVE/DEAD viability assay (Molecular Probes MP03224, Eugene, OR) was performed according to the manufacturer's recommendations. The samples were observed and scored using an epifluorescence microscope (Eclipse E600, Nikon, Tokyo, Japan). The excitation/emission filters were set at 488/530 nm to observe living (green) cells and at 530/580 nm to detect dead (red) cells. The cell viability was determined as the average ratio of vital to total cells in a sample, calculated from 4 randomly selected fields per scaffold.

Analysis of cytotoxicity of hydrogel materials

The cytotoxicity of the various hydrogels was assessed using the LIVE/DEAD viability assay described above. The cytotoxicity was investigated with non-printed, 1- to 2-mm thick hydrogel–BMSC disks, cast in 12-well plates, and analyzed after 5 hours, 1 day, 3 days, or 7 days in culture.

Fluorescent labeling of BMSCs

Before printing, 2 separate suspensions of BMSCs were fluorescently labeled using Calcein-AM (MP03224) (green) or CellTracker Red CMTPX (MP02925, Molecular Probes), both of which label the cytoplasmic components of viable cells. The labeled cells were mixed with ice-cold

Needle diameter (µm)	*Deposition pressure (bar)*	*Fiber diameter (mean +/- SD (µm))*
610	0.2	1280 +/- 96
210	2	430 +/- 42
180	2.5	350 +/- 24
150	3.5	320 +/- 41

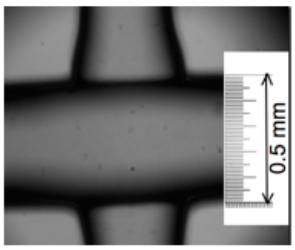

Figure 4.1: Printing parameters. Fiber size in 4-layered Lutrol F127 scaffolds using different needle diameters (n=5). Inset: Printed Lutrol F127 fibers, needle ø 210 µm. SD: standard deviation.

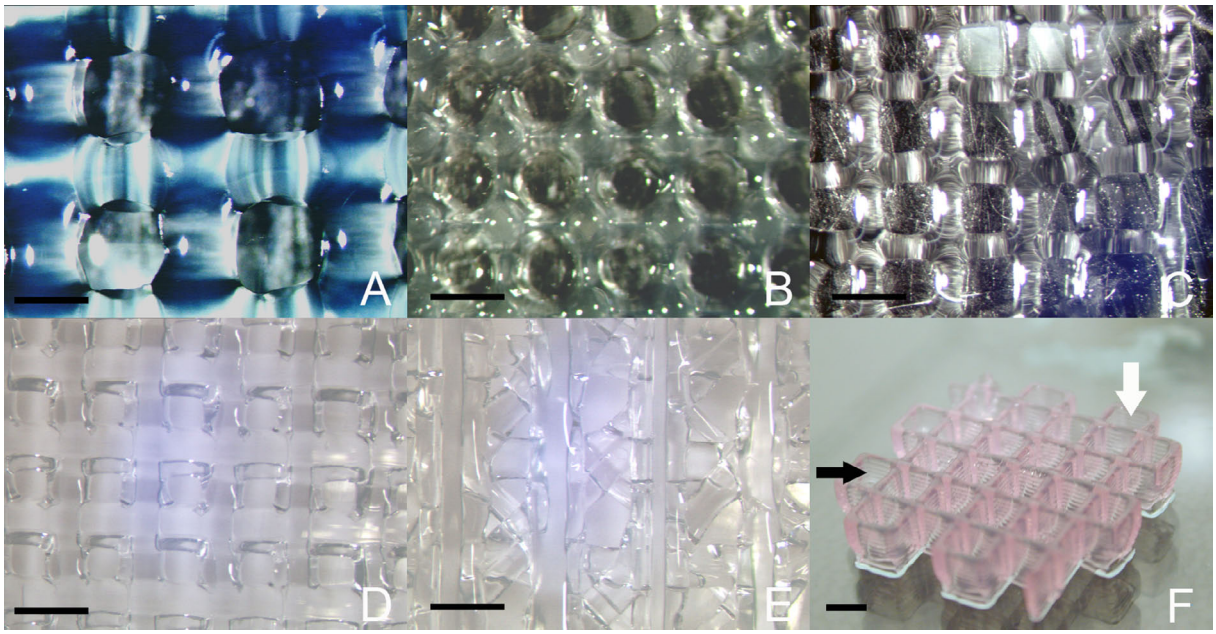

Figure 4.2: Printed hydrogel scaffolds. A: Agarose 5%, B: alginate 2%, C: methylcellulose 4%, D,E: Lutrol F127 25% in 2 different configurations of deposited fibers (0/90 and 0/45:0/90 configuration, respectively); F: Lutrol F127 10-layer scaffold with regular vertical channels (white arrow) and fused horizontal pores (black arrow). Scale bar A–E: 500 µm, scale bar F: 2.5 mm.

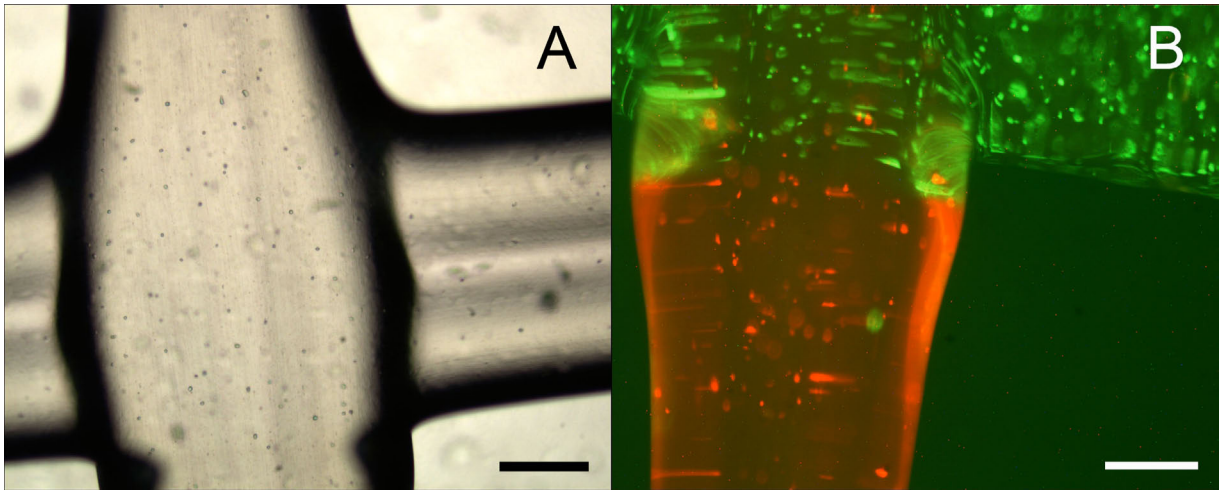

Figure 4.3: Encapsulation of cells during the deposition process. A: Bone marrow stromal cells (BMSCs) stained with Trypan blue embedded in Lutrol F127 25%; B: two BMSC populations printed in 1 scaffold labeled with calcein (green) or CellTracker Red. Scale bar: 100 μm.

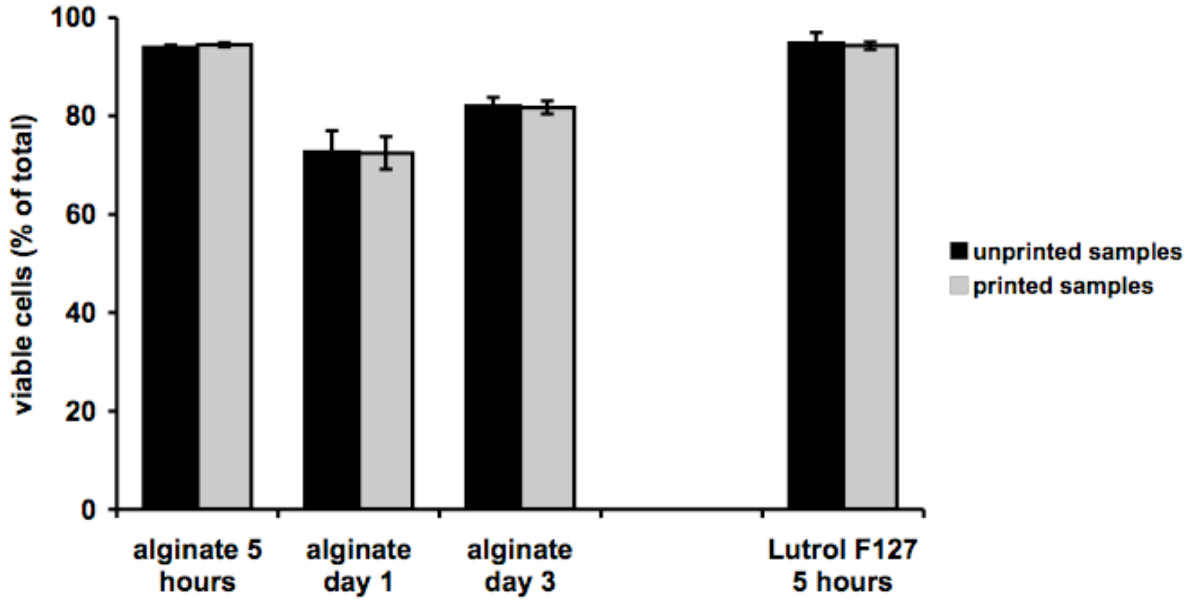

Figure 4.4: The effect of the printing process on cell survival. Bone marrow stromal cell viability in unprinted (black) and printed (light grey) samples (n=3); no significant differences between printed and unprinted samples were found (p=0.9).

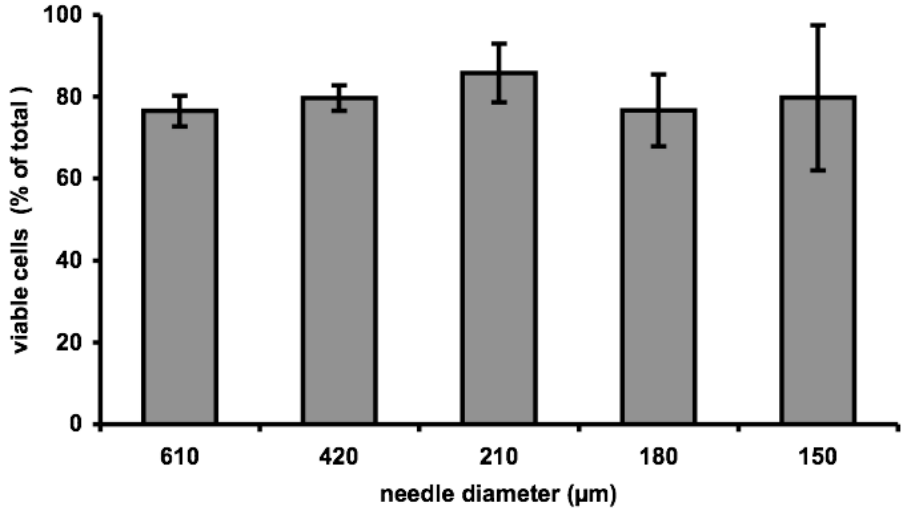

Figure 4.5: The effect of needle diameter on cell survival. Bone marrow stromal cell viability in printed Lutrol F127 samples (n=3); univariate analysis of variance: p=0.6.

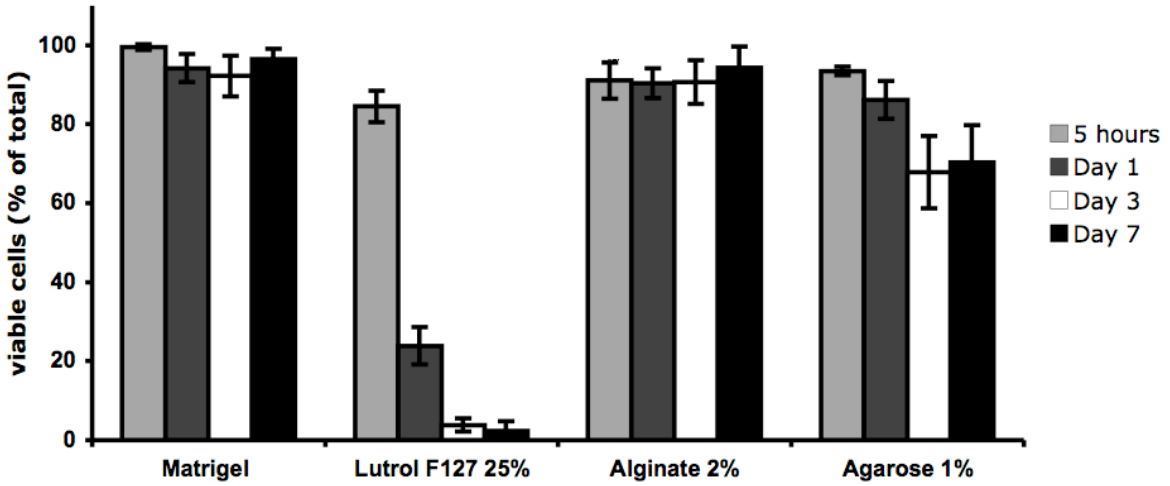

Figure 4.6: Survival in different hydrogels. Cell survival of bone marrow stromal cells in various hydrogels 5 h, 1 day, 3 days, and 7 days after encapsulation (representative experiment; n=3): 5 h: no significant differences between the groups (p=0.5); day 1: lower survival in Lutrol F127 than in other gels (p<0.001); day 3: lower survival in Lutrol F127 than in other gels (p<0.001), high viability in Matrigel and alginate (p<0.05 Matrigel and alginate vs agarose); day 7: lowest survival in Lutrol F127 (p<0.001), high viability in Matrigel and alginate (p<0.001 Matrigel vs agarose, p<0.05 alginate vs agarose).

Lutrol F127 at $0.5x10^6$ cells/ml hydrogel. Each labeled cell population was placed in a separate syringe and kept on ice. Four-layer constructs were printed with the Bioplotter, exchanging the syringes between each layer, resulting in interposed layers of red- and green-labeled cells. The constructs were evaluated using a Nikon epifluorescence microscope (Eclipse E600) directly after the deposition.

Differentiation assay

After 2 weeks of culture in osteogenic medium, the cell-laden scaffolds were tested for viability of the embedded cells, washed in phosphate buffered saline and embedded in Tissue-Tek® and 10 μm cryosections were cut. The sections were air-dried, fixed with 4% formaldehyde for 10 min, and washed with phosphate buffered saline–0.1% Tween20. The Fuchsin substrate-chromogen system (K0624, DAKO, Heverlee, Belgium) was applied for 30 min to stain alkaline phosphatase activity pink. Hematoxylin was used as a counter stain. The presence of pink cells was analyzed using an Olympus BX50 light microscope equipped with an Olympus DP 70 camera (Zoeterwoude, The Netherlands).

Statistical analysis

Statistical analysis was performed with SPSS 12.0.1 software (SPSS Inc, Chicago, IL). A Student's *t*-test was used to evaluate the viability data in printed and unprinted samples. Viability data at different needle diameters was performed using Kruskal-Wallis one-way analysis of variance (ANOVA). A two-way ANOVA was used to evaluate the viability measurements inside various hydrogels at three time points. *P*-values <0.05 were considered statistically significant. All values are reported as means ± standard deviations.

Results

Hydrogel deposition

We compared the 3DF deposition of Lutrol F127, agarose, alginate, and methylcellulose hydrogels. The resultant 4-layer scaffolds are depicted in Figure 4.2. Identical deposition speed (1000 mm/min) and needle diameter (210 μm) resulted in different fiber diameters and scaffold architectures because of the different gelation rates of the hydrogels. The slow gelation rate of agarose resulted in broad fibers that tended to fuse under their own weight, despite cooling on ice. Alginate layers gelled fast, which compromised the stacking of multiple layers. Lutrol F127 allowed easily controlled deposition, resulting in scaffolds with various fiber configurations and thickness of up to 10 layers. Vertical pores were regular throughout the samples, whereas transversal pores fused because of the softness of the material. For further analysis, we selected Lutrol F127 and alginate because of the ease with which they are processed and our experience with these materials.

Various needle diameters were tested to assess the processability of Lutrol F127 and alginate. Smaller needle diameters required higher dispensing pressures and lower deposition speeds to ensure uniform, continuous extrusion of fibers. The smallest internal needle diameter that yielded hydrogel deposition was 150 μm, which in turn determined the resolution of the printed scaffolds. Stacking of several hydrogel layers resulted in broader strands than the original needle diameter (Figure 4.1).

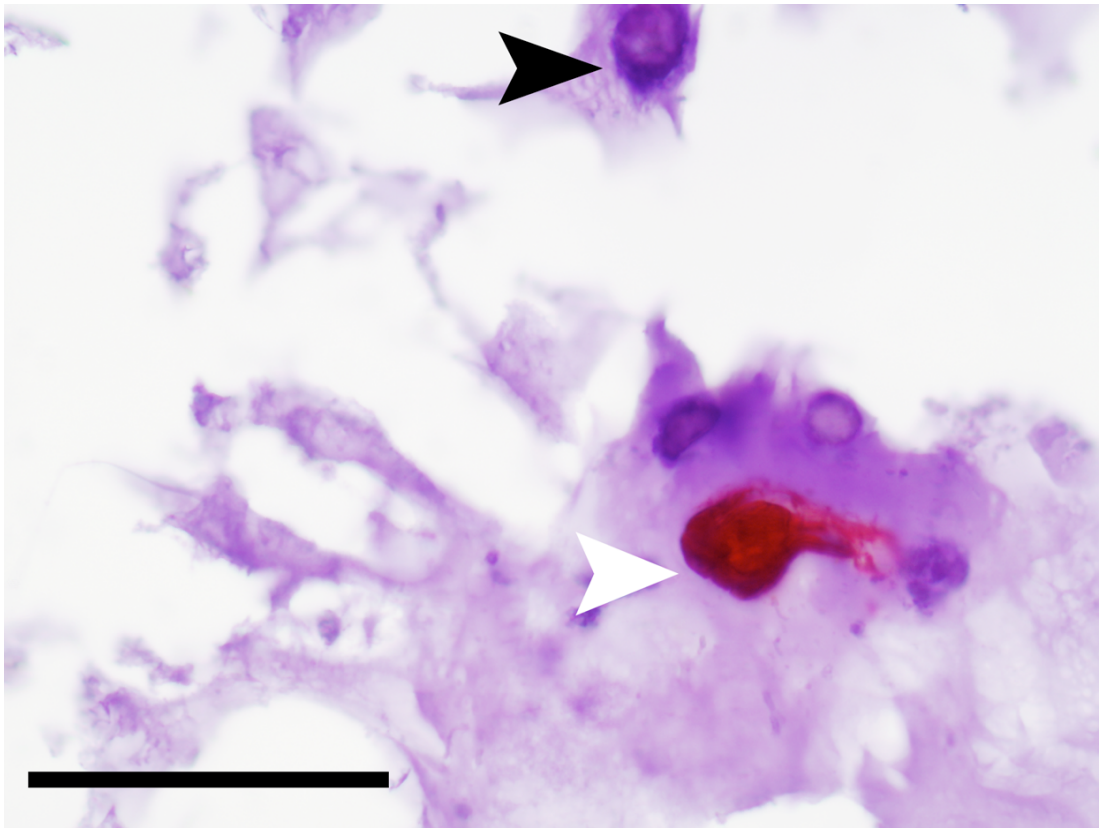

Figure 4.7: Osteogenic differentiation. Bone marrow stromal cells (BMSCs) embedded in alginate after 2 weeks of culture; white arrowhead: BMSCs expressing alkaline phosphatase, black arrowhead: negative cell; scale bar = 50 μm (representative figure of a single experiment performed in triplicate).

Cell encapsulation

Cells were encapsulated inside the hydrogels to assess the feasibility of 3DF for printing one or more cell populations within a single scaffold. Embedded cells were homogeneously distributed within the deposited hydrogel scaffolds, as illustrated in Figure 4.3A. Exchanging syringes between the deposition of each layer of the 4-layer model enabled 3D constructs containing interposing layers of green- and red labeled cells to be produced using 3DF (Figure 4.3B).

Cell survival

The effect of the printing process on the viability of the cells was determined by comparing the viability of printed constructs and cast gel discs for the alginate and Lutrol F127 hydrogels (Figure 4.4). There were no statistically significant differences in cell survival 5 hours after the printing, suggesting that the printing process itself does not induce immediate cell death. Also for days 1 and 3, there was no significant decrease in the viability of cells extruded with alginate, as compared with corresponding unprinted cell-laden alginate gels. This suggests that the printing process in general does not affect the survival of the cells. In a different hydrogel system, Lutrol F127, there were no significant changes between the printed and unprinted samples (Figure 4.4).
The effect of the applied pressure and inner diameter of the needle tip on the viability of the extruded cells were studied by measuring the fraction of viable cells 5 h after the deposition of cell-laden Lutrol F127. The results are summarized in Figure 4.5. There was no significant difference between the viability of cells extruded at a high pressure setting and those extruded through larger-diameter needles at lower pressure.
The cytotoxicity of the different hydrogels on BMSCs was investigated in thin hydrogel discs. The results are presented in Figure 4.6. The viability of cells was less after 1 and 3 days in culture than in corresponding samples analyzed 5 hours after printing. Cell survival was dependent on hydrogel type used. Although survival rates were comparable 5 hours after embedding (no significant differences between the hydrogel groups), we observed significantly lower cell survival in Lutrol F127 after 1, 3, and 7 days than with other hydrogels. Approximately 4% of BMSCs survived after 3 days in Lutrol F127. Matrigel and alginate provided significantly better conditions for the embedded cells over the course of 7 days than the other gels.

Osteogenic differentiation in printed scaffolds

The differentiation potential of the printed cells was determined by evaluating the activity of the osteogenic marker alkaline phosphatase in printed, cell-laden alginate scaffolds ($1.0x10^6$ BMSCs/ml) after 2 weeks of culture in osteogenic medium. The cells remained viable for up to 2 weeks of culture (viability 86% ± 1%; n=2) and expressed alkaline phosphatase, as illustrated in Figure 4.7. This shows that the cells not only survive the deposition process, but also retain the ability to differentiate to the osteogenic lineage after extrusion.

Discussion

In this study, we characterize the applicability of this 3DF system to print cell-laden hydrogels. We demonstrate for the first time that the Bioplotter 3DF system can be used for simultaneous deposition of cells and hydrogels, resulting in 3D defined scaffolds under semi-sterile conditions. To apply this 3DF system for design of tissue-engineered bone grafts, it is vital that the cells do not die during the deposition and retain the ability to differentiate. We show that the cells survive the deposition process and spread homogenously inside the gels. Neither the printing process nor the needle diameter, as used in this study, affect cell viability. The type of hydrogel determines

cell survival after embedding. Also, printed BMSCs retain the ability to differentiate toward osteogenic lineage.

We found that hydrogels vary greatly in their ease of processing with the Bioplotter system due to differences in gelation rate. With Lutrol F127, we were able to print regular scaffolds up to 10 layers thick with various fiber configurations under physiological conditions. Although some of the technologies applied for tissue printing are limited to cell deposition[111,190] or have a narrow processing window requiring specific materials to enable deposition,[176] dispensing systems like the Bioplotter can use various materials for printing scaffolds, including different hydrogels, as presented in this article, without the need for support materials. Furthermore, the 3DF dispensing system is able to print scaffolds with more complex 3D architectures comprising defined macroscopic pores and fiber configurations or even tubular structures than some of the other printing techniques that mainly attain simple layered structures.[189]

Due to the softness of the hydrogel matrices processed with 3DF in this study, the resultant fiber thickness is considerably broader than the needle diameter used, because the layers stack on top of each other, reducing the resolution of the printed scaffold. The low mechanical strength of the hydrogels used for printing, specifically of Lutrol F127, also compromise the formation of transversal pores, resulting in fusion of subsequent layers, with only vertical pores present in the printed scaffold. To solve this problem, inverse thermosensitive Lutrol F127 can be modified with chemical crosslinks,[308] yielding stiffer hydrogel fibers and stronger, more stable printed hydrogel scaffolds. Maintaining the stage at higher temperatures has been reported to aid the polymerization of the used thermosensitive hydrogels.[114] Although this approach can be used to ensure faster gelation of the inverse thermosensitive hydrogels, the conditions to induce crosslinking may significantly compromise the viability of the printed cells.

In this study, we demonstrate that cells survive the extrusion in two different hydrogels and are distributed homogeneously within the scaffold, with cells remaining intact after the deposition, irrespective of the needle diameter and pressures used.

The findings indicate that the printing process itself does not adversely affect the survival of cells, due to, for example, rupture of the membranes during extrusion. These results are in contrast with the expected enhanced shear stress experienced by the printed cells and findings by other research groups reporting reduced cell survival at comparable deposition pressures.[114] However, the use of cells from different species, goat cells versus human cells in other studies, and materials with different viscosities used at other extrusion rates resulting in different shear stress may explain these contrasting findings. Another factor that can influence the survival of the extruded cells is the air humidity during the printing process,[114] which has not been addressed in this study, because the current Bioplotter system is not equipped with humidity regulation. Nevertheless, we do not expect a large effect of this parameter, because we did not observe changes in cell survival when comparing printed and unprinted gels.

In the present study, we demonstrate the possibility of printing two distinct cell populations at predefined locations within a single hybrid construct. This means that we can use the 3DF system for simultaneous deposition of osteogenic and endothelial progenitors for development of vascularized bone grafts for bone tissue engineering. Not only does this method provide us with a tool for the development of novel, viable, spatially organized tissue engineered grafts, it also allows for differential growth factor placement, making it possible to guide cellular behavior *in vitro* and *in vivo*. Additionally, porous, printed hydrogel scaffolds allow for blood vessel ingrowth, making these scaffolds potentially suitable for angiogenesis studies.

Printed BMSCs express an early osteogenic marker, alkaline phosphatase, which indicates that printed cells are able to differentiate during subsequent culture. This suggests that the 3DF

approach can be used for 3D bone tissue printing. Future experiments will focus on analysis of extracellular matrix formation by the printed BMSCs, testing the functionality of the cells after the deposition.
An adequate hydrogel system is another essential factor in further development of this approach for bone printing. The direct effects of the printing such as shear stress and forces exerted on the cells do not affect cell viability in the first few hours after printing. Thereafter, environmental factors such as hydrogel formulation most probably have a profound influence on cell survival. In this study, we compared several hydrogel systems for cellular encapsulation, with variable outcomes. This finding may be partially due to impurities of the polymer sample or the intrinsic properties of the polymer compromising the integrity of the cell membrane.[304] Future studies will focus on further characterization of hydrogels with an optimal combination of good processability with 3DF and cytocompatibility, providing a suitable environment for cell survival and differentiation of osteogenic and endothelial progenitor cells. Newly developed interactive polymers, containing adhesion sequences and protease sensitive degradation sites for the embedded cells[129] could soon find application as bioactive scaffolds in organ printing.

Conclusion

This study characterizes the use of a 3DF dispensing system for the printing of cell-laden, spatially organized hydrogel scaffolds. Embedded BMSCs survived the deposition process and retained the ability for osteogenic differentiation after extrusion. Viability of embedded cells was dependent on the hydrogel matrix used. We demonstrated that the Bioplotter, a 3DF system, can deposit two distinct cell populations within a single scaffold and shows potential for the development of vascularized bone grafts.

Acknowledgements

The authors wish to thank Lorenzo Moroni for his assistance with the Bioplotter. This work was supported by the Mosaic Scheme 2004 of the Netherlands Organization for Scientific Research and Anna Fund in support of research of musculoskeletal conditions.

Chapter 5

The effects of photopolymerization on stem cells embedded in hydrogels

Fedorovich NE[1], Oudshoorn MH[2], van Geemen D[1], Hennink WE[2], Alblas J[1], Dhert WJA[1,3]

Biomaterials. 2009, 30(3):344-53

[1]Department of Orthopaedics, University Medical Center Utrecht, Utrecht, The Netherlands
[2]Department of Biopharmaceutics, Utrecht Institute for Pharmaceutical Sciences (UIPS), Utrecht University, Utrecht, The Netherlands
[3]Veterinary Medicine, Utrecht University, Utrecht, The Netherlands

Abstract

Photopolymerizable hydrogels, formed by UV-exposure of photosensitive polymers in the presence of photoinitiators, are widely used materials in tissue engineering research employed for cellular entrapment and patterning. During photopolymerization, the entrapped cells are directly exposed to polymer and photoinitiator molecules. To develop strategies that prevent potential photoexposure-damage to osteoprogenitor cells, it is important to further characterize the effects of photopolymerization on the exposed cells. In this study we analyzed the viability, proliferation and osteogenic differentiation of multipotent stromal cell (MSC) monolayers after exposure to UV-light in the presence of Irgacure 2959, a frequently used photoinitiator in tissue engineering research. Cell cycle progression, apoptosis and osteogenic differentiation of encapsulated goat MSCs were studied in photopolymerized methacrylate-derivatized hyaluronic acid hydrogel and methacrylated hyperbranched polyglycerol gel. We demonstrate adverse effects of photopolymerization on viability, proliferation and reentry into the cell cycle of the exposed cells in monolayers, whereas the MSCs retain the ability to differentiate towards the osteogenic lineage. We further show that upon encapsulation in photopolymerizable hydrogels the viability of the embedded cells is unaffected by the photopolymerization conditions, while osteogenic differentiation depends on the type of hydrogel used.

Introduction

Hydrogels are attractive materials for various tissue engineering (TE) applications as they can be used to homogeneously incorporate cells, growth factors and other bioactive compounds. Overall, hydrogels show a good biocompatibility, and provide the embedded cells with a highly hydrated environment that is amenable to rapid diffusion of nutrients and metabolites.[199,203,407] Hydrogels generally cause little irritation *in vivo* due to their high water content and the resulting low quantity of degradation products. Hydrogel-forming polymers can be tailored to present biochemical, cellular and physical stimuli to guide cellular processes such as migration, proliferation and differentiation.[129,210,408]

Some types of hydrogels are obtained by photopolymerization of liquid photosensitive polymer solution in the presence of photoinitiators using visible or ultraviolet (UV) light either *in vitro* or *in vivo*.[200,201,409] These gels are stable and mechanically strong, because the polymer networks are held together by covalent crosslinks. Furthermore, photopolymerization is an attractive technique as the conversion of liquid polymer solution to a gel occurs rapidly, under physiological temperature, with minimal heat production, and can be controlled in time and space.[201] Photopolymerization has been widely employed for drug delivery,[359,410] for controlled release of DNA and growth factors[411-413] and to create layered matrix devices for investigation of drug-release in non-uniform concentration profiles.[414]

In orthopaedic TE applications, photosensitive polymers are used as fillers for bone restoration[415] and for encapsulation of chondrocytes and osteogenic progenitors.[109,233,354,411,416] Photopolymerization provides the ability to gellify photosensitive polymers *in situ*, with a possibility to form complex shapes that adhere and conform to tissue structures.[201] Chondrocytes have already been encapsulated *in vivo* via transdermal photopolymerization as a minimally invasive technique.[354] Organ- or tissue printing (OP), based on layered deposition of (cell-laden) hydrogels is a novel technology suitable for application of photopolymerizable hydrogels.[407] This OP approach allows building of 3D organized scaffolds with multiple cell types at predetermined locations.

During the photopolymerization process (UV) light homolytically splits photoinitiator molecules into radicals, which initiates the formation of a polymer network. Free radicals can however also directly react with cellular components such as cell membranes, proteins and DNA, thereby directly inducing unwanted cellular damage, or indirectly via formation of reactive oxygen species (ROS). Despite the use of the exogenous defenses against oxidative damage and intracellular anti-oxidants to quench ROS, exposure to ultraviolet A (UVA) radiation can induce the formation of ROS. This can cause base lesions that could potentially lead to malignant transformation of photo-exposed cells, although UVA-induced lesions have low mutagenicity.[417] While many different methods exist to test for various DNA damage, most of the lesions are repaired quickly with little impact on cell homeostasis. Therefore, although these are unlikely to result from UVA irradiation,[418] it is desirable to detect the rare, not easily repaired damage such as double strand DNA breaks that can induce deleterious mutations and initiate carcinogenesis. To do this, detection of p53 binding protein-1 (p53BP1) is a useful tool. This mediator of a DNA damage checkpoint responds to, amongst others, DNA double strand breaks by quickly localizing to discrete nuclear foci.[419,420] Furthermore, exit from the cell cycle as a result of photoexposure-induced stress could lead to apoptosis or senescence, and is undesirable in a tissue engineering approach.

As further development of photopolymerizable hydrogels for TE has the potential to produce

structurally organized, cell-laden implants designed to repair or augment tissues, detailed studies are needed on the effect of photopolymerization on the exposed cells. Most studies in the literature provide a comparison between photoinitiator components with regard to their cytotoxicity, with[421] or without UV-exposure.[349,422] Several photoinitiators exhibit a good toxicological profile, with Irgacure 2959 providing the best results.[349] Photoinitiator concentrations and UV light intensity should be minimized to prevent adverse effects on the viability of the cells and their proliferation and/or differentiation potential.[201,350] Detailed studies describing the effect of UV-irradiation on cells in the presence of a photoinitiator and the hydrogel building blocks are lacking.
In our work we are interested in encapsulating bone marrow derived multipotent stromal cells (MSCs) in a photopolymerizable hydrogel for the development of printed bone grafts. The aim of this study was to analyze the effect of photopolymerization on the fate of photoexposed goat MSC monolayers, with regard to viability, DNA damage and subsequent cell cycle progression and differentiation. Examining these outcomes in the absence of hydrogel enables us to make general statements on effects of photoexposure, because additional interference from the hydrogel is excluded. Additionally, we have studied the behavior of these primary photoencapsulated cells in their microenvironment when entrapped inside two different hydrogels – a methacrylated synthetic and a methacrylated natural hydrogel – focusing on cell survival and osteogenic differentiation.

Materials and methods

Cells

Multipotent stromal cells (MSC) were obtained from iliac bone marrow aspirates of Dutch milk goats, and isolated by adherence to tissue culture plastic. The cells were culture-expanded as described previously,[18] in expansion medium consisting of aMEM (Gibco) supplemented with 100 U/ml penicillin, 100 μg/ml streptomycin (Gibco), 2 mM L-glutamine (Glutamax, Gibco) and 15% v/v Fetal Calf Serum (Cambrex). For osteogenic differentiation, expansion medium was supplemented with 10 nM dexamethasone (Sigma), 10 mM b-glycerophosphate (Sigma) and 0.1 mM L-ascorbic acid-phosphate (Sigma). Cell cultures were maintained in a humidified incubator at 5% CO_2 and 37°C. Cells of passage 2–6 were used in this study.

Hydrogel encapsulation

MSCs were encapsulated in two photopolymerizable hydrogels: methacrylate-derivatized hyaluronic acid (HA; Mw = 1700,000 g/mol; DS15; 2% (w/v) solution in expansion- or osteogenic medium),[423] and methacrylated hyperbranched polyglycerol (PG; Mw = 4000 g/mol; DS11; 30% (w/v) solution in expansion- or osteogenic medium).[424] Schematic representations of the two polymers are depicted in Figure 5.1. To study viability, the cells were encapsulated at 4.4 $x10^5$ cells/ml gel in expansion medium to facilitate counting of separate cells, and for osteogenic differentiation the cells were embedded at $5x10^6$ cells/ml gel in osteogenic medium. Gels were placed in 16-well chamber slides at 50 μl/well for photopolymerization. After the photopolymerization process, 100 μl of expansion or osteogenic medium was added to the well and changed every two days.

Photopolymerization presets

As photoinitiator, we used 2-hydroxy-1-[4-(2-hydroxyethoxy)phenyl]-2-methyl-1-propanone

(Irgacure 2959, Ciba Specialty Chemicals, Basel, Switzerland). A stock solution of 5% (w/v) in PBS was added to the culture medium or hydrogel to create final concentrations of 0% (w/v), 0.05% (w/v), or 0.1% (w/v). A Superlite S-UV 2001AV lamp (Lumatec, Munchen, Germany), which emits UVA and blue light (320–500 nm) was used to expose the MSC monolayers and cell-laden hydrogel discs at an intensity of ~6 mW/cm^2, measured at 365 nm.

Viability analysis

Monolayers of MSCs, plated in 96-wells plate at 10^4 cells/well, were exposed to UV light for 0, 30, 60 or 300 s, after a preculture step of one day, in three independent experiments. The total UV dose was 0 mJ/cm^2, 180 mJ/cm^2, 360 mJ/cm^2, or 1800 mJ/cm^2. The viability of the monolayers was measured within 1 h after photoexposure and after one and three days. Cell survival was determined with the LIVE/DEAD Viability/ Cytotoxicity Kit (Molecular probes, USA), used according to manufacturer's recommendations. The fluorescence emissions were acquired separately with a microplate reader (Flexstation, Molecular Devices, USA).
Viability of encapsulated cells was analyzed after one day in hyaluronic acid and hyperbranched polyglycerol solutions or hydrogels obtained by exposure to 360 mJ/cm^2 or 1800 mJ/cm^2 UV light in the presence of 0.05% (w/v) or 0.1% (w/v) Irgacure 2959. Stable hydrogels resulted from photoexposure of 1800 mJ/cm^2 in the presence of 0.05% (w/v) or 0.1% (w/v) Irgacure 2959, and were used to study cell-viability after one, two and three weeks in osteogenic medium. The hydrogels were incubated with a LIVE/DEAD solution according to manufacturer's recommendations and washed with PBS prior to analysis under a fluorescence microscope. Three samples per condition were measured using a microscope equipped with an epifluorescence set-up, excitation/emission setting of 488/530 nm to detect green fluorescence and 530/580 nm to detect red cells (Leica DM IRBE, Germany). Three randomly selected fields per sample were taken and cell viability was calculated as the average ratio of vital over total cells per sample using analySIS software (Soft Imaging System, Germany).

Proliferation analysis and colony-formation assay

The MSCs were plated at 5000 cells/cm^2 in culture medium and harvested (n = 2) on days 3, 5, 9, 12 and 16 with 0.25% Trypsin, 1 mM EDTA. The cells were counted using Trypan Blue exclusion. Additionally, the percentage of proliferating cells in UV-exposed MSC monolayers, cultured on 8-well chamber slides, was determined at days 1, 3 and 5 by immunocytochemical detection of Ki67, a proliferation marker.[425] Briefly, the monolayers were fixed in 4% formalin (Klinipath, The Netherlands), washed with PBS buffer and blocked with 5% (w/v) BSA in PBS. The coverslips were then incubated with mouse anti-human Ki67 antibody (0.8 μg/ml in 5% (w/v) BSA in PBS; DAKO M7240; crossreacts with goat) for 1 h, followed by incubation with goat anti-mouse Alexa fluor 488 (20 μg/ml in 5% (w/v) BSA in PBS; Molecular Probes, USA) for 1 h. Wash steps with 0.1% Tween20 in PBS were performed between the incubations. The sections were mounted with Vectashield containing DAPI for nuclear staining (Vector Laboratories) and analyzed under the fluorescence microscope. The percentage of proliferating cells was determined by calculating the average ratio of green, Ki67 positive nuclei, over total nuclei from four randomly selected fields in duplicate samples.
Colony formation capacity of UV exposed cells was analyzed by low-density plating. Non-exposed MSCs were used as controls. When colonies had formed, the cells were fixed for 10 min with 4% formalin and stained with methylene blue (Merck, Germany) for 5 min. The number of colonies per 10^5 seeded cells was determined in duplicate.

Apoptosis assay

Apoptotic cells were determined by caspase-3 immunocytochemistry (ICC). MSCs were seeded at 10^4 cells/cm^2, cultured for one day, and exposed to 0 mJ/cm^2, 360 mJ/cm^2 or 1800 mJ/cm^2 UV light in the presence of 0% (w/v), 0.05% (w/v) or 0.1% (w/v) Irgacure 2959. Twenty-four hours after the photoexposure, cells were fixed with 4% formalin for 10 min. After permeabilisation with 0.2% Triton X-100 (Fluka, Belgium) in PBS, the coverslips were incubated for 1 h with rabbit anti-active caspase-3 antibody (0.25 μg/ml in 5% (w/v) BSA in PBS; clone C92-605, crossreacts with goat; BD Biosciences, USA), washed with 0.1% PBS-Tween 20 and incubated with Powervision poly HRP goat-anti-rabbit IgG (Immunologic, The Netherlands). The staining was developed with diaminobenzidine (DAB; Sigma, The Netherlands) and hematoxylin was used as a counterstain. The fraction of apoptotic cells was calculated as the average ratio of apoptotic over total cells, by counting the caspase-positive cells in four randomly selected fields per slide (n = 4).

Senescence analysis

Senescent cells were identified by β-galactosidase staining in low-density culture. MSCs were seeded in 24-well plates at 5000 cells/cm^2 and exposed to 0 mJ/cm^2, 360 mJ/cm^2 or 1800 mJ/cm^2 UV light in the presence of 0% (w/v), 0.05% (w/v) or 0.1% (w/v) Irgacure 2959. One day after photoexposure, the cells were stained with senescence cells histochemical staining kit (Sigma-Aldrich, CS0030) according to manufacturer's recommendations and counted under the phase contrast microscope (n = 4 per condition).

DNA damage analysis

DNA damage in photoexposed MSC monolayers and hydrogel-embedded MSC was identified by staining nuclear p53 binding protein-1 (p53BP1) foci. MSCs were seeded at 5000 cells/cm^2, precultured for one day, and exposed to 0 mJ/cm^2, 1800 mJ/cm^2 or 3600 mJ/cm^2 UV light in the presence of 0% (w/v), 0.05% (w/v) or 0.1% (w/v) Irgacure 2959. Cells were fixed with 4% formalin for 10 min, at 1 h, one day and three days after the photoexposure.
To assess DNA damage of embedded MSC, cryosections from PG and HA hydrogel samples, obtained by exposure to 1800 mJ/cm^2 UV light in the presence of 0.05% (w/v) or 0.1% (w/v) Irgacure 2959 and cultured in osteogenic medium for one week, were cut at 5 mm, air dried and fixed with 5% formalin for 10 min. Upon permeabilisation with 0.2% Triton X-100 in PBS for 20 min, the coverslips were blocked in 5% (w/v) BSA in PBS for 1 h and incubated for 2 h with the rabbit anti-p53BP1 antibody (1 μg/ml in 5% (w/v) BSA in PBS; NB 100-304; Novus Biologicals), washed with 0.1% PBS-Tween 20, and incubated with goat anti-rabbit Alexa fluor 488 (2 μg/ml in 5% (w/v) BSA in PBS; Molecular probes, USA) for 1 h. The coverslips were mounted with Vectashield containing DAPI for nuclear staining and analyzed under the fluorescence microscope. The extent of DNA damage was analyzed by counting the percentage of cells with bright green p53BP1 foci in at least 100 nuclei per condition.

Osteogenic differentiation

Alkaline phosphatase assay

To analyze the effect of UV exposure on osteogenic differentiation of monolayers, we determined the presence of alkaline phosphatase activity in photoexposed MSCs seven days after exposure to 360 mJ/cm^2 or 1800 mJ/cm^2 UV light in the presence of 0.05% (w/v) or 0.1% (w/v) Irgacure 2959. The monolayers were fixed in 4% formalin and permeabilized in 0.2%

Triton X-100 in Tris buffered saline. The cells were then stained with Fuchsin Substrate-Chromogen system (DAKO, USA) according to the manufacturer's protocol. Cells were counterstained with hematoxylin and mounted with Aquatex. The ratio of alkaline phosphatase positive (pink-red) cells over total cells was determined in four sections per condition, using Image Pro Plus 5.1 software. To determine alkaline phosphatase activity of encapsulated cells after one or two weeks of culture in osteogenic medium, the medium was discarded, and the gels obtained by exposure to 1800 mJ/cm^2 UV light in the presence of 0.05% (w/v) or 0.1% (w/v) Irgacure 2959 were washed in PBS, embedded in Tissue-Tek_ and cryosections were cut at 10 mm. The sections were air-dried and fixed with 100% acetone for 10 min. The activity of alkaline phosphatase was determined by 30 min staining with the Fuchsin Substrate-Chromogen system. The presence of alkaline phosphatase positive cells was analyzed with an Olympus BX50 light microscope equipped with an Olympus DP 70 camera.

Collagen type I and osteocalcin immunocytochemistry

Osteogenic differentiation of photoexposed MSC monolayers was further determined by collagen type I- and osteocalcin ICC. The cells were plated on glass coverslips and exposed to UV light under conditions as described for alkaline phosphatase analysis. After two and three weeks, monolayers were fixed for 10 min in ice-cold 80% methanol, permeabilized with 0.2% Triton X-100 in PBS, blocked in 3% (w/v) BSA in PBS for 30 min and incubated with mouse anti-collagen type I antibody (2 μg /ml in 3% (w/v) BSA in PBS, clone I-8H5, Merck, Japan) or mouse anti-osteocalcin antibody (10 μg/ml in 3% (w/v) BSA in PBS, 804537, Alexis Biochemicals). The secondary antibody was goat anti-mouse Alexa fluor 488, used at 10 μg /ml in 3% (w/v) BSA in PBS. The coverslips were mounted with Vectashield with DAPI for nuclear staining and analyzed under the fluorescence microscope.

Statistical analysis

Statistical analysis was performed with SPSS 12.0.1 software. A one-way analysis of variance (ANOVA) was used to compare the amount of viable, senescent, and apoptotic cells between different photoexposure conditions, followed by the LSD post hoc test. A two-way ANOVA was used to evaluate the viability- and DNA damage measurements inside hydrogels obtained at different photoexposure presets, at various time points, followed by the LSD post hoc test. *P*-values of less then 0.05 were considered statistically significant. Values are reported as mean ± standard deviation.

Results

Viability of monolayers

In order to assess to which degree the survival of photoexposed cells is affected by the variables of photoexposure conditions, namely the time of UV exposure (and thus the irradiation dose) and presence of the photoinitiator molecules, the survival of MSC monolayers was studied after exposure to 6 mW/cm^2 of 362 nm UV light for varying periods of time (0–5 min) and various Irgacure 2959 concentrations (from 0 to 0.1% (w/v)). Irgacure 2959 was chosen for UV photoinitiation because it generally causes little cell death over a broad range of mammalian cell types and species.[349,350] A control population of MSCs in fresh media without irradiation was used to determine a relative cell survival. The fluorescence of viable control cells was set at 100, and for all other conditions relative survival directly after photopolymerization and after one and three days is presented in Figure 5.2.

One hour after photopolymerization, the viability of MSCs was comparable in all conditions. However, after one and three days, reduced survival in the photopolymerization conditions was observed, being around 53 ± 5% cell-survival at day one and 46 ± 7% at day three, using the more severe condition (i.e 0.1% (w/v) Irgacure 2959 and exposure to 1800 mJ/cm^2 UV light; Figure 5.2). The relative survival of MSCs, which were only exposed to UV in the absence of photoinitiator, was 86 ± 5% after three days, while it reached 96 ± 1% for MSCs incubated with 0.1% (w/v) Irgacure 2959 (without UV exposure), as shown in Figure 5.2. These findings indicate that more cell death occurs after exposure to UV light in combination with photoinitiator molecules than after exposure to the separate modalities alone, which suggests that the free radicals and/or ROS formed during the photopolymerization process mediate the deleterious effects on cell-survival.

Proliferation and cell cycle progression

To study how the photoexposure and the photoinitiator molecules affect cell proliferation, we analyzed the proliferative capacity of photoexposed monolayers by counting the MSCs (Figure 5.3A). This figure shows that while the control cells immediately started to proliferate and reached a plateau phase around day nine, the growth curve of photoexposed gMSC exhibited a lag phase, representing cells in the non-proliferative G_0 phase of the cell cycle. This phase appeared longer in the more severe photopolymerization conditions. To investigate which fraction of the exposed cells contribute to the growth curve, cells were stained with Ki67 as an indicator of active cycling. Figure 5.3B shows that the fraction of proliferating cells one day after photoexposure was very low in the more severe exposure condition, and progressively increased hereafter. Together these results indicate that although the majority of the cells survived the photoexposure, many of them exited the cell cycle.

To study which fraction of the cells reenters the cell cycle to the proliferating cell population after exposure to photopolymerization, a colony forming unit assay was performed (Figure 5.4). After UV-exposure, colonies were formed days later and at lower frequency than the control. Some MSCs started to form colonies after the lag phase, with 6 CFU per 10^4 cells when treated with 0.1% (w/v) Irgacure 2959 and 1800 mJ/cm^2 UV light, as compared to 2400 CFU per 10^4 cells in the unexposed group. These findings indicate that after photoexposure only a fraction of the cells that survive the treatment reenter the cell cycle and contribute to repopulation of the well.

DNA damage

To study the effect of UV-exposure on the extent of DNA damage, staining of photoexposed MSC monolayers for the presence of p53BP1 foci was determined as a measure of DNA damage in the cells. We compared the amount of p53BP1-positive cells in non-UV exposed and photoexposed monolayers and the results are presented in Figure 5.5A and Supplemental Figure 5.1. While the percentage of p53BP1-positive cells in the control group remained stable over the course of three days (around 10%), the percentage of positive cells in the photoexposed groups was considerably higher after one hour of exposure. The number of p53BP1-positive cells reached 66% in the sample exposed to the most severe condition, then decreased towards 20% within three days, most likely as a result of repair. The amount of positive foci per cell followed a comparable trend (Figure 5.5B).

The presence of p53BP1 foci was also assessed in embedded MSCs after one-week culture in HA en PG hydrogels (Figure 5.5C,D). The number of p53BP1-positive cells averaged 10% both in HA and PG gels, without differences between photopolymerization conditions.

Apoptosis and senescence analysis

Staining of caspase-3, a key protease activated during the early stages of apoptosis, demonstrated that around 2% of attached MSCs, treated with 0.1% (w/v) Irgacure 2959 and 1800 mJ/cm^2 of UV light were apoptotic after 24 h, as compared to less than 1% of the control cells (Figure 5.6 and Supplemental Figure 5.2).

Staining of β-galactosidase (Supplemental Figure 5.3), a biomarker that identifies senescent cells in low-density culture,[426,427] showed that more cells were senescent in more severe photoexposure conditions, reaching a maximum of 13% senescent cells in the group treated with 0.1% (w/v) Irgacure 2959 and 1800 mJ/cm^2 of UV light (Figure 5.7). These findings indicate that from all the adherent cells that survive the photoexposure only a small fraction is apoptotic or senescent.

Osteogenic differentiation of monolayers

Cell fate analysis includes the differentiation potential of the photoexposed osteoprogenitor cells. When determining alkaline phosphatase activity present early during osteogenic differentiation, we observed that seven days after photoexposure ALP activity was detected in all the conditions, when compensated for the cell-loss occurring during photoexposure (Figure 5.8A–D), without statistically significant differences between the photoexposure groups.

Immunocytochemical analysis of MSCs incubated for two and three weeks revealed the presence of the late osteogenic markers collagen type I and osteocalcin, in both the non-photoexposed and photo-treated cells (Figure 5.8E–H). This means that the photoexposed cells retain the ability to differentiate along the osteogenic lineage, comparable to unexposed control cells.

Effect of photopolymerization on encapsulated cell survival

Survival of cells encapsulated in two different photopolymerized hydrogels (namely methacrylated hyaluronic acid and methacrylated hyperbranched polyglycerol) was investigated. MSCs were dispersed in aqueous solutions of the hydrogel precursors and Irgacure 2959, and hydrogels with entrapped cells were then formed by UV irradiation (for details see materials and methods section). Survival of embedded MSCs was measured in unphotopolymerized hydrogels and compared to viability of cells embedded in photopolymerized hyaluronic acid (HA) and polyglycerol (PG) gels (n = 3 per condition) one day after hydrogel formation (Figure 5.9A). In HA hydrogels comparable MSC viability was observed for all photopolymerization conditions; overall we observed 80% cell-survival after one day of incubation. Also in PG hydrogels, comparable viability was seen for all photopolymerized gels and non-photoexposed gel, measuring around 75%. Importantly, this demonstrates that photopolymerization in the presence of the hydrogel precursors does not negatively influence cell-survival, whereas some cells damage is observed (Figure 5.2), once the cells are exposed to UV-light and photoinitiator only. This means that the radicals formed do their 'jobs' (initiating the polymerization) when hydrogels precursors are present and these reactive species are consequently unavailable to damage cellular components.

We also studied the viability of MSCs, embedded in hydrogels obtained by 1800 mJ/cm^2 UV exposure in the presence of 0.05% (w/v) or 0.1% (w/v) Irgacure 2959 for osteogenic differentiation, at one, two and three weeks (Figure 5.9B). After one week, 60% of the embedded cells were alive in HA gels, as compared to 50% viable cells encapsulated in PG gels. In the following two weeks, the percentage of viable cells embedded in photopolymerized HA and PG hydrogels increased to respectively 76% and 66% living cells, likely as a result of proliferation.

Osteogenic differentiation in gels

The presence of alkaline phosphatase in the encapsulated MSCs in HA and PG hydrogels, obtained by 1800 mJ/cm^2 UV exposure in the presence of 0.05% (w/v) or 0.1% (w/v) Irgacure 2959 (Figure 5.10A), was studied after one and two weeks. In PG gels, the cells exhibited a round morphology after one and two weeks, and expressed alkaline phosphatase to a higher level after two weeks, reaching a maximum of 6% of total cells (Figure 5.10B). The MSCs exhibited better stretching in HA gels, accompanied by a significantly higher expression of alkaline phosphatase after two weeks than after one week, reaching a maximum of 30% positive cells. The amount of ALP-positive cells was comparable between the two studied polymerization conditions, both for HA and PG hydrogels. Significantly more ALP positive cells were present in HA gels than in PG gels, obtained at the same photopolymerization presets, both after two and three weeks. This means that the natural HA hydrogel provided a better matrix for osteogenic differentiation of embedded MSCs than the fully synthetic PG gel.

General discussion

The current study evaluates the toxicity of a photopolymerization process to monolayers and encapsulated MSCs, and assesses the proliferation and differentiation of these cells upon exposure to UV-light and photoinitiator Irgacure 2959, under conditions regularly applied in numerous cell-based TE applications.[152,212,428] MSCs are widely used cells in TE research due to their multilineage potential and are often embedded in photopolymerizable hydrogels to study their differentiation capacity. While most of the studies evaluating the effect of photopolymerization on photoexposed cells solely focus on the viability of the cells, in this study we for the first time characterize in more detail further fate of the photoexposed cells. We demonstrate profound adverse effects of photopolymerization on viability and cell cycling capacity of the exposed cells, while the ability of MSCs to differentiate along the osteogenic lineage is retained. We further show that upon encapsulation in photopolymerizable hydrogels the viability of the embedded cells is no longer affected by the photopolymerization conditions, and that the osteogenic differentiation potential is dependent on the type of hydrogel used.

The wavelength of UV-light used in the study falls within the range of UVA, the radiation dose used is comparable to other cell encapsulation applications,[351] and is considered clinically safe.[351] The exposure conditions studied here provide acceptable photopolymerization times for gelation and cell encapsulation. Treating cells with only ultraviolet light at an intensity of 6 mW/cm2 exhibited a slight adverse effect for an exposure time of 300 s. This is in contrast to findings of others,[349] likely due to our longer follow-up time and the use of primary cells instead of a cell-line. We found that Irgacure 2959 concentrations used hardly affect cell viability and provide a sufficient rapid rate of photopolymerization at the studied light intensity (polymerization complete within minutes). Free radicals are formed when the initiator solution is exposed to the light of appropriate wavelength, and subsequently react with carbon–carbon double bonds of the monomers or can attack the encapsulated cells. The free radicals can potentially damage the photoencapsulated cells by their reaction with cell membranes, nucleic acids and proteins, which can lead to cell death.[429] The combined effect of photoinitiator and UV exposure is demonstrated by progressively lower cell survival of MSCs in our study. As UV exposure and photoinitiator show a synergistic (negative) effect on cell viability, we conclude that the production of free radicals is mainly responsible for the negative effect. Our findings are in contrast to studies conducted on fibroblast cell lines,[349,430] in which no detrimental effects with doses of 780–3600 mJ/cm2 and 0.05%–2% (w/v) Irgacure 2959 were observed. This could be explained by

differences in the sensitivity of the cells leading to a variable effect of photoexposure on different cell types.[350] When considering the proliferation of the photoexposed cells, we detect a lag phase in their growth curve, during which the exposed cells exit the cell cycle to remain in G_0, and where after the cells reenter the cell cycle and repopulate the well. Looking at the Ki67 staining and the CFU data of photoexposed MSCs, we observe that only a small fraction of the cells is responsible for the repopulation of the well. Finding that the fraction of Ki67-positive cells in the photoexposed groups is higher than the amount of the cells responsible for colony-formation indicates that many cells do not pass the checkpoint towards mitosis. We further demonstrate that part of the photoexposed cells exit the cell-cycle either towards apoptosis (2% in the photoexposed group versus 1% in regular culture) or towards irreversible cell cycle arrest (up to 13% senescent cells in the photoexposed group versus 1% in control culture).

As has been demonstrated in other studies, senescent and irradiated cells display DNA damage foci that contain p53BP1.[419,420] We demonstrate that already one hour after photoexposure, MSC monolayers contain an increased amount of p53BP1 foci compared to the unexposed controls indicating a certain degree of DNA damage. However, we also demonstrate that the percentage of positive cells and the amount of positive foci per cell drastically decrease within three days after exposure, suggesting that the damage is being repaired. As we found minimal proliferative capacity of photoexposed cells in the first days after exposure, this option is most probable.

Taken together, our findings indicate that of all the adherent, viable cells present after photoexposure, most are neither apoptotic, senescent nor replicating, but are in a resting state of quiescence, and in time most probably get overgrown by a small group of actively dividing cells. Regarding a substantial number of cells dying as a result of photopolymerization and a large fraction of resting cells in the photoexposed monolayers, it would be attractive to positively affect the survival and induce proliferation of the quiescent photoexposed cells. Measures to achieve this could include the addition of exogenous antioxidants,[431,432] induction of intracellular anti-oxidant synthesis[432] or targeting growth factors that affect proliferative capacity.[433-435]

The viability of hydrogel-encapsulated cells was not greatly affected by the various polymerization modalities. Both in hyaluronic acid and in polyglycerol gels, obtained at different photopolymerization conditions, we observed comparable viability of encapsulated cells, also at the most severe UV exposure of 1800 mJ/cm^2 in the presence of 0.1% (w/v) Irgacure 2959. This striking difference between moderate viability of monolayers and unaffected encapsulated cells could be explained by the presence of propagating macromers during photopolymerization. While monolayers are exposed to higher doses of free radicals reacting with the MSCs and partly with the serum, inside the gels most of the free radicals formed will quickly react with the photoresponsive groups of the surrounding monomers, and will not affect the cells to the full extent. This is substantiated by DNA damage analysis of encapsulated MSCs, which revealed an average 10% of p53BP1-positive cells, comparable to the degree of DNA damage in nonphotoexposed monolayers. Although we observed no differences between cell-survival at various photopolymerization conditions, the hydrogel type itself significantly influenced the survival and differentiation of encapsulated cells. Hyaluronic acid based
hydrogel, in essence a polysaccharide modified with photosensitive groups, provided an adequate environment to encapsulated cells, supporting survival of a larger fraction of MSCs as compared with polyglycerol-based hydrogel. Diverse adhesiveness of the two materials could in part explain the observed differences in survival, as hyaluronic acid provides the embedded cells with adhesive sequences, while cells are not able to interact with the polyglycerol to the same extent. This is illustrated by the observation that encapsulated cells adhered and stretched in crosslinked hyaluronic acid gels, but remained round in polyglycerol. Comparably, the hyaluronic acid gel

provided better conditions for osteogenic differentiation of encapsulated MSCs with up to 30% cells positive for the early osteogenic marker ALP, as compared to only 5% in crosslinked polyglycerol hydrogel. It was demonstrated for photopolymerizable hydrogels previously that addition of adhesive sequences indeed promotes survival and osteogenic differentiation of the embedded MSCs.[232,436]

When considering application of photopolymerizable hydrogels as scaffold matrices, employed for organ printing of TE grafts or as injectables, other factors than cytocompatibility will also affect the final choice of the material. Mechanical stiffness of the formed photopolymerized gels and their degradability have a profound influence on tissue development by the embedded cells.[220,387,394,437] With regard to the two hydrogels investigated in this study, we expect hyaluronic acid-based gels to clear in time by natural enzymatic degradation, while polyglycerol-based material is likely to be much less degradable, but forms a stable, mechanically stronger hydrogel scaffold.[423,424]

Conclusion

Photopolymerization is an attractive method to crosslink hydrogel-forming polymers, resulting in mechanically strong, stable matrices suitable for cell-encapsulation. We demonstrate adverse effects of photopolymerization on viability and cell cycle progression of exposed MSC monolayers, while their differentiation potential remains unchanged. We also show that the viability of encapsulated cells is not adversely affected by photopolymerization of the surrounding hydrogel, which is likely the result of lower amounts of free radicals available for cell-damage. We conclude that the influence of photoexposure on cell-cycle progression, which is often cautioned for in 2D, is well tolerated when applying the cells in hydrogels. The two hydrogels tested in this study support survival and osteogenic differentiation of the embedded cells to a variable degree, and constitute potential materials to create layered scaffolds for TE or for design of layered matrix drug release devices.

Acknowledgements

We would like to thank the department of Immunopathology of University Medical Center Utrecht, The Netherlands and Hugo Alves from the Department of Tissue Regeneration, University of Twente for their assistance with immunocytochemical stainings. We would like to acknowledge the financial support of the Mosaic scheme 2004 of the Netherlands Organisation for Scientific Research (NWO; grant number: 017.001.181), the Foundation De Drie Lichten and the Dutch Platform for Tissue Engineering (project number: UGT.6743).

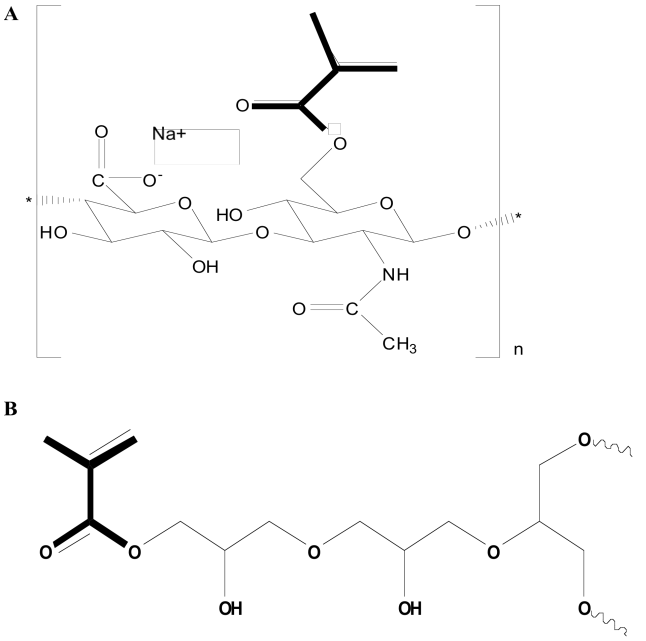

Figure 5.1 A schematic presentation of the crosslinkable methacrylated hyaluronic acid (A) and methacrylated hyperbranched polyglycerol, of which a fragment is depicted (B).

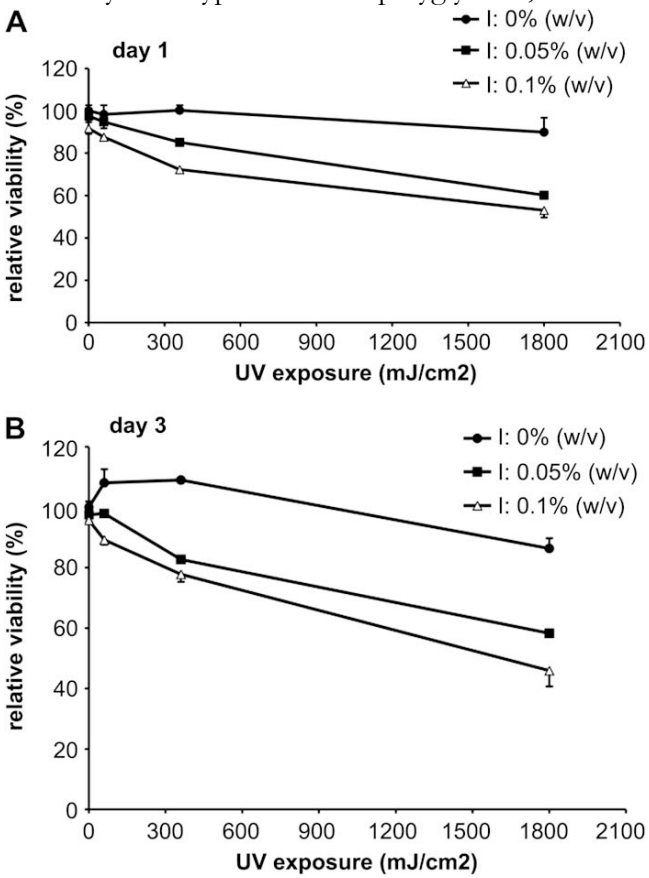

Figure 5.2: Viability of monolayers after photoexposure. Viability of MSC monolayers after exposure to UV light (0 mJ/cm^2, 60 mJ/cm^2, 360 mJ/cm^2 or 1800 mJ/cm^2) and Irgacure 2959 (referred to as I) at 0% (w/v), 0.05% (w/v) or 0.1% (w/v). The percentage of viable cells is presented relative to the non-exposed control (0 mJ/cm^2 UV; 0% (w/v) I), one day (A) and three days (B) after the photoexposure. Data are presented as mean ± standard error of the mean (SEM), determined in duplicate.

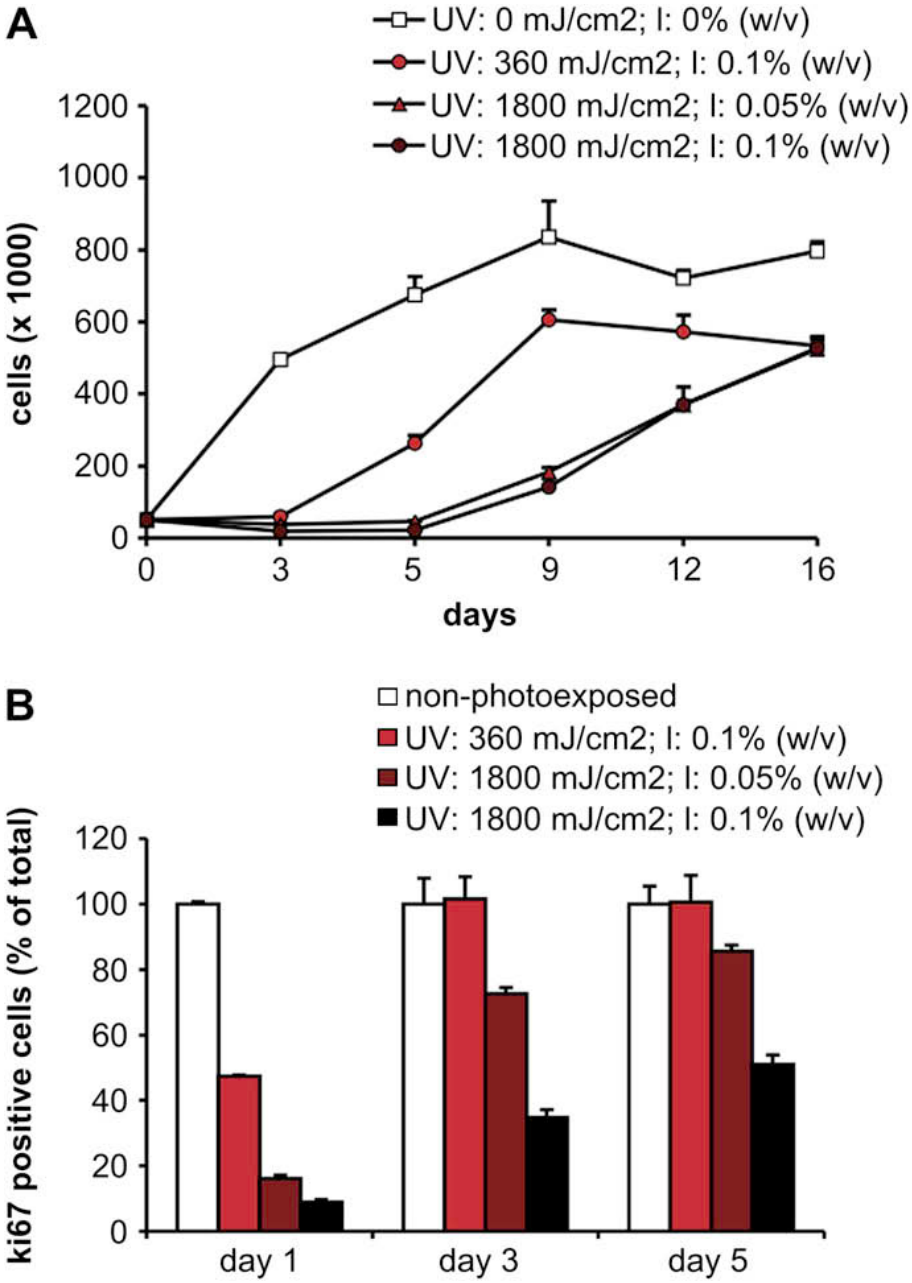

Figure 5.3: Proliferation of monolayers after photoexposure. Number of cells (A) and the percentage of proliferating MSCs after photoexposure (B). Proliferation in all photoexposed groups was reduced compared to the unexposed control. One day after exposure, the percentage of proliferating cells was lower in photoexposed groups than in unexposed controls. After five days, the percentage of proliferating MSCs exposed to most severe photopolymerization condition increased from 10% to 50%, but remained lower than in other groups. Data presented as mean ± SEM, determined in duplicate.

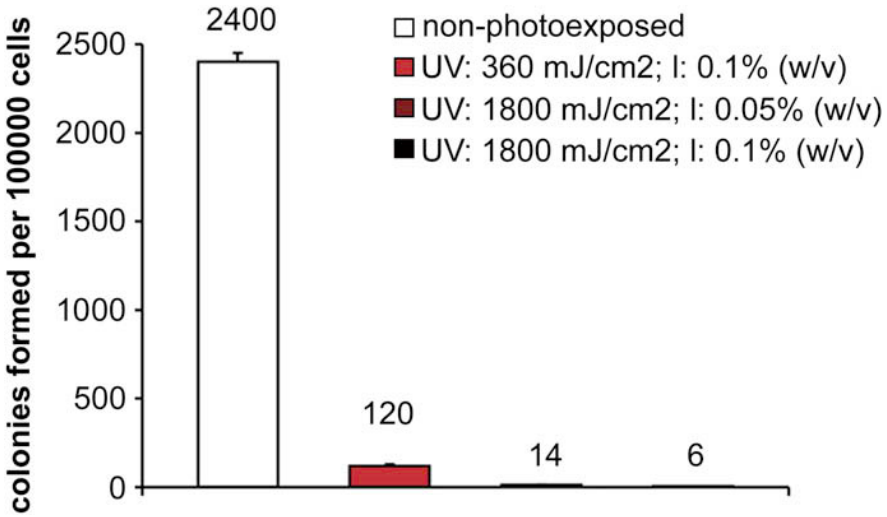

Figure 5.4: Colony-forming unit efficiency of MSCs after photoexposure. Data represent mean ± SEM, determined in duplicate.

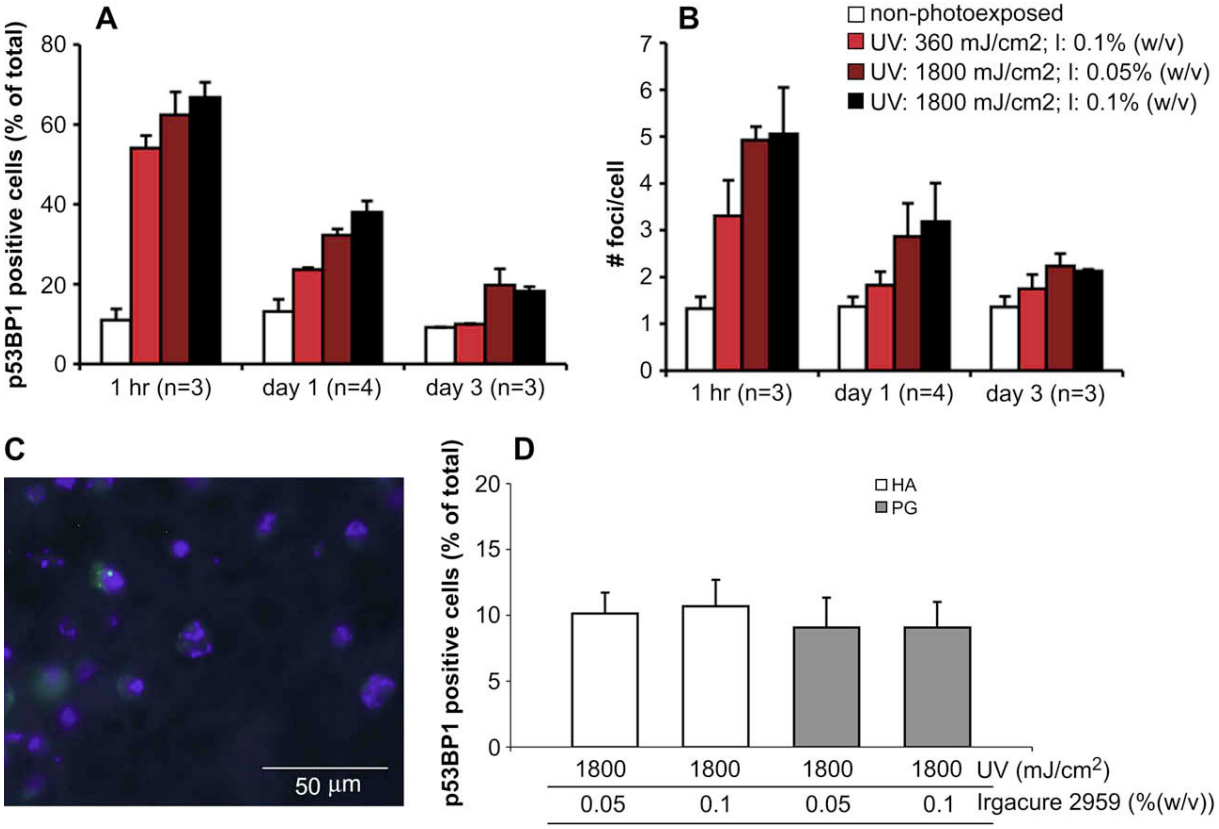

Figure 5.5: DNA damage after photoexposure. A–B: p53BP1-immunocytochemistry of MSC monolayers one hour, one day and three days after photoexposure. A: percentage of p53BP1-positive MSC; data presented as mean ± SD. After one day, the amount of p53BP1-positive cells was significantly higher in all photoexposed MSCs compared to unexposed control ($p < 0.01$). The percentage of p53BP1-positive cells remained stable at around 10% over the course of three days, while it significantly decreased from 54 ± 3% to 10% for cells exposed to 360 mJ/cm^2 UV and 0.1% (w/v) I ($p < 0.01$), from 62 ± 6% to 20 ± 4% for cells exposed to 1800 mJ/cm^2 UV and 0.05% (w/v) I ($p = 0.01$) and from 67 ± 4% to 18 ± 1% for cells exposed to 1800 mJ/cm^2 UV and 0.1% (w/v) I ($p < 0.01$). B: number of p53BP1-foci per cell. C: p53BP1-

immunocytochemistry of embedded MSCs seven days after photoexposure (PG gel exposed to 1800 mJ/cm^2 UV light and 0.05% (w/v) Irgacure 2959). All nuclei are stained blue with DAPI; p53BP1-positive cells contain bright green nuclear foci. D: percentage of p53BP1-positive hydrogel-embedded MSCs; data presented as mean ± SD, (n = 4).

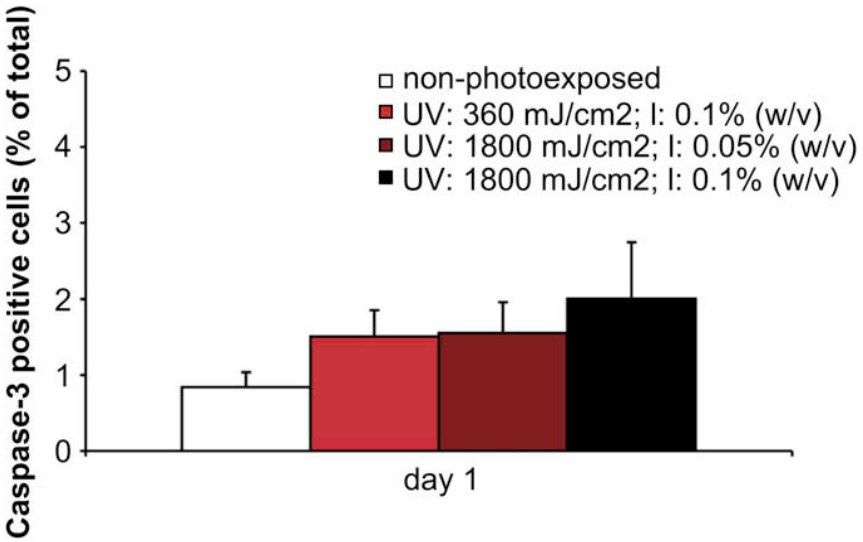

Figure 5.6: Apoptosis after photoexposure. Caspase-3 staining of MSC one day after photoexposure; percentage of apoptotic MSCs (n = 4) is presented as mean ± SD, The percentage of apoptotic cells in the group exposed to 1800 mJ/cm^2 UV light and 0.1% (w/v) Irgacure (2.0 ± 0.7%) was significantly higher than in the unexposed group (0.8 ± 0.2%; $p < 0.01$), while no statistically significant differences were found between the different photoexposure conditions.

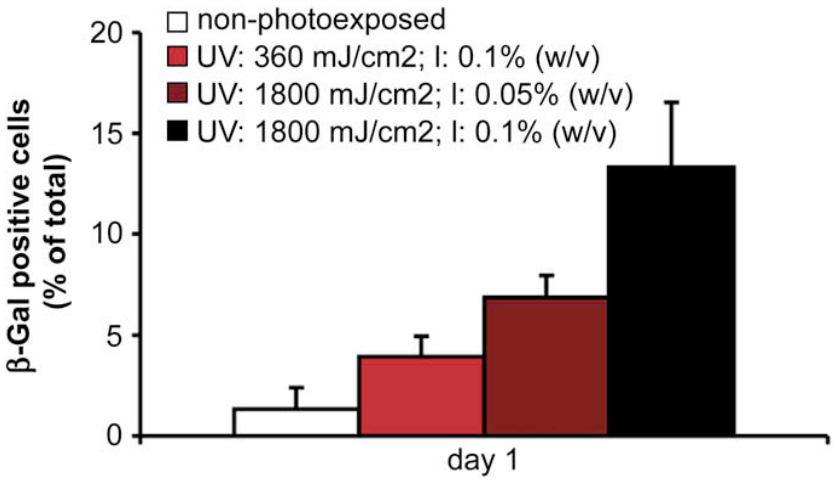

Figure 5.7: Senescence after photoexposure. β-Galactosidase activity in MSCs, one day after photoexposure; percentage of β-galactosidase-positive MSCs is presented as mean ± SD, (n = 4). The number of β-galactosidase-positive cells was significantly higher in the MSC exposed to most severe photopolymerization condition (1800 mJ/cm^2 UV light and 0.1% (w/v) Irgacure 2959), than in other groups ($p < 0.01$). There were more β-galactosidase-positive cells among MSCs exposed to 1800 mJ/cm^2 UV light and 0.05% (w/v) Irgacure 2959, than in MSCs exposed to 360 mJ/cm^2 UV light and 0.1% (w/v) Irgacure 2959 (7 ± 1% vs 4 ± 1%; $p = 0.045$).

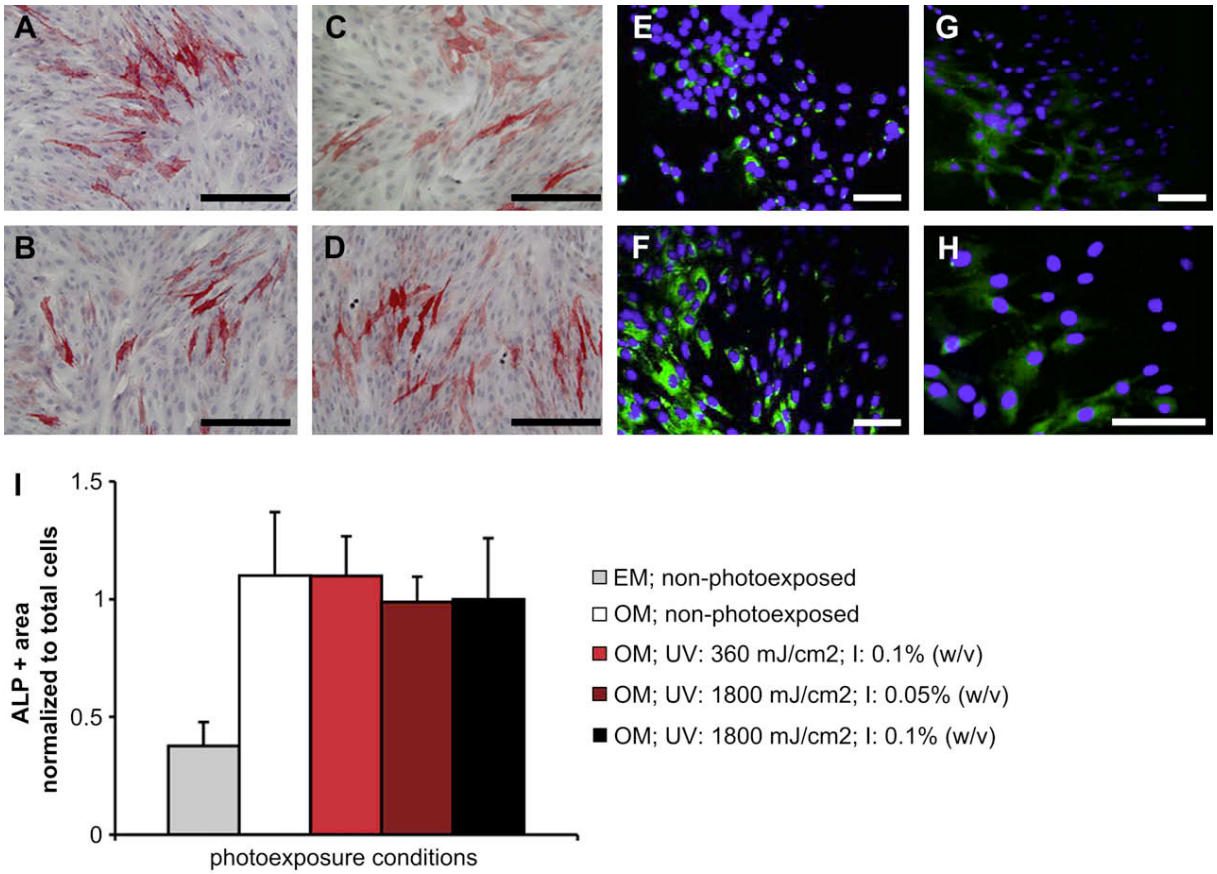

Figure 5.8: Osteogenic differentiation of MSC monolayers after photoexposure. A–D: Alkaline phosphatase (ALP) staining of MSCs, one week after exposure to UV light and Irgacure 2959; ALP-positive cells are stained red; counterstaining with hematoxylin; scale bar: 200 μm. A: non-photoexposed cells; B: MSCs exposed to 360 mJ/cm^2 UV light and 0.1% (w/v) Irgacure 2959; C: 1800 mJ/cm^2 UV light and 0.05% (w/v) Irgacure 2959; D: 1800 mJ/cm^2 UV light and 0.1% (w/v) Irgacure 2959. E–F: Collagen type I production after two weeks in nonphotoexposed (E) and MSCs treated with 1800 mJ/cm^2 UV light and 0.1% (w/v) Irgacure 2959 (F). Collagen type I is stained green, the nuclei of all the cells are stained blue by DAPI; scale bar: 100 μm. G–H: Osteocalcin production after three weeks in non photoexposed (G) and MSCs treated with 1800 mJ/cm^2 UV light and 0.1% (w/v) Irgacure 2959 (H), osteocalcin is stained green, the nuclei of all the cells are stained blue by DAPI nuclear stain; scale bar: 100 μm. I: Percentage of ALP-positive cells in different conditions one week after photoexposure; EM: expansion medium, OM: osteogenic medium. Data is presented as mean ± SD, from two independent experiments (total of n = 8). Percentage of ALP-positive cells was significantly smaller in the expansion medium than in groups treated with osteogenic medium ($p < 0.01$); there were no statistically significant differences between the photoexposure groups.

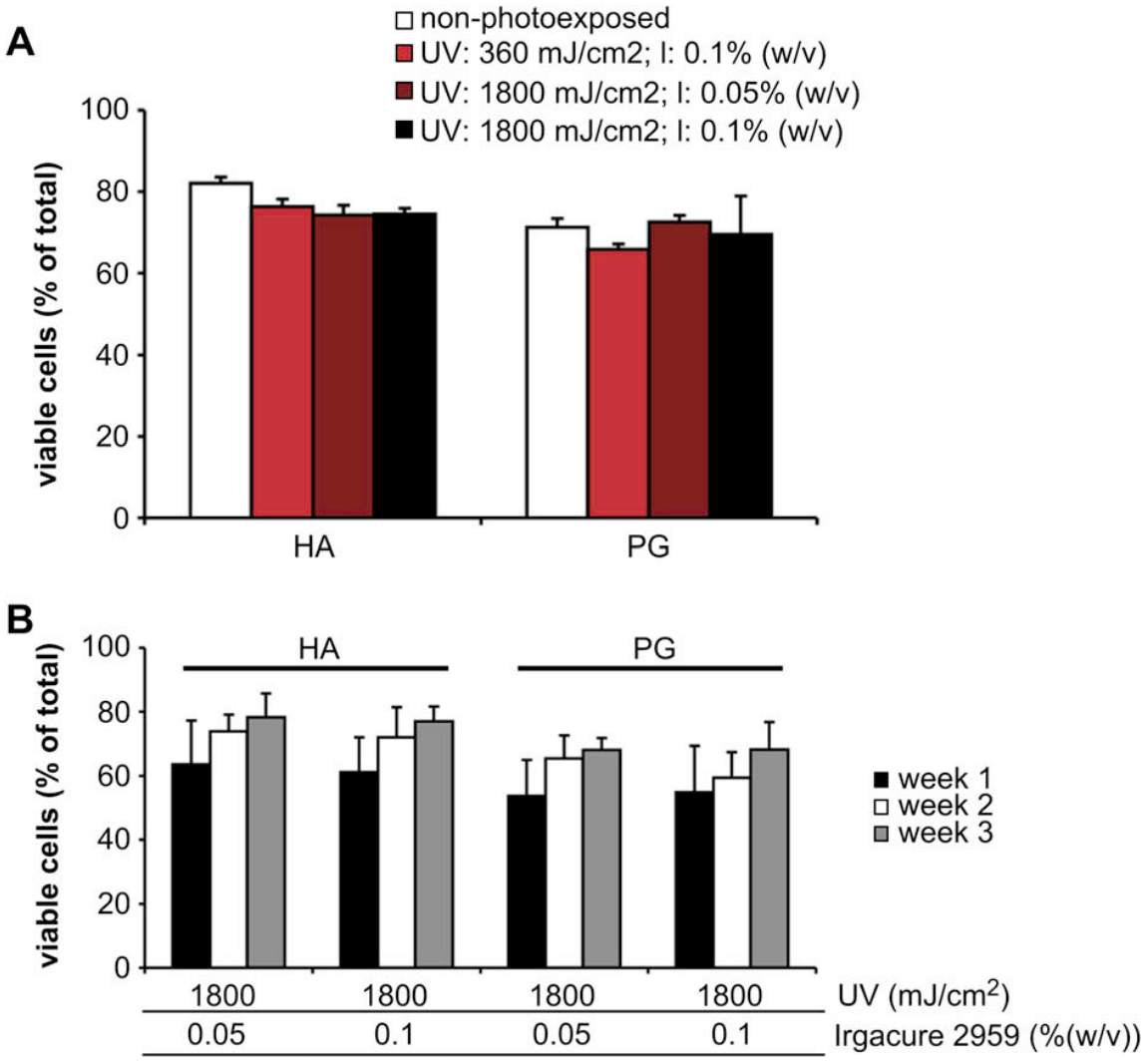

Figure 5.9: Viability of encapsulated MSCs. Viability in photopolymerized hyaluronic acid hydrogel (HA) and polyglycerol hydrogel (PG) as measured with LIVE/DEAD staining. A: viability one day after photoexposure; data presented as mean ± SD, (n = 3). No statistically significant differences were seen between the photoexposure conditions, both for HA and PG. B: viability of MSCs at one, two and three weeks after photoexposure; data presented as mean ± SD, from two independent experiments (total of n = 5). After three weeks, the percentage of viable MSCs was higher in HA obtained by 1800 mJ/cm^2 UV light and 0.05% (w/v) Irgacure 2959 than in both PG gels (76 ± 7% vs 68 ± 4% and 68 ± 9%; p = 0.033 and p = 0.027, respectively).

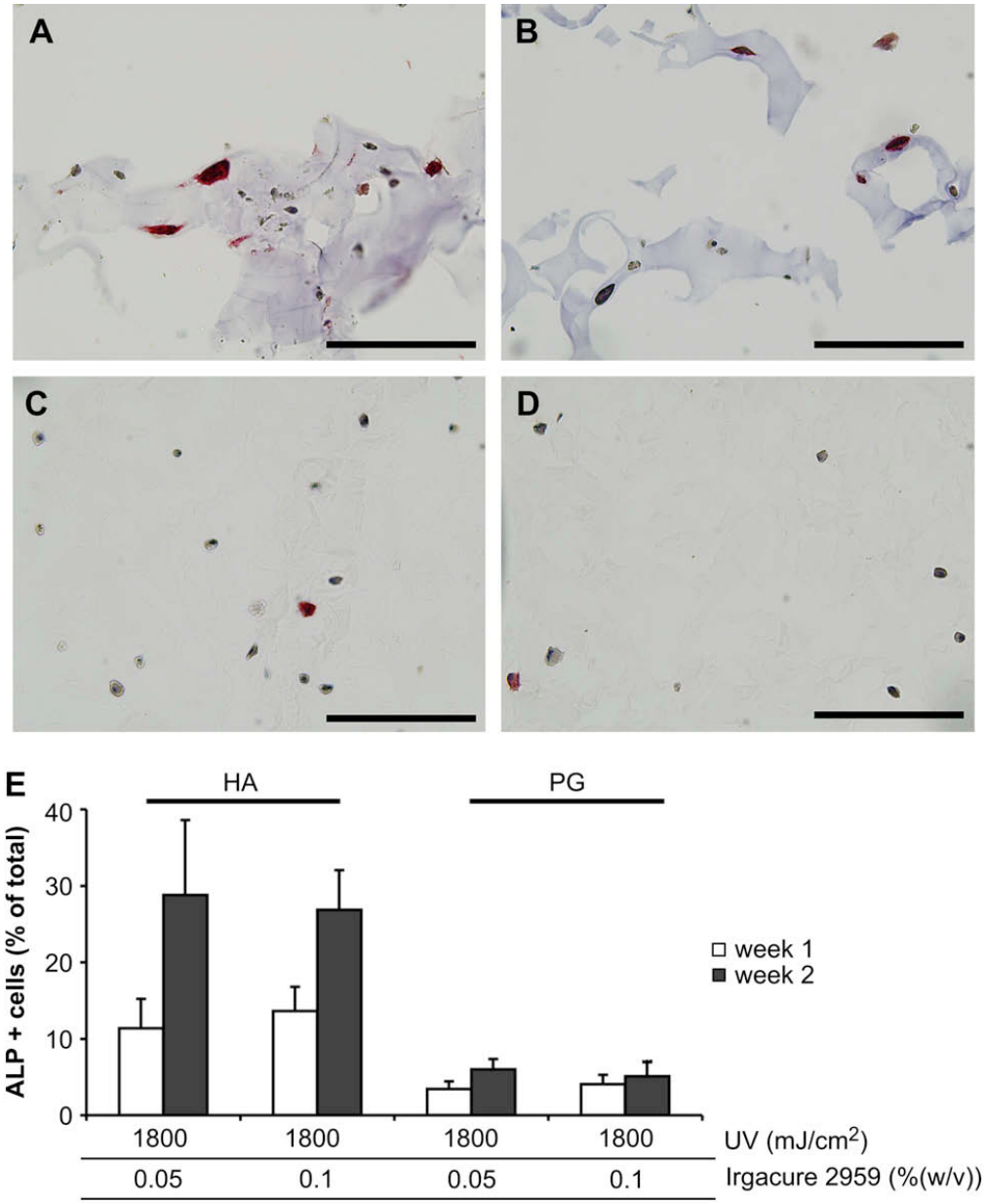

Figure 5.10: Osteogenic differentiation of MSCs in photogels. Alkaline phosphate (ALP) activity of MSCs embedded in HA and PG gels for one or two weeks. A–D: representative pictures of MSCs in HA and PG gels after two weeks of encapsulation; ALP-positive cells are stained red; nuclei are stained blue; scale bar: 100 μm. A–B: HA gels obtained by exposure to 1800 mJ/cm^2 UV light and 0.05% (w/v) and 0.1% (w/v) Irgacure 2959 respectively. C–D: PG gels exposed to 1800 mJ/cm^2 UV light and 0.05% (w/v) and 0.1% (w/v) Irgacure 2959 respectively. E: Percentage of ALP-positive cells in photopolymerized gels; data presented as mean ± SD, from two independent experiments (n = 4). After one and two weeks, the percentage of ALP-positive cells in both HA gels was higher than in PG gels ($p < 0.01$), and was not significantly different between the gels obtained at different photoexposure conditions.

Supplementary material

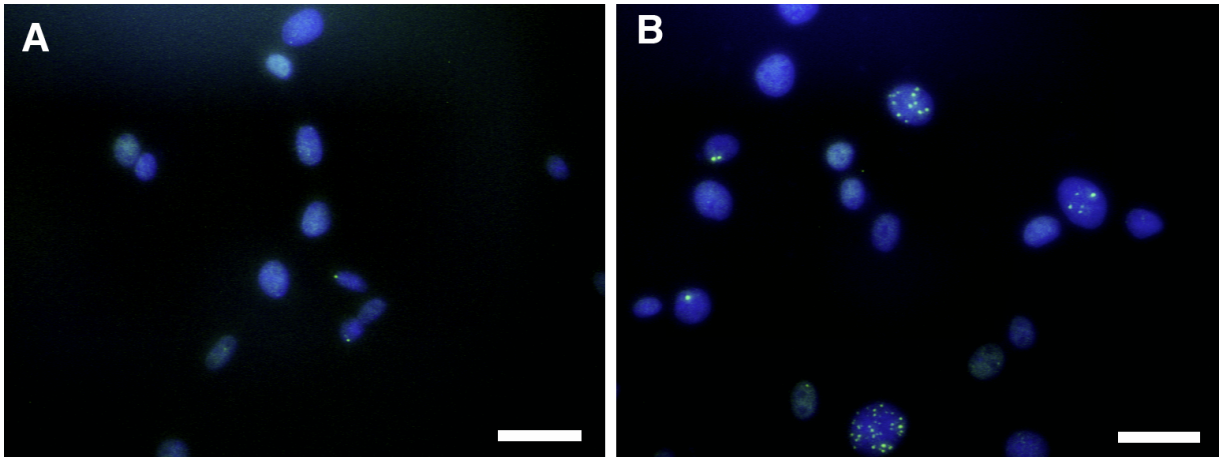

Supplemental Figure 5.1: p52BP1-positive cells after photoexposure. Representative pictures of p53BP1-stained cells one day after photoexposure: A: non-photoexposed cells; B: MSCs exposed to 1800 mJ/cm^2 UV light and 0.1% (w/v) Irgacure 2959; scale bar: 50 μm. All nuclei are stained blue with DAPI; p53BP1-positive cells contain bright green nuclear foci.

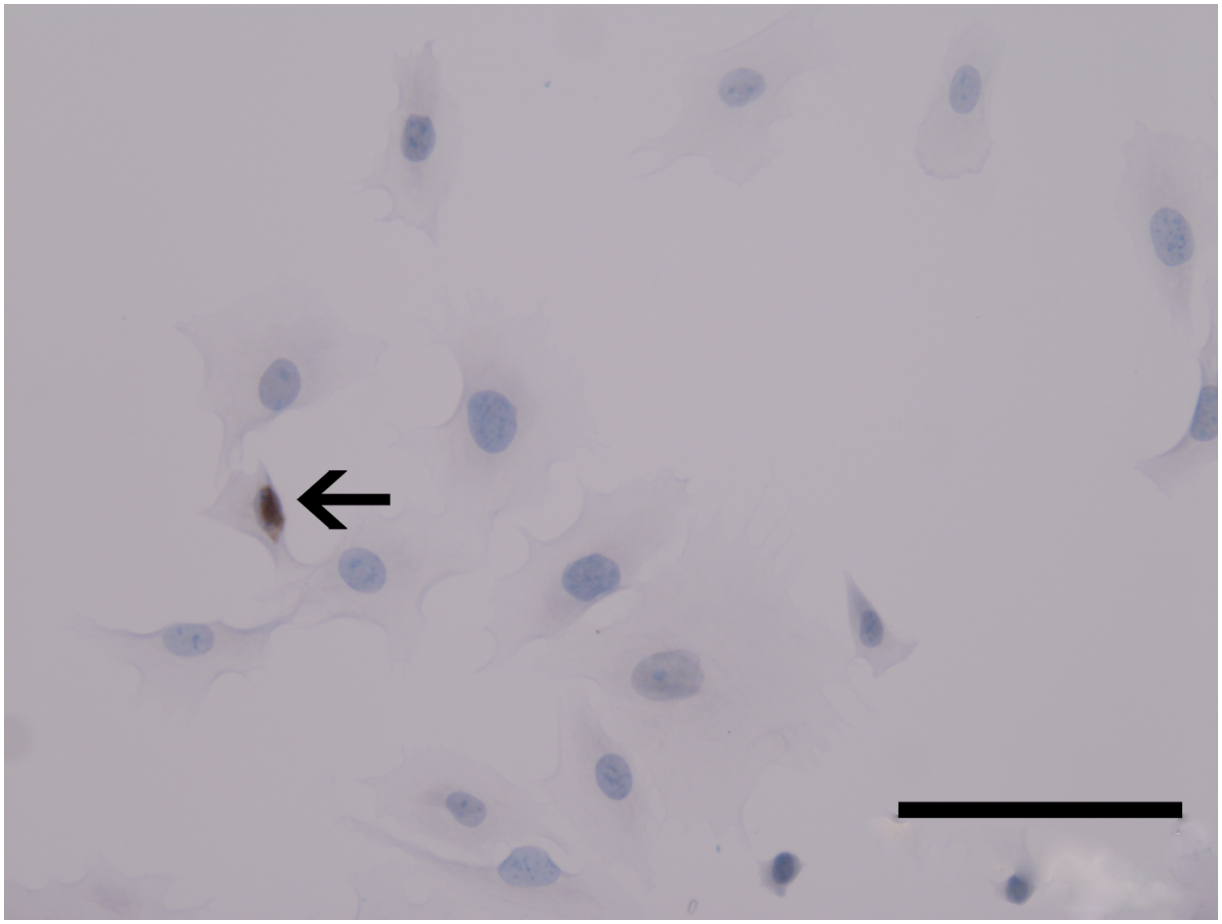

Supplemental Figure 5.2: Apoptosis after photoexposure. Representative picture of MSCs exposed to 360 mJ/cm^2 UV light in the presence of 0.1% (w/v) Irgacure; active caspase-3 positive cell is stained dark brown (arrow), scale bar: 100 μm.

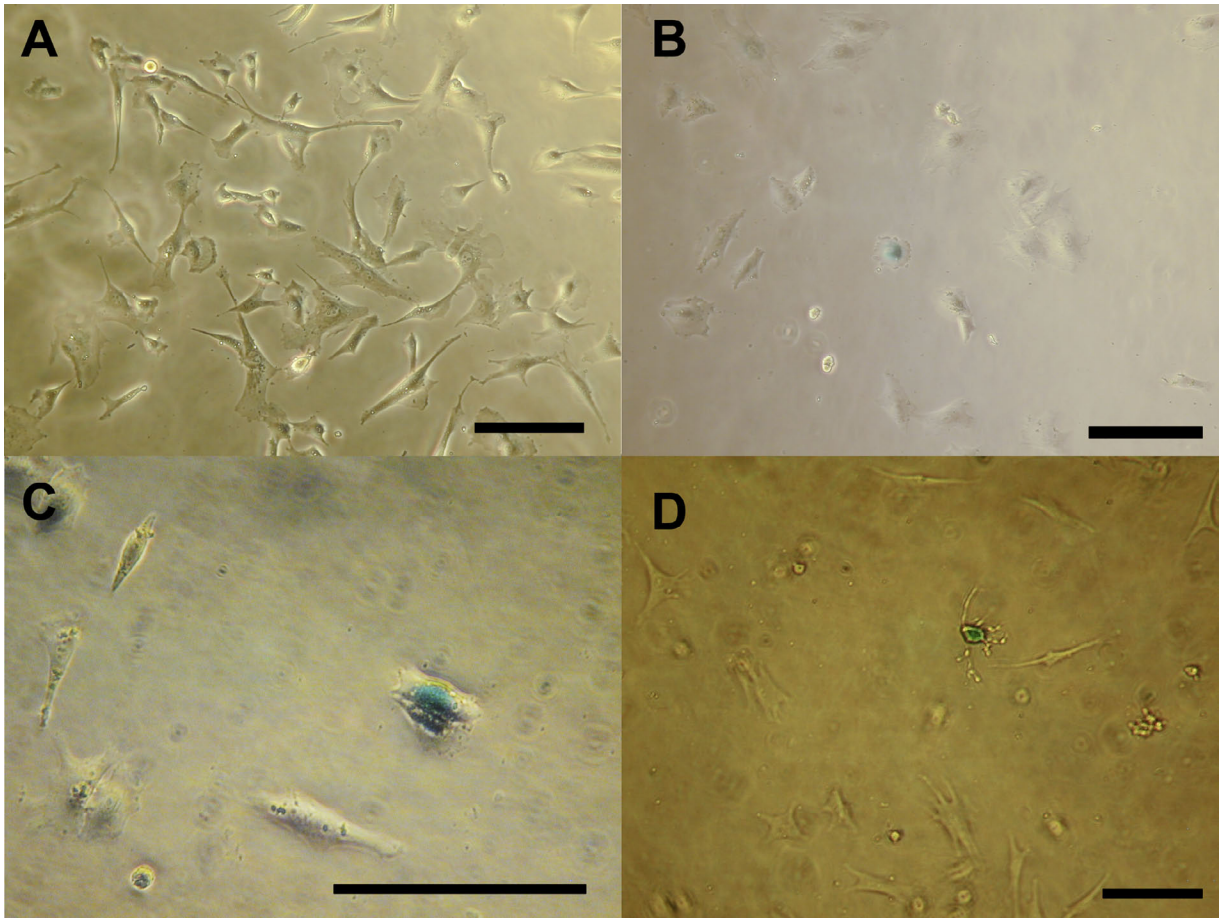

Supplemental Figure 5.3: Senescence after photoexposure. Representative pictures of ß-galactosidase-positive cells (blue) at different photoexposure conditions, scale bar: 100 µm. A: non-photoexposed cells; B: MSCs exposed to 360 mJ/cm^2 UV light and 0.1% (w/v) Irgacure 2959; C: 1800 mJ/cm^2 UV light and 0.05% (w/v) Irgacure 2959; D: 1800 mJ/cm^2 UV light and 0.1% (w/v) Irgacure 2959.

Chapter 6

Evaluation of photocrosslinked Lutrol hydrogel for tissue printing applications

Fedorovich NE[1], Swennen I[2], Girones J[2], Moroni L[3], van Blitterswijk CA[3], Schacht E[2], Alblas J[1], Dhert WJA[1,4]

Biomacromolecules. 2009, 10(7):1689–1696

[1]*Department of Orthopaedics, University Medical Center Utrecht, Utrecht, The Netherlands*
[2]*Polymer Chemistry and Biomaterials Research Group, Ghent University, Ghent, Belgium*
[3]*Institute for BioMedical Technology (BMTI), University of Twente, Enschede, The Netherlands*
[4]*Veterinary Medicine, Utrecht University, Utrecht, The Netherlands*

Abstract

Application of hydrogels in tissue engineering and innovative strategies such as organ printing, which is based on layered 3D deposition of cell-laden hydrogels, requires design of novel hydrogel matrices. Hydrogel demands for 3D printing include: 1) preservation of the printed shape after the deposition; 2) maintaining cell viability and cell function and 3) easy handling of the printed construct. In this study we analyze the applicability of a novel, photosensitive hydrogel (Lutrol) for printing of 3D structured bone grafts. We benefit from the fast temperatureresponsive gelation ability of thermosensitive Lutrol-F127, ensuring organized 3D extrusion, and the additional stability provided by covalent photocrosslinking allows handling of the printed scaffolds. We studied the cytotoxicity of the hydrogel and osteogenic differentiation of embedded osteogenic progenitor cells. After photopolymerization of the modified Lutrol hydrogel, cells remain viable for up to three weeks and retain the ability to differentiate. Encapsulation of cells does not compromise the mechanical properties of the formed gels and multilayered porous Lutrol structures were successfully printed.

Introduction

Organ printing is a novel approach in tissue engineering, based on layered strand- or drop wise deposition of cell-laden hydrogels.[28] This rapid prototyping-derived approach yields structured 3D scaffolds, with predetermined external shape and internal morphology, and can ensure defined cell placement. By printing different cell types at defined locations within a single scaffold, one could mimic natural cell distribution. So far, the organ printing approach has been used to make tubular-like structures of hydrogel laden with endothelial cells[112] and to design various coculture systems.[106,120,438] To use organ printing to construct vascularized bone grafts, endothelial cells together with bone progenitors might be a good combination, as both cell types showed enhanced functionality in cocultures.[71]

Hydrogels can be processed by a manifold of organ printing techniques and allow homogeneous encapsulation of cells and bioactive molecules.[407] For embedded cells, hydrogels provide a support matrix with a highly hydrated microenvironment that is amenable to nutrient and oxygen diffusion. For optimal use in organ printing, fast gelation is necessary during stacking of subsequent layers. Furthermore, the gel must be noncytotoxic and have an adequate stability and mechanical properties for *in vitro* culture and *in vivo* implantation. Depending on the type of tissue that is printed, the gel should ideally provide the embedded cells with the proper biochemical and physical stimuli to guide cellular processes such as migration, proliferation, and differentiation. Hydrogels used for organ printing so far include sodium alginates,[112,115] collagen and Pluronics,[198] each suffering from their own drawbacks like lack of adhesive/biomimetic sequences, low mechanical properties, and instability in culture, respectively. The development of more suitable, tailored hydrogel matrices is therefore highly desirable.

Solutions of thermosensitive polymers undergo a temperature-dependent gel formation, based on physical interactions between the polymer units. Particularly, inverse thermogelling polymers exhibiting lower critical solution temperature (LCST) behavior are popular as injectable matrices for tissue engineering (TE)[202] but may also be used for organ printing. Such gels can preserve their shape very well during printing, but they dissolve relatively fast after gelation.[308,430,439]

Crosslinking by photopolymerization of water-soluble polymers containing methacrylate groups using UV or visible light in the presence of photoinitiators offers spatial and temporal control over polymerization, with high polymerization rates at physiological temperatures and minimal heat production.[201] Some of the photoinitiators, including Irgacure 2959, were shown to exhibit adequate toxicological profile, with good cytocompatibility measured through analysis of cellular metabolic activity at concentrations ≤0.05% (w/v).[349,350] Therefore, the addition of photosensitive groups to a thermosensitive hydrogel would be ideal for organ printing, with additional covalent crosslinks allowing manipulation and subsequent culture of the printed scaffolds. Low photoinitiator concentrations and low intensity UV-light should be used to minimize possible adverse effects of exposure of the embedded cells to free radicals. Findings from earlier studies indicate that higher doses of photoexposure compromises proliferation and cell cycle progression of the exposed MSC.[440] Therefore, a balance between UV dosage ensuring adequate photocrosslinking of the polymer while maintaining functionality of the exposed cells is required.

In this study, the concept of organ printing is combined with a recently developed photopolymerizable Lutrol hydrogel to benefit from its fast temperature-responsive gelation properties and from the additional stability provided by covalent crosslinking. This photopolymerizable thermosensitive hydrogel is a modification of thermosensitive Lutrol F127 (Lutrol-T in this paper), a pharmaceutical grade of Pluronic F127. The hydrogel is based on

triblock of polyethylene-oxide and polypropylene-oxide modified with methacrylamide groups: Lutrol F127 AlaL polymer (Lutrol-TP from hereon). Photopolymerization of Lutrol-TP yields hydrogels with enhanced mechanical properties, while the degradation profile of this hydrogel can be tuned by varying the chemical composition of the depsi-peptide sequence groups. *In vitro* biological studies, including viability studies, have demonstrated that the materials are well tolerated by human cells.[441,442]

Here, we analyze the applicability of Lutrol-TP hydrogel for bone tissue printing, by investigating the cytotoxicity of original (Lutrol-T) and photosensitive Lutrol-TP hydrogels and by printing cell-laden Lutrol-TP scaffolds. We compare the effect of photopolymerization conditions on cell behavior, both for seeded and hydrogel-embedded goat multipotent stromal cells (MSC). Special focus is put on survival and differentiation of the embedded cells, assessed by viability/cytotoxicity assay and (immuno)cytochemical detection of early and late osteogenic markers, respectively. Further, we demonstrate the feasibility of printing the (cell-laden) Lutrol-TP scaffolds and analyze the mechanical properties of the formed gels.

Materials and methods

Hydrogel

Lutrol F127 (Poloxamer 407; Pluronic F127) was obtained from BASF, ExAct, and is termed Lutrol-T in this paper. Lutrol F127 AlaL (Figure 6.1), termed Lutrol-TP, was synthesized as described in detail.[441] In short, a solution of dehydrated Lutrol F127 (BASF, Germany) in dichloromethane (DCM) was reacted with bromoacetylbromide or 2-bromopropanoylbromide in the presence of poly(4-vinylpyridine) as proton acceptor. The purified F127-di(α-bromoesters), designated as F127-L-Br and F127-G-Br, were used in a reaction with *N*-2,3-dimethylmaleimidoalanine to obtain the modified, photosensitive Lutrol F127-AlaL.

Photopolymerization presets

The photoinitiator used was 1-[4-(2-hydroxyethoxy)-phenyl]-2-hydroxy-2-methyl-1-propane-1-one (Irgacure 2959, Ciba Specialty Chemicals, Basel, Switzerland). A stock solution of 5% (w/v) in PBS (obtained by 30 min incubation at 70°C) was added to the culture medium or hydrogel to create final concentrations of 0, 0.05, or 0.1% (w/v). A Superlite S-UV 2001AV lamp (Lumatec, Munchen, Germany), which emits UVA and blue light (320-500 nm) was used to expose the cells and (cell-laden) hydrogels to the UVA intensity of ~6 mW/cm^2 (X9$_2$ photometer, Gigahertz-Optik GmbH, Puchheim, Germany), for periods up to 300 s.

Cells

Multipotent stromal cells (MSCs) were obtained from iliac bone marrow aspirates of Dutch milk goats, and isolated by adherence to tissue culture plastic. The cells (passage 2-6) were culture-expanded as described previously.[18] Briefly, aspirates were resuspended by using 20-gauge needles, plated at a density of 5x10^5 cells per square centimeter and cultured in MSC culture medium consisting of αMEM (Gibco) supplemented with 100 U/ml penicillin, 100 μg/ml streptomycin (Gibco), 2 mM L-glutamine (Glutamax, Gibco) and 15% v/v fetal calf serum (Cambrex). Cells were maintained in a humidified incubator at 5% CO_2 and 37 °C. Medium was refreshed twice a week and cells were used for further subculturing or cryopreservation. The cells from passage 2-6 were used in the experiments.

Cell seeding on top of hydrogels

Upon trypsinization, MSCs were seeded on hydrogels discs (n = 4; 150 μL) at 10^4 cells/cm^2 in a total volume of 50 μL. The gels were prepared in 16-well chamber slides by 1800 mJ/cm^2 UV exposure of 25% (w/v) Lutrol TP polymer in the presence of 0.1% (w/v) Irgacure 2959. As a control, we used MSCs seeded on Lutrol-T gel surfaces and Matrigel (Growth Factor Reduced, BD Biosciences) discs. A total of 6 h after seeding, spreading of the seeded cells with and without the additional coating with poly-L-lysine (gel 5 min preincubated with 0.1 mg/ml poly-L-lysine in water, Sigma P4832) was analyzed by light microscopy. The viability of the seeded cells was studied 1 day after seeding with a LIVE/DEAD Viability/ Cytotoxicity Kit (Molecular Probes, U.S.A.). The samples were measured using a microscope equipped with an epifluorescence setup, excitation/emission setting of 488/530 nm to detect green fluorescence (living cells), and 530/580 nm to detect red (dead) cells (Leica DM IRBE, Germany). Three randomly selected fields per sample were counted under the fluorescence microscope (Leica DM IRBE, Germany) using analysis software (Soft Imaging System, Germany). The cells' viability was calculated as the average ratio of vital over total cells per sample.

Cell encapsulation in Lutrol-T and –TP

To study viability of encapsulated cells in Lutrol-T, the polymer was dissolved in culture medium with or without glycerol (10 mM, Merck) and hydrocortisone (60 nM, H6909, Sigma) as membrane stabilizing agents, at 20% (w/v) overnight at 4 °C. MSCs were harvested by trypsinization and encapsulated in hydrogels at 3.0x10^5 cells/ml, two samples per condition. Cells cultured on polystyrene tissue culture slides were used as control.

To study the fate of encapsulated cells in Lutrol-TP hydrogels, the polymer was either dissolved in culture medium, for viability studies, or in osteogenic medium, to study differentiation, at 25% (w/v) o/n at 4 °C. MSCs were harvested by trypsinization and resuspended in the triblock copolymer solutions at 4.4x10^5 cells/ml gel at room temperature. Hydrogel discs (6 mm Ø and 1 mm thick) were prepared in 16-well chamber slides by 60 or 300 s exposure of 50 μl Lutrol-TP in the presence of Irgacure 2959. The total UV doses used were 0, 360, or 1800 mJ/cm^2. For viability analysis, a nonphotopolymerized hydrogel was used as control. To promote cell distribution inside the gels, polymer solutions in culture medium were supplemented with poly-L-lysine (0.05 mg/mL Sigma) or fibronectin (human, 2.5 μg/ml, Harbor Bio-Products, 0172003). To study the osteogenic differentiation potential of MSCs inside the gels, cells were mixed with Lutrol-TP at 5x10^6 cells/ml gel. The gel discs (n = 3 per condition, 150 μl) were covered with 50 μL medium and cultured at 5% CO_2 and 37 °C. After the indicated period of incubation (6 h to 3 weeks), the viability of cells was measured with the use of LIVE/DEAD Viability/Cytotoxicity Kit, as described above.

Analysis of osteogenic differentiation

The activity of alkaline phosphatase (ALP), present early during osteogenic differentiation, was determined for the MSCs encapsulated in the Lutrol-TP hydrogels exposed to 1800 mJ/cm^2 UV-light in the presence of 0.1% Irgacure 2959 (n = 4). After 1 week of culture in osteogenic medium, the medium was discarded and the gels were washed in PBS and embedded in TissueTek. Cryosections of 10 μm were fixed in 100% acetone, washed with PBS-0.1% Tween, and Fuchsin Substrate-Chromogen System (DakoCytomation, Carpinteria, U.S.A.) staining was applied according to manufacturer's recommendations to detect alkaline phosphatase positive cells (pink staining). Hematoxylin was used as counter stain. The presence of ALP positive cells

was analyzed with an Olympus BX50 light microscope equipped with an Olympus DP 70 camera, by calculating the average ratio of ALP positive over total cells from four randomly selected fields per sample.
For detection of collagen I production, hydrogel samples were imbedded in TissueTek after 2 weeks of incubation, and 10 μm cryosections were cut. The sections were blocked with 5% (w/v) BSA in PBS and incubated with mouse anticollagen type I antibody (2 μg/ml in 5% (w/v) BSA in PBS, clone I-8H5, Merck, Japan) for 1 h, followed by incubation with goat anti-mouse-Alexa488 (20 μg/ml in 5% (w/v) BSA in PBS, Molecular Probes, U.S.A.) for 30 min. Wash steps with 0.1% Tween20 in PBS were performed between the incubations. The sections were mounted with Vectashield containing DAPI for nuclear staining (Vector Laboratories) and analyzed under the fluorescence microscope.

Mechanical properties of photopolymerized hydrogels

To test how cellular encapsulation affects mechanical properties of the formed gels, Lutrol-TP hydrogel discs (25% (w/v) polymer in culture medium) with (n = 3; 1x10^6 cells/ml gel) or without cells (n = 4) were prepared by exposure of 250 μL triblock solution in the presence of 0.1% (w/v) Irgacure 2959 to UV light at 1800 mJ/cm^2. The stiffness of the hydrogel samples was measured at room temperature 4 h after photopolymerization, using a dynamic mechanical analyzer (DMA 2980, TA Instruments, Etten-Leur, The Netherlands) in controlled force mode. Hydrogels of 6.4 x 6 mm (height x diameter) were placed between the parallel plates (diameter upper plate 6 mm, diameter lower plate 45 mm) and a static force was applied between 0 and 1 N, and varied at a rate of 0.05 N/min. The Young's modulus (E) was determined as described previously,[443] by measuring the variation of stress/strain ratio.

Printing of Lutrol-TP scaffolds

The Bioplotter pneumatic dispensing system (Envisiontec GmbH, Germany) was used for 3D printing of hydrogel scaffolds. This system was previously employed for extrusion of hydrogels and is described in more detail elsewhere.[187] Briefly, the Bioplotter is a three-axis dispensing machine, which builds up 3D constructs by coordinating the motion of a pneumatic syringe dispenser. The dispenser deposits extrudate consisting of empty or cell-laden hydrogel on a stationary platform. Models of the scaffolds are loaded via the Bioplotter CAD/CAM software, which translates this information for the layer-by-layer fiber deposition by the Bioplotter. In the current study, the speed of deposition was set at 16 mm/sec and the pneumatic pressure that was applied to the dispensing syringe (containing 25% (w/v) Lutrol-TP in culture medium, without cells, at 4 °C) was set at 2 bar to yield uniform, continuous extrusion of fibers. An inner nozzle diameter of 210 μm was used. Two different configurations of deposited fibers (0/90 and 0/45:0/90 configuration) were tested for Lutrol-TP. Rectangular 3D scaffolds of 20 x 20 mm with spacing between fibers of 300 μm and a layer thickness of 150 μm were constructed in a Petri dish. Ten-layer scaffolds of Lutrol-TP were constructed and subsequently photopolymerized under the UV lamp as indicated.

Statistical analysis

Statistical analysis was performed with SPSS 12.0.1 software. A two-way analysis of variance (ANOVA) was used to evaluate the viability measurements of seeded and encapsulated MSCs. LSD and Bonferroni post hoc tests were used to compare the groups. A Student's t test was used to compare the mechanical properties of Lutrol-TP gels cast with and without the cells. P-values of less than 0.05 were considered statistically significant. All values are reported as mean ± SD.

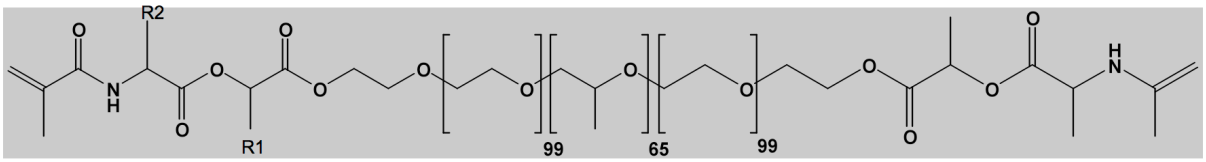

Figure 6.1: Structure of Lutrol F127 AlaL. R_1=CH_3; R_2=CH_3

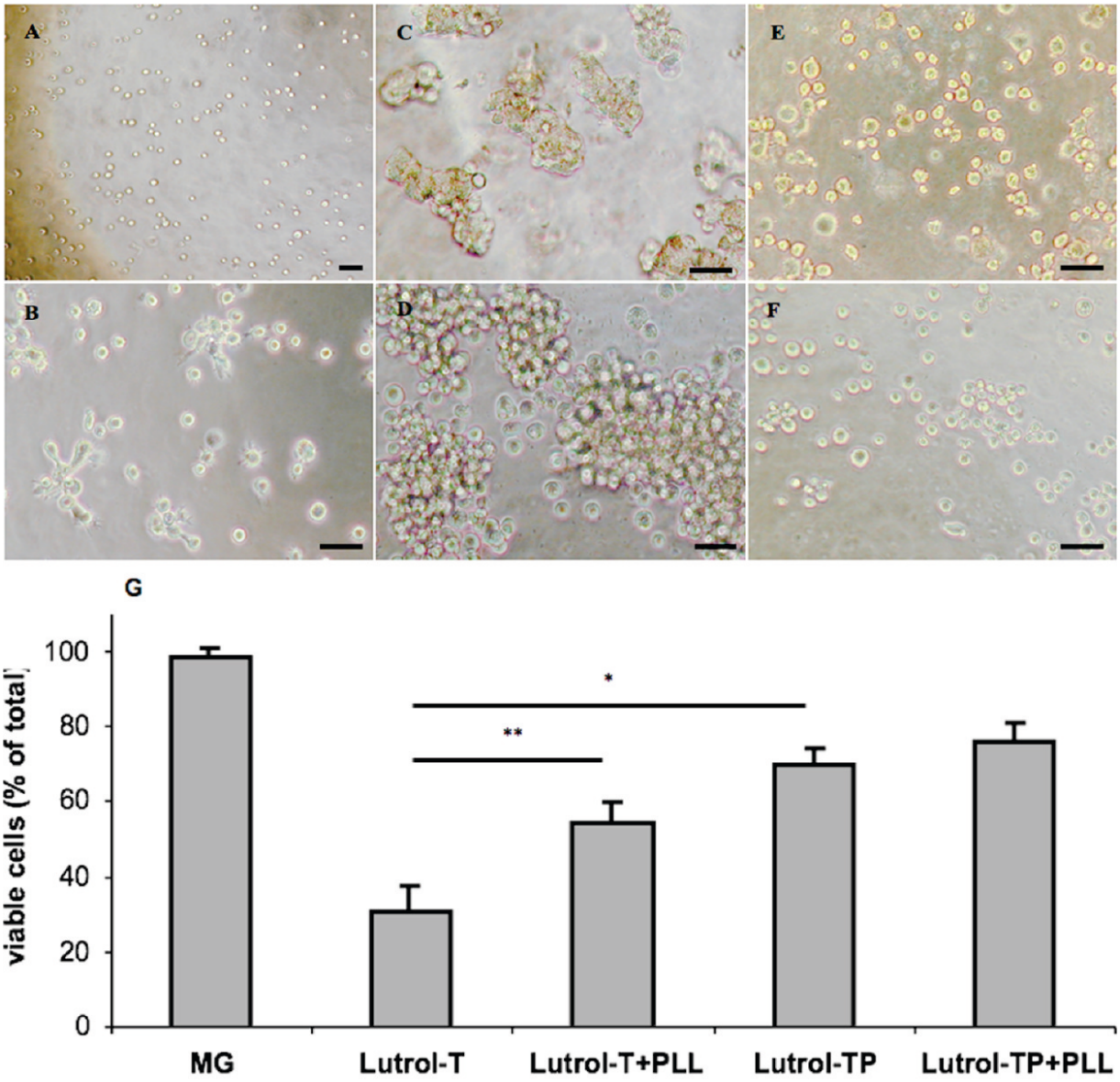

Figure 6.2: Effect of poly-L-lysine coating on cell morphology and viability. A-F: Cell morphology of MSCs seeded on Lutrol hydrogels; A: directly after seeding on Lutrol-T (formed by 1800 mJ/cm^2 UV exposure with 0.1% Irgacure); B-D: 6 h after seeding of MSCs on Matrigel (B), Lutrol-T (C), and Lutrol-TP uncoated (D); E,F: cells 6 h after seeding on Lutrol-T coated with PLL (E) and Lutrol-TP coated with PLL (F); scale bar: 50 µm; G: Cell survival of seeded MSCs after one day on various hydrogel surfaces (n = 4 per condition). MG: Matrigel.

Results

Effect of gel surfaces on cell distribution and viability

Analysis of cell distribution directly and 6 h after seeding of MSCs on top of Lutrol-T and photopolymerized Lutrol-TP hydrogel discs revealed that the cells aggregate toward the center of the hydrogel disk forming cell clusters on the hydrogel surface (Figure 6.2A,C,D). Coating of the hydrogel surface with poly-L-lysine resulted in more uniform distribution of the cells on the surface, although no stretching of the MSCs was observed (Figure 6.2E,F), as was seen when using Matrigel (Figure 6.2B). Viability analysis 1 day after seeding indicated that the survival on photopolymerized Lutrol-TP surface (formed by 1800 mJ/cm^2 UV exposure with 0.1% Irgacure) was significantly higher than on Lutrol-T gels: (70 ± 4% vs 30 ± 7%; $p < 0.05$*; Figure 6.2G). Additional coating with PLL promoted survival of the seeded MSCs on Lutrol-T (Lutrol-T vs Lutrol-T+PLL: 30 ± 7% vs 54 ± 5%; $p < 0.05$**) and not on Lutrol-TP surfaces.

Cell encapsulation and viability analysis

No significant differences in cell survival between the groups were seen after 6 h for all the tested conditions. After 1 and 3 days, TCPS-cultured MSCs were significantly more viable than the cells embedded in hydrogels. Analysis of cell survival of MSCs encapsulated inside Lutrol T hydrogels demonstrated progressive cell death of embedded cells, with around 30% survival after three days (Figure 6.3). It has been reported previously that the viability of cells embedded within the Pluronic hydrogel was significantly enhanced by the addition of hydrocortisone and glycerol,[304] and therefore, we used these supplements in similar concentrations in this study. Addition of hydrocortisone enhanced the survival of the cells after 1 and 3 days, although a persistent decline in cell survival over the course of three days was observed. After 1 day, viability inside gels supplemented with H was significantly higher than control Lutrol-T gels (70 ± 7% vs 52 ± 11%; $p = 0.021$). After 3 days of encapsulation, survival in the gels supplemented with either H (52 ± 0.5%) or H+G combination (47 ± 6%) was significantly higher than in control Lutrol T gels (31 ± 8%; $p = 0.009$ and $p = 0.025$, respectively). This was not the case for gels supplemented with only glycerol (39 ± 6.5%; $p = 0.06$ compared to control).

Lutrol-T hydrogels are highly unstable in culture starting to dissolve within minutes after incubation in culture medium. Cell-laden Lutrol-TP gels exposed to 360 mJ/cm^2 of UV light in the presence of 0.1% Irgacure formed gel discs, which dissolved after 6-7 days. Lutrol-TP gels polymerized by 1800 mJ/cm^2 UV exposure in the presence of 0.05 or 0.1% Irgacure were more stable, with the latter hydrogel discs remaining stable in culture for up to three weeks postpolymerization. MSCs embedded within photopolymerized Lutrol-TP were distributed evenly throughout the gels with formation of clusters (Figure 6.4A). Addition of poly-L-lysine (PLL) or fibronectin (FN) to the gels promoted more homogeneous dispersion of the cells, after 1 day of encapsulation, although cell clusters were still present in gels supplemented with PLL (Figure 6.4B,C). Initial cell survival of encapsulated MSCs in photopolymerized Lutrol-TP hydrogels obtained at different polymerization conditions was assessed after 1 day of incubation (Figure 6.4D). Analysis after 1 day ($n = 3$ or 5 per condition) indicated a statistically significant difference between unphotopolymerized and photopolymerized gels ($p \leq 0.001$), without a significant effect of the different photopolymerization conditions. Addition of PLL and fibronectin did not significantly contribute to cell survival (Figure 6.4D). Viability in unphotopolymerized Lutrol-TP was significantly lower than in photopolymerized gels (Figure 6.5A), after both 2 and 7 days ($p \leq 0.001$;*), measuring 6 ± 3% after 7 days. Viability of MSC inside Lutrol-TP exposed to 360 mJ/cm^2 UV light, in the presence of 0.1% Irgacure, decreased

with time and was significantly lower than in the two other photopolymerized conditions after both 2 ($p < 0.05$;**) and 7 days ($p < 0.001$;***), with 32 (3% viable cells after seven days, as compared to 59 ± 5% and 57 ± 1% in Lutrol-TP obtained by 1800 mJ/cm^2 UV exposure with 0.05% and 0.1% Irgacure, respectively. Survival of the embedded MSCs at 2 and 3 weeks is presented in Figure 6.5B, and measured around 60%.

Differentiation

Upon encapsulation, the MSCs retained a round morphology inside the gels (Figure 6.6) despite the addition of PLL or fibronectin to the hydrogel. To analyze the osteogenic differentiation of photoencapsulated MSCs, we determined the activity of alkaline phosphatase, an ectoenzyme produced by osteoblasts involved in ensuring a sufficiently high local concentration of phosphate for mineralization to occur. After a 1-week incubation in osteogenic medium, ALP was present in 10.2 ± 2.7% of the embedded MSCs (Figure 6.6A). To further assess osteogenic differentiation, collagen I, a major specific marker of bone matrix highly expressed during the entire process of bone formation,[444] was measured. Figure 6.6B shows the presence of collagen I in a substantial amount of the embedded MSCs after 2 weeks, as determined by immunocytochemistry.

Mechanical properties of the formed gels

The Young's modulus of the empty and cell-laden hydrogels was determined as the absolute value of the slope from the graph plotting the compression force versus the observed strain. Average Young's modulus of cell-laden hydrogels measured 21 ± 3 kPa, comparable to 20 ± 2 kPa of the empty hydrogels ($p = 0.55$).

Printing of the scaffolds

Computer-controlled deposition of Lutrol-TP hydrogel resulted in scaffolds with a thickness up to 10 layers (Figure 6.7A) and regular vertical pores throughout the printed samples. It was possible to print the hydrogel with different fiber configurations. The weight of subsequent hydrogel layers resulted in broader strands than the original needle diameter and fusion of transversal pores during stacking of layers (Figure 6.7A). Prior to photopolymerization, the scaffold was soft and could be easily damaged, compromising handling (Figure 6.7B). After polymerization, a stabile, mechanically strong structure was formed (Figure 6.7C).

Discussion

In this study we analyze the applicability of a novel, thermosensitive, and photopolymerizable Lutrol hydrogel for 3D deposition of (cell-laden) hydrogel scaffolds to function as possible bone grafts. Lutrol-TP turned out to be very suitable for printing with a Bioplotter system, with thermosensitive gelation of the material ensuring easy 3D deposition and providing temporary support of the printed shape prior to photopolymerization, without collapsing. Subsequent photopolymerization resulted in organized 3D scaffolds that could be easily handled and cultured, with hydrogels retaining their stability for up to 21 days.[441] Adjusting the photopolymerization regime to photoexposure during deposition can possibly overcome the fusion of transversal pores.

The functionality of this new hydrogel as cell-supporting matrix for seeded and encapsulated cells was studied by measuring the cytotoxicity of the hydrogel and the effect of photoencapsulation on viability and osteogenic differentiation of goat osteogenic progenitor cells, MSCs. Our findings indicate that the majority of the cells are able to survive within the photopolymerized

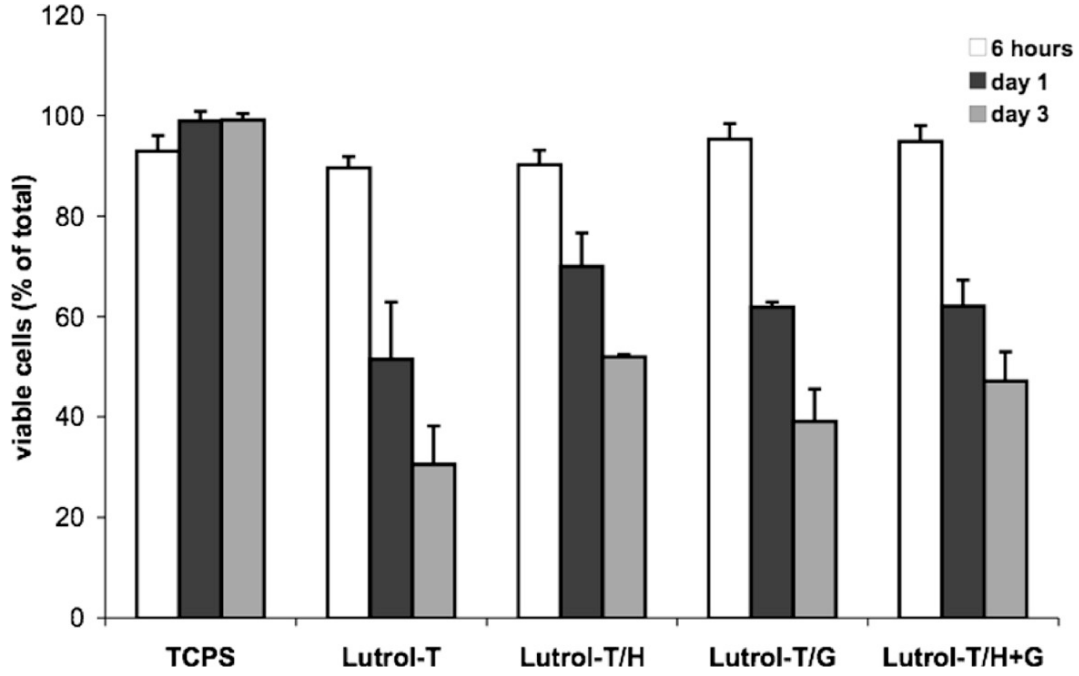

Figure 6.3: Survival of embedded cells. Viability of MSCs in Lutrol-T gels (25% w/v), control or supplemented with 60 nM hydrocortisone (H) and 10 mM glycerol (G), as compared to viability of MSCs seeded on tissue culture polystyrene surfaces (TCPS), n = 3 per condition, per time point.

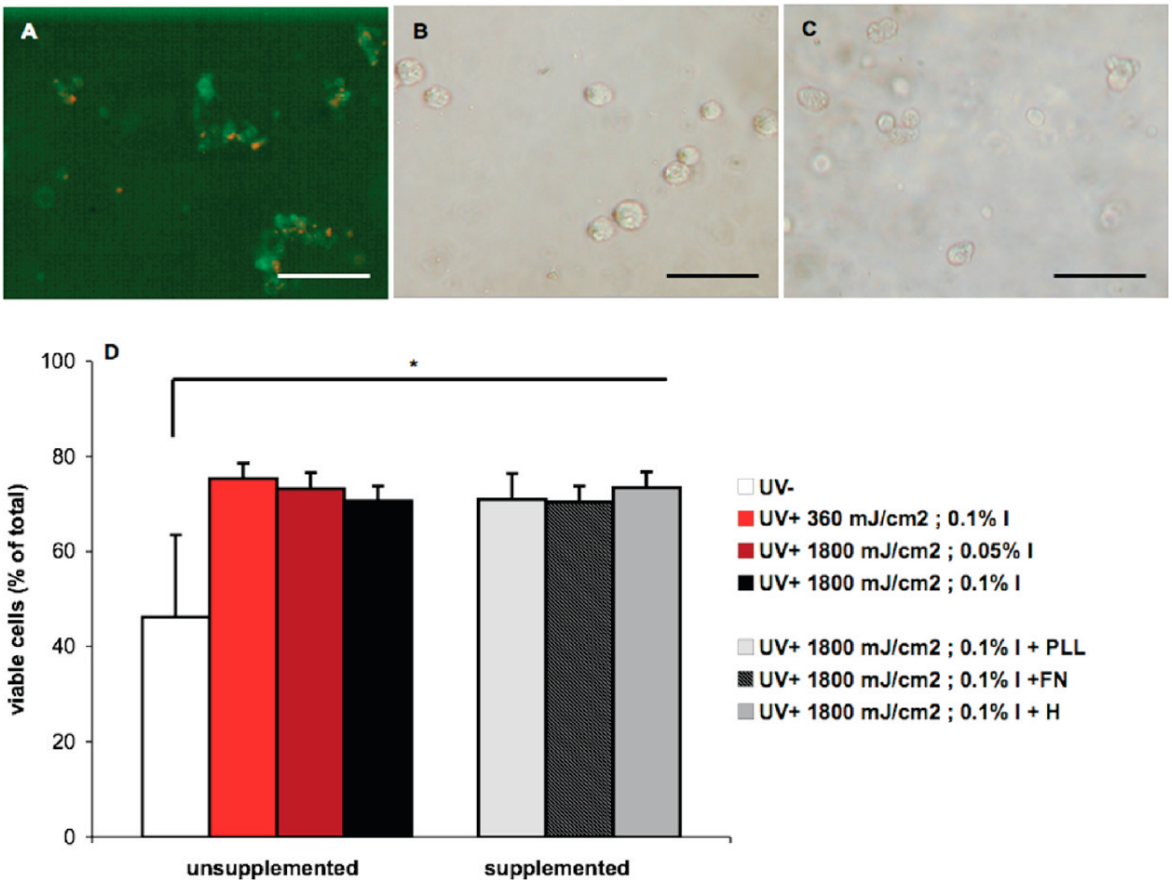

Figure 6.4: MSCs after one day of encapsulation in Lutrol-TP. A: Live/dead assay on MSCs in Lutrol-TP polymerized in the presence of 0.05% (w/v) Irgacure and 1800 mJ/cm^2 UV

exposure; live cells, green; dead cells, red; bar = 100 μm; B,C: MSCs 1 day after encapsulation in Lutrol-TP, supplemented with fibronectin (B) and PLL (C), bar = 50 μm. D: Viability of MSCs embedded in Lutrol-TP gels obtained under different photopolymerization conditions (UV: unphotopolymerized, UV+: photopolymerized, I: Irgacure) and the effect of modified Lutrol-TP gels on cell viability, asterisk: $p < 0.05$. Lutrol-TP gels were supplemented with 0.05 mg/ml poly-L-lysine (PLL), or 2.5 μg/ml fibronectin (FN), or 60 nM hydrocortisone (H) and exposed to 1800 mJ/cm^2 UV in the presence of 0.1% Irgacure.

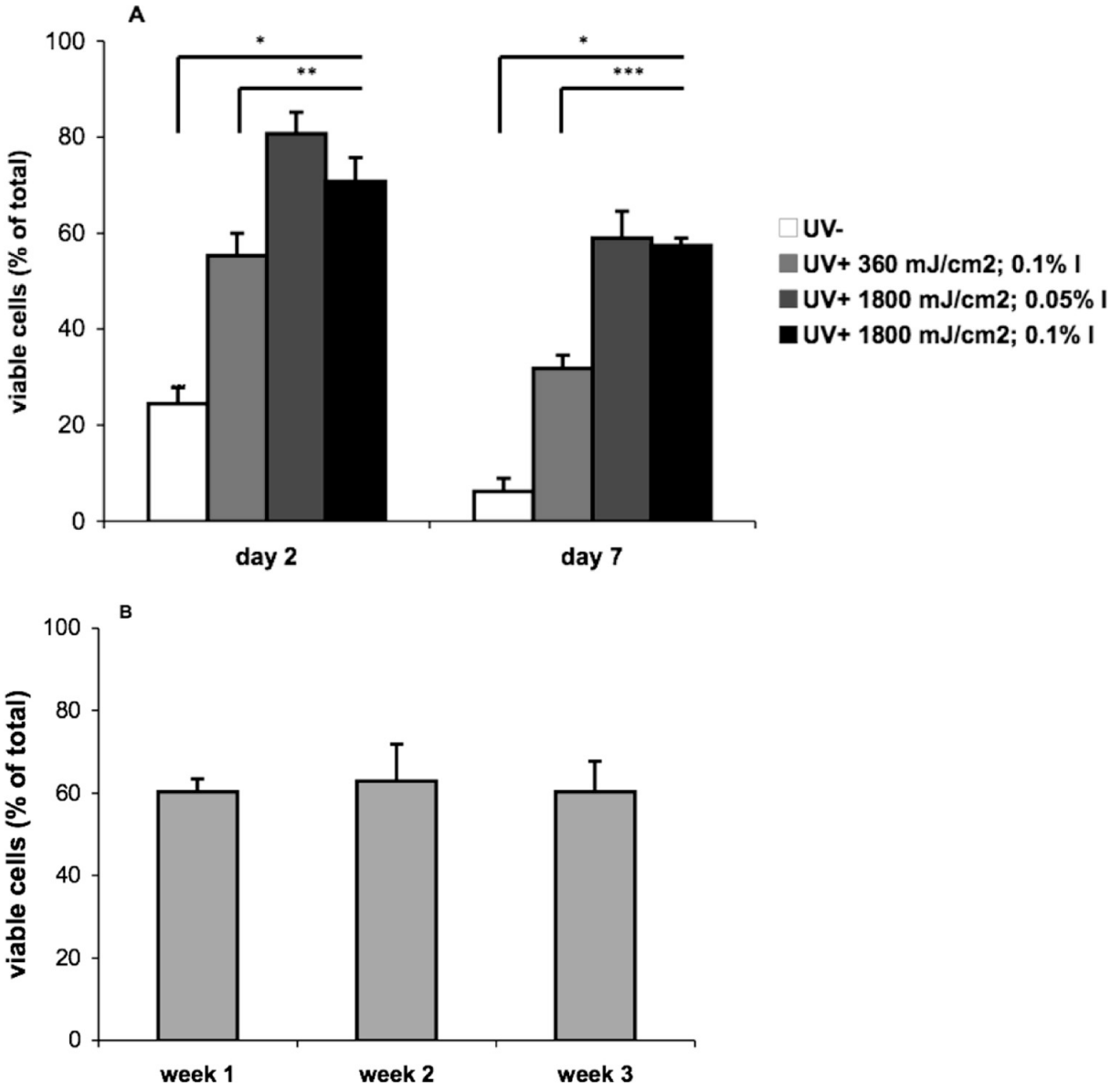

Figure 6.5: Long-term viability of MSCs in Lutrol-TP. A: Survival of embedded MSCs after 2 and 7 days incubation in Lutrol-TP ($n = 3$ per condition, per time point). B: Long-term survival of MSCs embedded in Lutrol-TP gels, formed by exposure to 1800 mJ/cm^2 UV light in the presence of 0.1% (w/v) Irgacure ($n = 5$ per time point).

Lutrol-TP hydrogels for up to 3 weeks and retain the ability to differentiate after encapsulation.
Goat MSCs encapsulated in non-photopolymerized Lutrol-T gels, dispersed throughout the gels with formation of clusters. Only a fraction of cells survived the encapsulation, with as minimal as 6% viable cells in 25% (w/v) Lutrol-T after 7 days of encapsulation. This low viability inside Pluronics has been reported previously also by other research groups and was in part attributed to disturbed membrane stability of the cells exposed to triblock-polymer units.[304] Therefore, we added hydrocortisone and glycerol to the polymer solutions prior to gelation, as addition of these media to Pluronics was shown to enhance cell viability through an unknown mechanism.[304] Although adding hydrocortisone could alleviate part of the cytotoxicity of the gels, an ongoing decrease in viability of MSCs remained. Furthermore, Lutrol-T gels were instable and could not be retrieved from culture after 3 days of incubation.
Additional photopolymerization of the Lutrol-TP gels renders the material more stable with regard to degradation, as covalent crosslinks prevent the dissolution of the gel. Hydrogel discs, obtained by photopolymerization of Lutrol-TP gels in the presence of 0.1% Irgacure and 1800 mJ/cm^2 UV exposure, persisted in culture for up to 3 weeks, and were evaluated for viability of encapsulated cells during a three-week period. Photopolymerization of the gel had a positive effect on shortterm cell viability with a substantially higher amount of viable cells than in the unphotopolymerized controls (50% vs 5%). A similar effect was seen for MSCs seeded on top of photopolymerized Lutrol-TP surfaces when compared to Lutrol-T gels. The positive effect of photopolymerization on cell survival may be attributed to crosslinking of the polymer that diminishes the dissolution of the gel and reduces the amount of triblock polymer molecules in direct contact with the cells. Notably, after crosslinking of Lutrol-TP, hydrocortisone no longer promotes cell viability, in accordance with the proposed effect of monomers on plasma membrane stability.[304]
We did not detect differences in cell survival between gels obtained at different photopolymerization conditions, indicating that the more stringent conditions can be applied to form scaffolds without directly harming cell viability. The long-term effects of UV-exposure and photoinitiator on protein and DNA damage in this hydrogel setting must still be determined. Cell survival around 60% is representative for unmodified, synthetic photopolymerized hydrogels.[355] Survival of encapsulated MSCs, even in hydrogels acknowledged as fully biocompatible can be as low as 15% after one week of encapsulation,[232] largely due to minimal interaction between hydrogel matrix and cells. It has been previously shown that integrins play a central role in adhesion, resistance to apoptosis, and promotion of cell survival.[445]
When MSCs were seeded on Lutrol-T and the photopolymerized Lutrol-TP hydrogel surfaces, the cells exhibited clustering and additional coating of the surfaces with poly-L-lysine promoted more homogeneous cell distribution. Poly-L-lysine and fibronectin also enhanced the distribution of cells embedded in the gels. Polylysines, polycations that mediate integrinin-dependent adhesion, as well as fibronectin, a high-molecular-weight glycoprotein that interacts with cell surface expressed integrins, have been used to successfully promote cellular attachment and spreading of cells in hydrogels and on hydrogel surfaces.[221,446] Additional modification of the synthetic photopolymerizable hydrogels with the arginine-glycine-aspartate (RGD) adhesive sequence found in fibronectin and many other extracellular matrix proteins drastically enhances cell attachment and spreading of osteoblasts[212] and significantly promotes survival of the embedded hMSC.[232,436] In this study we observed no positive effect of FN or PLL on stretching or survival of cells embedded in Lutrol-TP, possibly because the supplements were simply mixed with the gels and not grafted or otherwise covalently attached.
Photoencapsulated MSCs retained the ability to differentiate toward the osteogenic lineage, with

over 10% of the embedded cells exhibiting alkaline phosphatase activity and producing collagen I. A higher degree of osteogenic differentiation would be required for future use of this photopolymerizable gels in printed bone grafts. The use of high density culture contributes to the formation of vital intercellular contacts, and this is expected to enhance the differentiation of encapsulated cells:[447] the so-called "community-effect". Osteogenic differentiation can be further enhanced by grafting phosphoester groups,[448] heparin,[436] or collagen mimetic peptides[225] to the polymer chains.

Addition of the photosensitive groups to the Lutrol-T increases the mechanical properties of the formed gels after photopolymerization. The Young's modulus of the formed gels fall in the range of other photopolymerizable gels used for cellular encapsulation.[449] Addition of cells to the gels did not significantly alter the compressive modulus of the gels, indicating that initially, the embedded cells do not diminish the mechanical properties of the gels by distorting the photogel structure. Matrix stiffness is expected to have a significant effect on tissue development by the embedded cells,[450] with osteogenic differentiation possibly requiring stiffer hydrogels than the materials used in this study. Enhancing of crosslink density could be useful in this respect.

Conclusions

Modification of Lutrol F127 polymers with photosensitive groups renders thermosensitive hydrogels more stable in culture, making them attractive to design scaffolds for TE applications. MSCs embedded in photopolymerizable Lutrol-TP gels remain viable during the study period, with a significantly higher viability as compared to the same unphotopolymerized hydrogel or to Lutrol-T gels, and are able to differentiate toward the osteogenic lineage. This novel biomaterial is highly suitable for 3D fiber deposition, enabling formation of organized 3D scaffolds.

Acknowledgment

We thank Dr. Joost de Wijn for valuable discussions. We acknowledge the financial support of the Mosaic scheme 2004 of The Netherlands Organisation for Scientific Research to N.E.F. (NWO; Grant No. 017.001.181), the Dutch Platform for Tissue Engineering to J.A. (Project No. UGT.6743), and the Flemisch Institute for Encouragement of Science and Technology (IWT) for providing a Ph.D. grant to I.S.

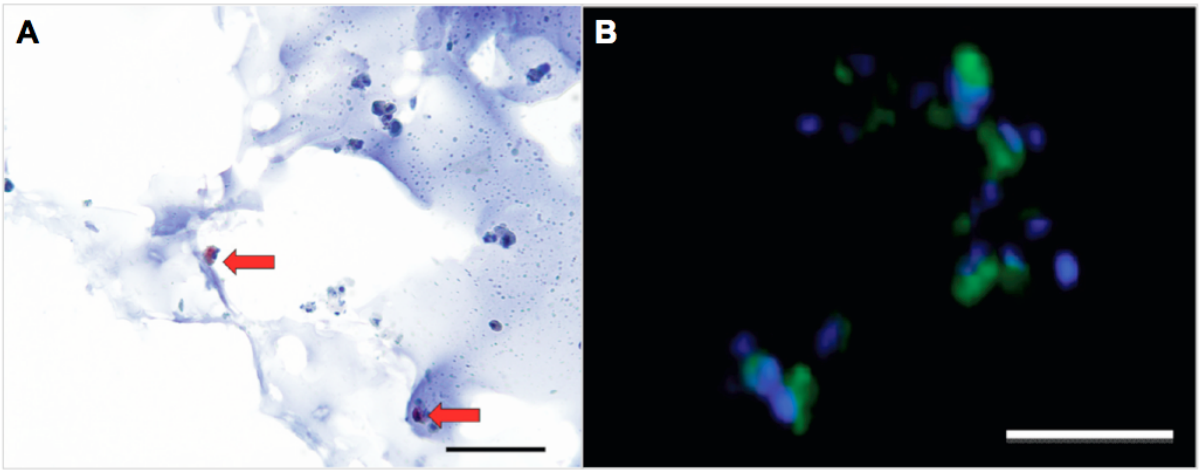

Figure 6.6: Osteogenic differentiation of MSCs in Lutrol-TP. A: MSCs embedded in polymerized Lutrol-TP (light blue) for 1 week in the presence of osteogenic medium; ALP-specific staining is indicated in red (red arrow); scale bar = 100 μm; B: Collagen I immunocytochemistry, 2 weeks after encapsulation; scale bar = 50 μm; collagen I (green); DAPI nuclear stain (blue).

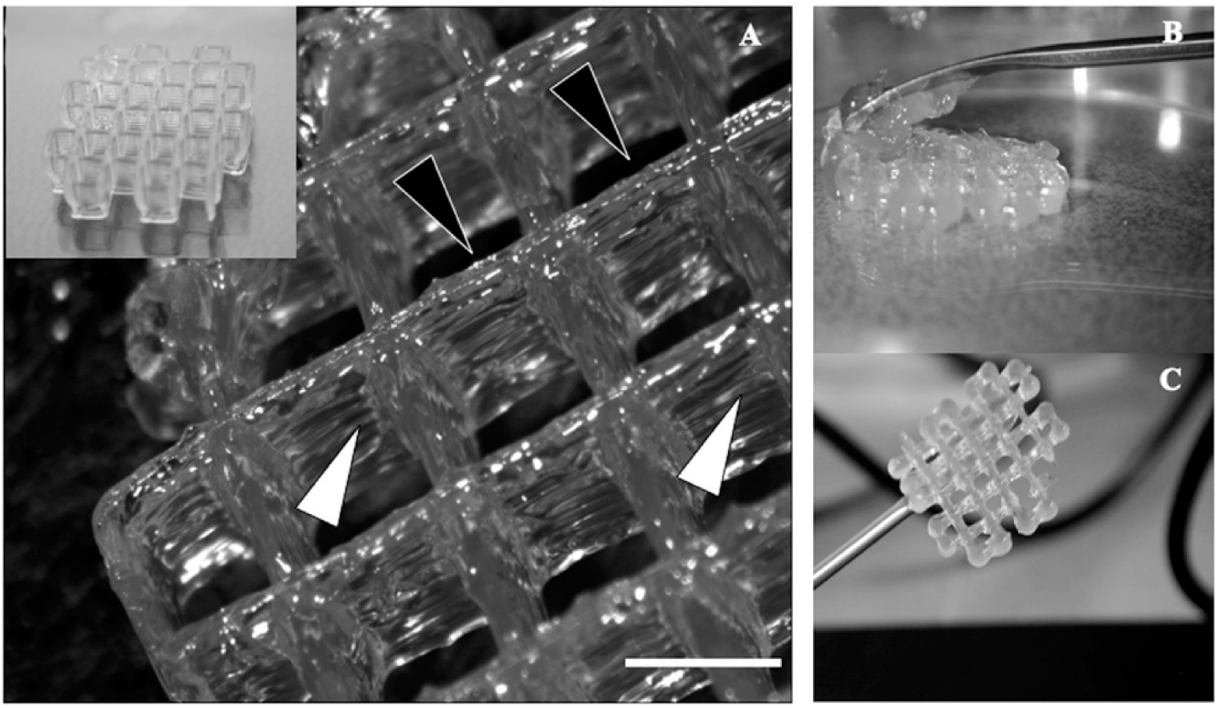

Figure 6.7: Printed Lutrol-TP scaffolds. A: Organized 3D structure (black arrowhead: vertical pores; white arrowhead: fused horizontal pores; bar: 2.5 mm); inset: total printed scaffold; B: printed unphotopolymerized structure; C: handling after photopolymerization.

Chapter 7

Scaffold porosity and oxygenation of printed hydrogel constructs affect functionality of embedded osteogenic progenitors.

Fedorovich NE[1], Kuipers E[1], Gawlitta D[1], Dhert WJA[1,2], Alblas J[1]

Manuscript submitted

[1]*Department of Orthopaedics, University Medical Center Utrecht, Utrecht, The Netherlands*
[2]*Faculty of Veterinary Medicine, Utrecht, The Netherlands*

Abstract

Insufficient supply of oxygen and nutrients throughout the graft is considered one of the principal limitations in development of large, tissue-engineered bone grafts. Organ- or tissue printing (OP) by means of three-dimensional (3D) fiber deposition is a novel modality in regenerative medicine that combines pore formation and defined cell placement, and is used here for development of cell-laden hydrogel structures with reproducible internal architecture to sustain oxygen supply and to support adequate tissue development.

In this study we tested the effect of porosity on multipotent stromal cells (MSCs) embedded in hydrogel constructs printed with a 3D fiber deposition (3DF) machine. For this, porous and solid alginate hydrogel scaffolds, with MSCs homogeneously dispersed throughout the construct, were printed and analyzed *in vitro* for the presence of hypoxia markers, metabolism, survival and osteogenic differentiation. We demonstrated that porosity promotes oxygenation of MSCs in printed hydrogel scaffolds and supported the viability and osteogenic differentiation of embedded cells. Porous and solid printed constructs were subsequently implanted subcutaneously in immunodeficient mice to analyze tissue formation in relation to hypoxia responses of embedded cells. Implantation of printed grafts resulted in ingrowth of vascularized tissue and significantly enhanced oxygenation of embedded MSCs. In conclusion, the introduction of pores significantly enhances the conductive properties of printed hydrogel constructs and contributes to the functionality of embedded osteogenic progenitors.

Introduction

One of the main restrictions in engineering of large, clinically relevant sized bone grafts is considered to be an insufficient supply of oxygen and nutrients throughout a construct, which would impair the development of tissue.[253,451-456] After implantation *in vivo*, cells in the engineered tissue consume the available oxygen within a few hours, but it takes days to weeks before new blood vessels have sufficiently invaded the implants to deliver oxygen and nutrients.[19] As a result, the transplanted cells often lose function or die after delivery to the recipient,[457] demonstrating the relevance of adequate oxygen tensions and sufficient nutrient levels for development of functional implants.

Oxygen is a prerequisite for aerobic metabolism and is one of the vital parameters affecting cellular processes including cell proliferation, differentiation, and cytokine production. Cellular responses to changes in oxygen tension are regulated by hypoxia-inducible factor (HIF)-1α, a transcription factor responsible for various functions including anaerobic energy supply, erythropoiesis, angiogenesis, and regulation of pH and cell survival.[458-460] Vascular endothelial growth factor (VEGF) and glucose transporter 1 (Glut-1) are some of the target genes upregulated by HIF-1α. GLUT-1 is responsible for transport of glucose across the cell membrane and is upregulated under hypoxic conditions, when cell changes its energy metabolism form aerobic to anaerobic and thus needs more glucose to generate enough ATP.

Culturing of stem and progenitor cell populations, including multipotent stromal cells (MSCs), under hypoxic conditions, lead to enhanced proliferation and preservation of stemness.[461-466] In the presence of chondrogenic stimuli, hypoxia supports expansion of MSC populations with chondrogenic potential[459,467,468] and promotes chondrogenic differentiation[469-471] by activating Sox-9 via a HIF-1α-dependent mechanism.[470] At the same time, hypoxia inhibits differentiation of MSCs along the osteogenic lineage.[72,462,463,466,472-474] The extracellular matrix formed by hypoxic osteoblasts is less abundant than in normoxic cultures, and has poor quality, highlighted by limited organization of weak collagen fibrils and increased sensitivity to pepsin degradation.[474] The survival of *in vivo* transplanted MSCs is strongly influenced by oxygen tensions, as is the homing to hypoxic locations to enable regeneration.[461] Also hypoxic preculturing of the cells prior to implantation may play a positive role in graft performance.[475] Overall, controlling the oxygenation of an engineered construct can influence tissue formation throughout the graft *in vitro* and to guide cell performance *in vivo*.

Limited presence of oxygen and nutrients in the core of the graft arises from several causes including restricted porosity of the scaffold and inhomogeneous distribution of seeded cells. Cells seeded on porous scaffolds often remain on the periphery of the scaffolds. A non-homogeneous nutrient distribution and oxygen gradients from the surface to the core of a scaffold,[476-479] will in turn result in heterogeneous cell function, associated with elevated proliferation and biosynthetic activity area at the periphery of the constructs[456] and non-viable areas in the center regions.[480] The size of necrotic areas increases with the scaffold thickness[481] or cell seeding density. If a non-porous material with limited diffusion properties is used, this will further enhance the development of steep oxygen gradients.[480]

In solving these limitations, the porosity of a graft is of particular importance since it enhances nutrient supply and waste product removal *in vitro* and allows blood vessel ingrowth *in vivo*. By using porous constructs together with perfusion bioreactor systems *in vitro*, relatively uniform oxygen-levels[479] can be achieved in engineered grafts. This would result in more homogeneous differentiation of cells,[451] and subsequent uniform formation of extracellular matrix *in vitro* and tissue *in vivo*. For example, in bone tissue engineering (TE), oscillatory flow conditions lead to

enhanced seeding efficiency and homogeneity, and facilitate not only uniform culture but also early osteogenic differentiation.[482] Altogether, this enables engineering of graft tissues with predictable mechanical properties and consistent quality. However, perfusion systems do not entirely eliminate three-dimensional (3D) culture–associated oxygen gradients.[479] Apart from transport restrictions, non-uniform matrix development can also be caused by inhomogeneous cell seeding or cell migration in the construct.[456,469] Uncontrolled, inhomogeneous matrix formation may in some cases be undesirable, as this can lead to inadequate overall mechanical properties of the construct.[483,484] When using static cell seeding it is hard to achieve desired cell dispersion and cell densities throughout the scaffold or to deliver cells deep into the scaffold.[485,486] Possible strategies for controlling cell distribution include the use of seeding techniques that promote spatial distribution of cells in the scaffolds, such as hydrogel encapsulation,[456] also in bone tissue engineering.[209]

Organ- or tissue printing is a novel modality in regenerative medicine that simultaneously addresses the issues of porosity and homogeneous cell seeding in cell-laden hydrogel constructs, based on rapid-prototyping (RP) technology.[487] With RP, 3D structures with highly reproducible architecture and compositional variation can be created. A main asset is that the interconnected porosity of the implants is easily tailored, which is important for conductive properties of the construct. 3D fiber deposition (3DF) is an organ printing technology based on layered deposition of cell-laden hydrogel fibers, creating viable grafts with cells homogeneously spread throughout the printed construct.[117]

Using 3DF printed constructs, we assessed the effect of porosity on osteogenic progenitor cell function. For this, porous and solid MSC-laden alginate hydrogel scaffold were printed and analyzed for cell dispersion, hypoxia responses, metabolism, viability and differentiation of the cells *in vitro*. Tissue formation and hypoxia of embedded cells were also investigated *in vivo* after subcutaneous implantation of the constructs in mice.

Materials and methods

Hydrogel preparation

High-viscosity alginate powder (International Specialty Products, ISP, Memmingen, Germany) was autoclaved and subsequently mixed (10% (w/v)) overnight at 37°C with expansion medium (αMEM (Invitrogen, Breda, The Netherlands), supplemented with 10% fetal bovine serum (FBS, Lonza, Basel, Switzerland), 0.1 mM ascorbic acid 2-phosphate (AsAP; Sigma-Aldrich, Zwijndrecht, The Netherlands), 2 mM L-glutamine (Glutamax, Invitrogen) and 100 U/ml penicillin, 100 μg/ml streptomycin (Invitrogen). To induce gel formation, alginate was incubated after printing with 102 mM $CaCl_2$ supplemented with 10 mM 4-(2-hydroxyethyl)-1-piperazineethanesulfonic acid (HEPES, Invitrogen) for 15 minutes.

Cell isolation and culture

Human and goat multipotent stromal cells (hMSCs/gMSCs) were isolated from iliac bone marrow aspirates,[488] obtained respectively from human donors undergoing hip arthroplasty after written informed consent or adult Dutch milk goats. For isolation of hMSCs the mononuclear cell fraction was acquired by centrifugation on Ficoll-paque and plated in expansion medium supplemented with 1 ng/ml rhFGF-2 (233-FB, R&D Systems). For isolation of gMSC the bone marrow aspirates were plated at a density of $5x10^5$ cells/cm^2 and cultured in expansion medium. Medium was refreshed twice weekly and cells were used for further subculturing or

cryopreservation. Cell cultures were maintained in a humidified incubator at 5% CO_2 and 37°C. hMSCs passage 3-4 and gMSCs passage 2-6 were used in the study.

Bioscaffolder and 3D fiber deposition presets

The Bioscaffolder pneumatic dispensing system (SYS+ENG, Germany) was used for 3-dimensional printing of hydrogel scaffolds. This system was previously employed for extrusion of (cell-laden) hydrogels and is described in more detail elsewhere.[117] Briefly, the Bioscaffolder is a three-axis dispensing machine, which builds up 3D constructs by coordinating the motion of a pneumatic syringe dispenser. The dispenser deposits fibers of extrudate consisting of cell-laden hydrogel. Models of the scaffolds are loaded via CAD/CAM software, which translates this information into layer-by-layer fiber deposition by the machine. In the current study, a syringe dispenser with an inner nozzle diameter of 210 μm was used. The deposition speed and pressure were set at 300 mm/min and 0.2 MPa, respectively. 3D block scaffolds of 10x10x1 mm with spacing between fibers of 0.8 (solid), and 2 mm (porous) and a fiber height of 100 μm were constructed.

Printing of porous and solid scaffolds

Trypsinized goat or human MSCs were mixed with alginate at 2.5, 5 and 10 x10^6 cells/ml gel to assess the degree of cell dispersion in hydrogel constructs. MSCs were mixed with alginate at 5-10x10^6 cells/ml for solid constructs and 10x10^6 cells/ml gel for porous constructs. This enables comparison between the scaffolds of equal cell density (solid versus porous construct with 10x10^6 cells/ml gel) or equal total cell number, when quantitative analysis per cell is performed (solid construct with 5x10^6 cells/ml versus porous construct with 10x10^6 cells/ml gel). Cell-laden gels were loaded into the syringe, kept at 4 ºC, and mounted onto the machine. Syringes were kept at 4 °C to uphold the viscosity of the hydrogel, enabling better scaffold formation. The printed scaffolds were subsequently crosslinked in $CaCl_2$ solution as indicated and further incubated in expansion or osteogenic medium (expansion medium supplemented with 10 nM dexamethasone (Sigma) and 10 mM β-glycerophosphate (Sigma)). For in vitro analysis the cell-hydrogel constructs were cultured in a humidified incubator at 21% oxygen, 37 °C and 5% CO_2. As a positive control for analysis of hypoxic markers, porous constructs (n=4 per time point) were cultured at 2% oxygen, 37 °C and 5% CO_2.

In vivo implantation

For *in vivo* implantation, four different constructs were prepared: porous implants with 5x10^6 goat MSCs/ml gel, solid implants with 10x10^6 goat MSCs/ml or 5x10^6 goat MSCs/ml gel respectively, and porous implants without cells. The samples were cultured in expansion medium for 24 hours prior to the implantation. Female nude mice (NMRI-Foxnu, Charles River, Belgium), six-weeks old, were anaesthetized with 1.5% isoflurane, after which the implants were placed in four separate subcutaneous dorsal pockets for a period of 4, 7 or 14 days (n=7 per group). The incisions were closed using a Vicryl 5-0 suture. The animals were postoperatively treated with the analgesic buprenorphine (0.05 mg/kg, sc; Temgesic, Schering-Plough) and housed together at the Central Laboratory Animal Institute, Utrecht University. Experiments were conducted with the permission of the local Ethical Committee for Animal Experimentation and in compliance with the Institutional Guidelines on the use of laboratory animals.

Sample processing

Part of the *in vitro* cultured constructs with gMSCs were incubated with 100 μM pimonidazole, an indicator of hypoxia (O_2<1.5 %; Hypoxyprobe-1 Omni Kit; Natural Pharmacia International, Burlington, USA), for 24 hours before termination of the experiment at days 2 and 7. The cultured samples were either analyzed for viability (n=4), or embedded in Tissue-Tek O.C.T. Compound (Sakura Finetek, Zoeterwoude, The Netherlands) for cryosectioning (n=4) or processed for paraffin sections (n=4) through graded ethanol series and xylene.
Pimonidazole was administered to the mice 2.5 hours prior to termination, after 4, 7 or 14 days, at a dose of 60 mg/kg body weight. The samples were then excised and processed for paraffin sectioning.

Analysis of cell distribution after printing

To assess the degree of cell dispersion in hydrogel constructs, printed cell-laden hydrogel (2.5, 5 and 10 x10^6 cells/ml gel) strands were incubated with DAPI nuclear stain (Sigma) directly after printing and the number of cells per mm^3 fiber (n=8) was scored using fluorescence microscopy.

Immunolocalization of endogenous hypoxia markers HIF-1α and GLUT-1 and hypoxia indicator pimonidazole

For analysis of hypoxia markers the *in vitro* and *in vivo* gMSC-laden samples were processed for paraffin histology and 5 μm sections were made. For HIF-1α localization, the sections were preincubated in 1.5% (v/v) H_2O_2 in Tris-buffered saline (TBS: 50 mM Tris, 150 mM NaCl, pH 7.6) supplemented with 102 mM $CaCl_2$ for 30 minutes, antigen retrieval was performed by 30-minute incubation in 10 mM Tris, 1 mM ethylenediaminetetraacetic acid (Tris-EDTA) buffer, pH 9.0 at 95°C, and the slides were blocked in 2% (v/v) normal goat serum in TBS-$CaCl_2$ for 30 minutes. The sections were subsequently incubated overnight at 4 ºC with rabbit primary antibody against HIF-1α (4 μg/ml; NB100-449, Novus Biologicals), before Powervision goat-anti-rabbit (Immunologic, DPVR-55HRP) was applied for 30 minutes. Rabbit immunoglobulin (4 μg/ml, DAKO X0903) was used as a control antibody.
For pimonidazole staining the sections were incubated in 0.3% (v/v) H_2O_2 in TBS-$CaCl_2$ for 10 minutes, followed by antigen retrieval with 1 mg/ml pronase and 10 mg/ml hyaluronidase in TBS-$CaCl_2$, each for 30 minutes at 37 ºC. The sections were then blocked in 5% (w/v) BSA in TBS-$CaCl_2$ for 30 minutes and incubated with rabbit primary antibody against pimonidazole (0.1 μg/ml; 2627, Hypoxyprobe™-1 Omni Kit; Natural Pharmacia International, Burlington, USA) for 1 hour. Goat anti-rabbit (2.5 μg/ml; P0448; DAKO) was applied as a secondary antibody for 1 hour. Rabbit immunoglobulin (0.1 μg/ml, DAKO; X0903) was used as a control antibody.
For Glut-1 staining the sections were incubated in 0.3% (v/v) H_2O_2 in TBS-$CaCl_2$ for 10 minutes, followed by antigen retrieval with 10 mM sodium citrate buffer, pH 6.0 for 30 minutes at 95 ºC. The sections were then blocked in 5% (w/v) BSA in TBS-$CaCl_2$ for 30 minutes and incubated with primary polyclonal antibody to human Glut-1 (cross-reacts with goat, 11 μg/ml, A3536, DAKO). Goat-anti-rabbit-Powervision (Immunologic, DPVR-55HRP) was used as a secondary antibody. Rabbit immunoglobulin (11 μg/ml; DAKO, X0903) was used as a control antibody. The amount of Glut-1 positive cells present in the constructs was determined by measuring the percentage of positive staining per total amount of present cells using Adobe Photoshop software, version 10.0 (Adobe Systems, San Jose, CA) and ImageJ software, version 1.42q (National Institutes of Health, Bethesda, MD) as previously described.[489,490]
All stainings were developed with 3,3'-diaminobenzidine (DAB) and counterstained with Mayer's hematoxylin (Merck).

VEGF analysis

Porous ($10x10^6$ hMSCs/ml gel) and solid ($5x10^6$ hMSCs/ml gel) alginate constructs were incubated in expansion medium for 3 and 7 days, and the medium fractions were collected for VEGF ELISA (n=4). Medium from porous constructs cultured in 2% O_2 for 3 and 7 days was used as positive control. Fresh medium served as a negative control. To collect VEGF residing in the gel, the alginate in the constructs was depolymerized by 30 minutes incubation with 10 mM sodium citrate buffer, pH 6.0 at 37 °C and gel fractions were analyzed next to culture medium fractions. Depolymerized alginate construct without cells served as a negative control. VEGF ELISA (R&D Systems human VEGF Quantikine Immunoassay DVE00) was performed on undiluted samples according to manufacturer's recommendations.

Glucose and lactate analysis

Porous (10^7 gMSCs/ml gel) and solid ($5x10^6$ gMSCs/ml gel) alginate constructs were incubated in expansion medium for 1, 2, 3 and 7 days, and the medium fractions were collected for glucose and lactate analysis (n=4 per group and time point). Fresh medium was used as a reference. The medium fractions were analyzed using a VITROS DT60 II chemistry system (Ortho-Clinical Diagnostics, Tilburg, The Netherlands).

Viability analysis

Four samples of each hydrogel (porous and solid) were evaluated with a LIVE/DEAD assay (Molecular Probes MP03224, Eugene, USA) at days 3 and 7 after printing, performed according to the manufacturer's recommendations. The samples were scored using a fluorescence microscope (Olympus BX51, Olympus DP70, Japan). The excitation/emission filters were set at 488/530 nm to observe living (green) cells and at 530/580 nm to detect dead (red) cells. The cell viability was calculated as the average ratio of vital to total cells in a sample, determined from four randomly chosen fields per scaffold.

TUNEL apoptosis assay

For terminal deoxynucleotidyl transferase dUTP nick end labeling (TUNEL) of fragmented DNA, indicative of late apoptosis, porous and solid gMSC-laden constructs were harvested at day 7 and fixed in 4% (v/v) formalin in 100 mM $CaCl_2$ in distilled water. The samples were processed for paraffin histology and 5 μm thick sections were cut, rehydrated in graded ethanol series and antigen retrieval was conducted by incubation with proteinase K (20 μg/ml in 10 mM Tris/HCl buffer; Roche Applied Science, Mannheim, Germany) at 37°C for 30 minutes. TUNEL reaction was performed using the Roche in situ cell death detection kit according to the manufacturer's instructions. Stained sections were washed in TBS and embedded in Vectashield containing DAPI nuclear stain. The excitation/emission filters were set at 365/450 nm for detection of DAPI (blue) and at 488/530 nm for detection of apoptotic cells (green). The number of apoptotic cells was calculated as the percentage of TUNEL-positive cells to total cells, calculated from four randomly selected fields in four constructs per group.

Proliferation analysis

Solid and porous gMSC-laden constructs were harvested on day 7 and the percentage of proliferating cells in cryosections was determined by immunocytochemical detection of Ki67, a marker of active cell-cycling.[425] Briefly, the cryosections were air dried, fixed in 100% acetone for ten minutes, washed in TBS/$CaCl_2$, and incubated with 0.3% (v/v) H_2O_2 in TBS for ten minutes

followed by a blocking step in 5% (w/v) BSA in TBS for 30 min. The sections were then incubated with mouse anti-human Ki67 antibody (cross-reacts with goat; 0.8 μg/ml in 5% (w/v) BSA in TBS; DAKO M7240) for 1 hour, followed by incubation with goat anti-mouse, 5 μg/ml in 5% (w/v) BSA in TBS; Immunologic) for 1 hour. Wash steps with 0.1% Tween20 in TBS-$CaCl_2$ were performed between the incubations. The staining was developed with DAB and counterstained with Mayer's hematoxylin. The percentage of proliferating cells was determined by calculating the average ratio of positive nuclei over total cells from three randomly selected fields in four constructs per group.

Analysis of osteogenic differentiation

For the evaluation of alkaline phosphatase activity of encapsulated gMSCs, the constructs cultured in osteogenic medium were harvested at day 7 and processed for cryosections. The sections were air-dried, fixed with 100% acetone for 10 minutes and incubated in 0.2% (v/v) Triton-X100 in TBS for 10 minutes. Wash steps were done in TBS supplemented with 102 mM $CaCl_2$. The activity of alkaline phosphatase was determined by 60-minute staining with the Fuchsin Substrate-Chromogen system (K0624, Dako, Carpinteria, USA). The sections were counterstained with Weigert's hematoxylin, and mounted with Aquatex. The presence of alkaline phosphatase-positive cells was analyzed with a light microscope equipped with an Olympus DP70 camera.

Presence of collagen type I was assessed by immunocytochemistry of gMSC-laden constructs harvested at day 14. For this, the paraffin sections were rehydrated and incubated in 0.3% (v/v) H_2O_2 in TBS for ten minutes followed by antigen retrieval in citrate buffer for 20 minutes. The sections were then blocked in 5% (w/v) BSA in TBS for 30 min and incubated overnight at 4 ºC with mouse anti-collagen type I antibody (20 μg/ml in 5% (w/v) BSA in TBS, clone I-8H5, Calbiochem, Darmstadt, Germany). A biotinylated secondary antibody was applied (5 μg/ml in 5% (w/v) BSA in TBS, biotinylated sheep anti-mouse, RPN1001V1, GE Healthcare, Diegem, Belgium) for one hour and the staining was enhanced by incubation with streptavidin-peroxidase for an additional hour (2 μg/ml, PN IM0309, Immunotec, Montreal, Canada). The staining was developed with DAB and counterstained with Mayer's hematoxylin.

The amount of hMSC-produced osteocalcin (OCN) in the medium and residing in the gel (n=4) was assessed by OCN ELISA (KAQ1381, Invitrogen) at day 21, according to the manufacturer's instructions. Samples of porous and solid constructs were depolymerized by 30-minute incubation in citrate buffer (150 mM sodium chloride, 55 mM sodium citrate, pH=7.4) at 37 °C and analyzed simultaneously with osteogenic medium fractions collected from the constructs. Depolymerized acellular alginate constructs served as negative controls.

Tissue development

Paraffin sections of *in vivo* implanted gMSC-laden constructs were stained with hematoxylin and eosin (HE) for general visualization of tissue development. The degree of tissue ingrowth was determined in transverse sections of the constructs (n=7 per group per time point) by measuring μm ingrown tissue as percentage of the thickness of the construct in μm.

To detect blood vessels, the sections were stained for endothelial marker von Willebrand factor (vWF) and α-smooth muscle actin (α-SMA). vWF detection was performed on rehydrated sections, which were preincubated in 3% H_2O_2 for ten minutes and 10% (v/v) normal goat serum in PBS for 20 minutes, and subsequently incubated with rabbit anti-human vWF antibody (15 μg/ml; DAKO). As secondary antibody we used powervision goat anti-rabbit HRP for one

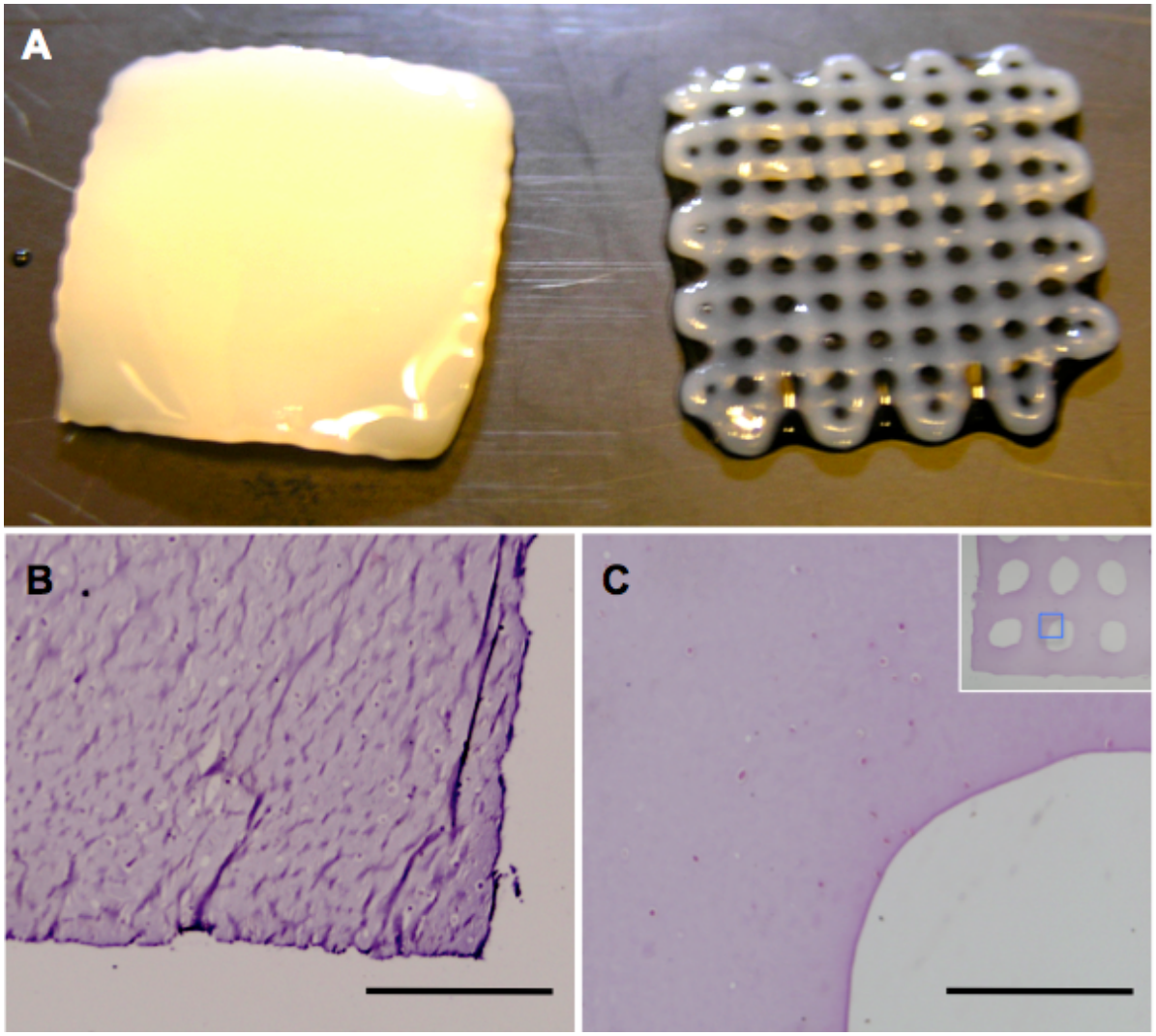

Figure 7.1: Printed cell-laden alginate constructs. A: Macroscopic view of the printed alginate constructs, B-C: HE staining, solid (left) and porous (right) printed construct; scale bar = 200 μm; D-G: see next page.

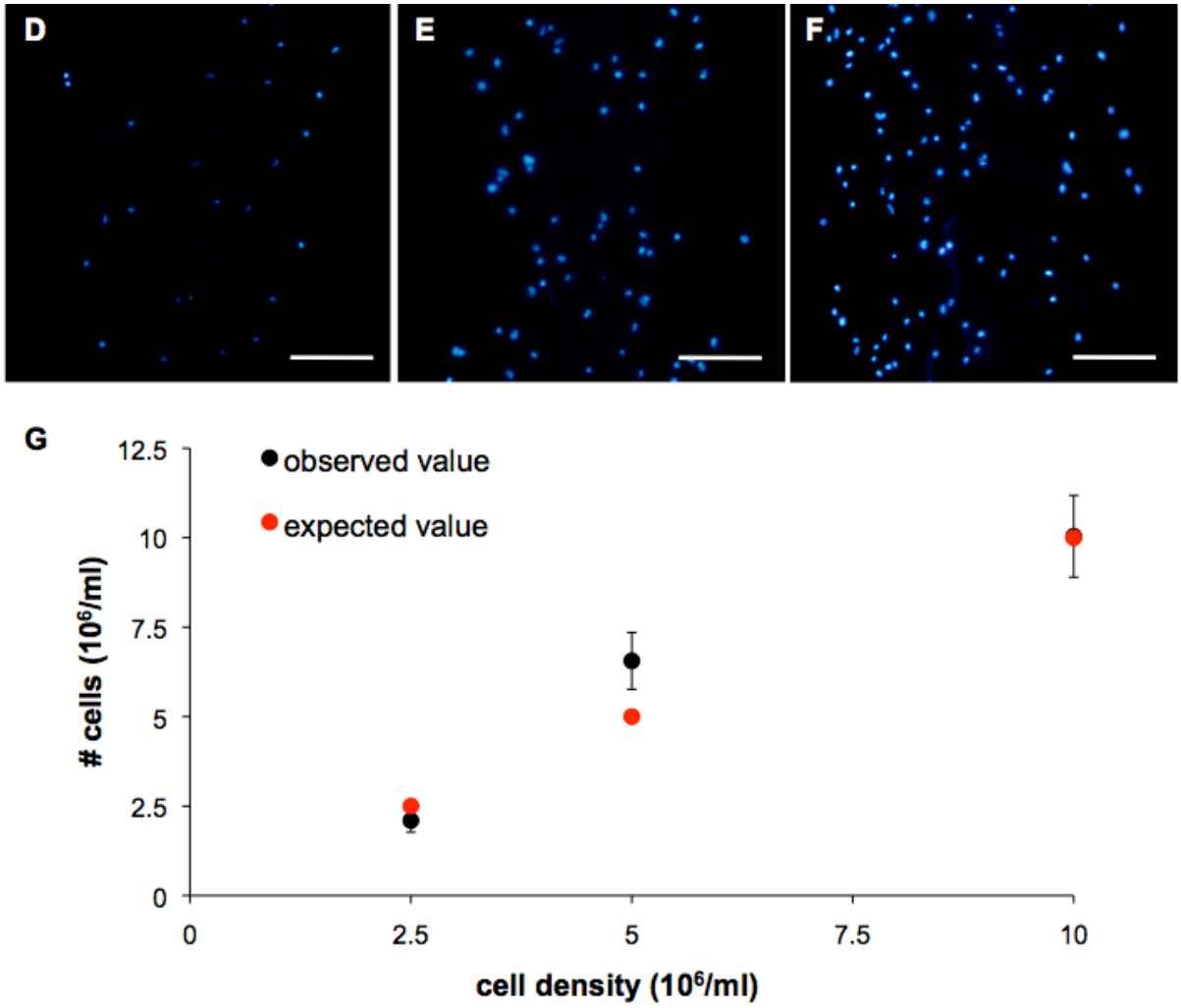

Figure 7.1: Printed cell-laden alginate constructs. A-C: see previous page. D: dispersion of hMSCs (DAPI nuclear stain (blue)) in alginate strands: $2.5x10^6$ cells/ml; E: $5x10^6$ cells/ml alginate, F: $10x10^6$ cells/ml alginate, scale bar = 50 μm; G: number of cells per ml printed gel (black), expected number of cells/ml gel (red), data presented as mean±SD (n = 8).

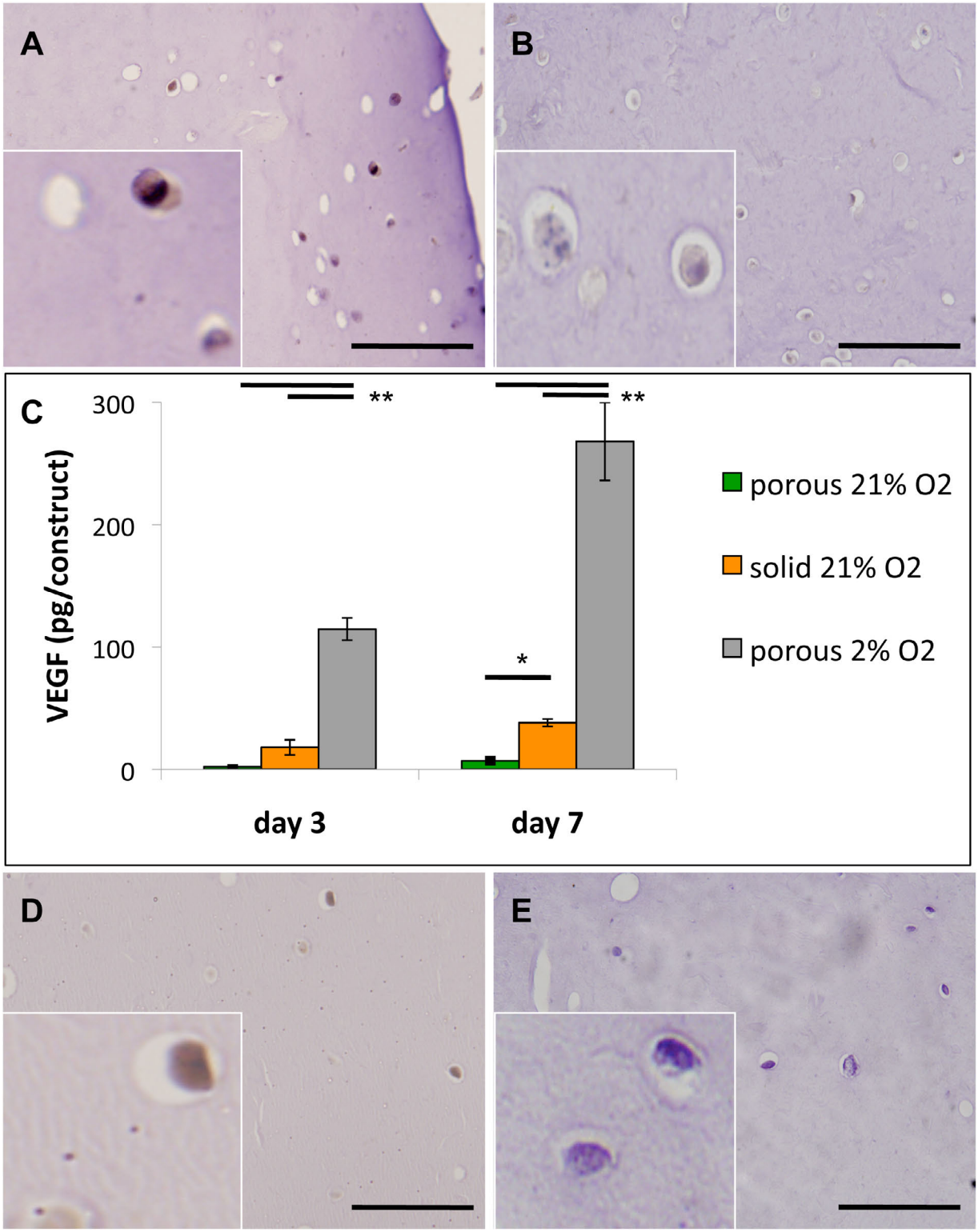

Figure 7.2: Hypoxia markers *in vitro*. A, B: HIF-1α immunohistochemistry on gMSCs (brown) in solid (left) and porous (right) constructs at day 2, scale bar = 100 µm; C: VEGF production by hMSCs per construct (in culture medium and depolymerized alginate) in printed alginate constructs, data presented as mean±SD (n = 4); *p<0.01; **p<0.001; D, E: pimonidazole staining (brown) of gMSCs in solid (left) and not in porous (right) constructs, at 7 days, scale bar = 100 µm.

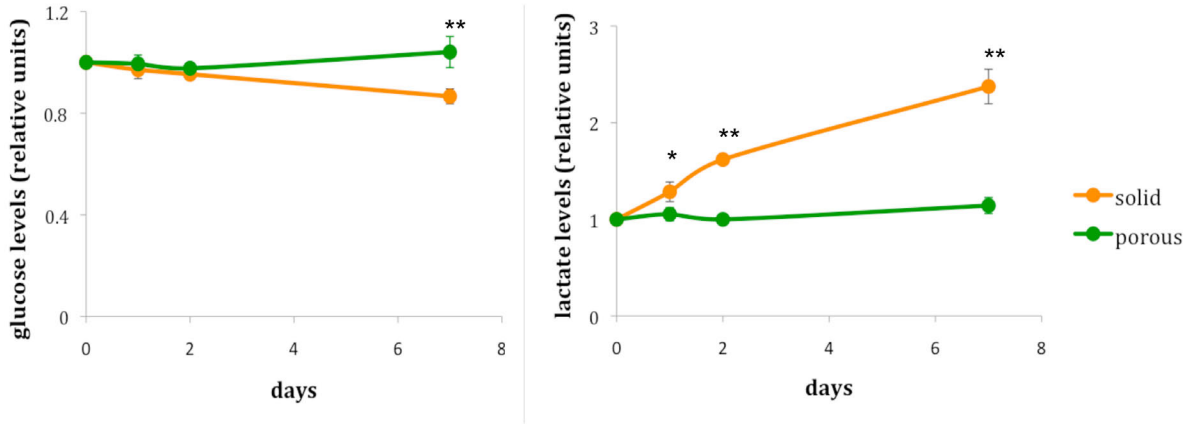

Figure 7.3: Metabolism of embedded gMSCs. Glucose (left panel) and lactate (right panel) levels in porous and solid constructs, presented relative to day 0 values, presented as mean ± SD (n=4), *p<0.05; **p<0.001.

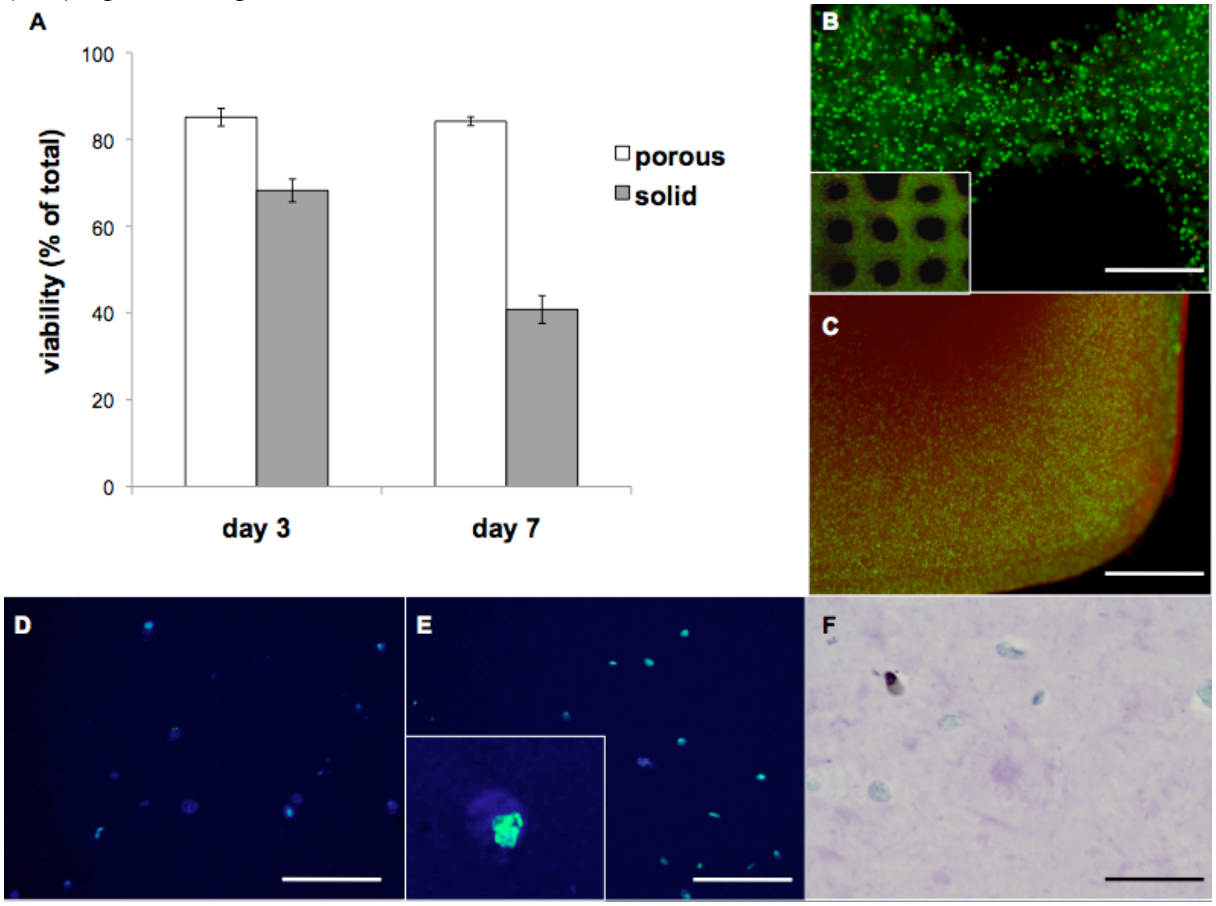

Figure 7.4: Viability and proliferation of MSCs in the printed constructs. A: Viability quantification of hMSCs, data presented as mean±SD (n = 4); B, C: LIVE/DEAD assay in porous (above) and solid (below) constructs, live cells (green), dead cells (red), scale bar = 500 µm and 1 mm, respectively; D, E: TUNEL staining of apoptotic cells (green) in porous (left) and solid (right) constructs, counterstaining with DAPI nuclear stain (blue), scale bar = 100 µm; F: Ki67-positive MSCs (brown), encapsulated in solid alginate (purple) scaffold at day 7; counterstaining with hematoxylin (blue), scale bar = 25 µm.

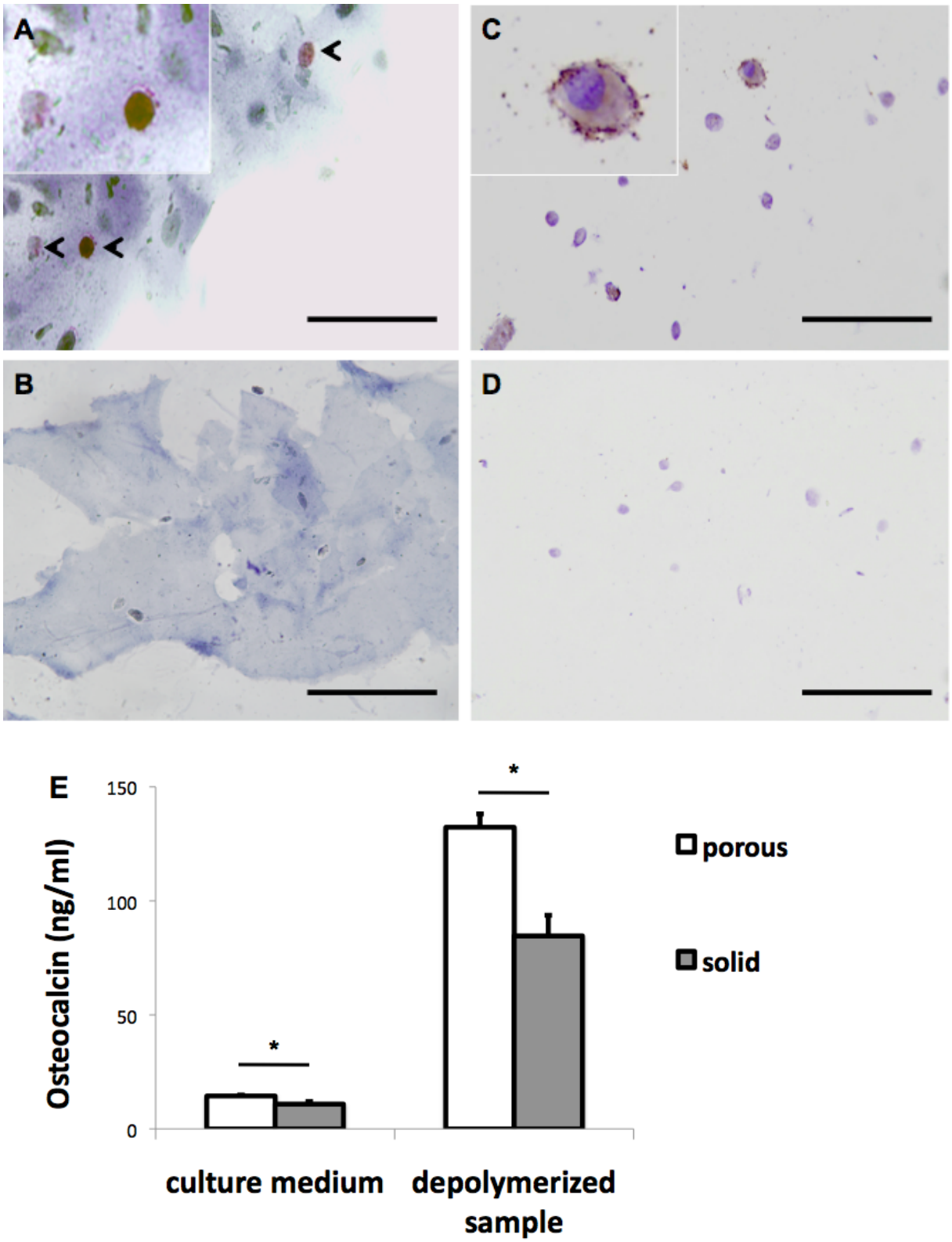

Figure 7.5: Osteogenic differentiation of MSCs in porous and solid constructs. A, B: ALP-staining of gMSCs (red, arrows) embedded for 7 days in porous (top) and solid (bottom) grafts; C, D: collagen type I immunohistochemistry (brown) on porous (top) and solid (bottom) constructs at 14 days, counterstained by Mayer's hematoxylin, scale bar = 50 µm; E: osteocalcin levels, determined by ELISA of culture medium and depolymerized gel of hMSC-loaded constructs after 21 days (*$p<0.05$), data presented as mean±SD, n = 4.

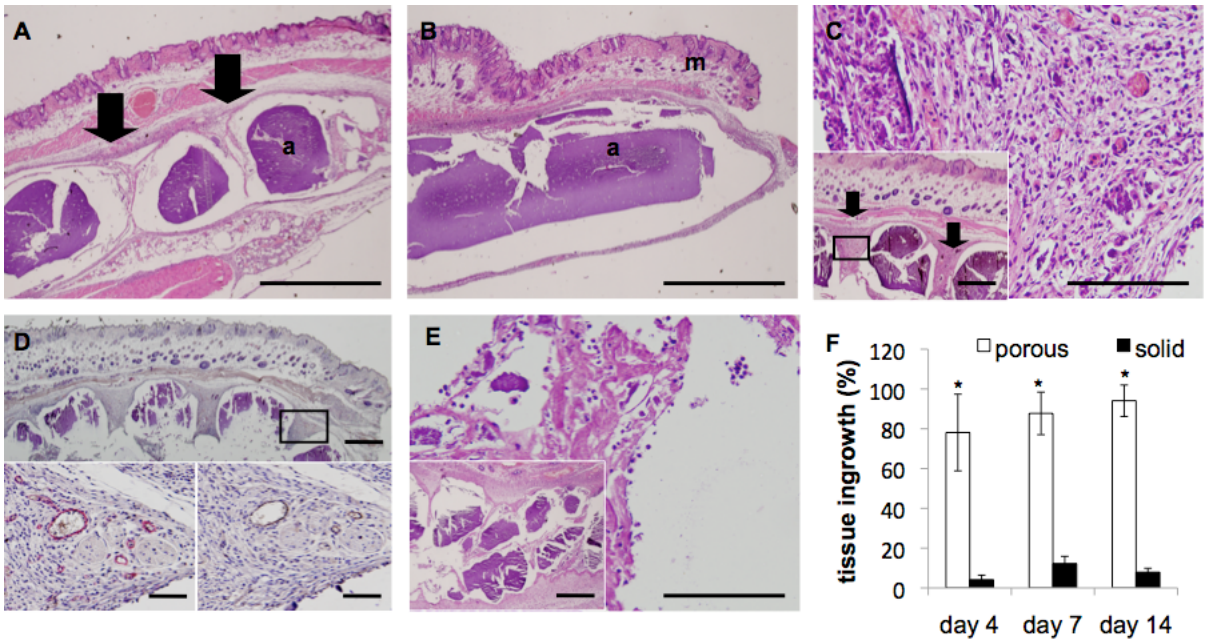

Figure 7.6: Histology of the implants. A, B: HE staining of cell-laden porous (left) and solid (right) graft, 4 days after implantation, a=alginate; m=mouse tissue; tissue ingrowth in the pores (arrows), scale bar = 1 mm; C, D: gMSCs-laden graft after 14 days, with C: tissue ingrowth in the pores (arrows), scale bar = 200 μm, (inset = overview of the graft; arrows indicate pores, scale bar = 500 μm); D: immunostaining of blood vessels in the pores of the construct, 14 days, scale bar = 500 μm; α-SMA (inset left, in red; scale bar = 100 μm) and vWF (inset right, in brown, scale bar = 100 μm); E: porous implant (acellular), 14 days, scale bar = 100 μm, (inset: overview of the graft, scale bar = 1 mm); F: quantification of tissue infiltration at 4, 7 and 14 days (*$p<0.01$; $n = 7$).

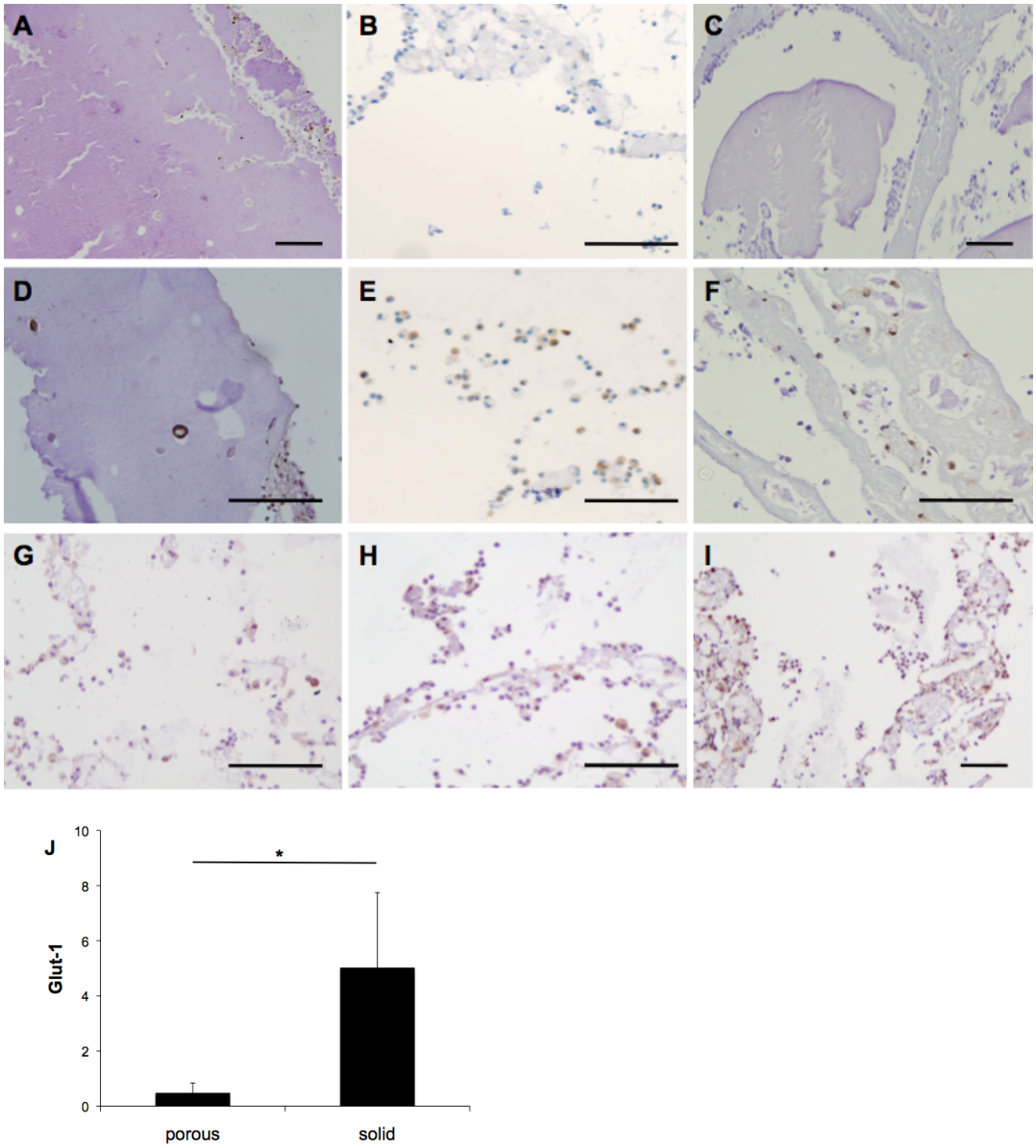

Figure 7.7: Hypoxia markers *in vivo*. A, D: HIF-1α staining (brown) in porous (top) and solid (below) grafts, 4 days post-implantation; B, E: GLUT-1 immunostaining (brown) in porous (top) and solid (below) implants, 7 days; C, F: pimonidazole staining (brown) in porous (top) and solid (below) implant, 14 days; G-I: GLUT-1 (brown) is less intense in solid implant with low gMSC concentration, (G: $5x10^6$ cells/ml), compared to constructs with high cell concentration (H, I: $10x10^6$ cells/ml) at day 4 (H) and at day 7 (I); scale bar = 100 μm; J: semi-automatic quantification of Glut-1 cell staining in porous and solid grafts, 4 days post-implantation, showed significantly more positive cells in solid implants (*$p<0.01$; n = 7), data presented as mean ± SD of Glut-1 positive area relative to total amount of nuclei per field of view.

hour. To detect α-SMA, rehydrated sections were incubated with alkaline-phosphatase conjugated mouse primary antibody against α-SMA (1:100 in 5% BSA/PBS; Sigma-Aldrich A5691, clone 1A4) for 1 hour and the presence of ALP was detected by incubation with Fuchsin Substrate-Chromogen system (DAKO) for 30 minutes. The vWF staining was developed with DAB and Mayer's hematoxylin was used for counterstaining. The presence of vWF-positive (brown) and α-SMA-positive (pink-red) structures was assessed in consecutive sections.

Statistical analysis

Statistical analysis was performed with SPSS 12.0.1 software (SPSS Inc, Chicago, IL). A two-way analysis of variance (ANOVA) with Bonferroni post-hoc test was used to compare cell viability (n=4), VEGF production (n=4), glucose/lactate values (n=4), the number of GLUT-1-positive cells (n=7) and the degree of tissue ingrowth (n=7) in porous and solid printed constructs at different time points. A Mann-Whitney test was done to compare osteocalcin production (n=4) in porous and solid constructs. *P*-values of less than 0.05 were considered statistically significant. All values are reported as means ± standard deviation.

Results

Printing of porous and solid scaffolds

Defined, 12-layer alginate constructs (10x10x1mm; Figure 7.1A-C) were printed by the BioScaffolder machine. Vertical pores were regular throughout the samples, while transversal pores fused due to the relative softness of the material. The weight of the porous constructs measured 52±6% (n=8) of the solid grafts, resulting in average porosity of 48%.
Analysis of cell dispersion after printing demonstrated homogeneous encapsulation of cells in hydrogel strands (Figure 7.1D-F). The observed number of cells corresponded to the theoretical calculation based on different prepared cell densities (Figure 7.1G), indicating the cells were not lost during the passage through the syringe and nozzles.

The influence of porosity on endogenous hypoxia markers and hypoxia indicator pimonidazole in vitro

Immunolocalization of hypoxia marker HIF-1α demonstrated intense staining of gMSCs at day 2 in solid constructs compared to porous grafts (Figure 7.2A-B). No staining was observed 7 days after printing (data not shown). Similarly, the production of VEGF by hMSCs was higher in solid grafts compared to porous constructs 7 days after printing (38±5 versus 7±1 pg VEGF, respectively ($p<0.01$); Figure 7.2C). These outcomes indicate that hMSCs embedded in solid constructs experienced more oxygen deprivation than cells in porous grafts. Control porous constructs cultured under hypoxic conditions of 2% O_2 exhibited significantly higher levels of VEGF production, both at 3 and 7 days, suggesting that hMSCs in solid normoxic samples were less hypoxic. Binding of pimonidazole 7 days after printing further corroborated the hypoxic status of gMSCs embedded in solid constructs while this hypoxic marker was not detectable in gMSCs of porous constructs (Figure 7.2D-E).

Cell metabolic activity in vitro

The metabolism of the printed gMSCs in porous and solid constructs was compared by measurement of glucose consumption and lactate production by embedded cells (equal number of cells at the start of experiment). Glucose and lactate values at day 1, 2, and 7, as presented in Figure 7.3, demonstrated that gMSCs in solid constructs consumed more glucose at day 7 and produced more lactate than in the porous grafts at each time point, indicative of a higher level of anaerobic respiration by MSCs in these scaffolds.

Cell survival and proliferation as a result of porosity in vitro

The viability of printed hMSCs, which was determined with LIVE/DEAD assays, measured around 85% in porous constructs both at days 3 and 7, and was as low as 68±3% and 41±3% in solid grafts after 3 and 7 days respectively ($p<0.01$; Figure 7.4A). In these grafts, viable cells were

mostly detected at the periphery of the construct (Figure 7.4C), while they were seen throughout the construct in porous grafts (Figure 7.4B).
The detection of apoptotic cells with TUNEL staining supported the findings of decreased viability of gMSCs embedded in solid constructs as compared to porous grafts (Figure 7.4D-E). After 7 days, in porous constructs 7.3±2.7% cells were apoptotic compared to 40±10.6% in solid grafts (n=4).
Proliferation analysis of gMSCs in porous and solid constructs was assessed by immunohistochemical staining of Ki67. Ki67 is a proliferation marker present during all active phases of the cell cycle (G1, S, G2 and mitosis), and is absent in resting cells (G0). Immunohistochemical analysis showed a small fraction of actively cycling cells in both construct types. The percentage of proliferating Ki67-positive cells (Figure 7.4F) was not different between the two groups, measuring 7.1±2.8% in porous scaffolds and 10.3±3.5% in the solid ones (n=4).

Analysis of osteogenic differentiation in vitro

Osteogenic differentiation by MSCs in porous and solid grafts was assessed by staining for early osteogenic marker alkaline phosphatase (Figure 7.5A-B), and by detection of late osteogenic markers collagen type I (Figure 7.5C-D) and osteocalcin (Figure 7.5E). Only a fraction of the embedded cells differentiated towards the osteogenic lineage in printed alginate scaffolds. gMSCs encapsulated in porous constructs exhibited a higher degree of early osteogenic marker expression than cells in solid scaffolds, measuring around 20% and 5% ALP-positive cells, respectively. In the porous scaffolds, higher numbers of encapsulated gMSCs differentiated along the osteogenic lineage as evidenced by the deposition of collagen type I around the cells (Figure 7.5C, 40% in porous and 17% in solid constructs). Also, osteocalcin production by hMSCs was elevated in the porous constructs compared to solid grafts (both in the culture medium and matrix-bound, $p=0.02$, Figure 7.5E), stressing the importance of scaffold porosity for bone constructs.

Tissue development in vivo

After 4, 7 and 14 days of subcutaneous implantation at the dorsum of immunodeficient mice, the implanted hybrid constructs were well-integrated with the surrounding host subcutaneous tissue (Figure 7.6). Porous hydrogels demonstrated tissue formation in the pores of the construct at all time points, but not in the gel itself (Figure 7.6A). Ingrown tissue exhibited a certain level of maturation in time (Figure 7.6C), showing development of fibrous tissue and blood vessels, as evidenced by the presence of erythrocyte-filled lumina and expression of vWF and α-smooth muscle actin (Figure 7.6D). Porous constructs without cells also enabled tissue ingrowth, but the ingrown tissue demonstrated a lower degree of extracellular matrix organization comprising loose matrix without concomitant formation of new blood vessels (Figure 7.6E). Unseeded porous scaffolds exhibited limited tissue infiltration (Figure 7.6B) at all time points (Figure 7.6F), with some novel tissue development after 14 days, most probably due to degradation of the alginate. The tissue that colonized the degraded regions did not contain blood vessels, yet.
Staining for hypoxia markers HIF-1α and GLUT-1 and hypoxia indicator pimonidazole demonstrated a large fraction of positive cells in solid constructs, compared to low numbers in porous grafts (Figure 7.7A-F, J). Comparison of GLUT-1 staining between solid grafts with high or low concentrations of embedded gMSCs indicated that more positive cells were present in constructs with the higher cell concentration (Figure 7.7G-H), which may indicate higher oxygen consumption by gMSCs in these grafts. The most evident differences in GLUT-1 staining were

observed at day 4. GLUT-1 staining in solid grafts at later time points was less intense (Figure 7.7I).

Discussion

One of the challenges in development of large engineered bone grafts is to ensure the survival and functionality of transplanted cells. In this study we demonstrate that porosity introduced in cell-laden scaffolds by 3DF affects the *in vitro* and *in vivo* oxygenation and functionality of embedded cells. The use of 3DF also implies controlled cell placement of defined cell numbers in printed constructs, which is in contrast to other printing techniques that are limited in that respect.[111,118,176] Control over cell distribution and cell density throughout the construct is thought to be important for tissue development and maturation in cell-laden TE constructs.[491,492] As differentiation is influenced by cell density, cell-laden constructs are expected to profit from techniques that allow deposition of defined and variable cell numbers.[493,494]

In the current study we demonstrate that MSCs embedded in solid constructs are less viable than their counterparts in porous grafts. The initial presence of viable cells inside the graft is crucial for bone formation *in vivo*.[18] Their presence may be essential not only because they actively participate in bone formation, but also due to their stimulatory role in subsequent bone remodeling by paracrine signaling.[11]

It is known that in static cultures of engineered grafts, after as little as 5 days, central oxygen levels can drop to 0%, while at the periphery ambient oxygen levels sustain the viability of the cells.[479] The problem of core hypoxia is aggravated in 3D cultures when diffusion limitations are even more severe, due to increased matrix production and cell density of cells on the outer surface of the graft.[495] A drop in cell viability in solid constructs observed by us is in line with findings in hydrogels[496,497] and in porous, thermoplastic scaffolds.[477] Oxygen consumption is lower in natural matrices, such as collagen and is attributed to an inhibitory effect on cell biosynthetic activity of a natural matrix when compared to a synthetic one.[498,499]

Porosity markedly affects oxygen diffusion in TE constructs.[469,476] This was reflected in our study as the presence of HIF-1α is evident in solid constructs after 2 days of culture, whereas in porous constructs HIF-1α is not detected after 7 days. This observed transient increase of HIF-1α is most probably due to a change in regulation of protein breakdown.[500] Similar to the rise in HIF-1α, its response gene VEGF is increasingly produced by MSCs and more hypoxia indicator pimonidazole is bound by embedded MSCs in solid constructs than in porous grafts. It was indeed reported previously that MSCs cultured under hypoxic conditions show enhanced VEGF production.[72,475,501] Considerably higher amounts of VEGF in control hypoxic samples indicate that the embedded cells in solid grafts are not as hypoxic as MSCs cultured under 2% O_2. In line with the above findings we also show that MSCs embedded in solid constructs produced more lactate, and consumed more glucose, indicative of higher levels of anaerobic metabolism. In this study cell density of 5-10x10^6 cells per ml gel was used, a concentration which lies in the lower range of densities commonly used for hydrogel encapsulation in bone tissue engineering.[70,233,502] As oxygen gradients correlate with cell density and viability[477,496] the use of higher cell concentrations and/or high cell proliferation rates are expected to result in more pronounced cell hypoxia, also eventually inside the printed grafts, warranting the need to adjust the strand thickness in printed scaffolds to smaller diameters.

Scaffold properties interact with metabolic demand of the cells modulating their performance.[496] The proliferation of embedded cells was not affected by porosity of the printed constructs in this study. In the literature both decrease and increase of proliferation by osteogenic cell lines and hMSCs have been described.[464,479] Dimensions of the construct and corresponding cell-oxygenation also influence the differentiation of embedded cells.[453,476] In this study we demonstrated that cells embedded in porous constructs are committed to the osteogenic lineage as evidenced by expression of early osteogenic marker ALP and production of collagen type I and osteocalcin, while osteogenic differentiation in solid constructs is limited.

This study is the first to compare the expression of hypoxia markers by embedded cells in printed porous and solid hydrogel scaffolds upon implantation *in vivo*. We demonstrated that analogous to *in vitro* data, also cells that were implanted *in vivo* in solid constructs expressed higher levels of hypoxia markers GLUT-1, HIF-1α and binding of hypoxia indicator pimonidazole. The correlation found between HIF-1α and pimonidazole measurements is high.[503,504] HIF-mediated transcription of GLUT-1 is dually stimulated in response to hypoxia and low glucose, which in turn promote anaerobic glycolysis in favor of oxidative phosphorylation.[459] We showed that the presence of hypoxia marker GLUT-1 *in vivo* subsides after 7 days, either due to protein breakdown or decreased hypoxic responses by the cells. This finding is supported by hypoxia analysis of cells in tissue-engineered chambers with AV loops, where hypoxia occurs in the first 10 days and then declines.[505] In parallel, protein expression studies of GLUT-1 in colorectal cancer indicate a fast rise of protein two hours after oxygen deprivation, which lasts for one day and subsides to basal levels thereafter.[506]

Ingrowth of blood vessels into the pores of the scaffold promotes oxygenation of engineered grafts[505] and is widely thought to be crucial for new bone formation. *In vivo*, it appears to be a good strategy to engineer vasculogenesis-promoting features such as interconnected channels in biomaterials capable of serving as conduits for neovascularization in TE grafts.[249] Engineered microchannels facilitate *in vivo* sprouting angiogenesis and host tissue ingrowth in TE constructs, providing the basis for inducing neovascularization *in vivo*.[507] In the current study, tissue ingrowth was pronounced more in porous constructs compared to solid constructs, at all time points. Although the origin of the ingrown tissue was not confirmed by additional staining, we are confident it is of host origin, based on the finding that transplanted cells only form very limited ECM in alginate *in vivo*. Blood vessel formation in the newly formed tissue, assessed by immunolocalization of endothelial marker vWF, started within 7 days and was abundant after 14 days of *in vivo* implantation. The presence of erythrocytes indicates the patency of the formed vessels. Our results correspond well to findings by others, reporting a peak in vascular development between 7 and 10 days, with sprouting of capillaries from day 3, arterioles from day 7 and venules a few days later.[508]

Unexpectedly, no tissue formation occurred inside the alginate hydrogel after 14 days of implantation. The seaweed-derived polysaccharide supports osteogenic differentiation,[509] and provides a relatively strong (5-15 kPa), yet non-interactive encapsulation matrix to the embedded cells. This material is widely used for organ printing applications,[115,116] however, the interaction of the cells with alginate is limited. The MSCs exhibit a round morphology upon encapsulation and do not actively degrade this matrix, demonstrating ECM formation that limited to direct surroundings of the cell. More interactive matrices such as for example alginate modified with adhesive RGD sequences or collageneous matrices (e.g. Matrigel), demonstrate more widespread deposition of ECM. *In vivo,* alginate elicits a limited foreign-body response, degrades by bulk erosion and is engulfed by the macrophages, demonstrating formation of collagen type I-rich

ECM after 6 weeks of implantation when supplemented with osteoinductive calcium phosphate particles (unpublished data).

The present study identifies the introduction of printed pores in TE constructs as an effective strategy to increase oxygenation and differentiation of embedded cells. Future directions further promoting the oxygenation of the embedded cells may include scaffolds containing oxygen-generating materials that maintain elevated levels of oxygen when incubated under hypoxic conditions. These biomaterials are able to extend cell viability and proliferation under hypoxic conditions,[510] and are based on chemical decomposition of solid sodium percarbonate to produce oxygen over a period of hours.[511] Ultimately, printed porous scaffolds with oxygen-generating materials might be combined with prevascularization of the graft with endothelial cells, or their progenitors[167] - another promising strategy to enhance oxygen delivery to the interior of the grafts. This combined approach could potentially lead to development of large bone grafts for clinical application.

The currently used soft hydrogels can hardly meet the requirement of bone tissue biomechanics. An important advance is the development photoliable synthetic hydrogels, in which the desired viscoelasticity can be tuned.[129] An alternative lies in combined printing of stiff materials with mechanically weak hydrogels.[102] This approach profits from, respectively, cell-supportive properties of gel matrices and increased elasticity of the resultant scaffolds for implantation, although full load bearing application remains an unmet challenge. For many tissue defects it might not be necessary to provide implants with the original biomechanical properties of the regenerated tissue, because the scaffold is meant to be completely remodeled.

Conclusions

Organ printing is a potent tool for the construction of cell-laden hydrogel constructs, which enables creation of porous hydrogel grafts. In this study we demonstrate that the porosity of MSC-laden hydrogel constructs affects the functionality of the embedded progenitors, enhancing their oxygenation, viability, and osteogenic differentiation *in vitro*. Porous grafts support oxygenation of the embedded cells *in vivo* and enable host tissue ingrowth and vascularization.

Acknowledgements

We thank E. Bosman for her assistance with immunocytochemical stainings. We acknowledge the financial support of the Mosaic scheme 2004 of the Netherlands Organization for Scientific Research (NWO; grant number: 017.001.181), the Dutch Program for Tissue Engineering (project number: UGT.6743), the Anna Foundation, the Smart Mix Program of the Netherlands Ministry of Economic Affairs and the Netherlands Ministry of Education, Culture and Science, and the support from the UMC Utrecht Regenerative Medicine Strategic Program.

Chapter 8

The osteoinductive potential of printable, cell-laden hydrogel-ceramic composites

Fedorovich NE[1], Leeuwenburgh S[2], van der Helm Y[1], Alblas J[1], Dhert WJA[1,3]

Manuscript in preparation

[1]*Department of Orthopaedics, University Medical Center Utrecht, Utrecht, The Netherlands*
[2]*Department of Biomaterials, Radboud University Nijmegen Medical Center, Nijmegen, The Netherlands*
[3]*Faculty of Veterinary Medicine, Utrecht University, Utrecht, The Netherlands*

Abstract

Unmodified hydrogels used as injectables or in organ printing often lack the appropriate stimuli to direct osteogenic differentiation of embedded multipotent stromal cells (MSCs), resulting in limited bone formation in these matrices. Addition of calcium phosphate (CaP) particles to the printing mixture is hypothesized to overcome this drawback. In this study we have investigated the effect of CaP particle characteristics on the osteoinductive potential of cell-laden hydrogel-CaP composite matrices printed with 3D fiber deposition. To this end, apatitic nanoparticles have been included into injectable Matrigel constructs whereafter the viability of embedded progenitor cells was assessed *in vitro*. In addition, the osteoinductive potential of cell-laden Matrigel containing apatitic nanoparticles was compared *in vivo* against composites containing osteoinductive biphasic phosphate (BCP) microparticles by subcutaneous implantation in immunodeficient mice, followed by histological and immunohistochemical analysis of the general tissue response as well as *in vivo* bone formation. For the time point as evaluated in this study, BCP particles lead to elaborate bone formation at ectopic location, while apatitic nanoparticles induced osteoclastogenic tissue response without bone formation.

Introduction

Successful closure of large osseous defects is an active area of basic and clinical research in regenerative medicine. In order to make clinically relevant sized grafts, the technique must be improved to optimize the growth rate, strength and yield of the newly formed bone.[512] Attention has therefore been given to approaches that can stimulate the osteogenic differentiation of multipotent stromal cells (MSCs) *in vitro* and promote bone formation *in vivo*. A wide variety of supportive matrices, including hydrogel-forming polymers often used as injectables, have been combined with MSCs to repair bone defects.[407] Recently, organ printing has received increasing interest as a novel approach in regenerative medicine towards deposition of cell-encapsulating hydrogels to yield 3D-structured hybrid constructs.[513] Using this rapid prototyping (RP)-based technique, heterogeneous constructs can be printed with distinct materials and cell populations at defined locations within one construct.[117] Several rapid prototyping fabrication approaches have been recently use for construction of 3D calcium phosphate-laden scaffolds with predefined architecture.[514] Most of these RP approaches are based on computer-aided design of 3D structures of a predefined external shape and internal morphology without the need for successive machining. The resulting (acellular) 3D scaffolds can be built using three-dimensional ink-jet printing (3DP) and injection molding,[19,385,515] stereolithography,[516] robocasting[517] and direct-write assembly.[514] Organ printing with 3D fiber deposition (3DF) combines simultaneous dispensing of viable cells with the RP-based fabrication of a scaffold,[117] and offers an attractive tool to process MSC-laden hydrogels supplemented with calcium phosphate particles for bone regeneration.

Hydrogels used as injectables or for printing often lack the appropriate stimuli to direct osteogenic differentiation of embedded MSCs, resulting in limited bone formation in these matrices. Addition of bioactive calcium phosphates to the printing mixture is hypothesized to overcome this drawback, and in previous studies it was indeed shown that injection of MSCs with hydrogel/HA/TCP/microparticles results in elaborate bone formation at both ectopic and orthotopic locations.[327,375,518,519] The most widely investigated calcium phosphates are hydroxyapatite (HA) and β-tricalcium phosphates (β-TCP)[520] and mixtures thereof that are referred to as biphasic calcium phosphates (BCP). Above-mentioned materials are osteoconductive and can be osteoinductive depending on the specific preparation conditions.[521-523] The ratio of HA and TCP in BCP can be varied to alter the degree of degradation of the BCP. Gradual degradation of BCP at the implant site releases calcium and phosphorus ions into the microenvironment of the cells, creating a favorable medium for new bone formation. The surface chemistry and microstructure are also thought to play an important role in osteoinduction, possibly because of differences in protein adsorption, ion release and bone-like apatite formation.

Over the past decades, extensive research efforts have been dedicated to the use of calcium phosphates as injectables for development of minimally invasive techniques, either as injectable cements or as particulates in suspension with hydrogels.[518] In order to prepare injectable osteoinductive formulations with hydrogels, ceramic microparticles are preferred to larger granules of mm-cm range. Injectable particles-based implants can be used next to calcium phosphate blocks of cm-scale for bone induction as they demonstrate bone formation throughout their cross-section caused by the high specific surface area and corresponding accessibility for tissue infiltration.[524] Generally, the injectability of calcium phosphate pastes increases with decreasing filler particle size.[525] Therefore, nanoparticles could be an interesting alternative to microparticles for inclusion in injectable - and thus printable - formulations for

bone regeneration. Besides the practical benefits of the use of CaP nanoparticles in injectable hydrogel-CaP composites, it should be realized that the mineral phase of bone is also comprised of a nanostructured CaP phase.[526] The inorganic phase of bone matrix - carbonate-substituted hydroxyapatite (HA; $Ca_{10}(PO_4)_6OH_2$) - consists of thin, flat plate nanocrystals (50 nm in length, 25 nm in width, and 2-5 nm in thickness) that lie parallel to each other in alignment with the continuous matrix that consists of tropocollagen molecules. Besides mechanical reinforcement of the composite, apatititic nanoparticles are known to increase the biological performance of bone-substituting materials owing to the formation of a chemical bond with surrounding bone tissue as well as their intrinsic affinity to biologically active proteins such as growth factors. Polymer/HA nanocomposites have enhanced cell-attachment, spreading and proliferation on their surfaces ascribed to higher hydrophilicity and serum protein adsorption on the surface of the nanocomposites.[527-529] Generally, a major challenge in synthesis of nanoceramic-reinforced polymers is the achievement of a fine dispersion of nanoparticles throughout the (hydrogel) polymer, since the unique properties of nanocomposites are lost when nanoparticles aggregate.[530] In this study we have investigated the osteoinductive effect of CaP particles on in cell-laden hydrogel-CaP composite matrices printed with 3DF. To this end, apatitic nanoparticles have been included into injectable Matrigel constructs whereafter the viability of embedded progenitor cells was assessed *in vitro*. Matrigel was chosen due to its processability with 3DF, high cytocompatibility and ability to support osteogenic differentiation of embedded MSCs *in vitro* and bone formation *in vivo*.[407] In addition, the osteoinductive potential of cell-laden Matrigel containing apatitic nanoparticles was compared *in vivo* against Matrigel composites containing osteoinductive BCP microparticles. To this end, the cell-laden hydrogel/CaP constructs were implanted ectopically in subcutaneous pockets in immunodeficient mice followed by histological and immunohistochemical analysis of the general tissue response as well as *in vivo* bone formation.

Materials and Methods

Synthesis of biphasic calcium phosphate microparticles

Irregularly shaped microparticles of biphasic calcium phosphate (BCP) were supplied by Progentix Orthobiology BV. BCP was composed of 80±5 wt% of hydroxyapatite (HA) and 20±5 wt% of β-tricalcium phosphate (β-TCP) as determined using X-Ray Diffraction, and particles were sintered for eight hours at 1150°C.[531] The particle size ranged from 100 to 200 micrometers (Figure 8.1A)

Synthesis of nanoparticles

Apatitic nanoparticles were prepared using a well-known wet-chemical neutralization reaction between phosphoric acid and calcium hydroxide.[532-534] Briefly, a concentrated slurry of poorly crystalline carbonate apatite nanoparticles was produced at a Ca/P ratio of 1.67 by slowly dripping 10 mL of a phosphoric acid solution in PBS (10.73 M) to 40 mL of a basic suspension of calcium hydroxide in PBS (4.42 M) at a temperature of 25 °C yielding a suspension in PBS with a final apatite content of 35 w/v% (Figure 8.1B).

Isolation and culture of multipotent stromal cells

MSCs were isolated from iliac bone marrow aspirates of Dutch milk goats and culture-expanded as described previously,[18] in the medium consisting of α-minimum essential medium (Gibco) supplemented with 100 U/mL penicillin, 100 μg/mL streptomycin (Gibco), 2 mM L-glutamine (Glutamax; Gibco), and 15% (v/v) fetal calf serum. For osteogenic differentiation, the culture medium was supplemented with 10^{-8} M dexamethasone (Sigma), 10 mM β-glycerophosphate (Sigma) and 0.1 mM ascorbic acid (Sigma). Medium was refreshed twice a week and cells were used for further sub-culturing or cryopreservation. MSCs passage 2-6 were used in these experiments.

Assessment of in vitro cell viability

Monolayers of MSCs, plated in 96-wells plate at 10^4 cells/well, were exposed to culture medium supplemented with nanoparticle-slurry (15 % (v/v)), as described above. Viability analysis was performed after 24 hours of incubation using a LIVE/DEAD assay according to the manufacturer's recommendations (Molecular Probes MP03224, Eugene, USA) (n=4). Living and total cell numbers were scored using a fluorescence microscope. The cell viability was calculated as the average ratio of vital over total cells in a sample, determined from four randomly chosen fields per sample.

To investigate the effect of the addition of apatitic nanoparticles on the viability of embedded MSCs, cell viability was measured in MSC-laden Matrigel plugs containing nanoparticles. Control Matrigel plugs were MSC-laden. The constructs (n=4 per group) were cultured for up to one week in expansion medium, and the viability of the cells was determined at one and seven days of culture using a LIVE/DEAD assay (as described above).

Preparation of hybrid constructs for ectopic implantation

Dry BCP particles and apatitic nanoparticle slurry as described above were mixed with culture medium containing cells and kept on ice. Growth factor depleted Matrigel (#356320, BD Biosciences) was added to the mixture, yielding hybrid gels with BCP (15% (w/v)) or nanoparticles (15 % (w/v)) and $5x10^6$ cells/ml gel. Samples of 200 μl were transferred to syringes of 1 ml (BD Plastipak) and allowed to solidify on a roller bank at 37 °C for 24 hours.

In vivo implantation

For *in vivo* assessment, tissue formation was studied in composite constructs (200 μl) composed of i) Matrigel/MSC constructs containing BCP microparticles and ii) Matrigel/MSC constructs containing apatitic nanoparticles. Matrigel plugs laden with MSCs served as negative controls. The constructs were implanted into immunodeficient mice for six weeks (n=8). For this, female nude mice (NMRI-Foxnu, Charles River, Belgium, six-weeks old) were anaesthetized using 1.5% isoflurane followed by injection of the implants in separate subcutaneous dorsal pockets. The incisions were closed using a Vicryl 5-0 suture. The animals were postoperatively treated with the analgesic buprenorphine (0.05 mg/kg, sc; Temgesic, Schering-Plough) and housed together at the Central Laboratory Animal Institute, Utrecht University. Experiments were conducted with the permission of the local Ethical Committee for Animal Experimentation and in compliance with the Institutional Guidelines on the use of laboratory animals.

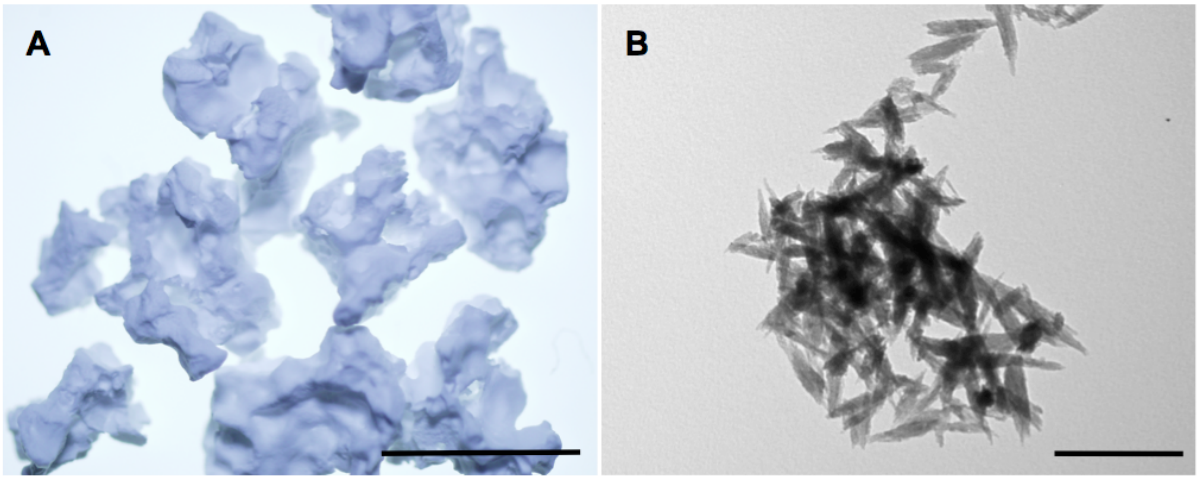

Figure 8.1: Calcium phosphate particles. A: Biphasic (BCP) microparticles, scale bar = 200 µm; B : apatitic nanoparticles, scale bar = 200 nm.

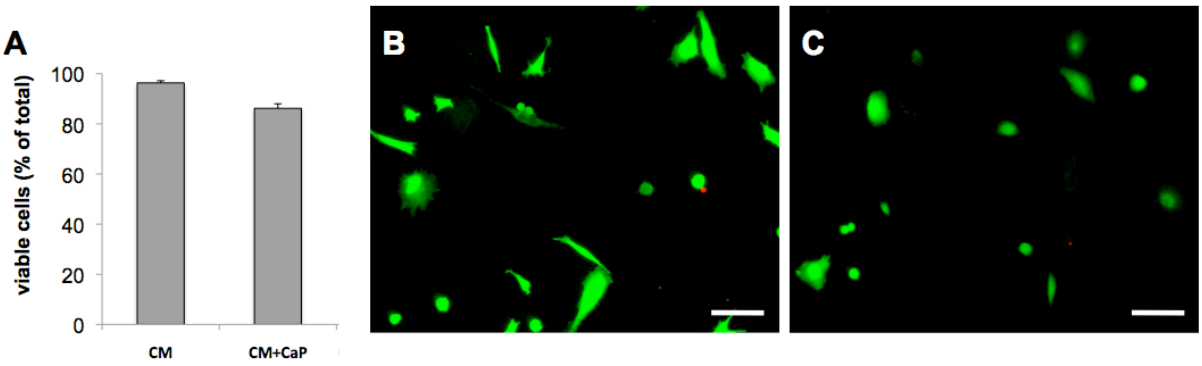

Figure 8.2: Viability of MSC monolayers. A: MSCs viability after 24 hours (n=4); B: In culture medium (CM); C: In culture medium supplemented with nanoparticles (CM+CaP), live cells (green), nuclei of dead cells (red), scale bar = 50 µm.

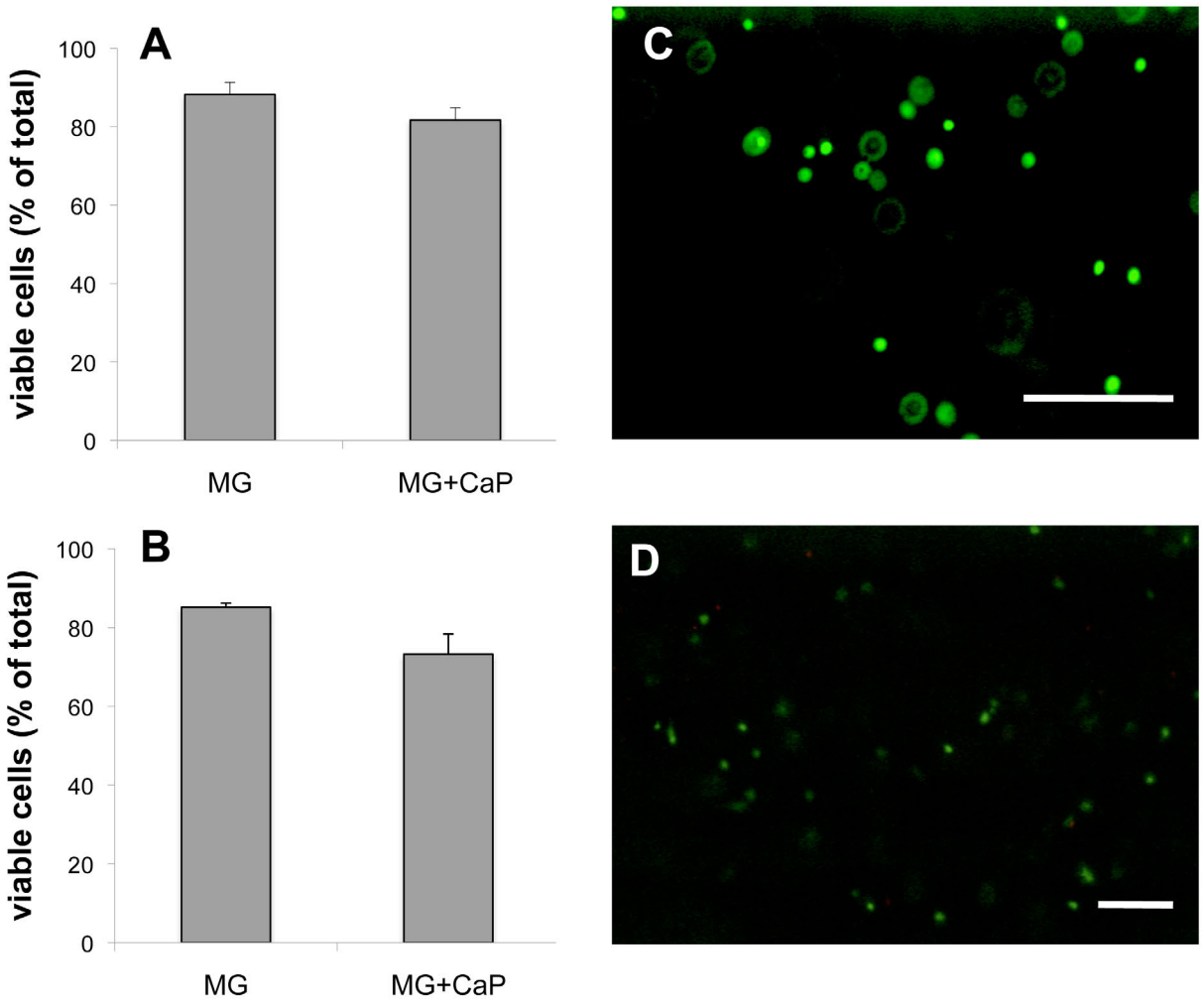

Figure 8.3: Viability of encapsulated MSCs. A: Viability after 24 hours; B: Viability after 7 days (n=4); C: Embedded MSCs in Matrigel (MG); D: MSCs in Matrigel supplemented with nanoparticles (MG+CaP) after 7 days, live cells (green), dead cells (red), scale bar = 200 μm.

Evaluation of tissue formation in vivo

The implants were retrieved six weeks after implantation, and fixed overnight in 4% buffered formalin. To study tissue development and bone formation the samples were subsequently decalcified in Luthra's solution (0.35 M HCl and 2.65 M formic acid in distilled water) for 24 h and processed for paraffin sectioning (5 μm, hematoxylin/eosin (HE) and Goldner's trichrome staining).

Collagen type I immunohistochemical analysis was performed on rehydrated sections that were preincubated in 0.3% H_2O_2 for ten minutes, followed by antigen retrieval with 10 mM sodium citrate buffer, pH 6.0 for 30 minutes at 95 ºC. The sections were then blocked in 5% (w/v) BSA in PBS for 30 minutes and incubated with rabbit polyclonal antibody to collagen type I (3.3 μg/ml in 5% BSA/PBS; Abcam 34710) overnight at 4 °C. As secondary antibody goat anti-rabbit HRP (2.5 μg/ml in 5% BSA/PBS; DAKO) was applied for one hour.

Osteocalcin immunohistochemical analysis was performed on rehydrated sections that were blocked in 5% (w/v) BSA in TBS for 30 minutes and incubated with rabbit polyclonal antibody to osteocalcin (2 μg/ml in 5% BSA/TBS; Alexis ALX-210-333) overnight at 4 °C. As secondary antibody goat anti-rabbit HRP (1.6 μg/ml in 5% BSA/TBS; DAKO) was applied for one hour.

Fibrotic marker collagen type III was stained on paraffin sections, which were rehydrated and blocked in 0.3% (v/v) H_2O_2 in PBS for ten minutes followed by antigen retrieval in pronase (1 mg/ml, 10165921001 Roche Diagnostics, Mannheim, Germany) for 30 minutes at 37 ºC followed by antigen retrieval in hyaluronidase type II (10 mg/ml, H2126; Sigma-Aldrich) for 30 minutes at 37 ºC. The sections were then blocked in 5% (w/v) BSA in PBS for 30 minutes and incubated for one hour with rabbit anti-collagen type III antibody (1/300 in 5% BSA/PBS; MD20311, MD Biosciences). As secondary antibody goat anti-rabbit HRP (2.5 μg/ml in 5% BSA/PBS; DAKO) was applied for one hour. Above immunocytochemical stainings were developed with 3,3'-diaminobenzidine (DAB) and counterstained with Mayer's hematoxylin (Merck).

For Cathepsin K immunolocalization, deparaffinised sections were blocked in 0.3% (v/v) H_2O_2 in PBS for ten minutes and in 5% (w/v) BSA in PBS for 30 minutes. Rabbit polyclonal antibody to Cathepsin K (ab19027, Abcam) was incubated at 1μg/ml in 5% (w/v) BSA in PBS for one hour, followed by one-hour incubation with a biotinylated secondary antibody (biotinylated goat-anti-rabbit, 7.5 μg/nl; BA-1000, Vector Laboratories) and the staining was enhanced by incubation with streptavidin-peroxidase for an additional hour (2 μg/ml, PN IM0309, Immunotec, Montreal, Canada).

For detection of F4/80, antigen retrieval in 10 mM sodium citrate buffer (pH 6.0) was performed on deparaffinised sections for 20 minutes at 95 ºC. The sections were then blocked in 0.3% (v/v) H_2O_2 in PBS for ten minutes and in 5% (w/v) normal goat serum (NGS) in PBS for 30 minutes. The sections were subsequently incubated with rat monoclonal antibody against F4/80 (0.4 μg/ml in 5% (w/v) NGS in PBS; clone C1:A3-1; MCA497; Serotec) for one hour, followed by incubation with rabbit-anti-rat antibody (13 μg/ml in 5% (w/v) BSA in PBS; DAKO) for 30 minutes and incubation with goat anti-rabbit HRP (2.5 μg/ml in 5% BSA/PBS; DAKO) for one hour. The stainings were developed with DAB, and Mayer's hematoxylin was used for counterstaining.

Results

Cytotoxicity of nanoparticles

In order to assess to which degree the survival of MSCs is affected by the presence of apatitic nanoparticles, the viability of MSCs was studied after 24 hours exposure of monolayers to suspensions of nanoparticles solution. Viability of MSCs measured 96±1% in regular culture medium, and was 88%±5% and 86±2% in medium supplemented with nanoparticles, respectively (Figure 8.2).

Viability of MSCs in hybrid constructs

Viability of MSCs that were encapsulated in hydrogels after 1 day of culture was equal to 88±3% for Matrigel and 81±3% for Matrigels supplemented with apatitic nanoparticles (Figure 8.3A). After 7 days of culture, cell viability values were 85±1% for Matrigel alone and 70±2% for Matrigels supplemented with nanoparticles (Figure 8.3B).

Tissue formation in vivo

After six weeks of implantation no bone formation was seen in MSC-laden Matrigels (Figure 8.4A,D). In samples supplemented with BCP, bone formed around the particles as evidenced by HE and Goldner's trichrome staining (Figure 8.4B,E). Bone lining cells and osteocytes were observed inside the newly formed bone (Figure 8.4B), while surrounding matrix was positive for osteogenic marker collagen type I (Figure 8.5B). In addition to new bone formation, some cartilage formation was observed (Figure 8.5C). In MSC-laden Matrigel samples marginal collagen type I staining was seen (Figure 8.5A), indicating that differentiation of MSCs into the osteogenic lineage was very limited in unmodified gels.

In implants containing apatitic nanoparticles elaborate fibrous-like tissue formed around the islands of particles (Figure 8.4C,F). Around the particles a band of tissue formed that stained dark green with Goldner's trichrome (Figure 8.4F) and was positive for collagen type I and osteocalcin (Figure 8.5D,E), indicating early osteogenesis around the particles after six weeks. This tissue was not positive for collagen type III (Figure 8.5F), corresponding to the limited fibrotic reaction around the CaP-loaded gels.

To determine the nature of cellular infiltrate around the particles of the hybrid construct, we performed a direct tartrate-resistant-acid-phosphatase (TRAP) staining,[535] and to verify the presence of osteoclasts an immunohistochemical detection of Cathepsin K,[536] which is predominantly expressed by osteoclasts, and immunostaining of F4/80, which identifies murine macrophages, with low levels in monocytic cells.

Host tissue response to the nanoparticles was observed after six weeks, as evidenced by the presence of multinucleated giant cells (MNGCs) lining the periphery of the nanoparticle-islands (Figure 8.6). These cells were absent in samples with Matrigel alone or with BCP particles. MNGC were mostly confined to the periphery of the particles, and were not observed in the rest of the host tissue. Concomitant infiltration of granulocytes was not observed.

Immunohistochemical analysis confirmed the osteoclastic phenotype of the MNGCs. These cells were positive for staining with TRAP and the majority of the cells was positive for Cathepsin K, an osteoclast marker. MNGCs were negative for F4/80 indicating that they lost the general macrophage phenotype.

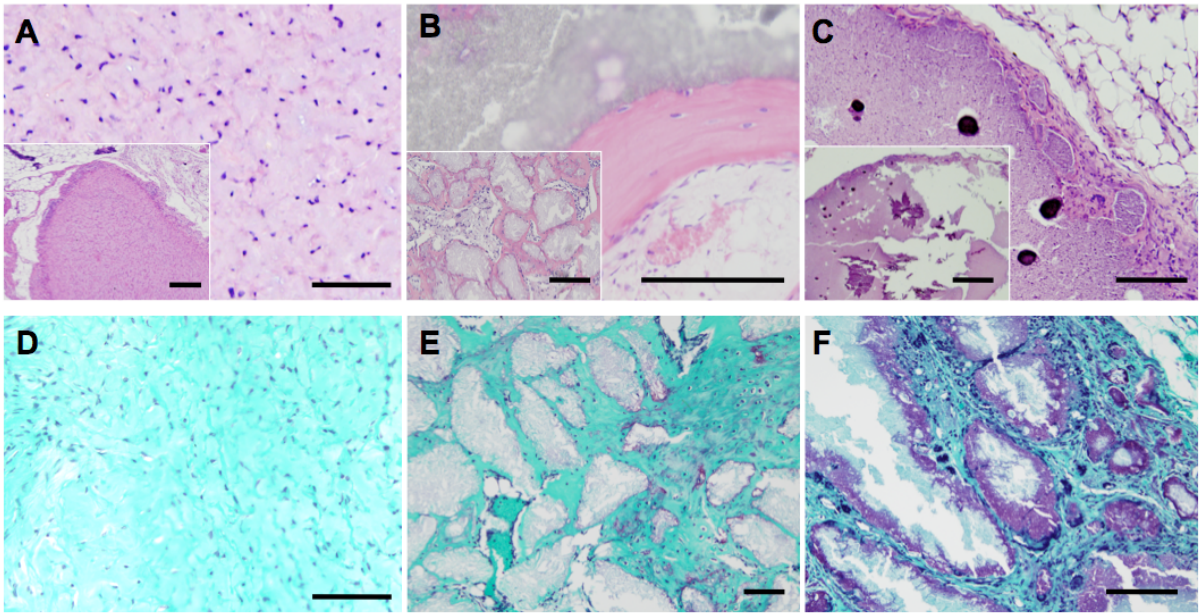

Figure 8.4: Tissue formation after six weeks *in vivo*. A-C: HE staining; A: MSC-laden Matrigel, Matrigel (pale pink); cells (blue), inset: sample overview (scale bar = 200 µm); B: MSC-laden Matrigel with BCP, bone (dark pink); cells (blue); BCP (grey), inset: sample overview (scale bar = 200 µm); C: MSC/Matrigel/nanoparticles, inset: sample overview (scale bar = 200 µm), clusters of nanoparticles (light purple), new tissue formation (dark pink), cells (blue); D-F: Goldner's trichrome staining; D: MSC-laden Matrigel, Matrigel (light green), cells (blue); E: MSC-laden Matrigel with BCP, bone (dark green); cells (blue), BCP (grey); F: MSC/Matrigel/nanoparticles, islands of nanoparticles (light green), degrading particles (purple), new tissue formation (dark green), cells (blue); scale bars = 100 µm.

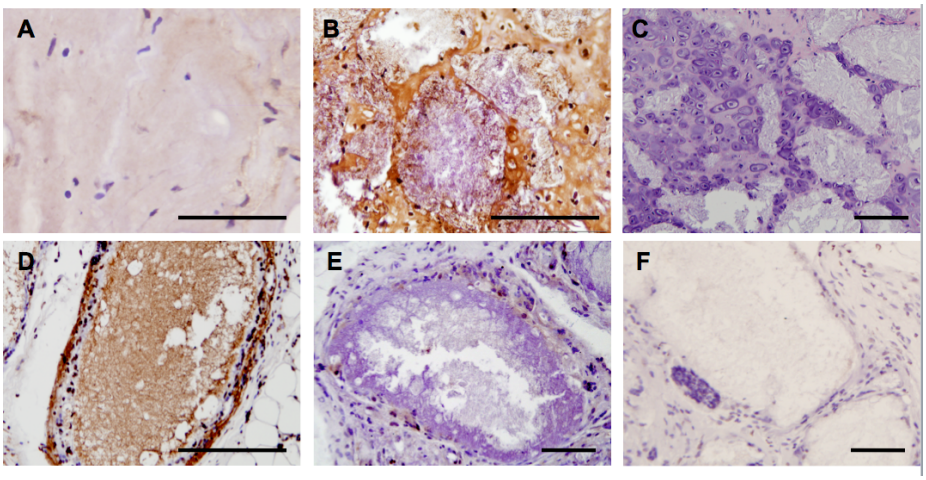

Figure 8.5: Osteogenesis after six weeks *in vivo*. A: MSC-laden Matrigel, collagen type I staining, Matrigel (light brown), cells (blue), scale bar = 50 μm; B: MSC-laden Matrigel with BCP, collagen type I staining (dark brown), scale bar = 100 μm; C: MSC-laden Matrigel with BCP, HE staining, cartilage formation (purple), scale bar = 100 μm; D: MSC/Matrigel/nanoparticles, collagen type I (dark brown) formation around the island of the nanoparticles (light brown), scale bar = 100 μm; E: MSC/Matrigel/nanoparticles, osteocalcin staining (brown), cells (blue); scale bar = 50 μm; F: MSC/Matrigel/nanoparticles, collagen type III staining (brown), cells (blue), scale bar = 50 μm.

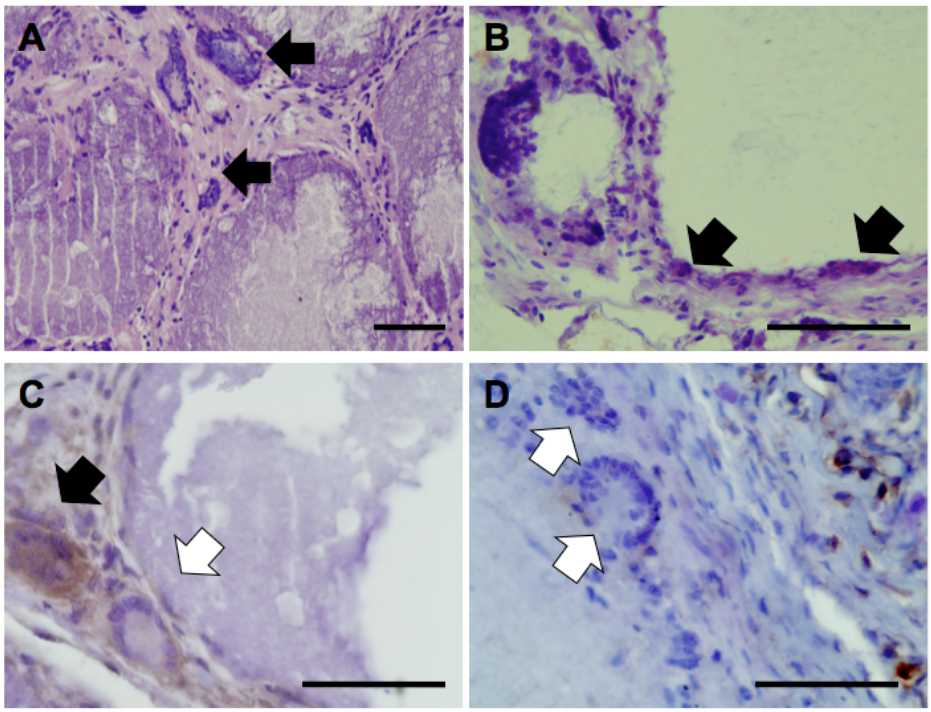

Figure 8.6: Host tissue reaction to the MSC/Matrigel/nanoparticles implants at six weeks. (A) HE staining; MNGCs (arrows); (B) TRAP staining (red) of MNGC (arrows), cells (blue); (C) Cathepsin K staining (brown) of MNGC shows both positive (arrow) and negative cells (white arrow); (D) F4/80 staining (brown), cells (blue) demonstrates F4/80-negative cells (white arrow); scale bars = 100 μm.

Discussion

Hydrogels are popular materials for use as injectables. Addition of bioactive calcium phosphates to hydrogel matrices laden with osteogenic cells is expected to stimulate bone formation after *in vivo* implantation for application in bone tissue engineering. In the current study the osteogenic performance of cell-laden hydrogels has been assessed for both the inclusion of CaP micro- and nanoparticles.

Abundant bone formation and newly formed cartilage was observed *in vivo* upon implantation of BCP-loaded and cell-encapsulating Matrigel whereas only limited osteogenesis occurred in Matrigel-alone samples after six weeks. These results are in line with previous studies on the osteoinductive capacity of BCP (microparticles).[25,537-539] Regarding the effect of incorporated apatitic nanoparticles to cell-laden hydrogel mixtures, *in vitro* analysis demonstrated that nanoparticles are not cytotoxic to both MSC monolayers and encapsulated MSCs. No bone formation *in vivo* occurred in samples supplemented with apatitic nanoparticles. However we did observe osteogenesis around the particle-loaded plugs as evidenced by collagen type I and osteocalcin staining. Around the plugs also osteoclastogenic response was seen as illustrated by the presence of TRAP and cathepsin K-positive multinucleated giant cells. It can be concluded that gels containing apatitic nanoparticles lack sufficient osteoinductive cues to induce bone formation at an ectopic location six weeks after implantation despite the observed signs of osteogenesis as well as the osteoclastic response. It is likely that combined application of nanoparticles and hydrogels in an orthotopic defect would lead to higher bone yield profiting from the osteoconductive properties of apatitic nanoparticles. Apatitic nanoparticles combined with glycerol hydrogel without cells for treatment of calvarial defects recently demonstrated bone formation in the samples.[540] However, no significant effect of this mixture on bone repair was found in the resultant (nonporous) implants.

Besides differences in particles size, which can have a profound effect on cell functioning *in vitro*[541] and bone formation *in vivo*, [512,542] the CaP particles used in the current study also differ considerably regarding their chemical stability. BCP microparticles were sintered at elevated temperatures of 1150 °C, whereas the apatitic nanoparticles were prepared using wet-chemical precipitation reactions without any further sintering treatment. Consequently, it is hypothesized that the CaP nanoparticles were more reactive than sintered BCP particles of higher chemical stability due to the higher surface area and lower crystallinity of CaP nanoparticles. The higher degradability c.q lower chemical stability of the nanostructured versus the microstructured mineral phase might have rendered the hydrogel containing the apatitic nanoparticles more prone to osteoclastic degradation[543] and less stimulatory to osteogenesis than the gels containing BCP microparticles as observed *in vivo*.

Apart from bone formation, elaborate tissue reaction was seen around the samples containing 15 % (w/v) nanoparticles after 6 weeks, while addition of 15 w/v% BCP particles did not provoke host response at this timepoint. Also in other studies in which small sintered calcium phosphate particles of 40-80 μm or apatitic nanoparticles were implanted *in vivo*, macrophage-like cells devouring the particles were observed.[540,544] The smaller the microparticles the higher number of macrophages can be expected in the implants. [545] Phagocytic cells with osteoclast phenotype possibly play a role in inductive bone formation.[546] The characterization of these cells in this study indicated that multinucleated giant cells surrounding the clusters of nanoparticles exhibited an osteoclastic phenotype, without macrophage markers. This suggests that the presence of these

cells is a specific osteoclast response to apatitic nanoparticles present at the scene, and to a lesser degree a general particle-induced effect.
Overall conclusion is that for the time point as evaluated in this study, BCP particles that enable cell attachment lead to bone formation at ectopic location, while nanoparticles in the context of Matrigel only induce osteoclastogenic tissue response without bone formation. It is likely that combined application of nanoparticles and hydrogels in an orthotopic defect would lead to higher bone yield due to the osteoconductive properties of apatitic nanoparticles.[547] Application of novel printing strategies for deposition of calcium phosphate-laden matrices is expected to promote development of structured engineered grafts with high bone yield.

Acknowledgements

We acknowledge the financial support of the Mosaic scheme 2004 of the Netherlands Organization for Scientific Research (NWO; grant number: 017.001.181), the Dutch Program for Tissue Engineering (project number: UGT.6743), the Dutch Technology Foundation STW (VENI grant 08101), the Anna Foundation and the Smart Mix Program of the Netherlands Ministry of Economic Affairs and the Netherlands Ministry of Education, Culture and Science.

Part II: Performance of heterogeneous cell-laden constructs

Chapter 9

The role of endothelial progenitor cells in prevascularized bone tissue engineering: development of heterogeneous constructs

Fedorovich NE[1], Haverslag RT[1], Dhert WJA[1,2], Alblas J[1]

Tissue Engineering Part A. 2010, 16(7):2355-67

[1]*Department of Orthopaedics, University Medical Center Utrecht, Utrecht, The Netherlands*
[2]*Faculty of Veterinary Medicine, University Utrecht, Utrecht, The Netherlands*

Abstract

In vitro prevascularization of bone grafts with endothelial progenitor cells (EPCs) is a promising strategy to improve implant survival. In this study we show bone formation in constructs that contain multipotent stromal cells (MSCs) and EPCs. Early and late EPCs from peripheral blood and bone marrow of adult goats were characterized for differentiation markers and functional responses. EPCs from peripheral blood are more proliferative than bone-marrow-derived EPCs, express higher numbers of endothelial markers for longer periods of time, and form more intricate networks. We demonstrate that EPCs derived from peripheral blood contribute to osteogenic differentiation by MSCs *in vitro*, and that MSCs support the proliferation of EPCs and stabilize the formed cellular networks. *In vivo*, EPCs from peripheral blood assemble into early blood vessel networks, which are more pronounced in the presence of MSCs. These results show that the EPCs isolated from peripheral blood are suitable for prevascularization strategies, and that coseeding of EPCs and MSCs is favorable for bone formation after 6 weeks.

Introduction

One of the major limitations in the size of tissue-engineered bone grafts is the distance over which nutrients and oxygen have to diffuse from the surrounding blood vessels before reaching the cells.[19,142,548] There is a strong association between bone formation and angiogenesis in bone development and healing,[140-142] and in formation of tissue-engineered bone.[549,550] There is evidence that the implantation of osteoprogenitor cells promotes bone formation only if the seeded cells are viable.[18] To engineer bone of clinically relevant size and volume, strategies that promote vascularization of tissue-engineered grafts are imperative.[19,143,551] Prevascularization of engineered grafts markedly improves *in vivo* performance of the tissue constructs and is a promising strategy to enhance graft survival after transplantation.[134,552,553]

Cell-based therapies using endothelial cells (ECs) accelerate vascularization of tissue-engineered implants by creating a blood vessel network in the graft before implantation that would connect to the host vasculature.[134,170,551,554-556] Besides their contribution to better vascularization and bone graft survival, ECs support osteogenesis by additional mechanisms. Coculture of (microvascular) ECs and osteoprogenitors[66,67] has a positive influence on osteogenic differentiation[71] and bone formation, both at ectopic and at orthotopic locations in rodents.[26,71] Communication between the two cells types is mediated both by soluble factors,[557-560] and directly by intercellular gap junction proteins.[66,561,562]

Drawbacks on the use of ECs for neovascularization include their limited proliferative ability and the necessity for an inhibition of the apoptotic response[556] or stabilization with co-seeded cells[170,554] to sustain the formation of capillary-like networks *in vitro*. Endothelial progenitor cells (EPCs) have a greater doubling ability than mature ECs[563] and are a potent source of ECs for prevascularization applications in regenerative medicine.[564-566] EPCs enriched from mononuclear cells (MNCs) of bone marrow,[567] peripheral blood,[568] and umbilical cord blood[569,570] can differentiate into ECs *in vitro*, and contribute to the formation of vascular networks through postnatal vasculogenesis.[564] EPCs are highly proliferative and exhibit a stable endothelial phenotype.[571] EPCs support neovascularization of the ischemic hindlimb[568,569,572] and can regenerate infarcted myocardium.[573] Under comparable conditions, EPCs perform better than ECs with respect to blood vessel network formation.[574]

The term EPCs represents al least two distinct types of cells, depending on source and isolation procedure used.[563,575-577] Early-outgrowth cells are spindle shaped and develop colonies after 4–7 days,[572] whereas late-outgrowth colonies form after 3 weeks of culture.[563] Early EPCs show limited proliferating potential in long-term culture and recede after 4–6 weeks.[568,576] Late-outgrowth cells are cobblestone shaped, much more proliferative,[563,578] and are widely considered "true EPCs."[579] Differences in isolation and cultivation procedures of EPCs make it difficult to directly compare studies on the outcomes of EPC functionality.[574] Although *in vitro* performance of ECs (human vascular ECs, circulating ECs, and microvascular ECs) was previously directly compared to EPCs,[563,574,580,581] so far no comparisons were made between EPCs isolated from peripheral blood and bone marrow. In turn, early and late EPCs are often compared with regard to their vasculogenic potential, but the cells are then cultured under distinct conditions.[576] In this study we isolated and characterized for the first time EPCs from peripheral blood and bone marrow of goats, a widely used animal to study bone regeneration in orthopedic applications.[25,233,582-585] We explored whether the isolated EPCs remain functional with respect to network-forming capacity upon implantation in immunodeficient mice and how addition of goat EPCs contributes to osteogenic differentiation and bone-forming capacity of goat multipotent stromal cells (MSCs) for bone tissue engineering purposes.

Materials and Methods

Isolation of goat EPCs and cell culture

Bone marrow and peripheral blood samples were harvested from adult Dutch milk goats, which had not received prior stimuli to mobilize EPCs from the bone marrow. MNCs were isolated by density gradient centrifugation with Ficoll solution (Ficoll Paque™ Plus; GE Healthcare Biosciences AB). Cells from individual goats were plated in 25cm^2 culture flasks coated with fibronectin (2.5 μg/mL in phosphate buffered saline (PBS), 1 h; Harbor Bioproducts) in EBM-2 (Cambrex), supplemented with singlequots (human endothelial growth factor, vascular endothelial growth factor, human fibroblast growth factor-B, R3-insulin-like growth factor-1, ascorbic acid, heparin, and gentamicin-amphotericin-B) and 20% fetal calf serum (Cambrex), and cultured at 37°C and 5% CO_2 in a humidified chamber. After 4 days of culture, non-adherent cells were removed by washing with PBS, a fresh medium was applied, and cells were cultured for at least 6 weeks, replating them twice a week. Colonies from a single donor were cultured together. Fibronectin coating and collagen coating (bovine collagen type I, 0.125mg/mL in 0.1 M acetic acid, 30 min; BD Biosciences) were compared during the first 2 weeks of culture.

Goat vein EC isolation and culture

Goat vein ECs (GVECs) were obtained by collagenase I (0.2% [w/v] in PBS; Sigma) digestion of freshly isolated goat jugular vein for 15 min at RT and subsequent flushing of the vein with the culture medium. Cells were cultured in EBM-2 medium with singlequots. GVECs from passage 3 were used as positive controls for angiogenesis assays and immunocytochemical staining of early endothelial markers.

Goat MSC isolation and culture

MSCs were isolated from iliac bone marrow aspirates of Dutch milk goats and culture-expanded as described previously,[18] in the medium consisting of α-minimum essential medium (Gibco) supplemented with 100 U/mL penicillin, 100 μg/mL streptomycin (Gibco), 2mM L-glutamine (Glutamax; Gibco), and 15% [v/v] fetal calf serum. For osteogenic differentiation, the culture medium was supplemented with 10^{-8} M dexamethasone (Sigma), 10mM β-glycerophosphate (Sigma), and 0.1 mM ascorbic acid (Sigma).

Colony-formation efficiency of EPCs

The cells were plated at 10^5 cells/cm^2 in fibronectin- or collagen-coated culture flasks. When colonies had formed, the cells were fixed for 10 min with 4% formalin and stained with methylene blue (Merck). The number of colonies per 10^6 seeded cells per donor was determined in duplicate.

Proliferation rate of EPCs

EPCs were counted at each passage to assess their proliferation capacity, and the cumulative population doublings (PDs) were calculated as ∑([log(#harvested cells/#plated cells)/log(2)]).

Characterization of EPCs by early endothelial markers

EPCs were incubated with DiI-labeled acetylated-low density lipoprotein (LDL) complex (2.5 μg/mL in α-minimum essential medium; Molecular Probes) at 37°C for 2 h and with fluorescein-labeled isolectin B_4 (10 μg/mL in PBS; Vector Laboratories) for one hour. After

washing with PBS, the coverslips were mounted with Vectashield containing DAPI.
(Vector Laboratories) for nuclear staining. Three samples per condition were measured using a microscope equipped with an epifluorescence setup, excitation/emission setting of 488/530 nm to detect green fluorescence, and 530/580 nm to detect red cells (Leica DM IRBE). Three randomly selected fields per sample were scored and the percentage of double positive cells was calculated.

Characterization of EPCs by late endothelial markers

To analyze the presence of cell-surface marker PECAM-1 (CD31) using flow cytometry, cells were detached from culture plates with trypsin/ethylenediaminetetraacetic acid and kept in suspension culture overnight. The cells were incubated with the primary murine monoclonal antibody against ovine CD31 (100 μg/mL; Serotec) for 1 h at 4°C, followed by incubation with Alexa Fluor 488 goat anti-mouse IgG (20 μg/mL in PBS; A11001; Invitrogen) for 45 min at 4°C and resuspended in PBS for analysis with flow cytometer (FACS Calibur; Becton Dickinson) and CELLQuest software (Becton Dickinson).
To detect the von Willebrand factor (vWF), cells were cultured on coverslips fixed with ice-cold methanol 80%. We used primary polyclonal rabbit antibody against human vWF (6 μg/mL; Dako) and Alexa Fluor 488 goat anti-rabbit IgG (10 μg/mL in PBS; Invitrogen) as a secondary antibody, and mounted the slides with Vectashield/DAPI.

Functionality analysis of goat EPCs: angiogenesis Matrigel assay

Matrigel (*In vitro* Angiogenesis Assay; Chemicon) was thawed on ice overnight, and 50 μl aliquots were deposited in a 96-well plate and incubated for 1 h at 37°C. About 10^4 cells were seeded in triplicate wells/condition, and plates were incubated for 15 h at 37°C and 5% CO_2. For quantification, in four random fields per sample the branch points and the number of tubular structures were counted under a phase-contrast microscope. Results are expressed as mean ± SD.

Coculture: proliferation analysis

To assess the proliferation of EPCs and MSCs, either cell type was labeled with carboxyfluorescein-diacetate succinimidyl ester (0.5 μM; Molecular Probes) and cocultured at different ratios (0.25–4), in a 1:1 mixture of osteogenic/endothelial medium. Fluorescence-activated cell-sorting analysis of the cocultures was conducted directly after labeling and after 3 days.

Coculture: in vitro analysis of 2D Matrigel network formation

To study the effect of coculture on cellular 2D network formation, the cells were detached from the culture flasks, washed, and seeded at 10^4 cells per Matrigel (BD Matrigel™; BD Biosciences) disc (0.6 cm ø). Five groups were formed - EPCs alone, MSCs alone, MSCs/EPCs = 4 (8000/2000), MSCs/EPCs = 1 (5000/5000), and MSCs/EPCs = 0.25 (2000/8000) - and cultured in the mixture of osteogenic and angiogenic medium for 15 h (three samples per group). The contribution of EPCs and MSCs to the formed tubular networks was analyzed by fluorescent labeling of the two populations (EPCs labeled red with PKH26 [Sigma-Aldrich] and MSCs labeled green with carboxyfluorescein-diacetate succinimidyl ester). The presence of fluorescent cells was analyzed under a microscope equipped with an epifluorescence setup (Leica).

Coculture: in vitro analysis of 3D network formation

To investigate the effect of coculture on cellular 3D network formation, the cells were encapsulated in an angiogenic matrix (10^6 cells/ml Matrigel) for 2 weeks. Four groups were formed - Matrigel with only EPCs, only MSCs, MSCs/EPCs = 1, and MSCs/EPCs = 0.25 (200,000/800,000). The groups were cultured in the mixture of osteogenic and angiogenic medium for 14 days and embedded in TissueTek (Sakura) for cryosectioning. The number of tubular structures relative to total cells was scored in cryosections, stained with Mayer's hematoxylin and eosin (four samples per group). To assess the contribution of EPCs to the formed networks, air-dried cryosections were fixed in acetone, blocked with 5% bovine serum albumin (BSA) in PBS for 30 min, and incubated with polyclonal rabbit anti-human vWF antibody (6 μg/mL; Dako) overnight at 4 °C. As a secondary antibody, we used polyclonal goat anti-rabbit horseradish peroxidase (HRP) (1.5 μg/mL; Dako), applied for one hour. The staining was developed with dimethylaminobenzaldehyde (DAB), counterstained with hematoxylin, and analyzed under the light microscope Olympus BX50 with Olympus DP70 camera.

Coculture: in vitro analysis of osteogenic differentiation

To assess the effect of coculture on early osteogenic differentiation by MSCs, the cells were seeded in fibronectin-coated 16-well chamber slides, in the mixture of osteogenic and angiogenic medium for 7 days. Six groups - 10^4 EPCs, 10^4 MSCs, 10^4 MSCs + $0.2x10^4$ EPCs, $1.2x10^4$ MSCs, 10^4 MSCs + $0.5x10^4$ EPCs, and $1.5x10^4$ MSCs - were tested for the activity of alkaline phosphatase, an early osteogenic marker. For this, the monolayers were fixed in 4% formalin and permeabilized in 0.2% Triton X-100 in Tris-buffered saline. The cells were then stained with Fuchsin Substrate–Chromogen system (Dako), counterstained with hematoxylin, and mounted with Aquatex. The ratio of alkaline phosphatase positive (pink-red) cells over total cells was determined in four samples per condition, using Image Pro Plus 5.1 software.

In vivo coimplantation of EPCs and MSCs

To evaluate the *in vivo* network formation by peripheral blood (PB)-derived EPCs (PB-EPCs) and bone-forming capacity of the MSCs coimplanted with EPCs, we combined MSCs with EPCs (1:1) in Matrigel at 10^6 cells/ml gel. We either constructed 200 μl cell-laden Matrigel plugs for analysis of blood vessel formation at 2 weeks or added 200 μl Matrigel to three 2–3-mm biphasic calcium phosphate (BCP) particles for analysis of bone formation at 6 weeks. Samples contained $2x10^5$ cells per construct. The BCP particles were prepared and sintered at 1150 °C as described previously.[582] The hybrid constructs, that is, EPCs and MSCs seeded in Matrigel alone or combined with BCP particles, and control constructs with EPCs alone and MSCs alone, were incubated overnight *in vitro* in the culture medium. As negative controls, we used acellular Matrigel plugs and Matrigels laden with EPCs devitalized by three freeze–thaw cycles. Female nude mice (Hsd-cpb:NMRI-nu; Harlan) were anaesthetized with 1.5% isoflurane, after which the implants were placed in separate subcutaneous dorsal pockets (n = 4 per time point). The animals were postoperatively treated with the analgesic buprenorphine (0.05mg/kg, sc; Temgesic; Schering-Plough) and housed together at the Central Laboratory Animal Institute, Utrecht University. Experiments were conducted with the permission of the local Ethics Committee for Animal Experimentation and in compliance with the Institutional Guidelines on the Use of Laboratory Animals.

Evaluation of in vivo blood vessel and bone formation

The implants were retrieved 2 and 6 weeks after implantation to analyze the blood vessel formation and bone formation, respectively. Samples were fixed overnight in 4% buffered formalin and 2-week samples were processed for paraffin sections. To analyze the formation of the blood vessel networks, 5-μm-thick paraffin sections were cut and general histological staining was performed with hematoxylin/eosin (HE) and Goldner's trichrome. Extracellular matrix formation was detected by Picrosirius red staining. To assess the differentiation status of the EPCs inside the Matrigel, the sections were stained for endothelial markers vWF and caveolin-1. vWF detection was performed on rehydrated sections that were blocked in 3% H_2O_2 for 10 min and 10% (v/v) normal goat serum in PBS for 20 min, and subsequently incubated with rabbit anti-human vWF antibody (15 μg/mL; Dako). As secondary antibody, we used powervision goat anti-rabbit HRP (Immunologic) for 1 h. To detect caveolin-1 the sections were blocked with 1.5% H_2O_2 in PBS, and antigen retrieval in pepsin (0.1% [w/v] in glycine buffer) was performed for 15 min. After blocking with normal goat serum (10% [w/v] in PBS), the sections were incubated with rabbit anti-human caveolin-1 primary antibody (2.5 μg/mL; Abcam), and as secondary antibody we used powervision goat anti-rabbit HRP. The stainings were developed with DAB or Vector NovaRED (Vector Laboratories), and Mayer's hematoxylin was used for counterstaining.

To assess the contribution of mouse ECs to the vessel networks observed in the Matrigel, the sections were stained for endothelial marker mouse-specific (not cross-reactive with goat) CD31 (PECAM-1). For this, the paraffin sections were rehydrated in graded ethanol series followed by antigen retrieval in pronase (1 mg/mL, 10165921001; Roche Diagnostics) for 30 min at 37°C and hyaluronidase type II (10 mg/mL, H2126; Sigma-Aldrich) for 30 min at 37°C. The sections were then blocked in 0.3% (v/v) H_2O_2 in PBS for 10 min. The M.O.M.™ Kit for detecting mouse primary antibodies on mouse tissue was used, according to manufacturer's recommendation (BMK-2202; Vector). Anti-CD31 mouse primary antibody (P2B1-s; Developmental Studies Hybridoma Bank) was incubated at 1.1 μg/mL in 5% (w/v) BSA in PBS, followed by streptavidine peroxidase (2 μg/mL in 5% [w/v] BSA in PBS; Beckman Coulter) for 1-h and 10-min incubation with DAB. Mayer's hematoxylin was used for counterstaining.

To study bone formation, 6-week samples containing BCP particles were decalcified in Luthra's solution (0.33 M HCl and 2.65M formic acid in distilled water) for 24 h and processed for paraffin sections. At least four sections from each sample were stained with HE. The amount of formed bone was quantified by histomorphometry. A custom program was used to measure the area of interest, the area of the scaffold, the area of bone, the scaffold outline available for bone apposition, and the contact length of bone and scaffold.[586] This allowed the calculation of the bone contact% = (bone-to-scaffold contact length/scaffold outline) x 100%, and bone area% = (bone apposition/available pore surface) x 100%.

Statistical analysis

Statistical analysis was performed with SPSS 12.0.1 software. A paired Student's *t*-test was used to compare the amount of formed bone in MSC-laden and MSC/EPC-seeded scaffolds after *in vivo* implantation of 6 weeks. A one-way analysis of variance with Bonferroni post hoc test was used to compare the numbers of branching points and tubular networks in 2D, the numbers of luminal structures in 3D, and alkaline phosphatase production. *P*-values less than 0.05 were considered statistically significant. All values are reported as mean ± SD.

Results

Isolation and proliferation of bone marrow (BM)-EPCs and PB-EPCs

Goat EPCs isolated either from bone marrow or peripheral blood by density gradient and seeded in fibronectin-coated flasks exhibited distinct morphology and growth characteristics as presented in Supplemental Figure 9.1A–D. Initially, the seeded cells were round, but when colonies appeared, the cells displayed their morphology as shown in Supplemental Figure 9.1A–C. Bone-marrow-derived cells formed colonies of spindle-shaped cells within 5 days after isolation, had a population doubling (PD) time of 2.5 days, and reached 20 PDs. The population of cells arising from peripheral blood was heterogeneous in character. Part of the cultures formed colonies within 1 week after isolation (early PB-EPCs). In other cultures, late outgrowth population arose around 2–3 weeks after isolation. Proliferation of early PB-EPCs was high for up to 3 weeks after isolation (PD time of 21 h), and reached a plateau after that (28 PDs). Late PB-EPCs colonies, arising from peripheral blood fractions after 2–3 weeks, exhibited more pronounced endothelial morphology (cobblestone monolayer). Late-outgrowth EPCs exhibited more extensive proliferation (PD time of 31 h) than BM-EPCs and could be kept in culture for at least 32 PDs.

CFU efficiency

Mononuclear fractions from goat bone marrow plated in fibronectin-coated flasks formed 5.2 ± 2 colonies per 10^6 cells. The number of colonies formed from PB-MNC on fibronectin- and collagen-I-coated surfaces was comparable, and measured 1.1 ± 0.7 and 1 ± 0.2 colonies per 10^6 cells, respectively.

Characterization of EPCs

Early (day 5) attached BM-EPCs exhibited spindle-shape morphology and showed well-known markers of EPCs (isolectin B_4 binding and acetylated LDL-incorporation, Figure 9.1A), but lost most of the double-positive cells within 1 week after isolation (Figure 9.1D). These cells expressed endothelial antigen CD31 only transiently (Figure 9.2A,D) and were negative for endothelial marker vWF (data not shown). Endothelial surface marker expression was more distinct in PB-EPCs (Figures 8.1B, C and 8.2B, C). The number of double-positive PB-EPCs after isolation was comparable for cells cultured on fibronectin- and collagen-I-coated surfaces, respectively, 91 ± 2% and 91 ± 5%. Most of the late PB-EPCs remained double positive for lectin binding and acetylated LDL-incorporation in culture (Figure 9.1D), expressed CD31 for up to 3 weeks (Figure 9.2F), and were positive for endothelial-specific marker vWF (Figure 9.2G).

2D in vitro angiogenesis characteristics of BM-EPCs and PB-EPCs

Because of the differences in cell surface marker expression, it was hypothesized that EPCs from PB and BM may also differ in their ability to form tubular networks in a Matrigel angiogenesis assay. BM-EPCs did not form tubes on Matrigel (Figure 9.3A), as compared to elaborate network formation by EPCs isolated from peripheral blood (Figure 9.3B,C) or GVECs (Figure 9.3D). Network formation *in vitro* was more evident in late-outgrowth EPCs (Figure 9.3C) than in early EPCs (Figure 9.3B).

Coculture

Given stable endothelial profile and good functionality of the differentiated late-outgrowth EPCs

isolated from peripheral blood, these cells were used in all subsequent coculture and coimplantation experiments with MSCs.

Coculture: proliferation analysis

Both EPCs and MSCs exhibited enhanced proliferation in coculture compared to monoculture, for all the coculture ratios tested. EPCs proliferate faster when more MSCs are added to coculture; similarly, MSCs exhibit higher proliferation rates when more EPCs are introduced (Supplemental Figure 9.2).

Coculture: in vitro analysis of 2D network formation on Matrigel

Scoring of tubular structures by EPCs with and without addition of MSCs revealed that branch points and tubular networks were formed in coculture (Figure 9.4A,B). Although EPCs alone exhibited significantly more branching points and tubular networks than other groups ($p<0.001$), relatively high network formation efficiency was found at MSCs/EPCs ratios of 1 and 4, while MSCs alone demonstrated least branching and tubular structures ($p<0.001$ compared to all other groups). Fluorescent labeling of each cell type demonstrated that in 2D cocultures on a Matrigel surface, both cell types contributed to the newly formed networks (Figure 9.4C).

Coculture: in vitro analysis of 3D network formation in Matrigel

After 1 and 2 weeks in 3D Matrigel, EPCs started to organize into elongated structures that connected to each other and formed a 3D network (Figure 9.4D). HE-stained cryosections revealed that MSCs alone did not form luminal structures. Networks formed by EPCs alone were immature without a lumen; in a few cases, a lumen was seen inside the structures (Figure 9.4E). Coseeding of EPCs with MSCs promoted the degree of network formation. Significantly more luminal structures were present inside Matrigel in groups seeded with MSCs/EPCs ratios 1 and 4 compared to EPCs alone ($p<0.05$ and $p<0.001$, respectively; Figure 9.4F). Staining with endothelial-specific marker vWF demonstrated that cells surrounding the lumen were positive, indicative of EPC's contribution (Figure 9.4G). However, involvement of MSCs cannot be excluded.

Coculture: in vitro analysis of osteogenic differentiation

Osteogenic differentiation analysis revealed that after 1 week of culture bone-marrow-derived EPCs were positive for alkaline phosphatase (Figure 9.5E), which was not the case for EPCs derived from peripheral blood (Figure 9.5D). The coculture of MSCs with PB-EPCs enhanced osteogenic differentiation of MSCs, compared to the equal amounts of MSCs alone (Figures 9.5A–C,F). The effect of cell density was assessed by including two groups with equal amounts of total cells (Figure 9.5F, green bars). Our findings indicate that relative ALP production per MSC is increased in the cocultures. ALP production in coculture groups (10^4 MSCs + 2000 EPCs and 10^4 MSCs + 5000 EPCs) was significantly higher than production of MSCs-alone (10^4 MSCs) samples ($p<0.001$).

In vivo vascularization

In vivo implantation of Matrigel constructs containing PB-EPCs or MSCs/EPCs = 1 resulted in formation of vessel-like networks (Figure 9.6A,B). Empty scaffolds showed no ingrowth of host cells and no indirect effect of cell loading was seen in samples containing dead EPCs (Figure 9.6C,D). Lumina were frequently formed by the vessel-like structures in Matrigel plugs with

MSCs/EPCs = 1 (Figure 9.6E), while networks formed by EPCs alone were less luminal and more compact (Figure 9.6A). In EPC-alone samples, we were not able to confirm whether the implanted prevascular network was connected to the host circulation, as no erythrocytes were detected inside the lumina. We observed erythrocytes in lumina of vessels in MSCs/EPCs samples (Figure 9.6F). However, this finding was not elaborate. The EPCs encapsulated in Matrigel stained positive for endothelial-specific marker vWF (Figure 9.6G) and caveolin-1 (Figure 9.6H), a protein involved in receptor-independent endocytosis that is highly expressed in ECs.[571,587]

The cells present in the constructs, responsible for observed network formation, were not stained by mouse-specific antibodies against ECs, whereas skin vessels clearly were (Supplemental Figure 9.3). The embedded cells produced large amounts of collagen-rich extracellular matrix, a prerequisite for bone tissue formation (Figure 9.6I).

In vivo bone formation

After 6 weeks of implantation, bone tissue formed inside BCP scaffolds loaded with MSCs alone and MSCs/EPCs = 1. Bone lining cells were clearly visible throughout the grafts, as well as osteocytes embedded in newly synthesized osteoid, typical for newly formed bone (Figure 9.6J–L).

Inflammatory cells, such as granulocytes, macrophages, and mononuclear giant cells were present at similar numbers in MSCs and MSCs/EPCs samples, and the degree of the response was host dependent (evidence of host reaction in some mice, and very small numbers of granulocytes and absence of mononuclear giant cells in other mice). No differences were found between the implanted groups (results not shown).

The percentage of area occupied by bone, as quantified by histomorphometry, was not different between implants seeded with MSCs alone ($2x10^5$ cells) and MSCs/EPCs combined ($1x10^5$ MSCs and $1x10^5$ EPCs) (30 ± 12% vs. 38 ± 10%, p = 0.177; Figure 9.6M). The bone contact% was significantly higher in the MSCs/EPCs1 = 1 combination group (40 ± 8% vs. 52 ± 4%; p = 0.026; Figure 9.6M). Note that in the MSCs/EPCs combination group, only half the amount of osteoprogenitors is present.

Discussion

In this study we describe for the first time the isolation and characterization of EPCs from peripheral blood and bone marrow of goats, an important animal model in orthopedic surgery. We demonstrate that EPCs derived from peripheral blood contribute to osteogenic differentiation by MSCs *in vitro*, and that MSCs support the proliferation of EPCs and stabilize the formed cellular networks. *In vivo*, PB-EPCs assemble into early blood vessels, which are more pronounced in the presence of MSCs. We show that some of these networks connect to the host circulation, as confirmed by the presence of erythrocytes in the lumina. Finally, coseeding of PB-EPCs with MSCs leads to efficient bone formation in ectopic implants after 6 weeks in immunodeficient mice. Although not much more bone formed in the coseeding group compared to constructs with MSCs alone, it is noteworthy that only half the amount of osteoprogenitors was present in the former constructs. It is not known at this stage whether the higher amount of bone found in the MSCs/EPCs group was the result of an earlier onset of bone formation. To monitor possible inflammatory responses that could influence bone formation, the presence of innate immune cells was analyzed. From these findings, we conclude that a limited chronic inflammation occurred in the samples, and that this reaction was host dependent and comparable

for MSCs and MSCs/EPCs implants.

When comparing EPCs from different sources, it appeared that (especially late) PB-EPCs exhibit extensive proliferation, perform well on the Matrigel angiogenesis assay, and present relevant endothelial markers during *in vitro* culture. Although more colonies arose from BM-EPCs cultures, these cells exhibited minimal expression of early and late endothelial markers, which is in line with previous findings.[588] Further, bone marrow-derived EPCs had a limited proliferative potential and did not form tubular structures in the angiogenesis assay, indicative of their low functionality. Studies by others suggest that these may be myeloid linage cells, often characterized as endothelial but with limited proliferative ability and expressing monocyte/macrophage markers.[589] Expression of ALP by this cell population in the osteogenic medium in our study suggests that at least part of the cell isolate consists of MSCs. Evidence is accumulating that EPCs from peripheral and umbilical cord blood are indeed superior to bone marrow-derived cells in their proliferative and vasculogenic potential,[590,591] confirming our findings.

Certain heterogeneity was observed in cultures of PB-EPCs. In part of the cultures, colonies formed within 10 days after plating; in other cultures, colonies formed after 24 days. Both cell groups presented endothelial markers, although the early PB-EPCs did so to a lesser extent than the late-outgrowth PB-EPCs. Late-outgrowth cells proliferated extensively and formed tubular networks on Matrigel, although these were less elaborate than those formed by GVECs. Our outcomes with these two subtypes of PB-EPCs are supported by previous findings,[563,576,581] suggesting that early and late PB-EPCs originate from different subpopulations of MNCs.[575] While early EPCs are derived from the vessel wall,[572] late-outgrowth EPCs originate from bone marrow.[563] Although both EPC populations exhibit endothelial markers, early EPCs do not build into the newly formed blood vessels, but rather support the angiogenesis by release of proangiogeneic factors, while late EPCs directly contribute to vasculogenesis by incorporation into the vessels.[575,576]

Given the good *in vitro* vasculogenic performance and stable endothelial phenotype of PB-EPCs, these cells were further used for coculture studies to mimic complex interactions between cells, necessary to create and maintain vascularization. In this study, we demonstrate a positive effect of coculture on proliferation and vasculogenic potential of EPCs in 3D *in vitro*, as well as enhanced vasculogenesis by EPCs *in vivo* when coimplanted with MSCs. The presented data show that seeded EPCs organize *in vivo* and only form functional, perfused networks upon coseeding with MSCs. This effect is supported by literature evidence that the presence of non-ECs, such as MSCs, smooth muscle cells, and osteoblasts, improves the survival, proliferation, and formation of microvessel-like structures by ECs,[560,592-594] by mechanism of direct physical contact between the cells.[595] We show that although both cell types contribute to the formed networks on Matrigel in 2D, most networks in 3D are formed by EPCs. The results of vessel formation in 3D environment are more relevant and might better predict tissue formation *in vivo*. The formation of vascular networks in coculture gels was dependent on the ratio of used cells, showing a decrease in network formation when higher numbers of EPCs were added. MSCs/EPCs ratios of 1 and 4 appeared optimal, both for 2D and 3D network formation. We demonstrate that EPC-networks anastomose with the host circulation, but only a few perfused vessel structures could be detected inside the coseeded implants. These results are consistent with findings by others, who also only sporadically observed some anastomosis at the periphery of their implants.[166] Host ECs did not participate in network formation inside the gels.

We further demonstrate that cocultures of MSCs and EPCs promote proliferation and osteogenic differentiation by MSCs, and positive effects of communication between ECs and osteoblasts on osteogenic differentiation and bone formation are well described.[166,557,561] In this study we show

that goat EPCs coimplanted with MSCs sustain bone formation *in vivo*. As cell numbers per implant were kept constant, half of the osteogenic MSCs coimplanted with EPCs was sufficient to make a similar amount of bone. EPCs contribute to bone formation either by enhancing the bone-forming capacity of MSCs or by transformation toward osteogenic lineage.[566] Our finding that, contrary to the BM-EPC, PB-EPCs did not exhibit ALP activity *in vitro* culture under osteogenic conditions makes bone formation by EPCs unlikely. Since EPCs can be easily isolated from peripheral blood, thereby eliminating donor-site morbidity, they are an ideal autologous cell source for vascularization of engineered bone tissue.

While prevascularization with EPCs is expected to be valuable in generating larger bone grafts (cm size), the interactions between ECs and osteogenic progenitors remain controversial,[596] and the ideal ratio and organization of cells that would yield functional grafts need to be further determined.[166] Organ- or tissue printing technology based on layered deposition of cell-laden hydrogels[28] creates novel opportunities to study 3D interactions between the two cells types, and it would be interesting to see to which extent imposed organization of the EPCs could add to the self-organization capacity they already have.

Conclusions

In vitro prevascularization of grafts with EPCs is a promising strategy to improve implant vascularization in the field of bone TE, in which the lack of sufficient vasculature is regarded a limiting factor for survival of implanted osteoprogenitors. In this study we demonstrate that coimplantation of EPCs isolated from peripheral blood significantly enhances osteogenic differentiation *in vitro* and supports bone formation *in vivo*.

Acknowledgments

We thank J.W. Leeuwis and D.M. van der Giezen from the Department of Pathology and P. Westerweel from the Department of Vascular Medicine of University Medical Center Utrecht, The Netherlands, for their assistance with immunocytochemical stainings. We thank H. Yuan from Progentix BV for kindly providing BCP particles. We acknowledge the financial support from the Mosaic scheme 2004 of the Netherlands Organization for Scientific Research (NWO; Grant no. 017.001.181), the Dutch Program for Tissue Engineering (Project no. UGT.6743), the Anna Foundation and the Smart Mix Program of the Netherlands Ministry of Economic Affairs, and the Netherlands Ministry of Education, Culture, and Science.

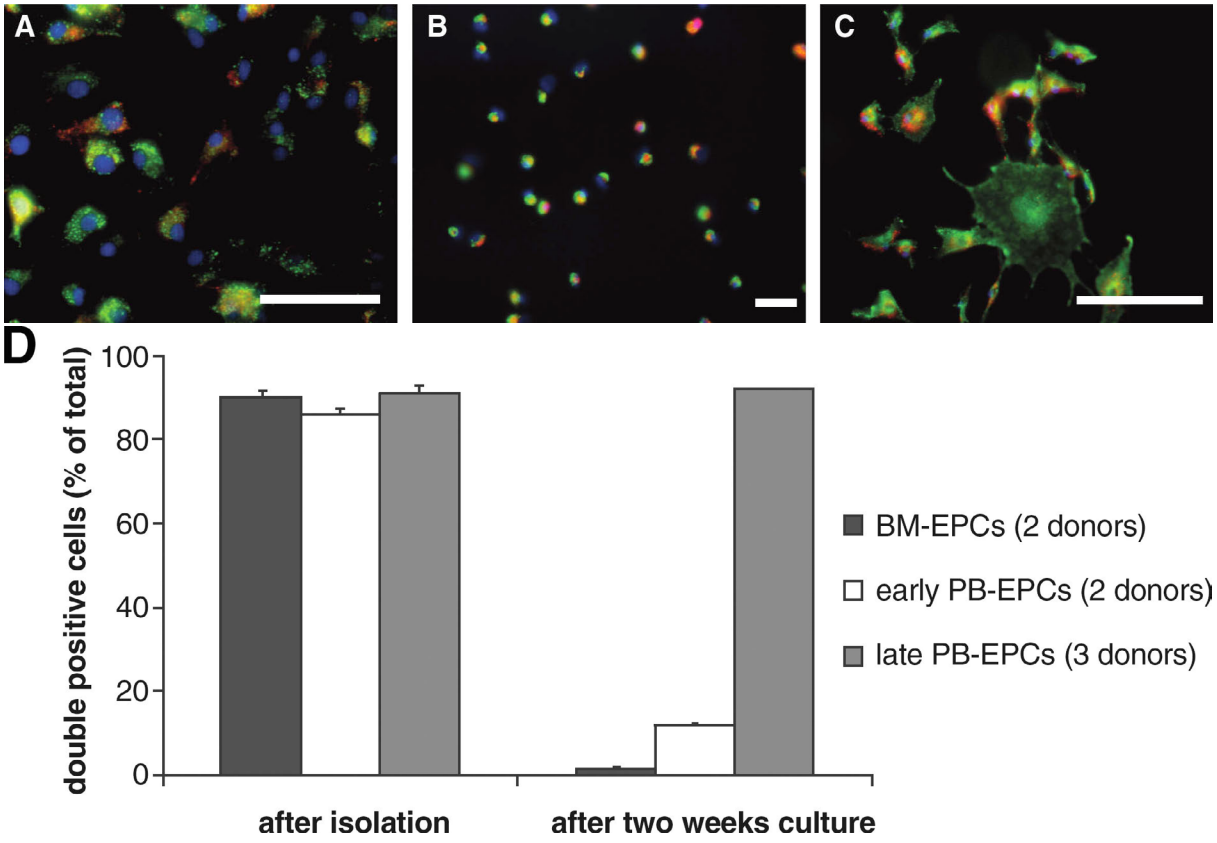

Figure 9.1: Expression of early endothelial markers. Uptake of acetylated LDL [red] and binding of isolectin B_4 [green]) in all the isolated endothelial progenitor cell (EPC) populations 4 days after colony formation [bone marrow (BM)-derived EPCs (A), early peripheral blood (PB)-derived EPCs (PB-EPCs) (B), and late PB-EPCs (C)]; DAPI nuclear stain (blue); scale bar = 25 μm; After 2 weeks of culture the percentage of double-positive cells is strongly reduced in BM-EPCs and early PB-EPCs, but remains high in late PB-EPCs (D).

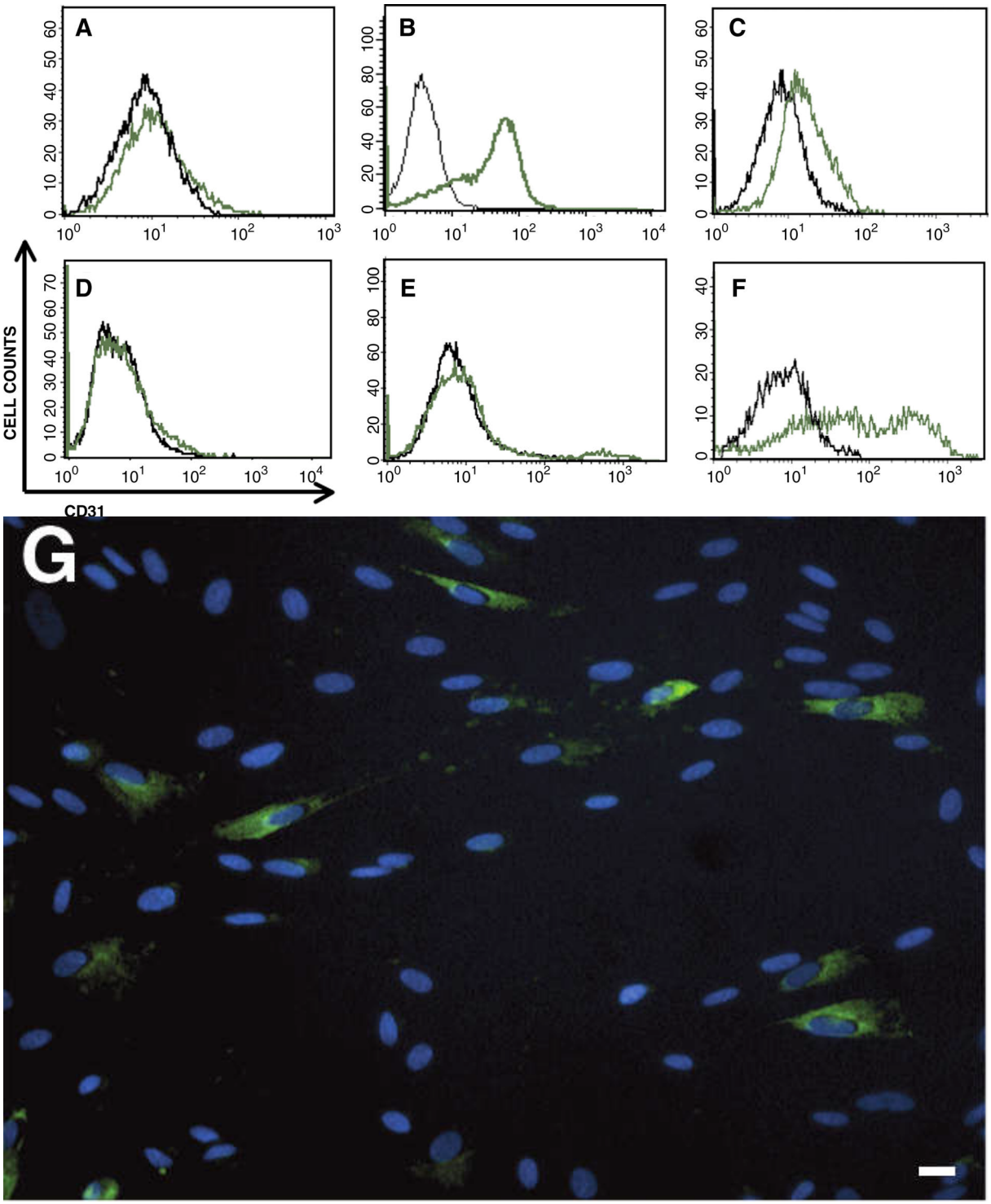

Figure 9.2: Expression of late endothelial cell markers. A–F: Fluorescence-activated cell-sorting analysis of CD31 (PECAM-1, green line) on isolated EPCs [(A, D) BM-EPCs; (B, E) early PB-EPCs; (C, F) late PB-EPCs], isotype-matched control (black line); (A–C) after 1 week and (D–F) after 3 weeks of culture. G: Immunocytochemistry of von Willebrand factor (vWF) on late PB-EPCs (green), DAPI nuclear stain (blue); scale bar = 10 μm.

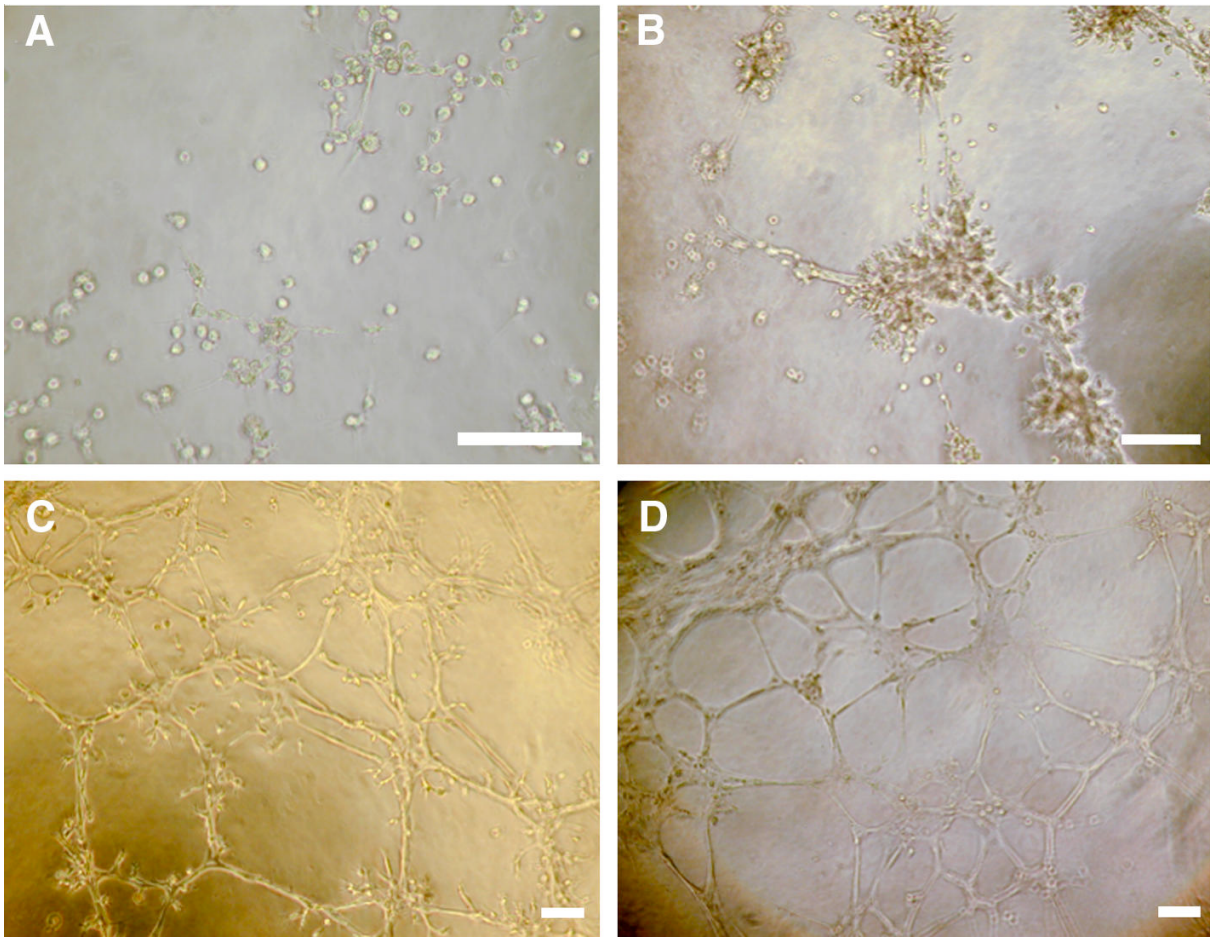

Figure 9.3: Angiogenesis assay showing network formation by isolated EPCs on Matrigel. A: BM-EPCs stretched on Matrigel, but hardly formed networks. B: Early PB-EPCs formed networks on Matrigel; these early vascular structures were less extensive than those formed by late PB-EPCs (C) or goat vein endothelial cells (D); scale bar = 100 μm.

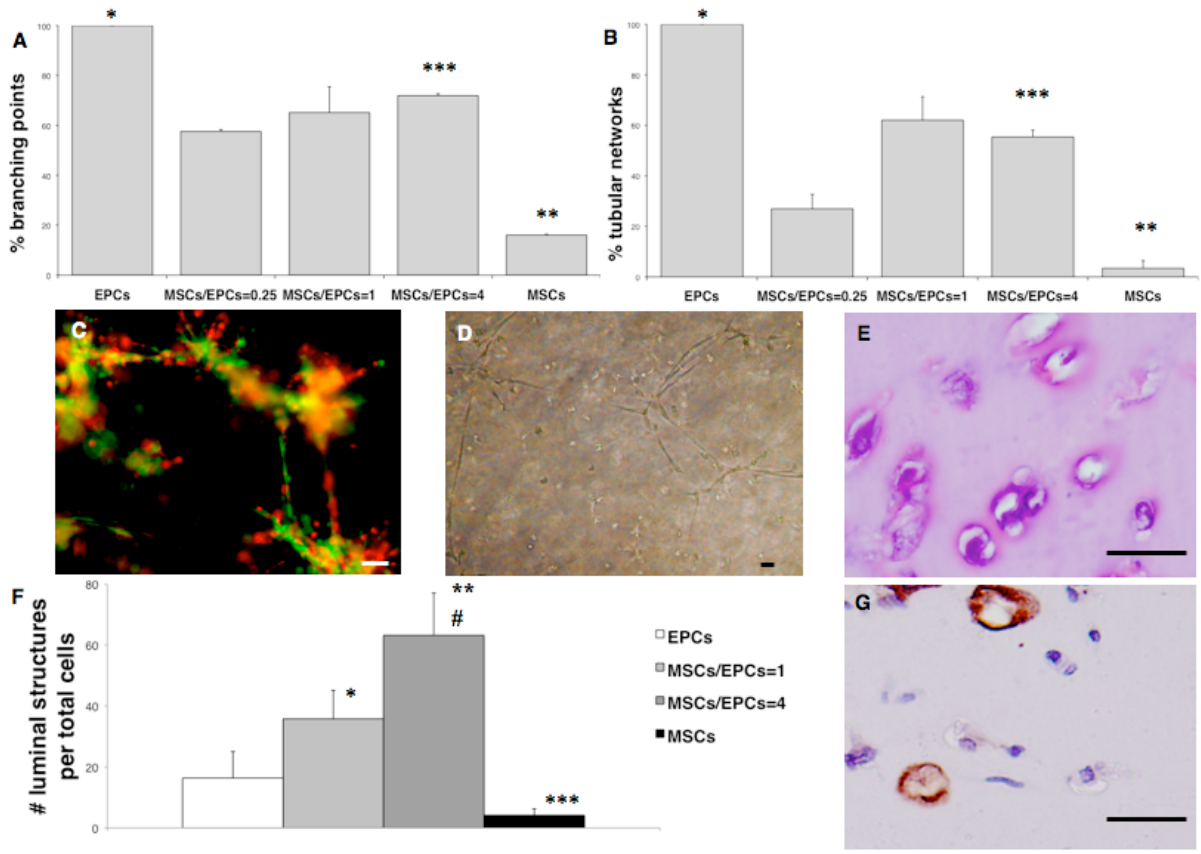

Figure 9.4: Tubular network formation of cocultures on and in Matrigel. A, B: The number of branching points and tubular networks seen on top of Matrigel as percentage of network formation by EPCs alone (15 h after cell seeding; two independent experiments); number of branching points and tubular structures was significantly higher in EPC-alone group compared to other groups, *$p<0.01$; multipotent stromal cell (MSC)-alone group was lower than all other groups, **$p<0.001$; cocultures of MSCs/EPCs = 4 yielded significantly more branching points and tubular structures than the MSCs/EPCs = 0.25 group, ***$p<0.05$. C: Coculture of fluorescently labeled MSCs (green) and EPCs (red) at the ratio of 0.25 in Matrigel; D: EPCs after 1 week in Matrigel; E: formation of luminal networks by EPCs, section stained with hematoxylin/eosin; F: scoring of the formed luminal structures at different MSCs/EPCs ratios in 3D, data presented as mean ± SD (n = 4); significant differences were detected between EPC-alone group and MSCs/EPCs = 1 and 4 (*$p<0.05$; **$p<0.001$), between MSC-alone groups and MSCs/EPCs = 1 and 4 (***$p<0.001$), and between MSCs/EPCs = 1 and 4 (#$p<0.01$). G: Networks immunostained for endothelial-specific marker vWF (brown). Scale bar = 20 μm.

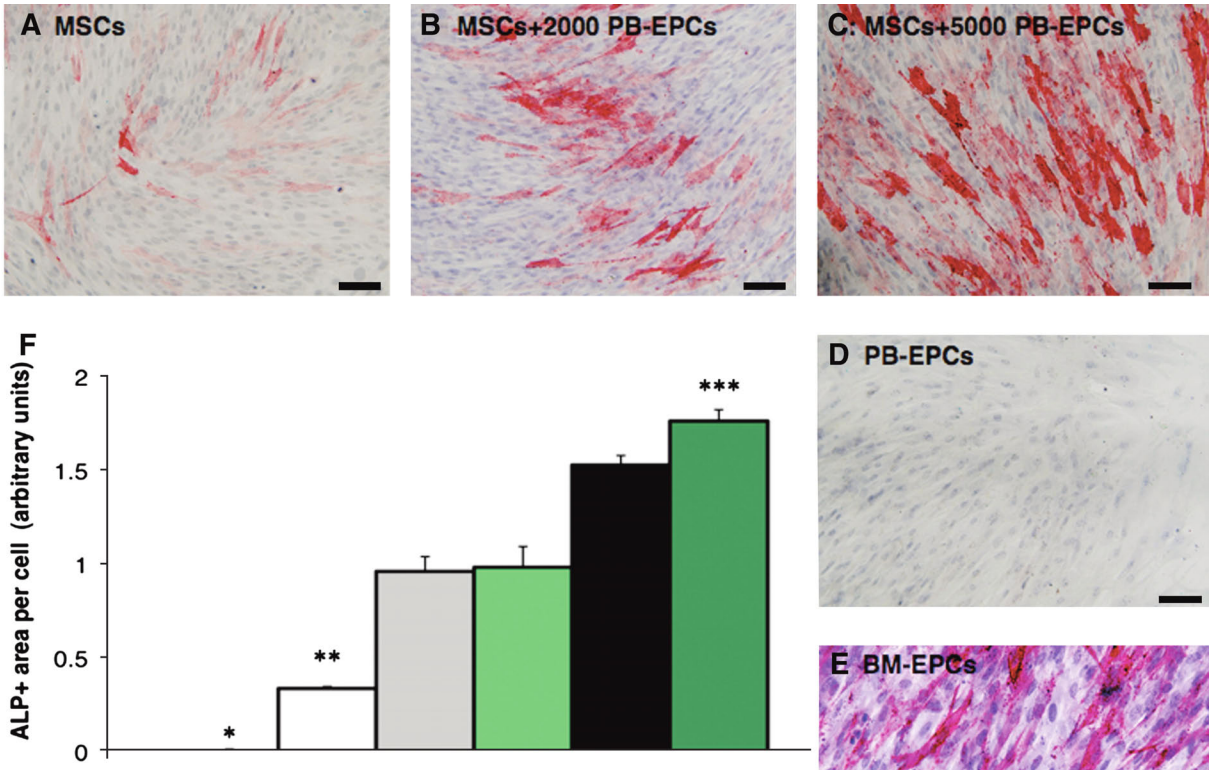

MSCs	-	10.000	10.000	12.000	10.000	15.000
PB-EPCs	10.000	-	2.000	-	5.000	-
Total cells	10.000	10.000	12.000	12.000	15.000	15.000

Figure 9.5: Osteogenic differentiation in coculture. Differentiation of MSCs in coculture with peripheral blood (PB)-EPCs: alkaline phosphatase (ALP) staining after one week of coculture (A–E); ALP-positive cells are stained red with fuchsin chromogen; counterstaining with hematoxylin; scale bar = 100 μm. (F) The fraction of ALP-positive cells in different coculture ratios of MSCs/EPCs; data presented as mean ± SD (n = 4); 10^4 EPCs compared to other groups (*$p<0.001$), 10^4 MSCs compared to the other groups (**$p<0.01$), $1.5x10^4$ MSCs produced more ALP than 10^4 MSCs + 5000 EPCs (***$p<0.01$), while difference between $1.2x10^4$ MSCs and 10^4 MSCs + 2000 EPCs was not significant.

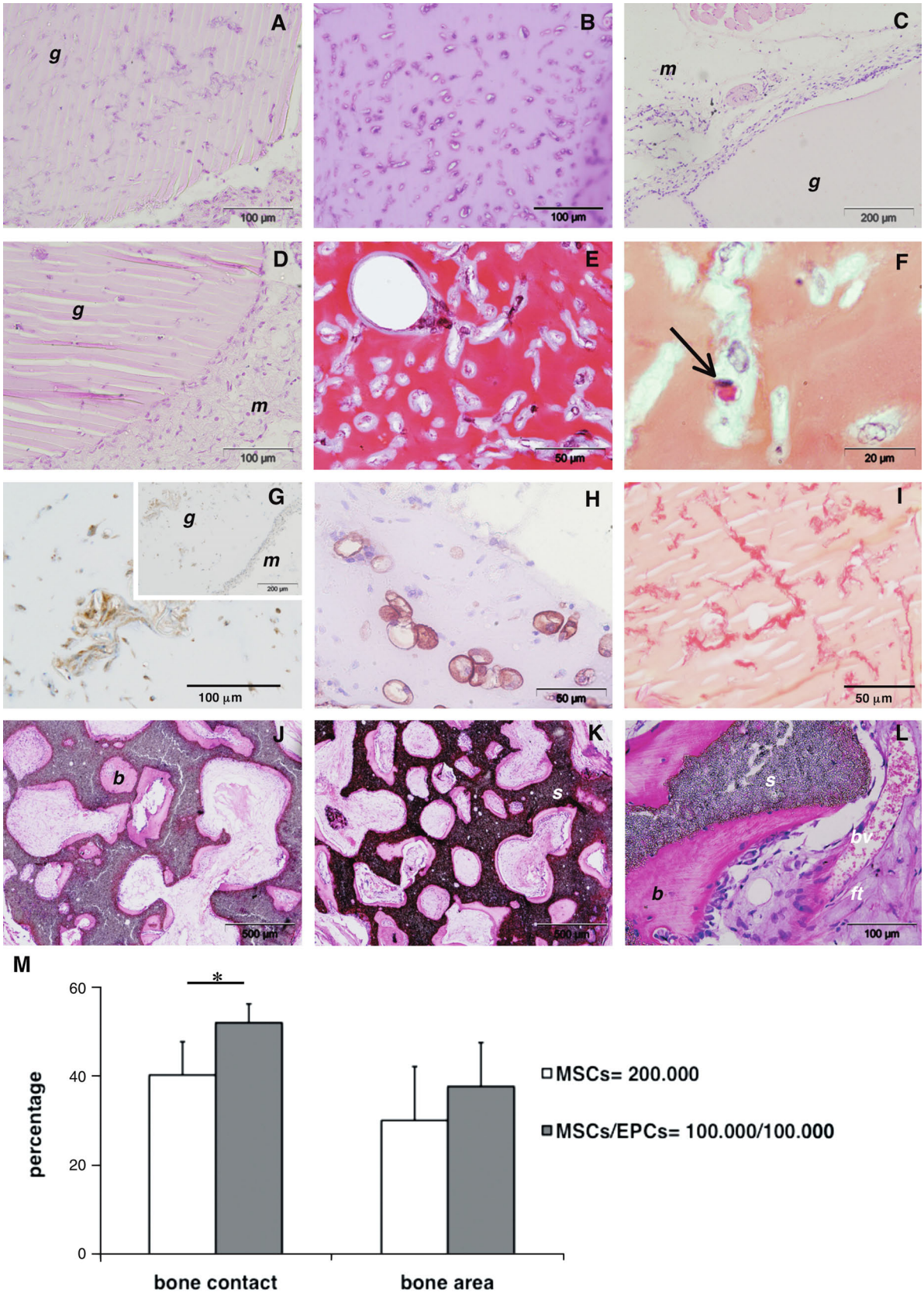

Figure 9.6: *In vivo* vascularization in Matrigel plugs after 2 weeks and bone formation after 6 weeks. A–E: Hematoxylin/eosin staining of Matrigel plugs revealed no network formation in control acellular gels (C) and Matrigel seeded with dead EPCs (D), compared to

compact network formation in viable EPC-laden hydrogel (A) and luminal networks in MSCs/EPCs-laden Matrigel (B, E). g, gel, m, mouse tissue; F: Matrigel plugs containing EPCs coembedded with MSCs (Goldner's trichrome staining) had erythrocytes present in some lumina in the coseeded group (F, arrow); G, H: Immunohistochemical staining of the networks in EPC-laden gels for endothelial markers vWF (G, brown dye) and caveolin-1 (H, red dye) demonstrated endothelial phenotype of embedded EPCs; cells counterstained with hematoxylin; I: Picrosirius red staining of EPC-laden gels to indicate collagenous matrix. J–L: Bone formed after 6 weeks both in MSCs (J) and MSCs/EPCs = 1 (K, L) implants. s, scaffold; b, bone; bv, blood vessel; ft, fibrous tissue; M: Histomorphometric quantification of the bone contact% (MSCs vs. MSCs/EPCs = 1; *$p<0.05$) and bone area% (n.s.), n = 4.

Supplementary material

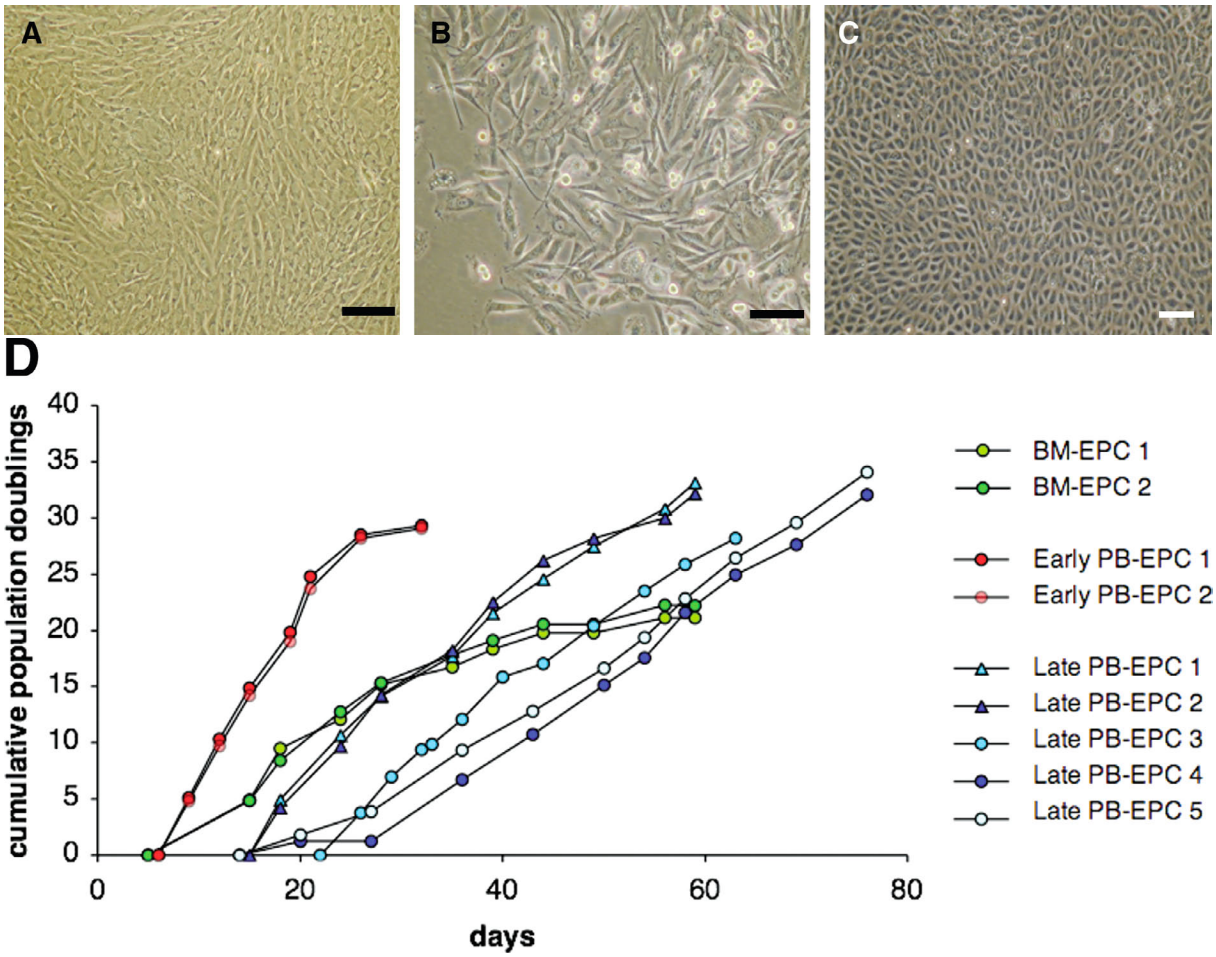

Supplemental Figure 9.1: Morphology and proliferation of isolated EPCs. Morphology of bone marrow (BM)-derived endothelial progenitor cells (EPCs) (A), early peripheral blood (PB)-derived EPCs (PB-EPCs) (B), and late PB-EPCs (C) after 1 week of culture, scale bar = 100 μm; D: Proliferation curves of BM-EPCs (two donors), early PB-EPCs (two donors), and late PB-EPC (five donors). Numbers 1–5 represent separate goat donors.

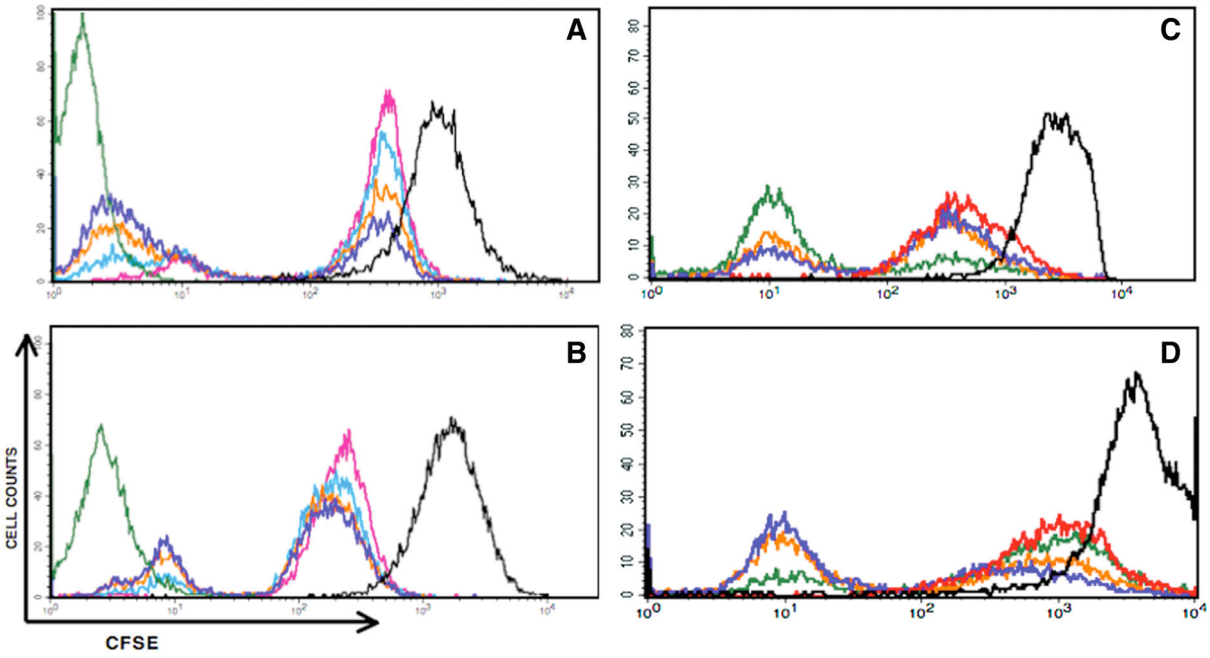

Line color, (day)	Figure A	Figure B	Line color, (day)	Figure C	Figure D
black, (0)	CFSE labeled MSCs	CFSE labeled EPCs	*black, (0)*	CFSE labeled MSCs	CFSE labeled EPCs
pink, (3)	15000 MSCs	15000 EPCs	*red, (3)*	100% MSCs	100% EPCs
light blue, (3)	15000 MSCs+5000 EPCs	15000 EPCs+5000 MSCs	*green, (3)*	MSCs/EPCs=0.25	EPCs/MSCs=4
orange, (3)	15000 MSCs+15000 EPCs	15000 EPCs+15000 MSCs	*orange, (3)*	MSCs/EPCs=1	EPCs/MSCs=1
dark blue, (3)	15000 MSCs+30000 EPCs	15000 EPCs+30000 MSCs	*blue, (3)*	MSCs/EPCs=4	EPCs/MSCs=0.25
green, (3)	Unlabeled MSCs	Unlabeled EPCs			

Supplemental Figure 9.2: Proliferation in coculture.

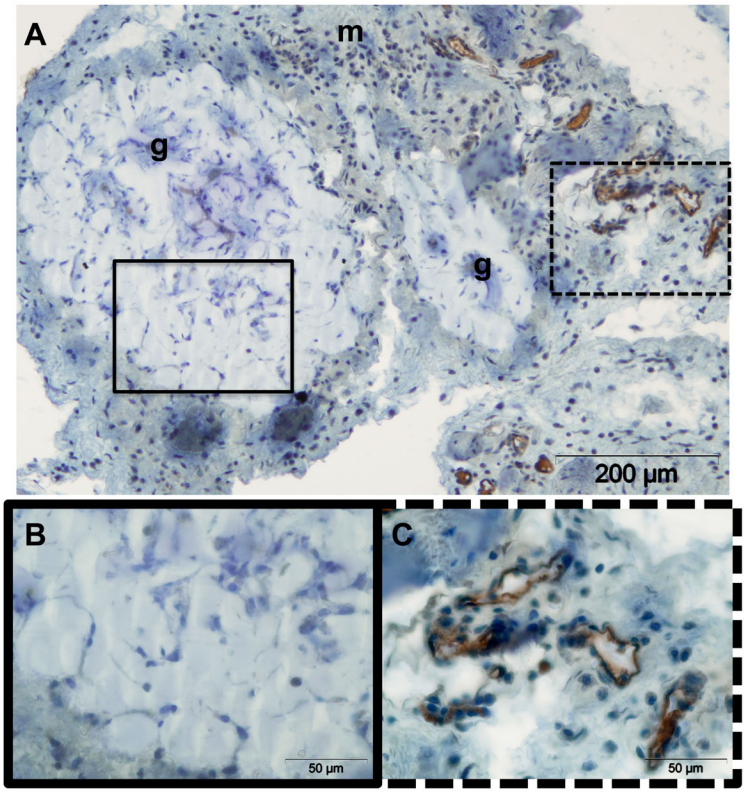

Supplemental Figure 9.3: *In vivo* vascularization.

Supplemental Figure 9.2: Proliferation in coculture. Proliferation analyzed by green fluorescent carboxyfluorescein-diacetate succinimidyl ester (CFSE) labeling, at constant target cell numbers (A, B) and at constant total cell numbers (C, D). Signal decreases when cells proliferate and the label is equally divided over the daughter cells; (A, C) CFSE-labeled multipotent stromal cells (MSCs) in coculture with PB-EPCs; (B, D) CFSE-labeled PB-EPCs in coculture with multipotent stromal cells.

Supplemental Figure 9.3: *In vivo* vascularization. Matrigel plugs after 2 weeks, mouse-specific CD31 (PECAM-1) staining; A: Overview of the sample: EPC-laden Matrigel (g), murine tissue (m), CD31 (brown); B: Close-up of the Matrigel part; C: Close-up of surrounding murine tissue.

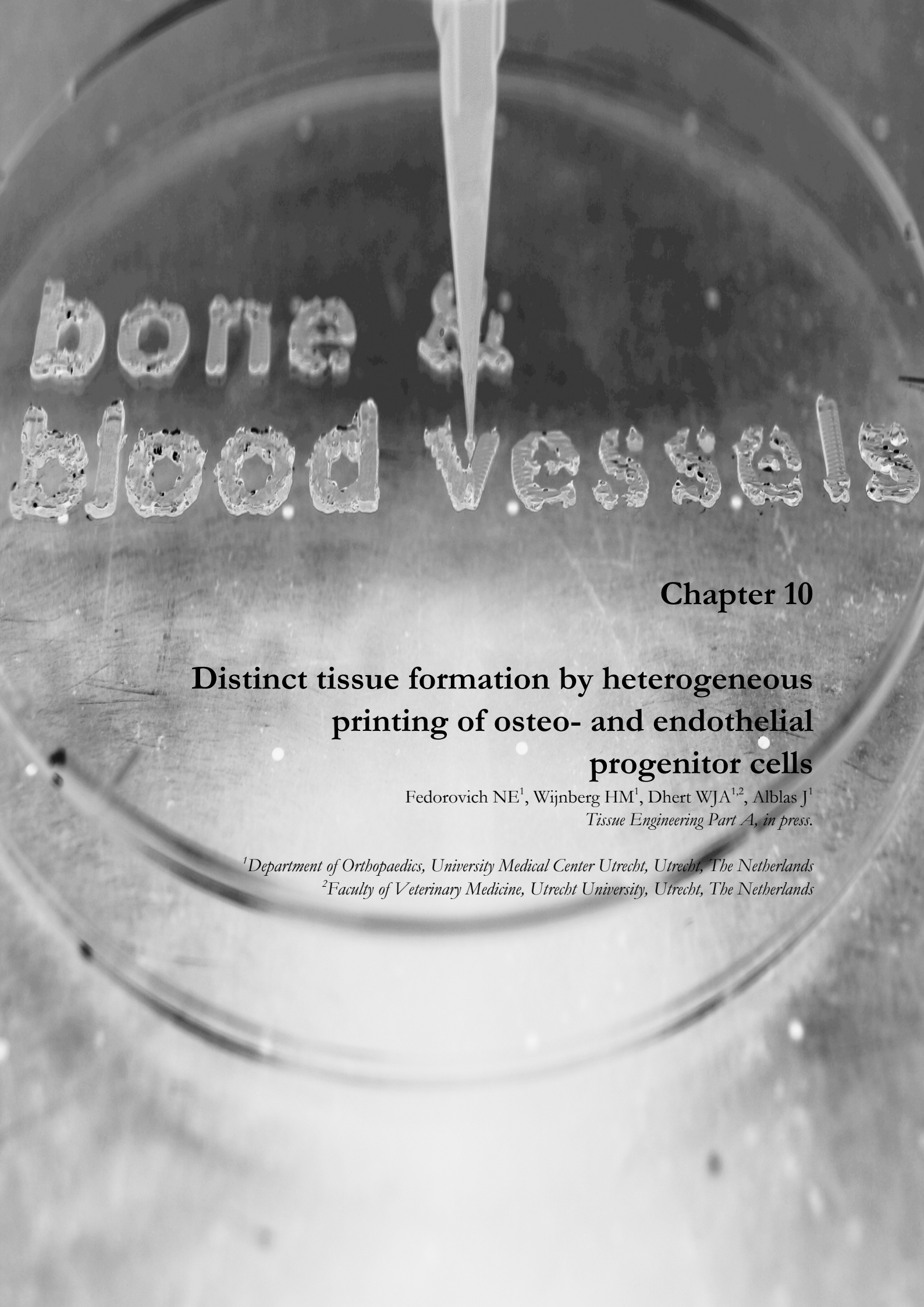

Chapter 10

Distinct tissue formation by heterogeneous printing of osteo- and endothelial progenitor cells

Fedorovich NE[1], Wijnberg HM[1], Dhert WJA[1,2], Alblas J[1]

Tissue Engineering Part A, in press.

[1]*Department of Orthopaedics, University Medical Center Utrecht, Utrecht, The Netherlands*
[2]*Faculty of Veterinary Medicine, Utrecht University, Utrecht, The Netherlands*

Abstract

The organ- or tissue printing (OP) approach, based on layered deposition of cell-laden hydrogels, is a new technique in regenerative medicine suitable to investigate whether mimicking the anatomical organization of cells, matrix and bioactive molecules is necessary for obtaining or improving functional engineered tissues. Currently data on performance of multicellular printed constructs *in vivo* is limited. In this study we illustrate the ability of the system to print intricate porous constructs containing two different cell populations - endothelial progenitors (EPCs) and multipotent stromal cells (MSCs) - and show that these grafts retain heterogeneous cell organization after subcutaneous implantation in immunodeficient mice. We demonstrate that cell differentiation leading to the expected tissue formation occurs at the site of the deposited progenitor cell type. While perfused blood vessels are formed in the EPC-laden part of the constructs, bone formation is taking place in the MSC-laden part of the printed graft.

Introduction

Successful engineering of tissues for regenerative medicine is expected to profit from strategies addressing the complex nature of natural tissue organization.[19,597,598] There is growing evidence that tissue formation can be significantly enhanced from combined use of multiple cell types and by building heterogeneously structured scaffolds. Specifically, the addition of endothelial (progenitor) cells to bone tissue engineered constructs is beneficial for the performance of the bone forming cells and stimulates neovascularization once the construct is implanted.[599] This is especially important for the survival of large, clinically relevant-sized tissue constructs. The bio-mimicking approach, which addresses the development of engineered tissues with design strategies that closely resemble the anatomical organization of cells, matrix and bioactive molecules of the native tissue,[47] is regarded as a potentially successful strategy to engineer functional bone grafts.

Organ- or tissue printing (OP) is a new technique in regenerative medicine that can help to investigate whether imposed cell organization is actually necessary for obtaining fully functional newly formed tissues, as it enables defined placement of different cell types in a construct. Using 3D fiber deposition, layers of cell-laden hydrogel strands are deposited according to a rapid prototyping design.[487] The resulting 3D scaffolds show a highly reproducible architecture (size, shape, porosity, interconnectivity, pore-geometry and orientation), while a great variation in material composition is possible. The porosity of the implants is easily tailored, which is important for mechanical and conductive properties of the construct. Pores enhance nutrient supply and waste product removal by allowing ingrowth of blood vessels and supporting homogeneous tissue formation. Furthermore, the 3D fiber deposition method can be used for rapid formation of constructs with defined organization of multiple cell types. Printable hydrogel matrices, including thermosensitive gelatinous protein mixtures such as Matrigel and seaweed-derived ion-sensitive alginates, are well suited materials for cell encapsulation and support viability and differentiation of embedded cells.[407] Previously, 3DF was used to print osteogenic progenitors in alginate scaffolds.[117] Multipotent stromal cells (MSCs) survive the deposition process and retain the ability to differentiate towards osteogenic lineage after printing. Deposition of multiple cell populations has also been achieved by other organ printing techniques including ink jet printing, laser deposition and dispensing tools.[118,513,600] However, limited evidence is available on the functionality of the designed cellular structures, due to short follow-up times after printing.

Currently no data are present on performance of multicellular printed constructs *in vivo*. It would be interesting to know whether *in vivo* heterogeneous cell organization introduced by printing is retained and is being translated to heterogeneous tissue formation. In this study we follow the retention of defined cell arrangement and heterogeneous tissue formation in printed grafts *in vivo*. We printed intricate, multicellular constructs using MSCs and endothelial progenitor cells (EPCs), and subsequently analyzed the nature of tissue formed after subcutaneous implantation in immunodeficient mice. Cells were fluorescently labeled to assess the dispersion of the transplanted cell populations *in vivo* and to determine whether the resulting tissue formation corresponded to the printed cell type.

Materials and methods

Cells

Goat multipotent stromal cells (gMSCs) obtained from iliac bone marrow aspirates of adult

Dutch milk goats were isolated by adhesion to tissue culture plastic.[11] Briefly, aspirates were plated at a density of $5x10^5$ cells/cm^2 and cultured in expansion medium consisting of αMEM (Invitrogen) supplemented with 10% FBS (Lonza), 2 mM L-glutamine (Glutamax, Invitrogen), 100 U/ml penicillin and 100 μg/ml streptomycin (Invitrogen). Medium was refreshed twice a week and cells were used for further subculturing or cryopreservation. Cell cultures were maintained in a humidified incubator at 5% CO_2 and 37 °C. gMSCs passage 2-6 were used in the study.

Goat endothelial progenitor cells (gEPCs) were isolated from peripheral blood. The peripheral blood samples were harvested from adult Dutch milk goats, which had not received prior stimuli to mobilize EPCs from the bone marrow. Mononuclear cells (MNCs) were isolated by density gradient centrifugation with Ficoll solution (Ficoll Paque™ Plus, GE healthcare Biosciences AB, Sweden). Cells from individual goats were plated in 25 cm^2 culture flasks coated with fibronectin (2.5 μg/ml in phosphate-buffered saline (PBS), one hour; Harbor Bioproducts, Norwood, USA) in EBM-2 (Cambrex, Verviers, Belgium), supplemented with singlequots (hEGF, VEGF, hFGF-B, R3-IGF-1, ascorbic acid, heparin, gentamicin-amphotericin-B) and 20% fetal calf serum (FCS, Cambrex), and cultured at 37 °C, 5% CO_2 in a humidified chamber. After 4 days of culture, non-adherent cells were removed by washing with PBS, fresh medium was applied and cells were cultured for at least 6 weeks, replating them twice a week. Colonies from a single donor were cultured together. After colony outgrowth, the cells were detached using 0.25% trypsin (Invitrogen) and stored in liquid nitrogen until further use.

Fluorescent labeling of cells

Prior to printing, cells were fluorescently labeled to facilitate distribution-analysis of the two cell types. For this, gEPCs were incubated with PKH26 (red; Sigma-Aldrich) and gMSCs with CFSE (green; Molecular Probes, Leiden, The Netherlands). The presence of fluorescent cells was analyzed directly after printing and after 1 and 2 weeks in *in vitro* samples and in frozen sections of *in vivo* samples after 2 weeks. For this, a fluorescence microscope (Olympus BX51 microscope, Olympus DP70 camera, Hamburg, Germany) was equipped with an epifluorescence set-up (Leica DM IRBE, Solms, Germany), excitation/emission setting of 488/530 nm to detect green-fluorescent gMSCs or 530/580 nm to detect red gEPCs.

Cell-laden hydrogel preparations

BD Matrigel™ Basement membrane matrix (#354234, BD Biosciences, Breda, The Netherlands) was used for encapsulation of EPCs at $5x10^6$ cells/ml gel. For encapsulation of MSCs we used alginate or growth factor depleted Matrigel (#354230, BD Biosciences) (both gels contained $5x10^6$ cells/ml gel), supplemented with osteoinductive biphasic calcium phosphate BCP microparticles (10% (w/v), see below for details).

Matrigel preparations were processed at 4 °C to keep the matrix fluid, and formed a gel at room temperature during printing. High-viscosity alginate powder (International Specialty Products, ISP, Memmingen, Germany) was autoclaved and subsequently mixed (10 % (w/v)) overnight at 37° with osteogenic medium (αMEM (Invitrogen, Breda, The Netherlands) supplemented with 10% FBS (Lonza, Basel, Switzerland), 0.1 mM ascorbic acid 2-phosphate (AsAP; Sigma-Aldrich, Zwijndrecht, The Netherlands), 2 mM L-glutamine (Glutamax, Invitrogen), 100 U/ml penicillin, 100 μg/ml streptomycin (Invitrogen), 10^{-8} M dexamethasone (Sigma-Aldrich) and 10 mM β-glycerophosphate (Sigma-Aldrich)). For gel formation, after printing alginate was incubated for 15 minutes with 102 mM $CaCl_2$ supplemented with 10 mM HEPES pH 7.4 (Invitrogen). BCP

microparticles (Progentix Orthobiology BV) were sintered at 1150°C and ranged from 106 to 212 μm in size. To assess contribution of BCP to bone formation *in vivo*, MSC-laden gel samples (alginate and growth factor depleted Matrigel) without BCP served as controls.

3D fiber deposition presets and printing of heterogeneous scaffolds

The BioScaffolder pneumatic dispensing system (SYS+ENG, Germany) was used for 3-dimensional printing of hydrogel scaffolds. This system was previously employed for extrusion of (cell-laden) hydrogels and is described in more detail elsewhere.[117,187] Briefly, the BioScaffolder is a three-axis dispensing machine, which builds up 3D constructs by coordinating the motion of a pneumatic syringe dispenser. The dispenser deposits extrudate consisting of empty or cell-laden hydrogel on a stationary platform. Composite models of the scaffolds are loaded via CAD/CAM software, which translates this information for the layer-by-layer fiber deposition by the machine.
To illustrate the ability of 3DF to print complex multicellular constructs, fluorescently labeled EPC and MSCs were mixed with a translucent thermosensitive hydrogel (Lutrol® F127 25 % (w/v) in medium; BASF) at 10^6 cells/ml and printed with the Bioscaffolder at two different configurations of deposited fibers (strand orientation of 90° relative to the underlying layer for MSCs and circular for EPCs). Each cell type was placed in a separate syringe loaded into the machine and a four-layer construct was printed by automatically exchanging the syringes between each layer, resulting in heterogeneous scaffolds with red- and green-labeled cell populations. Images were taken using an epifluorescence microscope (Leica, Germany) directly after the deposition.
Rectangular (10x20x1mm) ten-layer scaffolds were made with the CAD/CAM software for the study of cell dispersion *in vitro* and for design of *in vivo* implants, which consisted of two parts (10x10mm) directly adjacent to each other (experimental groups are described in Table 10.1). The speed of deposition was set at 300 mm/min and the pneumatic pressure that was applied to the dispensing syringe was set at 0.175 MPa to yield uniform, continuous extrusion of fibers. An inner nozzle diameter of 420 μm was used. The Bioscaffolder interchanged the cooled cartridges (4 °C) with the loaded syringes every two layers, in the case of heterogeneous scaffolds. The alginate containing scaffolds were subsequently crosslinked in $CaCl_2$ solution as indicated. Upon printing the constructs were cultured *in vitro* overnight and implanted the next day.

In vivo implantation

Tissue development in heterogeneous grafts was studied in composite constructs two and six weeks after implantation. Implanted constructs included Matrigel/Matrigel grafts (EPCs in Matrigel; MSCs in growth factor depleted Matrigel/BCP) and Matrigel/alginate grafts (EPCs in Matrigel; MSCs in alginate/BCP). Control samples included printed gel constructs (alginate or growth factor depleted Matrigel) without BCP and printed scaffolds without cells (all n=3 per time point). Female nude mice (NMRI-Foxnu, Charles River, Belgium), six-weeks old, were anaesthetized with 1.5% isoflurane, after which the implants were placed in separate subcutaneous dorsal pockets. The incisions were closed using a Vicryl 5-0 suture. The animals were postoperatively treated with the analgesic buprenorphine (0.05 mg/kg, sc; Temgesic, Schering-Plough) and housed together at the Central Laboratory Animal Institute, Utrecht University. Experiments were conducted with the permission of the local Ethical Committee for Animal Experimentation and in compliance with the Institutional Guidelines on the use of laboratory animals.

Sample processing

Two weeks after implantation, part of the implants was retrieved for analysis of cell distribution in printed grafts. For this, the samples were embedded in TissueTek and processed to frozen sections (5 μm). Another part of the samples was fixed overnight in 4% buffered formalin and processed for paraffin histology.
Implants retrieved after 6 weeks were fixed in 4% buffered formalin, decalcified in Luthra's solution (0.35 M HCl, 2.65 M formic acid in distilled water) for 24 h and processed for paraffin sections.

Cell dispersion

The constructs were assessed with a fluorescence microscope to analyze cell distribution *in vitro* and after *in vivo* implantation, and included samples cultured *in vitro* for 2 weeks (n=3) and grafts implanted *in vivo* for 2 weeks (n=3), respectively.
For analysis of *in vitro* samples, three groups were used: Matrigel/Matrigel scaffolds (EPCs in Matrigel; MSCs in growth factor depleted Matrigel), Matrigel/alginate constructs (EPCs in Matrigel; MSCs in alginate) and Matrigel/Matrigel constructs supplemented with BCP particles (EPCs in Matrigel; MSCs in growth factor depleted Matrigel/BCP). For analysis of cell distribution *in vivo*, two groups were compared: Matrigel/Matrigel scaffolds (EPCs in Matrigel; MSCs in growth factor depleted Matrigel), and Matrigel/alginate constructs (EPCs in Matrigel; MSCs in alginate).

Evaluation of tissue formation

To analyze tissue formation, 5 μm thick paraffin sections were cut and general histological staining was performed with hematoxylin/eosin (HE) and Goldner's trichrome.
To detect blood vessels, the sections were stained for endothelial marker von Willebrand factor (vWF) and α-smooth muscle actin (α-SMA). vWF detection was performed on rehydrated sections, which were preincubated in 3% H_2O_2 for ten minutes and 10% (v/v) normal goat serum in PBS for 20 minutes, and subsequently incubated with rabbit anti-human vWF antibody (15 μg/ml; DAKO) for 1 hour. As secondary antibody we used powervision goat anti-rabbit HRP for one hour. To detect α-SMA, rehydrated sections were incubated with alkaline-phosphate conjugated mouse primary antibody against α-SMA (1:100 in 5% BSA/PBS; Sigma-Aldrich A5691, clone 1A4) for 1 hour and the presence of ALP was detected by incubation with Fuchsin Substrate-Chromogen system (DAKO) for 30 minutes, and counterstained with Mayer's hematoxylin (Merck).
To demonstrate the presence of osteogenic marker collagen type I, immunohistochemical analysis was performed on rehydrated sections that were preincubated in 0.3% H_2O_2 for ten minutes and 5% BSA/PBS for 30 minutes, and subsequently incubated with rabbit polyclonal antibody against collagen type I (3.3 μg/ml in 5% BSA/PBS; Abcam 34710) overnight at 4°C. As secondary antibody we used goat anti-rabbit HRP (2.5 μg/ml in 5% BSA/PBS; DAKO) for one hour.
To illustrate cartilage formation, Safranin-O staining of proteoglycans and collagen type II immunolocalization were conducted. For detection of collagen type II, rehydrated sections were preincubated in 0.3% H_2O_2 for ten minutes and 5% BSA/PBS for 30 minutes, followed by antigen retrieval with 1 mg/ml pronase and 10 mg/ml hyaluronidase in PBS-0.1% Tween, each for 30 minutes at 37 ºC. The sections were subsequently incubated with rabbit polyclonal antibody against collagen type II (10 μg/ml in 5% BSA/PBS; Abcam 53047) overnight at 4°C. As

secondary antibody we used goat anti-rabbit HRP (2.5 μg/ml in 5% BSA/PBS; DAKO) for 1 hour. The immunohistochemical stainings were developed with 3,3'-diaminobenzidine (DAB) and counterstained with Mayer's hematoxylin (Merck).

Results

Printing of heterogeneous implants and analysis in vitro

To illustrate the possibilities of heterogeneous cell printing, EPCs and MSCs were each combined with a thermosensitive hydrogel and printed by the Bioscaffolder to yield structured scaffolds with distinct cell populations at predetermined locations (Figure 10.1). Cells were homogenously encapsulated throughout the gel, when placed in predefined strands within one construct (Figure 10.1D).

Cell distribution in dual heterogeneous grafts (Matrigel/Matrigel grafts (EPCs in Matrigel; MSCs in Matrigel±BCP) and Matrigel/alginate grafts (EPCs in Matrigel; MSCs in alginate; n=3 per group) was retained *in vitro* 2 weeks after printing in the three groups (Figure 10.2). The MSC-laden parts of the constructs containing BCP particles were opaque, and limited the analysis with fluorescence microscopy (Figure 10.2A). Some of EPCs, restricted to one part of the heterogeneous graft, formed networks (Figure 10.2D), while MSCs remained homogeneously dispersed in the other (Figure 10.2C). Cell distribution between alginate/Matrigel and Matrigel/Matrigel constructs differed. A distinct demarcation line was visible between green-labeled MSCs and red-labeled EPCs in alginate/Matrigel samples (Figure 10.2B), while a transition zone with both cell types was observed in Matrigel/Matrigel constructs (Figure 10.2A,C).

Tissue formation in heterogeneous grafts in vivo

Cell distribution

After 2 weeks *in vivo*, fluorescently labeled cell populations were observed in frozen sections of the printed heterogeneous scaffolds (Figure 10.3). In Matrigel/alginate constructs (Figure 10.3A), the cells were mostly restricted to the part of the scaffold they were printed in, while in Matrigel/Matrigel grafts (Figure 10.3B), a small fraction of the cells was observed to migrate into the transition zone between the two compartments.

Tissue formation

Upon retrieval, the constructs were well integrated and vascularized by the host tissue, both at 2 and 6 weeks. Heterogeneous ECM formation in printed Matrigel constructs was observed both macroscopically (Figure 10.4A) and upon histological evaluation (Figure 10.4B,C) and the overview is presented in Table 10.2.

After two week-implantation of heterogeneous Matrigel grafts, blood vessels started to form in EPC-laden part of the construct (Figure 10.4D). Some of the newly formed tubular structures were empty, and some were perfused with erythrocytes. No tubules were seen in control Matrigel without seeded cells (Figure 10.4E), indicating that inclusion of EPCs is crucial for tubule formation. Six weeks after implantation, erythrocyte-filled tubules were observed throughout the EPC-laden part (Figure 10.4F,G). Immunostaining for endothelial specific marker vWF and α-SMA underscored the formation of stabilized blood vessels structures (Figure 10.4H,I).

Early bone apposition and cartilage formation took place in the MSC/BCP-laden Matrigel part two weeks after implantation (Figure 10.5A-C). Here, osteoblasts lining the BCP particles were frequently seen (Figure 10.5A, inset). While cartilage formed in the vicinity of skin, early bone

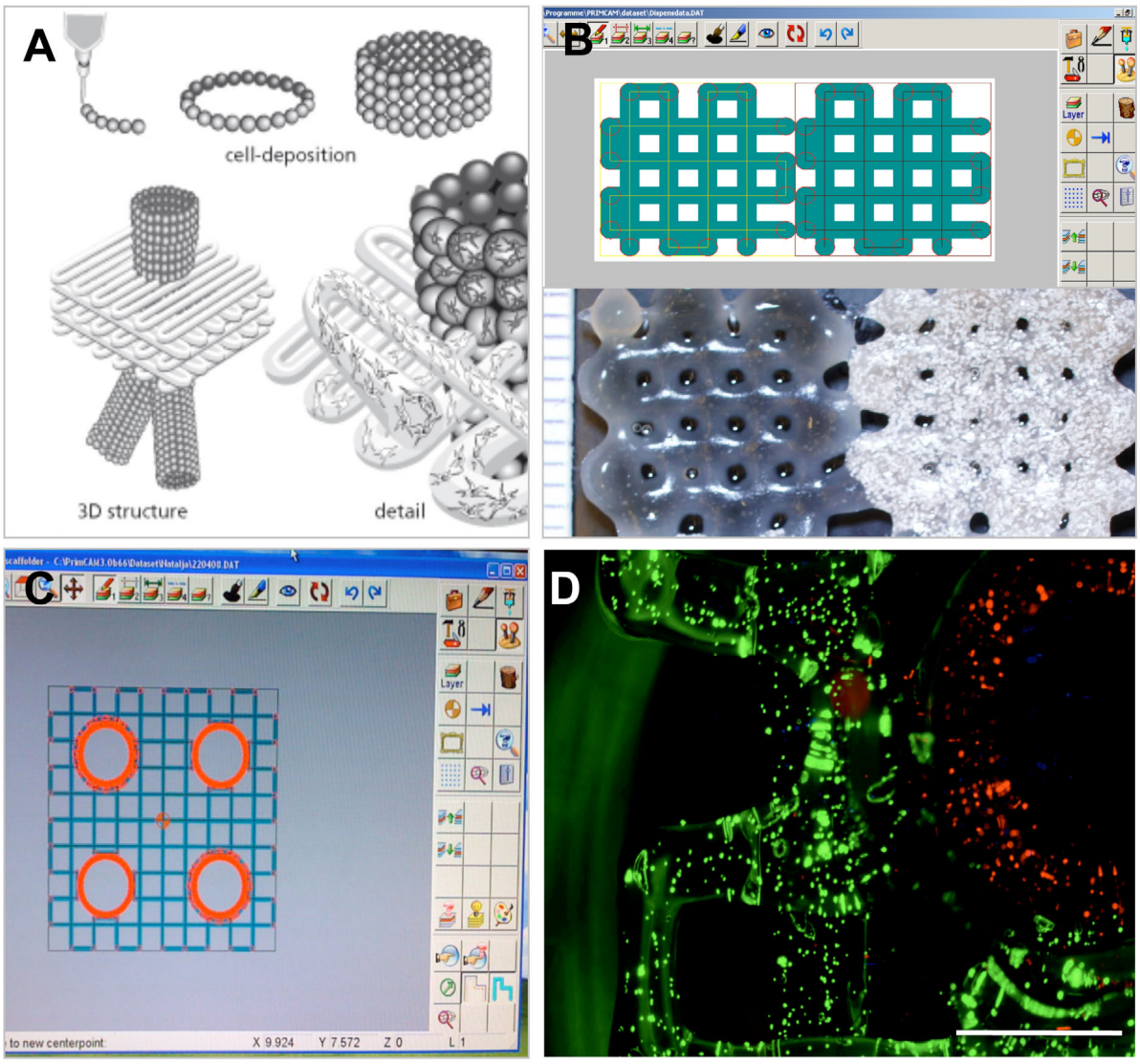

Figure 10.1: Printing heterogeneous constructs for vascularized bone tissue engineering. A: Schematic representation of the 3DF printing process; B: Model of the heterogeneous "dual" construct (top), printed graft (bottom); 10x20x1mm; EPC-laden Matrigel part (left), MSC-laden Matrigel part with added BCP (right); C: Model of the printed heterogeneous "tubes-in-cube" construct (20x20x1mm); D: Fluorescently labeled populations of EPCs (red) and MSCs (green) printed within one "tubes-in-cube" construct, scale bar = 1 mm.

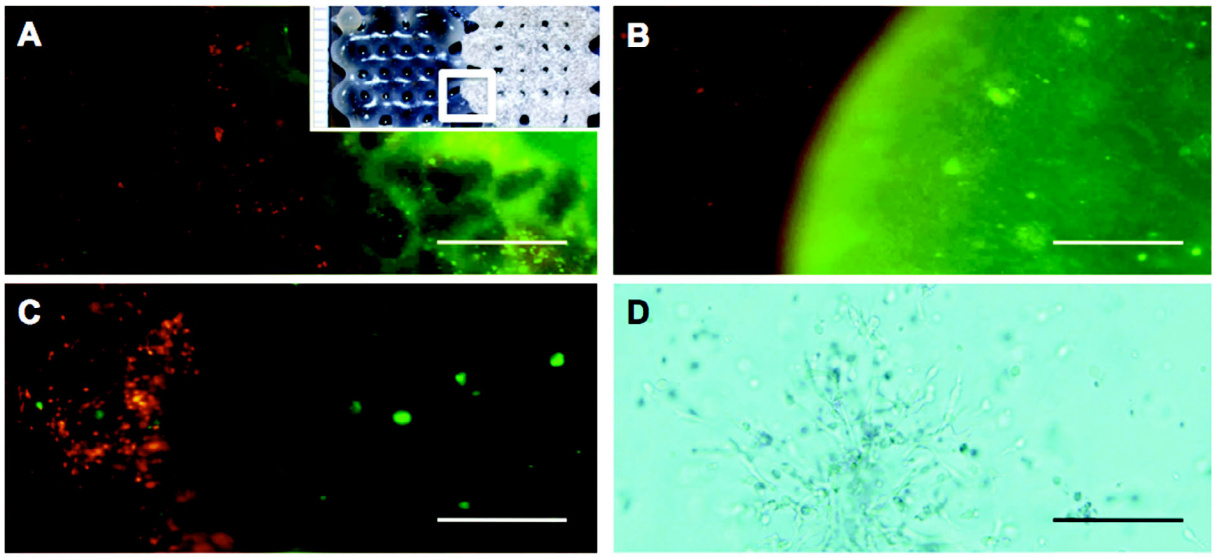

Figure 10.2: Cell dispersion in heterogeneous printed grafts *in vitro*. A: EPCs (red) in Matrigel, MSCs (green) in Matrigel with BCP, inset: overview of dual graft, showing BCP-containing gel on the right; scale bar = 200 µm; B: EPCs (red) in Matrigel, MSCs (green) in alginate, scale bar = 200 µm; C: EPCs (red) in Matrigel, MSCs (green) in Matrigel, scale bar = 100 µm; D: EPCs form networks in Matrigel, transmitted light view, scale bar = 200 µm.

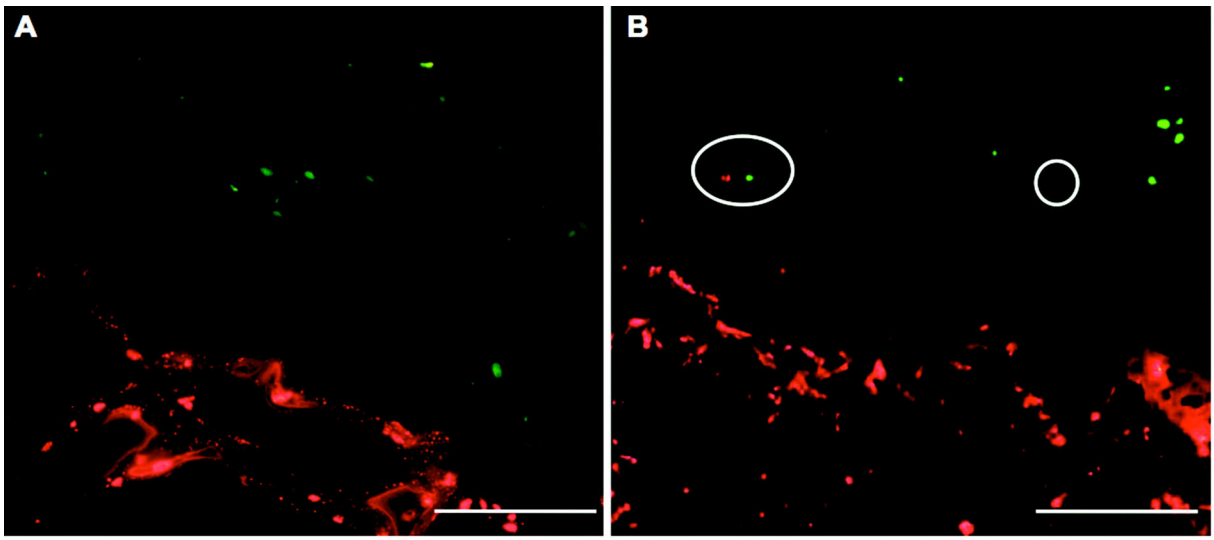

Figure 10.3: Cell dispersion in heterogeneous printed grafts *in vivo*. A: EPCs (red) in Matrigel, MSCs (green) in alginate; B: EPCs (red) in Matrigel, MSCs (green) in Matrigel, migrated cells in the transition zone (circle), scale bar = 200 µm.

development started in deeper regions of the constructs, adjacent to the muscle layer (Figure 10.5B,C). Very limited extracellular matrix formation was seen in the MSC-laden alginate part of the constructs (Figure 10.5B, inset), and no collagen type I staining was detected (data not shown).
After six weeks of implantation, the MSC-laden part of the construct with Matrigel and added BCP exhibited evident bone formation as confirmed by Goldner's trichrome staining and collagen type I immunolocalization (Figure 10.5D-F). In the MSC/Matrigel-part of the construct without BCP, very limited collagen type I formation occurred next to some cartilage development (Figure 10.5G,H), indicative of the osteoinductive role of the microparticles. Strikingly, again cartilage was detected in the MSC-laden part of the samples, as evidenced by Safranin-O and collagen type II stainings (Figure 10.5I,J). The MSC-laden part of the construct with alginate/BCP demonstrated regions of newly formed matrix (Figure 10.5K), which stained positive for osteogenic marker collagen type I (Figure 10.5L). No collagen type I formation was seen in control MSC-laden alginate without added BCP (data not shown), indicating that inclusion of osteoinductive particles plays a role in the observed early bone formation in this hydrogel.

Discussion

In this study we validate the development of tissue equivalents printed with 3DF. Dual, heterogeneous constructs comprising two parts with distinct cell types (EPCs and MSCs) are printed with a 3DF machine and exhibit heterogeneous ECM formation corresponding to the deposited cell type after *in vivo* implantation.
In literature, the interactions between endothelial cells and osteogenic progenitors are well described,[601] and require further research into the ideal combinations and ratio of cells that would yield functional grafts.[166] In this respect, our Bioscaffolder printing technique represents a unique tool to study 3D interactions between the two cells types and provides us with a model to analyze the relevance of anatomical structuring in TE. As an early step towards this goal, in this study we demonstrate that the two cells types can be combined during the deposition process.
Various patterning and organ printing techniques enable formation of multicellular, heterogeneous constructs. Among others, combined photo- and electropatterning technique,[109] optofluidic maskless lithography[602] and robotic dispensing[118] were recently used to build layered grafts to modulate cell's biosynthetic activity, to precisely study cellular interactions, and for defined arrangement of multiple cell populations in skin tissue engineering, respectively. However, all of the conducted studies were performed *in vitro* and commonly provide little evidence on retention of cell organization introduced by printing, limited by their short-term observation periods.[118]
In our experiments we demonstrate retention of printed cell organization 2 weeks after printing, both *in vitro* and after implantation *in vivo*. We observed that Matrigel/Matrigel composite scaffolds promote cell migration at the interface zone, compared to Matrigel/alginate constructs. This difference can be explained by low interactive properties of alginate, which as a rule entraps the cells and does not support their migration. The majority of the cells, however, is retained at its original printed location. In a recent *in vivo* study, which addressed short-term retention of stratified chondrocyte populations implanted in a patellofemoral defect in minipigs for one week, the stratified organization was lost after implantation.[31] Possibly, this could be explained by the mechanic pressure on the implants in the knee, which was much higher than at the ectopic location in our experiments. The organized deposition of cells and the subsequent development

of viable, 3D hydrogel structures is an important achievement of modern TE technologies, but it is unknown whether these constructs will lead to more functional tissues *in vitro* and *in vivo*. It was previously demonstrated that patterning and dispensing techniques can build viable cell-laden structures, that singular cell populations retain their functionality for several weeks *in vitro*[115,117,133] and that functionality of embedded cells can be further modulated by specific cell arrangement.[109] In this study we demonstrate for the first time that multiple printed cell types also retain their functionality after *in vivo* implantation, and produce extracellular matrix according to the deposited cell type. Blood vessel formation takes place in the EPC-laden part of the printed constructs, while bone formation occurs in the MSC-laden part, starting two weeks after implantation.

In the EPC-laden Matrigel part of the printed construct, we observed formation of erythrocyte-filled tubules. EPCs isolated from peripheral blood are a potent source of endothelial cells (ECs). Under comparable conditions, EPCs perform better than ECs with respect to blood vessel network formation.[574] EPCs are highly proliferative, exhibit a stable endothelial phenotype,[571] support neovascularization of the ischaemic hindlimb,[568,569,572] regenerate infarcted myocardium[573] and support bone formation upon co-implantation with MSCs.[603,167] In this study addition of EPCs was essential for the formation of potent, erythrocyte perfused vessels, whereas no vessel ingrowth was seen in acellular Matrigel. The newly formed vessels stained positive for endothelial specific marker vWF and were stabilized by smooth muscle cells. We cannot claim that the seeded EPCs actually form the blood vessels, as the exact origin of the cells forming the new blood vessel networks remains to be elucidated. It is likely that vWF positive endothelial lining is in part derived from the seeded progenitors, while α-SMA positive vessel-stabilizing cells are either host-derived pericytes or MSCs. Limited migration of cells in the hydrogel matrix makes the contribution of coprinted MSCs to blood vessel stabilization less likely.

Bone tissue started to form around the BCP particles in Matrigel scaffolds two weeks after implantation and progressed to abundant bone formed at 6 weeks, a potent outcome considering that the concentration of encapsulated MSC used for implantation in this study was lower than in other bone TE studies.[70,291] Inclusion of osteoinductive BCP particles has proven to be of importance for bone formation in this context. This finding is supported by other reports illustrating potent bone formation when calciumphosphate precipitates are added to the hydrogel.[519] The positive effect of microparticles on bone formation has been attributed to a number of factors, of which serum protein adsorption to the surface of particles is important.[604] Dissolution of calcium phosphates is responsible for calcium and phosphorus release into the microenvironment of the cells, which creates a favorable milieu for new bone formation, supported by the rough surface of the particles.

While a large amount of bone formed in the printed MSC-laden Matrigel part of the scaffold, as evidenced by Goldner's trichrome and collagen type I staining, limited bone formation was observed in alginate. A small degree of extracellular matrix development, as shown by Goldner's trichrome staining, next to some positive staining for collagen type I in alginate samples at six weeks, are indicative of osteogenesis taking place in this gel. Limited interaction of the alginate matrix with cells, restricting the migration of the cells through the matrix, and a relatively high concentration of this slowly resolving polysaccharide in the printed gel may be responsible for above findings. The degree of this delay in bone formation depends on the hydrogel type used and its degradation speed.[605]

We also observed formation of substantial amounts of cartilage in the MSC-laden part of the Matrigel grafts. The development of bone by endochondral ossification is a common mechanism displayed by transplanted MSCs at ectopic locations in the murine model.[24] Cartilage formation

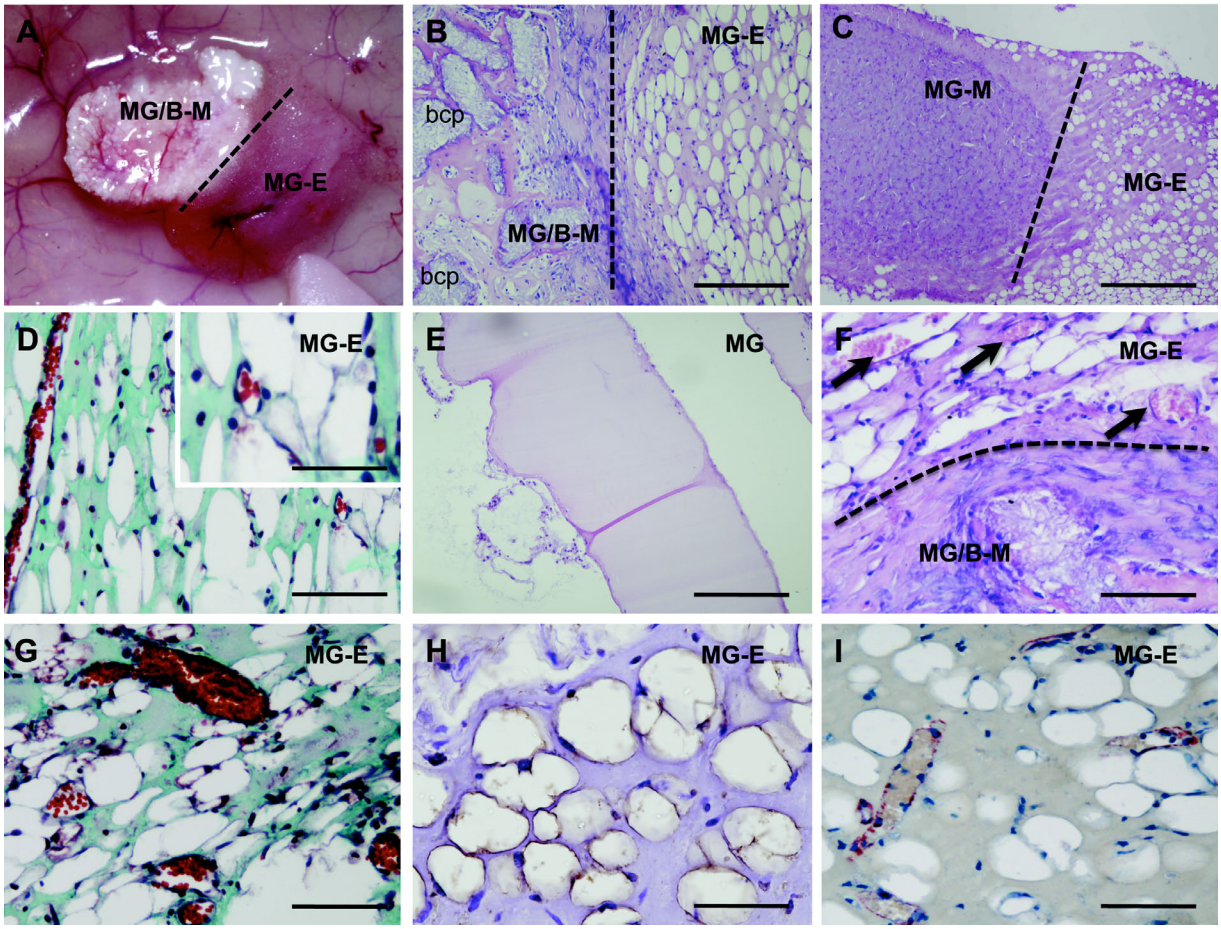

Figure 10.4: Heterogeneous tissue formation *in vivo*. A: Macroscopic view of heterogeneous graft at 6 weeks, dotted line represents the transition zone; B: HE staining, 6 weeks, scale bar = 200 μm; C: HE staining, 6 weeks, scale bar = 500 μm; D: Goldner's trichrome staining, 2 weeks, collagen in green, erythrocytes in red, cell nuclei are black, scale bar = 100 μm, (inset: close-up, scale bar = 50 μm); E: HE staining of unseeded Matrige at 6 weeks, scale bar = 100 μm; F: HE staining, 6 weeks, arrow: erythrocytes, scale bar = 100 μm; G: Goldner's trichrome staining, 6 weeks, erythrocytes: red, Matrigel: green, nuclei: black, scale bar = 100 μm; H: vWF staining (in brown) at 6 weeks, Matrigel: purple, scale bar = 100 μm: I: α-SMA staining (in red) at 6 weeks, Matrigel: grey, nuclei: blue, scale bar = 100 μm. bcp indicates the location of BCP particles in the sections.

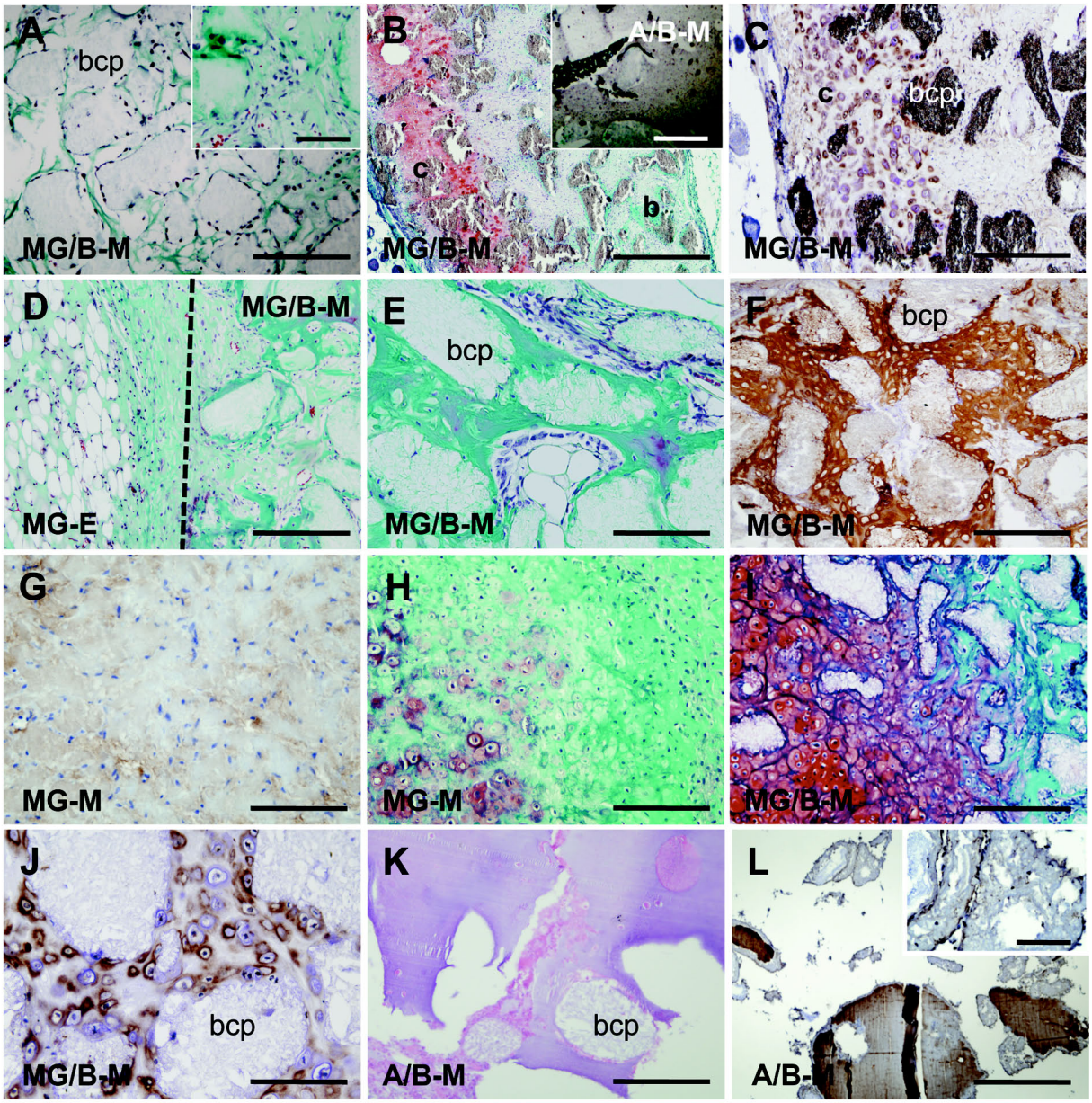

Figure 10.5: Bone tissue formation in MSC-laden part of the grafts *in vivo*. A: Goldner's trichrome staining at 2 weeks, scale bar = 200 μm, inset: early bone apposition (dark green), scale bar = 100 μm; B: Safranin-O staining at 2 week, c: cartilage (red); b: bone formation (dark green), scale bar = 500 μm, inset: alginate (grey) construct at 2 weeks, scale bar = 200 μm; C: collagen type II staining (brown) at 2 weeks, scale bar = 200 μm; D: Goldner's trichrome staining of transition zone at 6 weeks, scale bar = 200 μm; E: detail of bone (dark green) formation after 6 weeks, Goldner's trichrome staining, erythrocytes: red, scale bar = 100 μm; F/G: collagen type I immunostaining (brown) at 6 weeks, scale bar = 100 μm; H/I: Safranin-O staining at 6 weeks, proteoglycans: red, collagen: green, bone: dark green, scale bar = 100 μm; J: collagen type II immunostaining (brown) at 6 weeks, scale bar = 100 μm; K: HE staining of alginate (purple) construct at 6 weeks, ECM formation: pink, scale bar = 200 μm; L: collagen type I immunostaining (brown) at 6 weeks in alginate matrix and around BCP, scale bar = 500 μm (inset: detail, scale bar = 100 μm). bcp indicates the location of BCP particles in the sections.

Time point	**Study group I**	**Study group II**	**Acellular I**	**Acellular II**	**Fluorescence analysis (week 2) Control w/o BCP, I (week 6)**	**Fluorescence analysis (week 2) Control w/o BCP, II (week 6)**	**Implants per group**
Week 2	MG-E; MG/B-M	MG-E; A/B-M	MG; MG-B	MG; A-B	MG-E; MG-M	MG-E; A-M	3
Week 6	MG-E; MG/B-M	MG-E; A/B-M	MG; MG-B	MG; A-B	MG-E; MG-M	MG-E; A-M	3

Table 10.1: Experimental groups. MG=Matrigel, A=alginate, E=EPCs, M=MSCs, B=BCP.

Time point	**EPC-laden Matrigel**	**MSC-laden Matrigel**	**MSC-laden alginate**
Week 2	• some tubular structures • erythrocytes present in part of the lumina	• cartilage • early bone apposition	• limited matrix formation
Week 6	• tubular structures • erythrocytes in some lumina • vessels stabilized by smooth muscle cells	• cartilage • bone formation, only in BCP-laden gels	• early osteogenesis, only in BCP-laden gels

Table 10.2: Summary of the extracellular matrix formation in heterogeneous scaffolds.

appeared to be initiated at the skin-side of the constructs, while bone formation seemed to occur in deeper regions. The development of oxygen gradients that modulate the differentiation of MSCs[72,463] after implantation may be responsible for this phenomenon.
While mm-sized bone tissue implants are successful in animal models, formation of large-scale tissues is limited due to death and restricted osteogenic differentiation of transplanted cells. Currently, the formation of printed cm-scaled tissue equivalents like we presented here lies a considerable distance away from the actual printing of bone tissue. However, in the future 3DF may result in development of larger, clinically relevant-sized grafts. *In vivo* implantation of heterogeneous printed grafts at an orthotopic location will provide insight in the quality and quantity of tissue formation within the printed grafts. An important issue to investigate is whether the imposed cell organization is actually necessary for obtaining fully functional newly formed tissues upon *in vivo* implantation. Another essential matter to consider is the cell density in printed grafts, which is likely to have a profound effect on tissue formation[11,173,493] due to a strong positive effect that direct cellular interactions can have on ECM development. Controlled delivery of biological factors in printed constructs is expected to promote further functionalisation of complex tissue grafts.

Conclusions and future directions

In summary, we demonstrate here for the first time the retention of spatially organized, functional osteogenic and endothelial progenitor cells in printed grafts after *in vivo* implantation. Heterogeneous extracellular matrix formation in printed grafts occurs analogous to the deposited cell type. In the next step, it would be attractive to design more intricate printed bone structures with blood-vessel channels and test these implants *in vivo* in large animal model, also at orthotopic locations and to investigate the necessity of imposed organization.

Acknowledgements

We thank H. Yuan from Progentix Orthobiology BV (Bilthoven, The Netherlands) for kindly providing the BCP particles. We acknowledge the financial support by the Netherlands Organisation for Scientific Research to NF (NWO; grant number: 017.001.181) and the Smart Mix Program of the Netherlands Ministry of Economic Affairs and the Netherlands Ministry of Education, Culture and Science.

Chapter 11

Biofabrication of osteochondral tissue equivalents by printing topologically defined, cell-laden hydrogel scaffolds

Fedorovich NE[1], Schuurman W[1,2], Wijnberg HM[1], Prins HJ[3], van Weeren PR[2], Malda J[1,4], Alblas J[1], Dhert WJA[1,5]

Manuscript submitted

Fedorovich NE and Schuurman W contributed equally to the work described

[1]*Department of Orthopaedics, University Medical Center Utrecht, Utrecht, The Netherlands*
[2]*Department of Equine Sciences, Faculty of Veterinary Medicine, Utrecht University, Utrecht, The Netherlands*
[3]*Department of Immunology, University Medical Center Utrecht, Utrecht, The Netherland.*
[4]*Institute of Health and Biomedical Innovation, Queensland University of Technology, Brisbane, Australia*
[5]*Faculty of Veterinary Medicine, Utrecht University, Utrecht, The Netherlands*

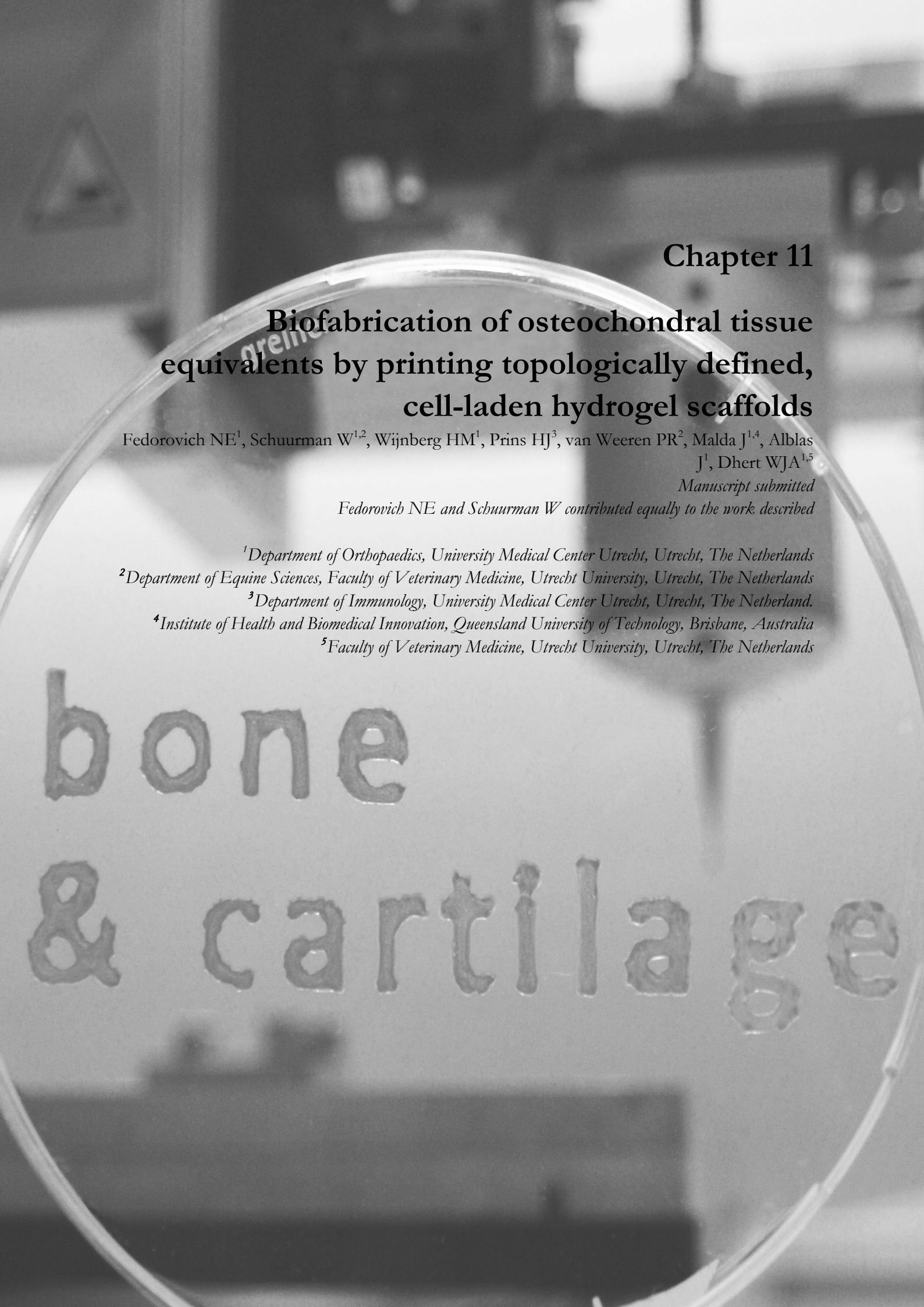

Abstract

Osteochondral defects are prone to induce osteoarthritic degenerative changes. Many tissue-engineering approaches that aim to generate osteochondral implants suffer from poor tissue formation and compromised integration. This illustrates the need for further improvement of heterogeneous tissue constructs. Engineering of these structures is expected to profit from strategies addressing the complexity of tissue organization and the simultaneous use of multiple cell types. Moreover, this enables the investigation of the effects of three-dimensional (3D) organization and architecture on tissue function.

In the present study, we characterize the use of a 3D fiber deposition (3DF) technique for the fabrication of cell-laden, heterogeneous hydrogel constructs for potential use as osteochondral grafts. Changing fiber spacing or angle of fiber deposition, yielded scaffolds of varying porosity and elastic modulus. We encapsulated and printed fluorescently labeled human chondrocytes and osteogenic progenitors in alginate hydrogel yielding scaffolds with distinct parts for both cell types. Cell viability remained high throughout the printing process, and cells remained in their compartment of the printed scaffold for the whole culture period. Moreover, distinct tissue formation was observed, both *in vitro* and *in vivo*, at different locations within one construct. These results demonstrate the possibility of manufacturing viable cm-scaled structured tissues by a 3D fiber deposition technique, which could potentially be used for the repair of osteochondral defects.

Introduction

Osteochondral defects, affecting both articular cartilage and the underlying subchondral bone, are prone to induce osteoarthritic degenerative changes over time.[606] Current strategies to restore the biological and mechanical functionality of the joint include microfracture and mosaicplasty (autologous osteochondral grafting),[607-609] but their clinical use suffers from several limitations, including compromised cartilage tissue formation and donor site morbidity.[39] Furthermore, in mosaicplasty it is difficult to match the shape of the injured site.[39] Current approaches for the engineering of osteochondral grafts suffer from poor tissue formation and compromised integration at the interface between the layers,[49,50,610] advocating the need for further improvement of these techniques.

An important focus in current cell-based tissue engineering lies on the development of engineered osteochondral tissues with design strategies that closely mimic the complex structure of matrix, cells and bioactive factors assorted in a distinct spatiotemporal order inside native tissue. Engineered (osteochondral) tissues can profit from the synergistic effects of combined growth factor delivery and heterotypic cell interactions on extracellular matrix (ECM) formation both *in vitro* and *in vivo*.[73,171,173] This bio-mimicking approach is expected to enhance graft functionality, render suitable mechanical properties to the engineered tissue,[34,611] and enhance the regenerative process. This was previously illustrated by the use of bilayered (hydrogel) scaffolds laden with distinct MSC and chondrocyte populations, which supports the integration between the two layers.[73,80,171-173]

Organ- or tissue printing by 3D fiber deposition (3DF) is an innovative approach in regenerative medicine, based on layered deposition of cell-laden hydrogel strands and is derived from rapid-prototyping (RP) technology. With RP, 3D scaffolds with highly reproducible architecture (size, shape, porosity, interconnectivity, pore-geometry and orientation) and compositional variation can be created.[30] The porosity of the implants is easily tailored, which is important for mechanical and cell/tissue conductive properties. Interconnected porosity is of particular importance since it facilitates nutrient supply and waste product removal[405] and allows ingrowth of blood vessels.[21] Using 3DF, living cells can be incorporated into the printed construct, creating grafts that further recapitulate the intricate 3D structure of cells and matrix in natural tissues.[117]

The aim of the present study is to build and characterize 3D structures for application in osteochondral tissue engineering and to validate organized cell placement inside printed grafts *in vitro* and *in vivo*. By combining human chondrocytes and human osteogenic progenitors with alginate hydrogel - a widely-used polysaccharide that supports both chondrogenic and osteogenic differentiation[509] - we printed porous, heterogeneous constructs. We tested the design of various heterogeneous scaffolds, and tailored the porosity and elastic modulus of grafts by modulating the distance between the strands and their configuration. The ensuing hybrid grafts were characterized for cell performance *in vitro* and for tissue development *in vivo*.

Materials and methods

Hydrogel preparation and viscosity measurements

High-viscosity alginate powder (International Specialty Products, ISP, Memmingen, Germany) was autoclaved and subsequently mixed (10 % (w/w)) overnight at 37°C either with MSC expansion medium ((aMEM (Invitrogen) supplemented with 10% FBS (Lonza, Basel, Switzerland), 0.1 mM ascorbic acid 2-phosphate (AsAP; Sigma-Aldrich, Zwijndrecht, The

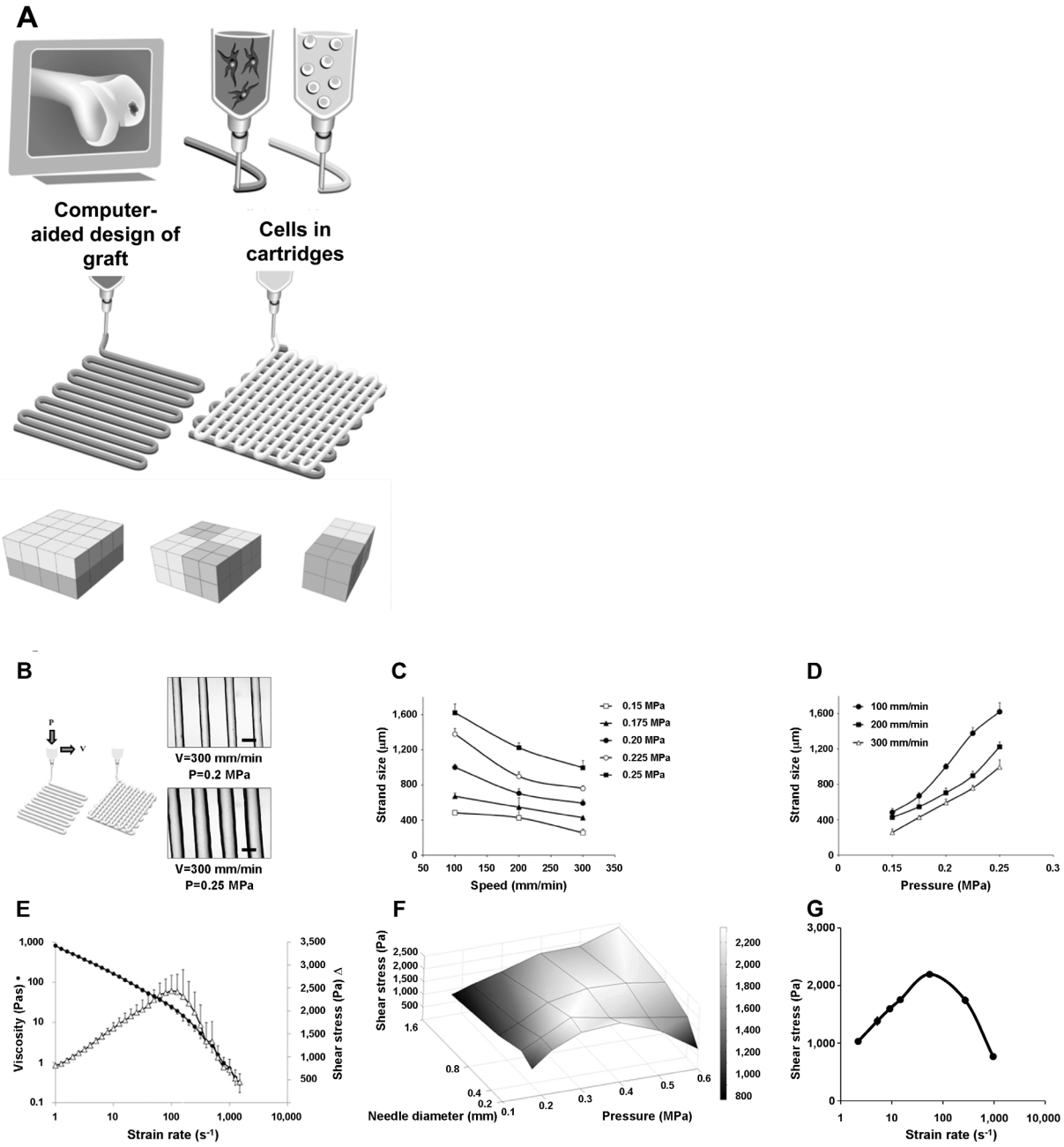

Figure 11.1: 3D fiber deposition and characterization of the printing parameters. A: Schematic representation of tissue printing using various cell types; the design of a construct is translated to a robot arm that drives a cartridge loaded with a cell-hydrogel mixture and extrudes fibers in a layered fashion; the bottom panel represents various scaffold designs used in this study; B: The effect of speed of deposition (V) and pressure (P) on strand size, scale bars: 500 µm; strand size as function of speed (C) and pressure (D), data presented as mean ± standard deviation (n=8); E: Viscosity (circles) and shear stress (triangles) of the hydrogel as a function of shear rate measured by rheometer (n=6); F: Shear stress as a function of needle diameter and pressure (n=4); G: Shear stress in the BioScaffolder, mean ± standard deviation (n=4).

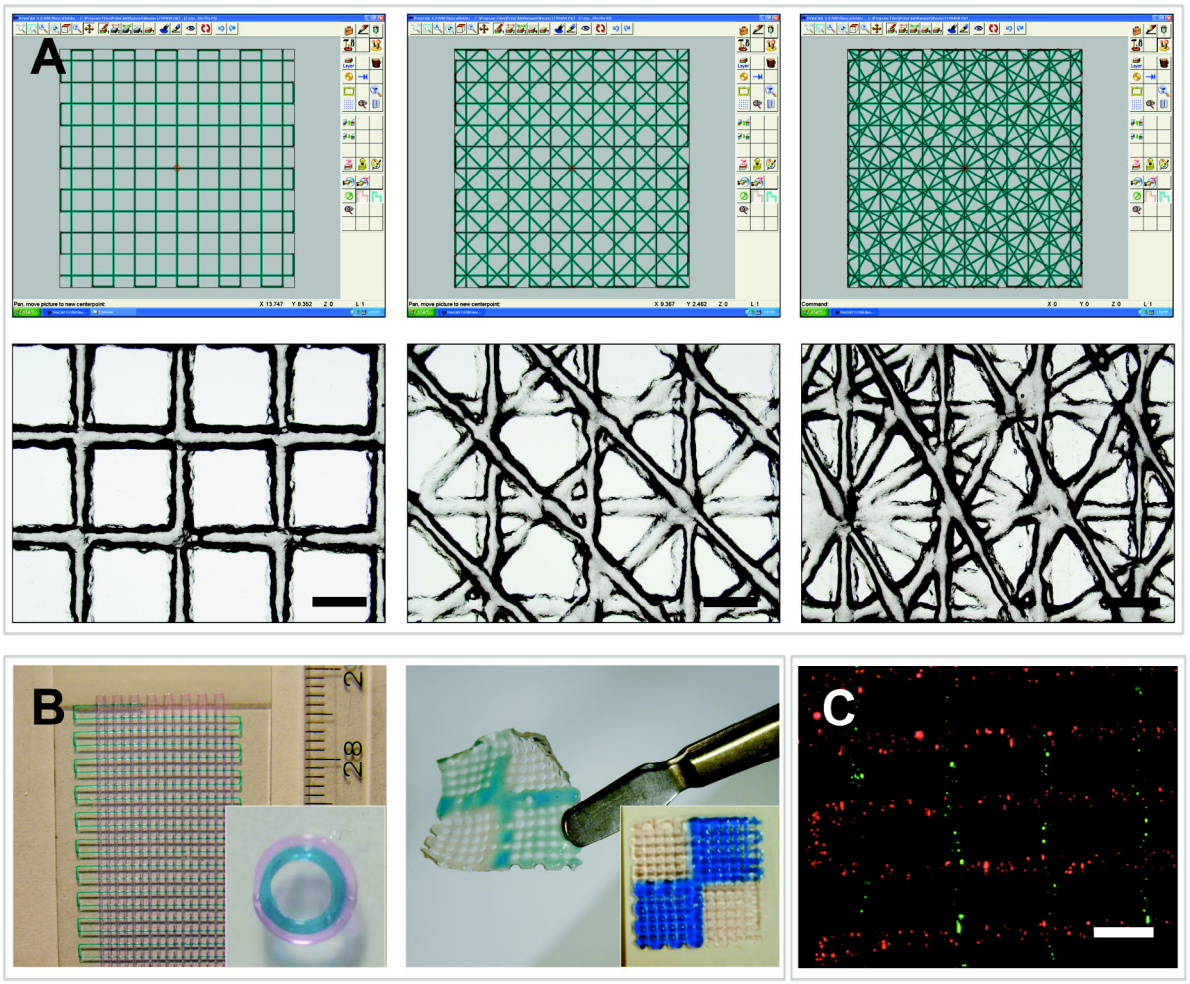

Figure 11.2: Scaffold architecture. A: A computer blueprint is used to construct scaffolds with variable strand orientation; CAD/CAM software design is shown in the top panels and light microscope images of resultant scaffolds in lower panels, scale bar: 1 mm; strand orientations of any layer in a design relative to the underlying layer from left to right is 90, 45, 30 (in °); B: Examples of heterogeneous acellular scaffolds (left: multilayer and a circular construct (inset); right: a chess-board construct, blue dye is used for illustration purposes; right: no delamination between the printed alginate compartments); C: Encapsulated cells (fluorescently labeled red and green) in a heterogeneous scaffold, (SO)90, scale bar: 1 mm.

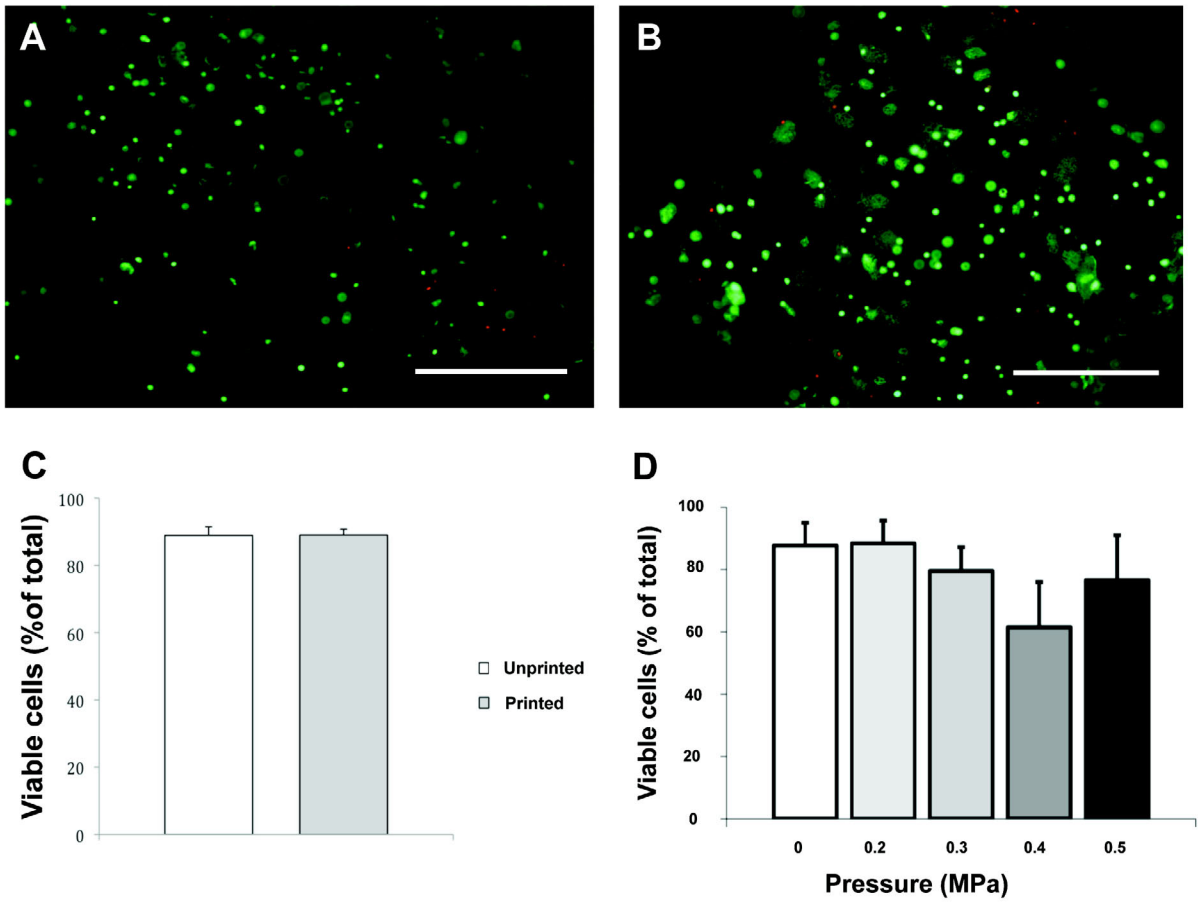

Figure 11.3: The effect of the printing process on MSCs survival. A: MSCs in unprinted control; red: dead cells, green: live cells; B: MSCs in alginate 5 hours after printing; C: Viability in unprinted (white) and printed (grey) samples (n=5) 5 hours after printing; no significant differences between printed and unprinted samples were found (p=0.94); D: Viability 24 hours after printing at various pressures (n=4), controls (0 MPa) are non-printed.

Netherlands), 2 mM L-glutamine (Glutamax, Invitrogen), and 100 U/ml penicillin, 100 μg/ml streptomycin (Invitrogen)), or osteogenic differentiation medium (MSC expansion medium supplemented with 10^{-8} M dexamethasone (Sigma-Aldrich) and 10 mM β-glycerophosphate (Sigma-Aldrich)), or chondrogenic differentiation medium (DMEM (Invitrogen) supplemented with 0.2 mM AsAP (Sigma-Aldrich), 0.5% human serum albumin (SeraCare Life Sciences, Milford, USA), 1% (v/v) insulin-transferrin-selenium mixture (ITS-X, Invitrogen), 100 U/ml penicillin, 100 μg/ml streptomycin and 5 ng/ml TGF-β_2 (R&D Systems, Abingdon, United Kingdom)). Alginate was crosslinked with 102 mM aqueous $CaCl_2$ solution supplemented with 10 mM HEPES (pH 7.4, Invitrogen, Carlsbad, USA) for 15 minutes.
To determine the viscosity of the 10% (w/w) alginate, rheology analysis was performed on an ARG2 1000N rheometer (TA Instruments, New Castle, USA) using a cone-plate geometry (steel, 40 mm diameter with an angle of 2°) at 4°C. Shear rates between 1/s and 1500/s were applied for ten minutes.

3D fiber deposition presets

The BioScaffolder pneumatic dispensing system (SYS+ENG, Germany) was used for 3D printing of hydrogel scaffolds. The prototype of this system is described in more detail elsewhere.[117,187] Briefly, the BioScaffolder is a three-axis dispensing machine, which builds 3D constructs by coordinating the motion of a pneumatic syringe dispenser (Supplementary Figure 11.1). The dispenser deposits extrudate consisting of hydrogel either or not supplemented with cells on a stationary platform. Models of the scaffolds are loaded via computer-aided design/computer-aided manufacturing (CAD/CAM) software, and translated for layer-by-layer fiber deposition by the machine (Figure 11.1).

Effect of nozzle diameter, deposition speed and pressure, and fiber orientation

The inner nozzle diameter, deposition speed and pressure were varied between, respectively, 210-1610 μm, 100 and 300 mm/min and 0.1 and 0.2 MPa in order to assess their influence on strand size. Ten-layer rectangular 3D scaffolds of 10x10 mm with spacing between fibers of 0.8- 2.5 mm and a layer thickness of 100 μm were constructed and subsequently crosslinked in $CaCl_2$ solution as indicated.
Fiber orientation was changed by plotting fibers with 45° or 90° angle steps between two successive layers (strand orientation (SO)45 and (SO)90, respectively). Flow rate of the hydrogel through a 210 μm inner nozzle diameter needle was determined for pressures of 0.15 - 0.6 MPa, by measuring the amount of extruded material per second (flow rate in ml/s). Shear stress was then determined according to the formula below, in which Q is flow rate (mm^3/s), r is radius of the needle (mm) and η is the viscosity (Pa*s):

$4Q / \pi r^3) \eta$ = shear stress.

Mechanical analysis of printed scaffolds of different porosity and strand orientation

Alginate scaffolds of 7x7x0.8 mm (wxlxh) were prepared by varying the strand distance (0.8 mm, 1.5 mm, 2 mm and 2.5 mm at (SO)90), i.e. 90º relative to the underlying strand) and (SO)90 and (SO)45 at 2 mm strand diameter). Subsequently, the scaffolds were crosslinked as described above.

Porosity was estimated by comparing the weight of the porous scaffolds to the weight of non-porous controls. The stiffness of the scaffolds was measured at room temperature using a dynamic mechanical analyzer (DMA 2980, TA Instruments) in controlled force mode. Scaffolds were placed between the parallel plates and a static force was applied between 0 and 1 N, and varied at a rate of 0.1 N/min. The Young's modulus (E) was determined as described previously,[443] by measuring the variation of stress/strain ratio.

Deposition of acellular heterogeneous scaffolds

Heterogeneous scaffolds consisting of two distinct materials were designed, as illustrated in Figure 11.1A. Alginate hydrogel was left translucent or stained with fast green, methylene blue or basic fuchsin (pink) for illustration purposes and loaded into the BioScaffolder. Unless stated otherwise, an inner nozzle diameter of 420 μm was used, the speed of deposition was set at 300 mm/min and the pneumatic pressure was set at 0.175 MPa to yield uniform, continuous extrusion of strands.

Cells

Human multipotent stromal cells (MSCs) were isolated from bone marrow aspirates, obtained from donors undergoing hip arthroplasty after informed consent with approval of the local medical ethical committee, and culture-expanded as described previously.[612] Briefly, aspirates were resuspended by using 20-gauge needles, plated at a density of $5x10^5$ cells per square centimeter and cultured in MSC expansion medium supplemented with 1 ng/ml basic recombinant human fibroblast growth factor ((rhFGF2), 233-FB, R&D Systems). Medium was refreshed twice a week and cells were used for further subculturing. MSCs passage 3-4 were used in these experiments.

Human articular chondrocytes (Chs) were isolated from cartilage, after informed consent with approval of the local medical ethical committee, from patients undergoing total knee arthroplasty. Cartilage was digested overnight using 0.15% collagenase type II (Worthington Biochemical, Lakewood, USA) at 37°C. The cell suspension was filtered through a 100 mm cell strainer and washed in phosphate buffered saline (PBS) (Invitrogen). Cells were resuspended in chondrocyte expansion medium (DMEM (Invitrogen), supplemented with 10% FBS (Biowhittaker), 100 U/ml penicillin, 100 μg/mL streptomycin (Invitrogen) and 10 ng/mL rhFGF2 (R&D Systems). Cells were then counted and seeded at a density of 5000 cells/cm^2 in expansion medium. After ten days, the chondrocytes were detached using 0.25% trypsin (Invitrogen) and stored in liquid nitrogen until further use. Expanded chondrocytes were combined with alginate (2% (w/w) in differentiation medium)[613] at a density of $1x10^7$ cells/ml. To create alginate beads, this solution was dripped with a 23G needle into 102 mM $CaCl_2$ solution supplemented with 10 mM HEPES pH 7.4 (Invitrogen). The beads were then cultured in chondrogenic differentiation medium for five days and subsequently, cells were retrieved from the beads using sterile citrate buffer (150 mM sodium chloride, 55 mM sodium citrate, pH = 7.4) for 15 minutes.

Viability analysis

To test the effect of shear stresses during the printing process on cell viability, hydrogel-embedded MSCs ($5x10^6$ cells/ml gel) were extruded through a needle with an inner nozzle diameter of 210 μm at various pressure settings (0.175-0.5 MPa). Unprinted cell-laden alginate was used as a control. The samples (n=5 per group) were incubated in $CaCl_2$ solution and

cultured for five or 24 hours in expansion medium. The viability of the cells was determined by a LIVE/DEAD assay (Molecular Probes MP03224, Eugene, USA) according to the manufacturer's recommendations. Living and total cells were scored using a fluorescence microscope. The cell viability was calculated as the average ratio of vital over total cells in a sample, determined from four randomly chosen fields per scaffold.

Fluorescent labeling and tracing of cells

Cells were fluorescently labeled for spatial distribution-analysis. For this, Chs were incubated with PKH26 (20 μM, red; Sigma-Aldrich) and MSCs with CFSE (1 μM, green; Molecular Probes, Leiden, The Netherlands). The presence of fluorescent cells was analyzed directly after printing and after 14 and 21 days under a fluorescence microscope (Olympus BX51 microscope, Olympus DP70 camera, Hamburg, Germany) equipped with an epifluorescence set-up, excitation/emission setting of 488/530 nm to detect green-fluorescent MSCs or 530/580 nm to detect red Chs (Leica DM IRBE, Solms, Germany).

Deposition of cell-laden scaffolds

To develop dual, heterogeneous scaffolds for *in vitro* use, fluorescently labeled MSCs and Chs were separately mixed with alginate at $5x10^6$ cells/ml and $3x10^6$ cells/ml respectively. A rectangular (1x2cm), ten-layer scaffold was designed, and consisted of two parts (1x1cm) directly adjacent to each other. The BioScaffolder interchanged the cooled cartridges (4 °C) with the loaded syringes every two layers. The scaffolds were subsequently crosslinked in $CaCl_2$ solution.
For building heterogeneous scaffolds for *in vivo* implantation, an analogous protocol was followed: Chs ($1x10^7$ cells/ml) were mixed with alginate, and MSCs ($1x10^7$ cells/ml) were mixed with alginate supplemented with 10% (w/v) osteoinductive biphasic calcium phosphate particles (BCPs, 80±5 % (w/v) hydroxyapatite and 20±5 % (w/v) β-tricalciumphosphate; total porosity 70 ± 5%, macroporosity 55 ± 5% and microporosity 20 ± 5%). Irregularly shaped BCP particles (kindly provided by Progentix Orthobiology BV, Bilthoven, the Netherlands) were sintered at 1150°C and ranged from 106 to 212 μm in size. Acellular printed grafts served as negative controls. After printing, the constructs were cultured overnight and subcutaneously implanted in mice (see section on *in vivo* implantation).

Heterogeneous scaffold culture and embedding

Heterogeneous scaffolds were cultured in a 1:1 mixture of osteogenic and chondrogenic differentiation medium for a period of 7 and 21 days (both n=4). Scaffolds were maintained in a humidified incubator at 5% CO_2 and 37°C, and the medium was exchanged every 3 days. Additionally, the scaffolds were incubated for 15 minutes in 102 mM $CaCl_2$ once a week to prevent gel weakening (unpublished observation, WS). Upon termination of the experiment, half of the experimental set of scaffolds was embedded in Tissue-Tek® (Sakura Finetek, Alphen aan den Rijn, The Netherlands) and the others were dehydrated through graded ethanol series and embedded in paraffin. Samples were cut to yield 5 μm sections.

In vivo implantation

For *in vivo* assessment, printed Ch/MSC-laden grafts (n=6) and acellular constructs consisting of an alginate part and an alginate/BCP part (n=4) were cultured in proliferation medium for 24 hours prior to implantation. Female nude mice (NMRI-Foxnu, Charles River, Brussels, Belgium),

6-weeks old, were anaesthetized with 1.5% isoflurane, after which the implants were placed in separate subcutaneous dorsal pockets. The incisions were closed using a Vicryl 5-0 suture. The animals were postoperatively treated with the analgesic buprenorphine (0.05 mg/kg, sc; Temgesic, Schering-Plough, Kenilworth, USA) and housed in groups at the Central Laboratory Animal Institute, Utrecht University. Experiments were conducted with the permission of the local Ethical Committee for Animal Experimentation and in compliance with the Institutional Guidelines on the use of laboratory animals. After 6 weeks, the mice were killed and the constructs were harvested, fixed in 4% buffered formalin, decalcified in Luthra's solution (0.35 M HCl, 2.65 M formic acid in distilled water) for 24 h and processed for sections.

Analysis of differentiation of MSCs and Chs in vitro

Osteogenic differentiation of embedded cells was assessed by alkaline phosphatase (ALP) staining, collagen type I and osteonectin immunohistochemistry, and Alizarin red staining.
For the evaluation of ALP activity of encapsulated cells, cryosections were air-dried, fixed with 100% acetone for 10 minutes and incubated in 0.2% (v/v) Triton-X100 in TBS for 10 minutes. The activity of ALP was determined by 30 minute staining with the Fuchsin Substrate-Chromogen system (Dako, Carpinteria, USA). The presence of ALP positive cells was analyzed with a light microscope and equipped with an Olympus DP70 camera. For immunocytochemical analysis, the paraffin sections were rehydrated and blocked in 0.3% (v/v) H_2O_2 in TBS for 10 minutes followed by antigen retrieval in pronase (1 mg/ml, 10165921001 Roche Diagnostics, Mannheim, Germany) for 30 minutes at 37 ºC and hyaluronidase type II (10 mg/ml, H2126; Sigma-Aldrich) for 30 minutes at 37 ºC. The sections were then blocked in 5% (w/v) bovine serum albumin fraction V (BSA, Roche, Almere, Netherlands) in TBS for 30 min and incubated overnight at 4 ºC with either mouse anti-collagen type I antibody (2 μg/ml in 5% (w/v) BSA in TBS, clone I-8H5, Calbiochem, Darmstadt, Germany) or mouse anti-osteonectin antibody (1/50 in 5% (w/v) BSA in TBS, clone AON-1, Developmental Studies Hybridoma Bank (DSHB, Iowa City, USA). A biotinylated secondary antibody was applied (1/200 in 5% (w/v) BSA in TBS, biotinylated sheep anti-mouse, RPN1001V1, GE Healthcare, Diegem, Belgium) for one hour and the staining was enhanced by incubation with streptavidine-peroxidase for an additional hour (2 μg/ml, PN IM0309, Immunotec, Montreal, Canada).
Chondrogenesis of encapsulated cells was assessed by Safranin-O staining and collagen type II and VI immunohistochemistry. To demonstrate proteoglycan production, alginate was removed from the sections by 10-minute incubation in citrate buffer and the sections were stained with Weigert's hematoxylin (Klinipath, Duiven, The Netherlands) and fast green (Merck, Darmstadt, Germany) for cells and with Safranin-O (Merck) for proteoglycans. Immunohistochemical analysis of collagens was performed using a rabbit polyclonal antibody against collagen type II (10 μg/ml in 5% (w/v) BSA/PBS; Abcam 53047) and mouse anti-collagen type VI antibody (1/10 in 5% (w/v) BSA in TBS, clone 5C6, DSHB). Subsequently the secondary antibody was applied for one hour, respectively goat-anti-rabbit Powervision (Immunologic, DPVR-55HRP) and goat anti-mouse HRP, 10 μg/ml in 5% (w/v) BSA in TBS). All immunohistochemical stainings were developed with DAB and counterstained with Mayer's hematoxylin.

Analysis of printed tissue formed in vivo

Sections were stained with hematoxylin and eosin (HE) and Goldner's trichrome for general visualization of tissue development. To demonstrate formation of cartilaginous tissue, collagen

types II and VI were immunolocalized, as indicated above. To determine the presence of osteogenic marker collagen type I, immunohistochemical analysis was performed on rehydrated sections that were pre-incubated in 0.3 % H_2O_2 for 10 minutes, followed by antigen retrieval with 10 mM sodium citrate buffer, pH 6.0 for 30 minutes at 95 ºC. The sections were then blocked in 5% (w/v) BSA in PBS for 30 minutes and incubated with rabbit polyclonal antibody to collagen type I (3.3 μg/ml in 5% BSA/PBS; Abcam 34710) overnight at 4 °C. As secondary antibody we used goat anti-rabbit HRP (2.5 μg/ml in 5% BSA/PBS; DAKO) for 1 hour. The stainings were developed with DAB and counterstained with Mayer's hematoxylin.

Statistical analysis

Statistical analysis was performed with SPSS 12.0.1 software. A Mann-Whitney U-test was used to evaluate the viability data in printed and unprinted samples (n=5). This statistical test was chosen because of the small number of samples. *P*-values of less than 0.05 were considered statistically significant. Values are reported as mean ± standard deviation.

Results

3D fiber deposition of structured hydrogel scaffolds

Defined, 3D hydrogel scaffolds consisting for up to ten layers (0.8 mm) were printed by the BioScaffolder machine (Supplementary Figure 11.1). Vertical pores were regular throughout the samples, while transversal pores fused due to the relative softness of the material. Strand size was tailored by adjusting the speed of deposition and the extrusion pressure (Figure 11.1B-D). The shear-thinning effect that occurred in the system resulted in a fall in shear stress at higher extrusion pressures (Figure 11.1E,F). The values calculated for the shear stress experienced by the (cell-laden) hydrogel inside the printer cartridge corresponded to those obtained using rheometer analysis (Figure 11.1G).

Modulating the strand distance during printing resulted in formation of scaffolds with different porosities, while the resulting pore architecture of the printed scaffolds followed the imposed strand orientation (Figure 11.2A). To illustrate the effect of strand orientation (SO) and strand distance (SD) on overall porosity and mechanical properties of the printed hydrogel scaffolds, SO and SD were varied between two successive layers. Increasing the strand distance from 0.8 mm to 1.5, 2.0 and 2.5 mm resulted in formation of scaffolds with 0, 35±3%, 48±7% and 66±4% porosity, respectively (Figure 11.2A). Porosity in turn influences the elastic modulus of the scaffolds (Table 11.1). Increased scaffold porosities corresponded with a decrease in the elastic modulus of the scaffolds (Table 11.1). Changing strand orientation relative to the underlying layer from (SO)90 to (SO)45 produced scaffolds with comparable porosity, but higher elastic modulus (Table 11.1).

Heterogeneous scaffolds, consisting of two differently stained hydrogels were printed according to the CAD/CAM design (Figure 11.2B). The adjacent compartments, here indicated by different colors, interacted well without visible signs of delamination (Figure 11.2B).

Printing of viable and heterogeneous cell-laden constructs

In the design of viable cell-laden structures, survival of the printed cells (Figure 11.3A,B) is a crucial factor, while homogeneous cell dispersion allows uniform cell distribution throughout the construct. There were no statistically significant differences in cell survival five hours after

	Solid	***Porous (SO)90***	***Porous (SO)90***	***Porous (SO)90***	***Porous (SO)45***
Porosity (%)	0	35 (3)	48 (7)	66 (4)	48 (2)
Modulus (kPa)	14.8 (3.6)	7.6 (0.6)	5.6 (0.6)	4.5 (0.1)	6.4 (0.2)
Strand distance	0.8 mm	1.5 mm	2.0 mm	2.5 mm	2.0 mm

Table 11.1: Scaffold strength as a function of porosity. Porosity (%), Young's modulus (kPa) and strand distance of the printed scaffolds (solid: n=2; porous: n=4), strand distance is the distance between the middle of two consecutive strands. A deposited strand distance of 0.8 mm yields solid constructs. (SO)90 and (SO)45 indicate a difference in strand orientation (SO) relative to the underlying layer of 90° and 45°, respectively. Data are presented as mean ± standard deviation.

printing (89±2% viable cells in printed gels (n=5) versus 89±3% in unprinted controls (n=5), p=0.94), indicating that the printing process did not induce immediate cell death in this system (Figure 11.3C). We analyzed the effect of shear stress on the viability of printed MSCs, showing that 3DF printing sustains high viability of MSCs after 24 hours in culture (viability of 88±6% and 89±7% in printed group (∅210 μm; 0.2 MPa) and unprinted control, respectively). Furthermore, the viability of MSCs extruded at different pressures, and at different shear stresses, follows the inverse pattern of shear stress values (Figure 11.3D).

An attractive feature of the 3DF approach is its ability to controllably place cells encapsulated in hydrogels and to combine different cell types. To illustrate the feasibility of printing cell-laden constructs with organizational diversity, different cell types were organized in layered configuration (Figure 11.2C). Fluorescent detection of the cells demonstrates that the designed scaffold geometry is sustained by the entrapped cellular patterns both *in vitro* (Figure 11.2C) and *in vivo* (Figure 11.5B).

Tissue formation by heterogeneous cell-laden constructs in vitro

To demonstrate the biological potential of 3DF using multiple cell types, we investigated cellular organization *in vitro*. Cell distribution differences in ECM formation were followed in time. For this, 10-layer alginate constructs were built, containing two adjacent regions with either MSCs or chondrocytes (Figure 11.4A). Gross appearance of the implants indicated formation of two distinct compartments starting two weeks after printing. The chondrocyte region exhibited thickening and increased opacity of the scaffold structure (Figure 11.4B), which was attributed to ECM deposition. In the MSC part, tissue formation was more subtle, as described below. The distribution of cell types was assessed for up to three weeks in culture by fluorescence labeling and showed strict containment of the printed population to either scaffold compartment, indicating a good retention of organization *in vitro* (Figure 11.5A, B). General histology of the composite scaffolds demonstrated appearance of cell-clusters confined to the chondrocyte compartment, rich in proteoglycans and the cartilage-specific markers collagen VI and II (Figure 11.4B and Figure 11.5E). Concurrently in the osteogenic part, the cells remained homogeneously dispersed and stained positive for osteogenic markers alkaline phosphatase, collagen type I, osteonectin and Alizarin red (Figure 11.4B and Figure 11.5). Together these findings illustrate heterogeneous extracellular matrix formation *in vitro* analogous to the deposited cell type.

Tissue formation by heterogeneous cell-laden grafts in vivo

To validate the retention of heterogeneous tissue organization *in vivo*, we investigated the effect of 3DF-defined cell placement on osteochondral tissue formation in mice. Grafts were composed of a chondrocyte-laden compartment and an MSC-laden compartment, which included osteoinductive ceramic particles. Constructs exhibited heterogeneous tissue formation corresponding to the deposited cell type (Figure 11.6) after six weeks. Extracellular matrix formation was evidenced by Goldner's trichrome staining, while almost no matrix developed in acellular control gels (Figure 11.6, inset Goldner's), signifying that embedded cells contribute substantially to formation of ECM in these grafts. Collagen type I-positive matrix enveloped the BCP particles (Figure 11.6, Col I), suggesting the onset of osteogenic differentiation in this part of the construct.

In the chondrocyte-laden region of the construct we observed dense matrix accumulations in alginate and formation of cell clusters positive for cartilage-specific markers collagen type II and

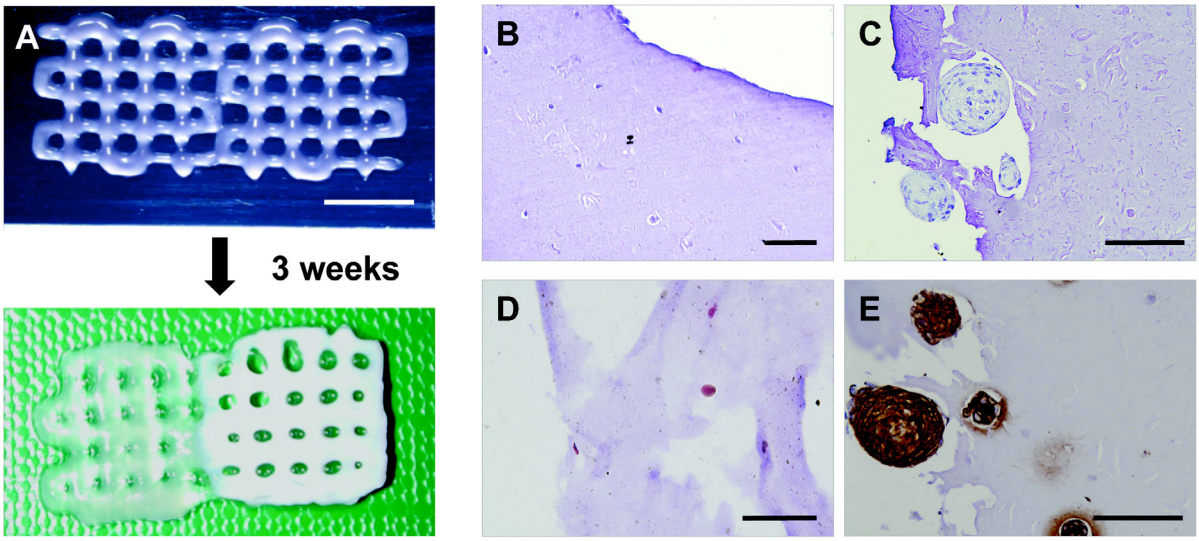

Figure 11.4: Appearance and cell function in printed grafts *in vitro*. A: Macroscopic appearance of printed composite constructs with a MSC-laden compartment on the left and a chondrocyte-laden compartment on the right, directly after printing (top) and after three weeks of culture (bottom), showing differences on a macroscopic level, scale bar: 500 µm; B, C: HE-staining after 21 days in osteogenic part (B) and chondrogenic part (C) illustrates clusters in the chondrocyte-part of the construct, while cells are dispersed in the MSCs-compartment; D: ALP-staining (red) after 7 days demonstrates positive cells in MSC-compartment of the construct; E: Immunolocalization of collagen type VI (brown) at 21 days in the chondrocyte-laden part of the scaffold, scale bars: 100 µm.

VI (Figure 11.6 and Figure 11.7). The latter marker is specific for human collagen VI and does not cross-react with mouse tissue, indicating that the newly formed collagenous matrix is derived from the transplanted cells.

Discussion

In the present study, for the first time the feasibility of 3DF to fabricate porous heterogeneous osteochondral constructs that encompass living chondrocytes and osteogenic progenitors is demonstrated. Printed cell-hydrogel constructs revealed differential lineage commitment and extracellular matrix formation. This study addresses recent development in the field of regenerative medicine that aims to recapitulate the complexity of natural biological tissues, consisting of different cell types with a specific organization and matrix composition.

Previously, 3DF has been developed as a rapid prototyping method to create 3D porous shapes of a range of materials, including thermoplastics[30,614] and hydrogels [187] and the adapted technology used by us can comply with several important prerequisites of tissue-engineered grafts, including tailorable mechanical properties, the introduction of sufficient interconnected porosity, the introduction of living (progenitor) cells, and the possibility to investigate organizational aspects in tissue regeneration. Moreover, 3DF is a robust dispensing technology, resulting in constructs that easily reach relevant (cm-scale) sizes for tissue replacement. Addition of cells to the process of hydrogel fiber deposition facilitates formation of cell-laden, viable printed scaffolds for tissue engineering purposes,[115,117] while local cell densities can be modulated and various types of cells can be deposited in tissue-like architectures.

When adding cells to the materials before printing, we demonstrated that human primary stem cells survive the shear stresses imposed on them during the deposition process, which is in line with previous reports.[117,118] A relatively high cell survival was observed at higher dispensing pressures, which is explained by shear thinning of the hydrogel resulting in a drop in shear stress. This phenomenon of shear-thinning is common behavior for (natural) polymers[615] and has been described in detail for minimal invasive material delivery.[616] As matrix stiffness is a known factor in cell differentiation,[387] modulating biomechanical properties by using various depositing configurations and materials is likely to influence tissue formation *in vitro* and *in vivo*.

The concurrent printing of different hydrogels illustrated the ability of the system to reproducibly print heterogeneous 3D structures comprising different matrices. The results show adequate integration between the adjacent layers of separately printed gels. As a following step we demonstrated the design of cell-laden heterogeneous scaffolds (*i.e.* printed with different cell types at different locations). In the heterogeneous grafts *in vitro* studies revealed that the cells remained located specifically in their original deposited position during the entire culture period. This limited interaction between the cells of the adjacent layers can be explained by the hydrogel matrix employed for the encapsulation of the cells. Due to the non-interactive nature of alginate, the cells are unable to adhere or degrade the surrounding gel matrix,[407] and will remain confined.

Our *in vivo* study demonstrated that in printed osteochondral grafts, specific structural arrangements imposed by 3DF may induce heterogeneous tissue formation and can lead to a stable cellular architecture, which is an important factor in the success of 3D constructs.[170] Another important characteristic for tissue engineering purposes is maintenance of the required phenotype.[121] Our printed osteochondral grafts exhibited heterogeneous extracellular matrix formation at distinct locations within one scaffold, corresponding to the deposited cell type. The transplanted human cells contributed to extracellular matrix formation, as evidenced by detection

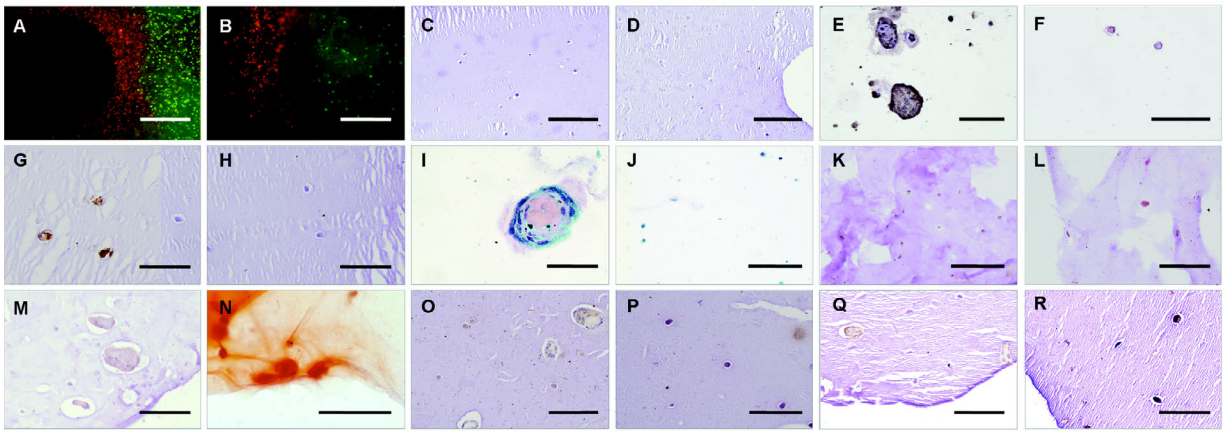

Figure 11.5: Analysis of extracellular matrix formation in printed grafts *in vitro*. A, B: Fluorescently labeled cells, MSC in green and chondrocytes in red, directly after printing (A) and after three weeks (B), scale bars: 500 µm; C, D: HE-staining after 7 days demonstrates homogeneous dispersion of cells in both regions of the scaffold, in chondrogenic part (C) and in osteogenic part (D), scale bars: 200 µm; E, F: Immunolocalization of collagen type II (brown) after 21 days, in chondrogenic part (E) and in osteogenic part (F), scale bars: 100 µm; G, H: Immunolocalization of collagen type VI (brown) after 7 days, in chondrogenic part (G) and in osteogenic part (H), scale bars: 100 µm; I, J: Safranin-O staining at 21 days indicates presence of proteoglycans (pink) in chondrocyte region (I), and not in osteogenic part (J), scale bar in I: 50 µm, in J: 100 µm; K, L: ALP-staining after 7 days demonstrates positive cells (red) in the osteogenic compartment of the construct (L) and not in chondrogenic part (K), scale bars: 100 µm; M, N: Alizarin red staining for calcium depositions (orange-red) after 21 days, in chondrogenic part (M) and in osteogenic part (N), scale bars: 100 µm; O, P: Collagen type I immunostaining (brown) at 21 days, in chondrogenic part (O) and in osteogenic part (P), scale bars: 100 µm; Q, R: Osteonectin immunostaining (brown) at 21 days, in chondrogenic part (Q) and in osteogenic part (R), scale bars: 100 µm.

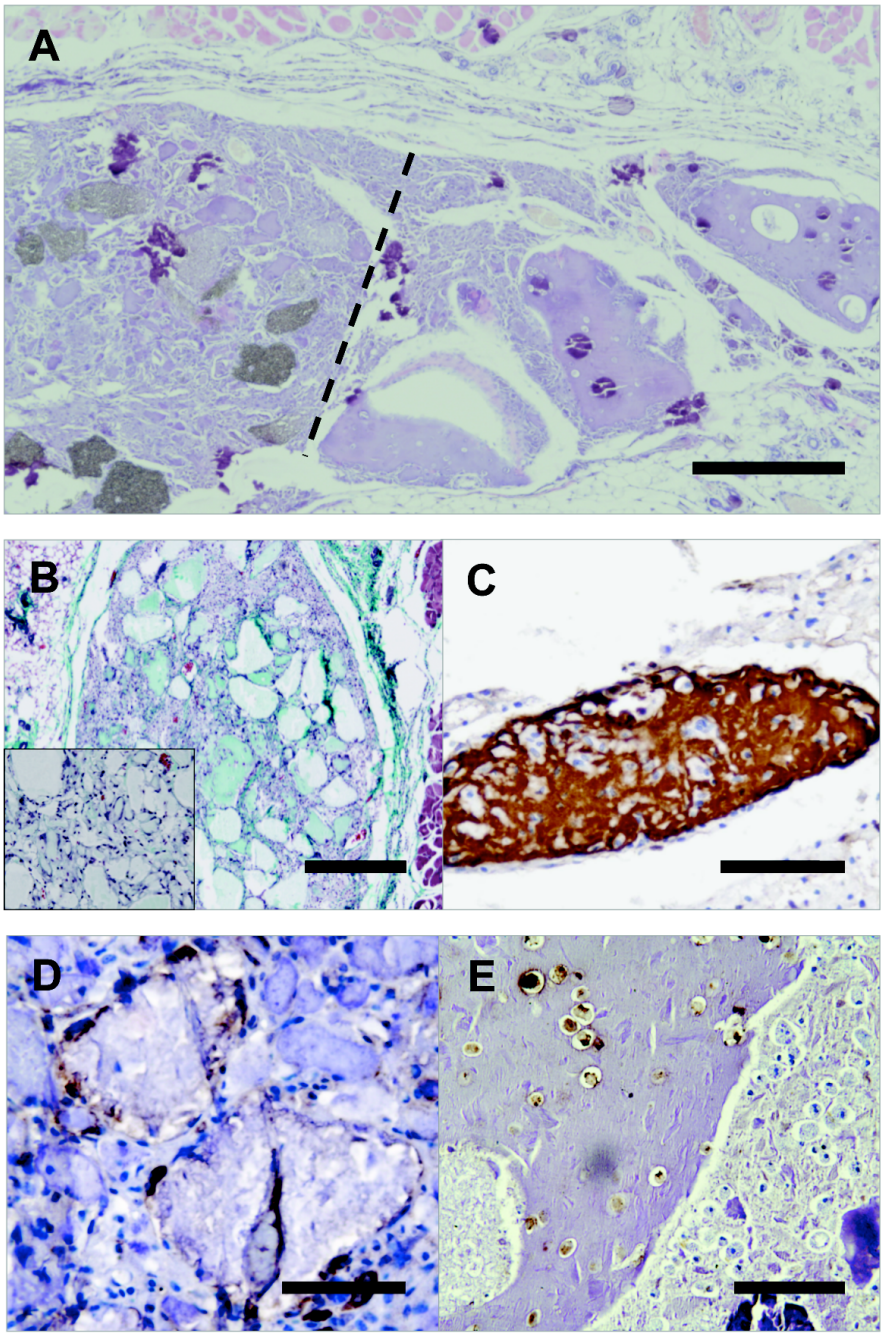

Figure 11.6: Tissue development in printed scaffolds *in vivo*. A: General histology (HE staining) of the graft illustrates heterogeneous tissue formation (dashed line represents the interface between MSC-laden region with BCP particles (left) and Ch-laden alginate (right)), scale bar: 500 µm; B: Goldner's trichrome staining in MSC-laden part demonstrates ECM formation in the cell-laden grafts, and limited tissue formation in acellular scaffolds (inset), scale bar: 500 µm; C, E: Immunostaining for cartilage–specific markers collagen types II (C) and VI (E) is positive in the chondrocyte-laden part of the grafts, scale bars: 100 µm; D: Immunostaining for collagen type I demonstrates osteogenic differentiation around the BCP-particles in MSC-laden part of the grafts, scale bars: 100 µm.

of substantial amounts of human collagen matrix in the cellular grafts and absence of ECM in acellular gels. The lack of abundant osteogenic tissue formation in the osteochondral printed grafts may be explained by the use of low interactive alginate matrix with a relatively high polymer concentration. The issue of vascularization of the bone grafts needs to be addressed in future studies in order to bring the scale-up of constructs to clinically relevant sizes within reach.
In order to design better cartilage implants, and larger bone grafts, design-strategies should mimic anatomical and biochemical organization of cells, matrix and growth factors found in the native tissue.[27,34,611] Various other cell printing approaches, including 3D ink-jet printing[28] and 3D robotic dispensing,[118] have previously been applied for precise patterning of various cell populations. Similarly, micropatterning approaches, such as microfluidic patterning[617] and microcontact printing,[180] allow the study of cellular interactions between various populations and at different ratios. Each of these technologies copes with specific challenges, like material choice, precision of the deposition, combining multiple components and cell types, stability of the construct and, depending on the application, the realization of relevant sized constructs. While most of these technologies are very precise and reach high resolutions, the attained scale of the constructs is at maximum mm-size. The 3DF technology presented in the current study is powerful in that respect, as cm-scale scaffolds are easily printed, making the technology an interesting option in tissue replacement therapies. Nevertheless, several important issues in 3DF still have to be addressed. First, the use of materials that possess the mechanical properties to enable printing and endure the forces acting on tissues, especially on cartilage and bone, and at the same time are biocompatible[618] should be considered. The materials so far used for 3DF, result in variable cell viability and tissue responses,[304,619] the seemingly best performers being natural hydrogels. However, using model alginate gels in this study, only a limited height of the construct could be achieved. The limitations of alginate with respect to its low mechanical strength could be alleviated by the use of thermo- and photo-curable hydrogels.[409,440,620] Further modulations of mechanical properties of these hydrogel scaffolds with 3DF can potentially meet the mechanical requirements needed for tailored tissue engineering applications. Future advances in biomaterial sciences may provide more sophisticated and tailored materials that meet the 3DF requirements better. An additional challenge will be the *in vivo* implantation of heterogeneous printed grafts at orthotopic locations, at the same time maintaining the external shape and internal organization of the printed constructs and ensuring good integration with the surrounding host tissue. With respect to the biology of self-organization, organ printing with 3DF is a powerful tool to study the relevance of biomimicking, also to address the question whether anatomical tissue design is an important prerequisite for the development of functional tissues.

Conclusions

In the present study, we demonstrate the possibility of manufacturing viable heterogeneous tissue constructs consisting of bone and cartilage matrix by a 3D fiber deposition technique. We printed cm-scale intricate hydrogel scaffolds with high cell viability. By encapsulating osteogenic progenitors and chondrocytes in different parts of a construct, the formation of distinct ECM regions *in vitro* and *in vivo* according to the anticipated tissue type was attained.

Acknowledgements

The collagen type VI antibody (developed by E. Engvall) and the osteonectin antibody (developed by J.D. Termine) were obtained from the Developmental Studies Hybridoma Bank. We thank Dr. T. Vermonden from the Department of Pharmaceutics, Utrecht University for the help with rheometry measurements. We acknowledge the financial support by the Anna Foundation, the Netherlands Organization for Scientific Research (NWO; grant number: 017.001.181), the Smart Mix Program of the Netherlands Ministry of Economic Affairs and the Netherlands Ministry of Education, Culture and Science and the Dutch Technology Foundation STW.

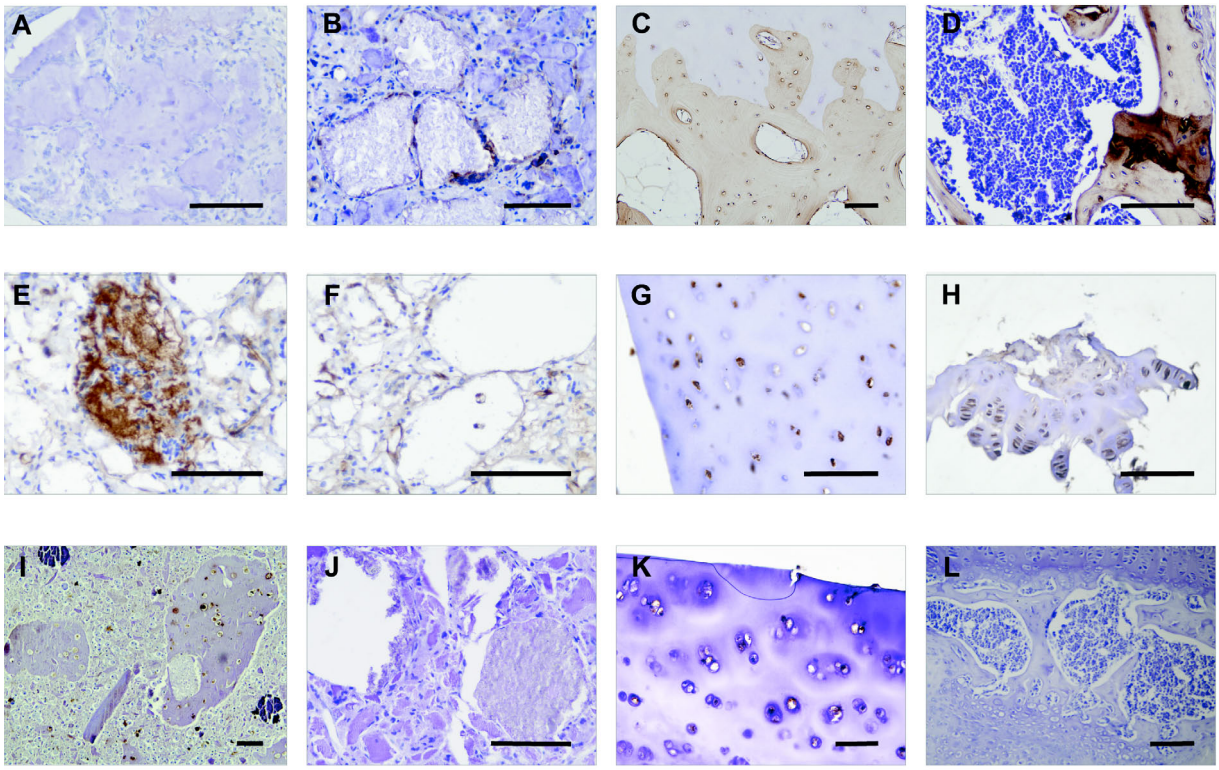

Figure 11.7: Collagen production in printed scaffolds *in vivo*. A-D: Collagen type I immunohistochemistry (brown) performed on explanted tissue after 6 weeks, in chondrocyte-laden region (A), MSC-laden region (B), human osteochondral control tissue (C), and a murine bone control (D); E-H: Collagen type II immunohistochemistry (brown) and (I-L): Collagen type VI immunostaining (brown) on chondrocyte-laden region (E, I), MSC-laden region (F, J), human cartilage (G, K) and murine cartilage (H, L), scale bars: 100 μm.

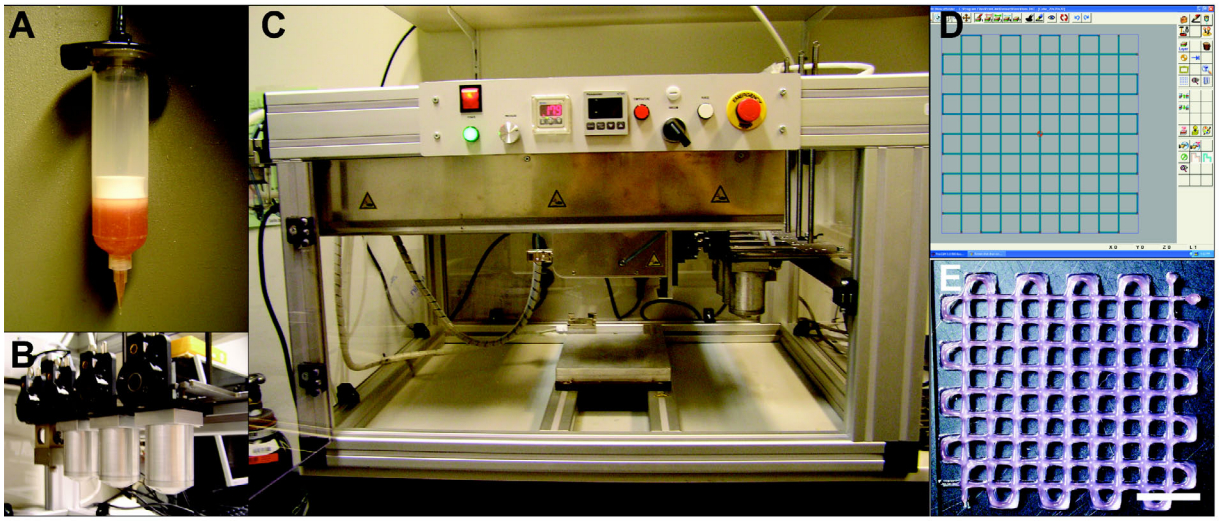

Supplemental Figure 11.1: The components of the 3D fiber deposition technology. Hydrogel is loaded into the syringe (A), which is placed in one of the cartridges (B) on the BioScaffolder (C). Hydrogel fibers are deposited according to a model for a scaffold that is designed by the CAD/CAM software (D). Pressure-driven extrusion in a layered fashion yields porous 3D constructs (E), scale bar: 500 μm.

Summary and discussion

However beautiful the strategy, you should occasionally look at the results.
Sir Winston Churchill

Chapter 12

General conclusions, discussion and future directions

General conclusions

In this thesis we studied the application of organ printing for development of (vascularized) bone grafts. Organ- or tissue printing is a novel approach of regenerative medicine, which enables mimicking anatomical organization of tissues by developing 3D-structured cell-laden multimaterial scaffolds. In **Chapter 2** we described the rationale behind the use of organ printing as a tool to study the role of anatomical organization and for development of 3D structured tissues. In a literature overview we presented research demonstrating that by organizing the cells and matrix in a way that mimics the anatomical distribution of these components in natural tissues, one can enhance the functionality of tissue-engineered grafts. We discussed the role of tissue self-assembly and speculated how organ printing can help investigating whether the imposed organization is actually necessary for obtaining fully functional tissues.

In the first part of this thesis we defined parameters necessary for printing of cell-laden constructs in their application as bone grafts. The hydrogel matrix is an important component of the printing process, thus we addressed this factor in the research question "*Which hydrogel materials are suitable for printing of viable bone tissue equivalents?"* For this, we first conducted a literature study on the use of hydrogels in skeletal tissue engineering in general, and for use in organ printing in particular. Hydrogels are highly hydrated polymer networks used as scaffolding materials in organ printing. These hydrogel matrices are natural or synthetic polymers that provide a supportive environment for cells to attach to and proliferate and differentiate in. Successful cell embedding requires hydrogels that are complemented with biomimetic and extracellular matrix components, in order to provide biological cues to illicit specific cellular responses and direct new tissue formation, and these materials are described in **Chapter 3**. Synthetic polymers are reliable in terms of tailored mechanical and degradation properties, together with uniformity. Of all synthetic hydrogels, photopolymerizable systems are currently one of the most promising materials for skeletal TE. Photopolymerizable hydrogels, formed by UV-exposure of photosensitive polymers in the presence of photoinitiators, are widely used materials in tissue engineering research for cellular entrapment and patterning. These gels have adequate mechanical properties and have been widely investigated with regard to incorporation of degradative and adhesive linkages to promote tissue formation. During photopolymerization the entrapped cells are directly exposed to polymer and photoinitiator molecules.

In the printing process, one of the other principal components is the 3D fiber deposition machine. To address the research question "*Can 3D fiber deposition tool be used for processing of osteoprogenitor cells?"* we characterized the applicability of 3DF system to print cell-laden hydrogels for the first time, as described in **Chapter 4**. We demonstrated that osteogenic progenitors and hydrogels can be deposited simultaneously, with cells dispersed homogeneously throughout the construct. To apply 3DF for the design of tissue-engineered bone grafts, it is vital that the cells do not die during the deposition and retain the ability to differentiate. We showed that the cells survive the deposition process and that osteogenic progenitors retain the ability to differentiate towards the osteogenic lineage after printing. Neither the printing process nor the needle diameters, as used in this study, affected cell viability. The type of hydrogel determined cell survival after embedding. Based on our findings we can conclude that 3DF is a well-suited tool for printing of viable osteogenic grafts.

Subsequently, in **Chapter 5** we characterized the effects of photopolymerization on the exposed goat multipotent stromal cells (MSCs). We demonstrated that the viability of encapsulated cells is not adversely affected by photopolymerization of the surrounding hydrogel, which is likely the

result of low amounts of free radicals causing cell-damage. We concluded that the influence of photoexposure on cell-cycle progression, which is often cautioned for, is well tolerated when encapsulating the cells in hydrogels. Although we observed no differences between cell-survival at various photopolymerization conditions, the nature of the hydrogel itself significantly influenced the survival and differentiation of encapsulated cells. For printing of 3D structured bone grafts we subsequently tested a novel, photosensitive hydrogel - Lutrol F127 AlaL, as described in **Chapter 6**. The printing process benefits from the fast temperature-responsive gelation ability of this thermosensitive Lutrol F127 AlaL, allowing organized 3D extrusion. The additional stability provided by covalent photocrosslinking allows handling of the printed scaffolds and renders the material more stable with regard to degradation. Lutrol F127 AlaL turned out to be highly suitable for 3D fiber deposition, enabling formation of organized 3D scaffolds. MSCs embedded in photopolymerizable Lutrol F127 AlaL gels remained viable in this matrix and were able to differentiate toward the osteogenic lineage.

The final printing parameter assessed in this thesis was scaffold design, which we addressed in two research questions: "*How do printing characteristics affect construct properties?"* and *"How does construct porosity affects functionality of embedded cells?"* To answer the first question, we described on pages 194-195 of **Chapter 11** (this chapter addresses questions related to the first and second part of this thesis) how tailoring of dispensing parameters such as fiber distance, orientation, pressure, speed and the used cell concentrations affect the characteristics of the printed scaffolds including their porosity, mechanical properties and cellularity. Using 3DF, alginate hydrogel strands were printed at variable pneumatic pressures, speeds and patterns of fiber deposition, demonstrating the ability of the system to modulate construct properties, such as strand thickness, porosity and mechanical characteristics. The number of printed cells corresponded to the cell-concentrations used for printing and human primary stem cells survived the shear stresses imposed on them during the deposition process. Due to the shear-thinning of the hydrogel, a relatively increased cell survival at higher dispensing pressures (explained by the drop in shear stress) was seen. To answer the second question ("*How does construct porosity affects functionality of embedded cells?")* we assessed how incorporated cells react to changes in porosity of the construct. To address the challenge of nutrient and oxygen diffusion, we embedded the cells in solid and porous hydrogel constructs, and compared the functionality of embedded cells in these grafts, as described in **Chapter 7**. Cells embedded in solid hydrogel scaffolds exhibited more hypoxia markers and higher rate of lactate production, indicative of a more anaerobic metabolism. Fewer cells were viable in solid constructs, and more cells underwent apoptosis inside these grafts. Similarly, porosity supported osteogenic differentiation of embedded MSCs as evidenced by detection of early (alkaline phosphatase) and late (collagen type I and osteocalcin) osteogenic markers. Further, porosity promoted oxygenation of embedded cells and ingrowth of blood vessels upon implantation *in vivo*. Based on our findings we can conclude that porous scaffold design is vital for functionality of embedded cells *in vitro* and supports tissue formation *in vivo*.

In an effort to further enhance bone formation in printed grafts upon implantation *in vivo* we investigated the effect of calcium phosphate (CaP) particle characteristics on the osteoinductive potential of printable cell-laden hydrogel-CaP composite matrices, as described in **Chapter 8.** Research question posed was: "*Does addition of calcium phosphate micro- and nanoparticles to cell-laden hydrogels lead to enhanced bone formation in vivo?"* We demonstrate that in comparison to absent bone tissue formation in MSC-laden Matrigels, BCP particles lead to elaborate bone formation at

ectopic location, while apatitic nanoparticles induce osteoclastogenic tissue response without bone formation.

The second part of this thesis addressed the development of multicellular grafts and validated whether heterogeneous cell arrangement introduced by the printing process is retained *in vitro* culture and after *in vivo* transplantation, and whether heterogeneous design is translated into heterogeneous tissue formation *in vivo*. First, in **Chapter 9,** we describe the isolation and characterization of goat endothelial progenitor cells (EPCs) that we want to use in combination with osteogenic progenitors to promote prevascularisation of printed bone grafts. Two research questions were addressed by this study: "*What are the characteristics of goat endothelial progenitor cells isolated from bone marrow and peripheral blood and do they form blood vessels in vivo?"* and *"Can we use endothelial progenitors to enhance osteogenic differentiation in vitro and bone formation in vivo?* To answer these questions, early and late EPCs from peripheral blood and bone marrow of goats were characterized for differentiation markers and functional responses. EPCs from peripheral blood were more proliferative than bone marrow-derived EPCs, expressed higher numbers of endothelial markers for longer periods of time and formed more intricate networks. We demonstrated that late EPCs derived from peripheral blood contribute to osteogenic differentiation by MSCs *in vitro*, and that MSCs support the proliferation of EPCs and stabilize the formed cellular networks. *In vivo*, EPCs from peripheral blood assembled into early blood vessel networks, which were more pronounced in the presence of MSCs. From these results we can conclude that the EPCs isolated from peripheral blood of goats are suitable for prevascularization strategies, and random coseeding of EPCs and MSCs does lead to significantly higher bone contact % in the newly formed bone.

Subsequently, the printing of structured, cell-laden grafts and incorporation of various cell populations in heterogeneous constructs is described in **Chapters 10 and 11,** to address the final research question of this thesis: "*Do printed heterogeneous constructs demonstrate osteogenesis in vitro and form heterogeneous tissues, including bone, in vivo?"* In **Chapter 10** we showed for the first time the printing of bone constructs that contain multipotent stromal cells and endothelial progenitor cells. Heterogeneous, printed constructs consisting of an MSCs-laden compartment and an EPCs-laden part were implanted *in vivo* and we demonstrated that heterogeneous tissue formation takes place in these printed dual implants, corresponding to the deposited cell type. Erythrocyte-filled tubuli, positive for endothelial marker von Willebrand factor, were observed in the EPC-laden part of the printed grafts, while bone and some cartilage formation were detected in the MSC-laden part of the grafts when BCP particles were added to the constructs. Similar dual scaffolds were printed consisting of an hMSC-laden part and a compartment with human primary chondrocytes (Ch) for use as osteochondral grafts, as described in **Chapter 11**. *In vitro*, cells remained in their compartment of the printed scaffold, and matrix formation was observed at distinct locations within one scaffold, corresponding to the deposited chondrogenic and osteogenic cell types. After implantation *in vivo*, cell organization introduced by the printing was retained and resulted in heterogeneous tissue formation. While early osteogenesis was observed around the BCP-particles in the MSC-laden part of the grafts, cartilage-like tissue developed in Ch-laden part of the constructs. Transplanted cells contributed to the newly formed ECM. From these findings we can conclude that printed heterogeneous grafts demonstrate retention of cell organization introduced by the printing and result in heterogeneous ECM formation, including bone-like tissue, both *in vitro* and *in vivo*.

Cumulatively, these results demonstrate the possibility of manufacturing viable and functional heterogeneous tissue constructs by a 3D fiber deposition technique, which could potentially be used for the repair of bone defects and osteochondral lesions.

Discussion

Tissue engineering and organ printing

Tissue engineering emerged in 1993 as a research discipline that was expected to meet the rapidly growing need for tissue replacement. In the past decades a vast amount of research has been dedicated to this field of regenerative medicine, in an attempt to engineer various tissue-types and even organs. Despite this great effort, so far few products or treatments modalities have been introduced from the laboratory bench to clinical practice.[621] In orthopaedic surgery, the novel TE strategies have only occasionally been translated to clinical application,[16] and the interpretation of outcomes suffers from low numbers of patients and the low level of evidence.[622] For many orthopedic TE treatment options, precise clinical indications, timing, dosage, and mode of action are unclear. Controlled randomized clinical trials will have to elucidate the superiority and cost effectiveness of the tissue engineering approach compared to other methods of bone reconstruction.[15] In case of bone tissue regeneration, promising early results with mm-scale tissue engineering unfortunately did not lead to an immediate breakthrough of this technique. Although regeneration of small volumes of bone tissue is a proven concept in for example maxillary sinus floor augmentation,[623] until now it has been challenging to engineer fully functional bone of clinically relevant centimeter-dimensions.[622] Low cell viability due to delayed vascularization, inadequate differentiation of transplanted stem cells and simplistic design have been named as possible confounders. The organ printing approach addresses some of these challenges in current cell-based tissue engineering and might contribute to making TE a clinical reality one day, by specifically addressing complex tissue design, including the prevascularization strategy.

Requirements of printed tissues

Development of functional printed grafts relies on determining the relevant printing parameters, defining the necessary material characteristics and understanding the cell-related effects. Printing parameters that affect the development of printed tissues include the resolution and stability of the printed construct, cytocompatibility of the printing process, the degree of cell distribution and porosity and interconnectivity of the printed graft for nutrient delivery *in vitro* and tissue formation and vascular ingrowth *in vivo*. Construct resolution should enable incorporation of structural features such as pores or cell-seeded channels. To enable deposition of cell-laden structures, the matrix should meet the requirement of good printability and provide support to embedded cells. The material should be stiff enough to enable fiber stacking and sustain forces associated with handling and implantation. After printing the material must ensure viability of embedded cells and should either support the differentiation and matrix formation by embedded cells or induce differentiation of encapsulated progenitors (and host) cells towards the desired lineage. The mechanical properties of the scaffold can be chosen to either maintain the integrity of the construct until the newly formed tissue is able to support itself in a bioreactor setting or to support the physical scaffold structure until full tissue remodeling occurs *in vivo*.[249] According to the first strategy the scaffold material is expected to eventually slowly degrade and resorb by bulk erosion, or following *in vivo* implantation route, the matrix should ideally be resorbed at a rate

similar to new tissue formation, if possible by surface degradation. Cell-related requirements include relevant cell density to achieve formation of extracellular matrix and adequate levels of oxygen and other nutrients to sustain survival and differentiation of embedded cells. Additionally, heterotypic cell interactions between seeded cell populations and anatomical organization of various cell types need to be addressed to promote tissue formation in general. For development of bone grafts in particular, important requirements are introduction of vascularization into engineered constructs and combining of organization introduced by cell-printing techniques with self-assembly potential of bone by remodeling.

Printing parameters

Organ- or tissue printing enables formation of 3D structures of defined shape and internal morphology and can combine different cell types at predetermined locations within one hybrid construct. In our application of organ printing for development of (vascularized) bone grafts we use 3D fiber deposition (3DF) dispensing machine to build porous, cell-laden hydrogel constructs. Such grafts can be prepared with desired compositional variation and external shape rendering the use of molds redundant. Next to dispensing techniques, 3D inkjet printing, laser deposition, microfluidic-, ultrasound-, electro- or photopatterning are some of the recently developed organ printing tools to pattern cell-laden matrices.[97] Despite the high resolution of patterning biofabrication methods, they present difficulties for scaling up and are limited in the possibility to create defined pores in the architectures. Dispensing systems such as 3D fiber deposition, and analogous machines such as 3D plotting, 3D deposition tools and volumetrical deposition tools, overcome these disadvantages by fast, layered deposition of polymer strands and formation of cm-scale porous constructs with tailored porosity, characterized by 100% interconnected pores.[30] These systems are able to print porous hydrogel scaffolds from agarose, chitosan or alginate,[407] and improve on the current use of solid hydrogel scaffolds with limited nutrient diffusion characteristics. Various materials can be easily processed with 3DF, while 3D ink-jet printing and laser deposition are limited in the range of materials they can print. Using 3DF, alginate hydrogel strands were printed at variable pneumatic pressures, speeds and patterns of deposition, demonstrating the ability of the system to modulate mechanical properties. Matrix stiffness is a known factor in cell differentiation,[387] and modulating biomechanical properties by using various depositing configurations and materials will influence tissue formation *in vitro* and *in vivo*.

The resolution of the constructs made with 3DF printing process is determined by the smallest needle diameter used to print the (cell-laden) gels, resulting in a strand diameter of at least 150 micrometers for the studies described in this thesis. This resolution is low relative to stereolithography and micropatterning techniques, but is sufficient for introduction of structural features including pores and cell-seeded channels into the scaffold. Taking self-organization of cells into account, maybe it is at all unnecessary to build structures cell by cell, which makes micropatterning techniques more suitable for design of *in vitro* models and dispensing systems applicable for printing hybrid grafts for implanation.

Materials

Due to their high water content hydrogels are highly attractive materials for developing printable matrices. Many hydrogels can be formed under mild, cytocompatible conditions. Characterization of hydrogels with an optimal combination of good processability with 3DF and

cytocompatibility, providing a suitable environment for cell survival and differentiation of osteogenic and endothelial progenitor cells, is an essential step towards future application of 3DF technique.

In most of the conducted studies we used alginate as a model hydrogel material for printing. This widely used polysaccharide, derived from seaweed, supports chondrogenic and osteogenic differentiation,[509] and provides a relatively strong (5-15 kPa), yet non-interactive encapsulation matrix to the embedded cells. This material is frequently used for organ printing applications.[112,115,116] We employ a relatively high polymer content of alginate in culture or osteogenic medium and uphold the viscosity of alginate during deposition by cooling the printing syringe to 4 ºC. After printing, the constructs are crosslinked by incubation with $CaCl_2$. We demonstrate that porous, cell-laden constructs are easily formed with this hydrogel, however the interaction of the cells with alginate is limited. The cells exhibit a round morphology upon encapsulation and do not actively degrade this matrix. Due to this, ECM formation by the MSCs is limited to direct surroundings of the cell, this in comparison to more interactive matrices such as Matrigel, where more widespread deposition of ECM occurs. *In vivo,* alginate elicits a limited foreign-body response, degrades by bulk erosion and is engulfed by the macrophages (unpublished data).

Furthermore, we tested the application of photopolymerizable hydrogels for encapsulation of osteogenic progenitors and printing of cell-laden constructs. Crosslinking of polymer chains, in the presence of photoinitiator molecules and UV light proceeds by covalent linkages and yields stable, mechanically strong gels (20 kPa) that allow easy handling and implantation. Photopolymerizable hydrogels are widely used materials for cell-encapsulation in TE and photopatterning. These gels can now also be used for (bone) printing applications, as photoinitiators do not have severe detrimental effects on survival and differentiation of embedded MSCs (Chapter 5). *In vivo* evaluation of these materials is vital for understanding of host responses to these synthetic materials and is a focus of current studies.

The majority of the hydrogels tested by us i.e. alginate, PEG and Lutrol, provide the cells with a non-interactive encapsulation matrix. These unmodified gels lack any group to directly promote cell attachment and migration and act mainly as a template for ECM deposition.[624] During conducted *in vitro* experiments we observed that the embedded cells do not attach to or degrade the surrounding matrix in the time frame for up to 4 weeks. Furthermore, osteogenic differentiation in these matrices is limited to small fractions of cells expressing the osteogenic phenotype. Modification of hydrogels with adhesive sequences such as RGD-peptides or heparin-groups has been proven to enhance the interaction between cells and matrices and to promote osteogenic differentiation in synthetic gels.[222,228]

Another potent way to promote bone formation *in vivo*, especially at ectopic implantation sites, is the addition of osteoinductive calcium phosphate ceramic particles to cell-laden hydrogel mixtures.[518] In our studies addition of BCP particles lead to elaborate bone formation, while nanoparticles only induced osteoclastic tissue response without bone formation. Potent osteoinduction by BCP is in line with studies by others[25,539] demonstrating osteoinductive capacity of BCP (microparticles). Nano-HA particles lack sufficient osteoinductive cues to induce bone formation at an ectopic location and their poor performance could be attributed by the inhibitory effect of small particle size on bone formation,[512,521] or insufficient nanoparticle content. In turn, CaP nanoparticles are more reactive than sintered BCP particles of higher chemical stability, most probably due to the higher surface area and lower crystallinity of CaP nanoparticles. The higher

degradability c.q lower chemical stability of the nanostructured versus the microstructured mineral phase might have rendered the hydrogel containing the apatitic nanoparticles more prone to osteoclastic degradation[543] and less stimulatory to osteogenesis than the gels containing BCP microparticles as observed *in vivo*. It is likely that combined application of nanoparticles and hydrogels in an orthotopic defect would lead to higher bone yield[547] due to the osteoconductive properties of nano-HA particles. Combined application of calcium phosphate particles with cell-laden hydrogels requires further development of printable pastes, which would surpass current printing-associated impaction and clogging issues associated with the use of microparticles by using particles of smaller size or addition of components that would promote the particle dispersion.

Cell printing

The use of novel inverse thermosensitive and photopolymerizable hydrogels and viscous ion-sensitive alginate matrices enables 3DF dispensing at physiological temperatures without elaborate and harmful postprocessing steps. Previously, inclusion of cells during the scaffold deposition process was impossible because of harsh postprocessing procedures, the use of high temperatures, or acidic conditions during processing. In particular, reactive plotting of gels is demanding, because it entails precise control of material and medium properties.[187] 3DF technique can easily be translated for organ/tissue printing by placing the extrudate of hydrogel mixed with cells in the printing syringe, followed by fast and efficient layered dispensing of cell-laden gels. Cell encapsulation in the gel ensures homogeneous cell distribution throughout the construct, surpassing uneven cell distribution associated with cell seeding approaches. Other cell printing approaches, including 3D ink-jet printing and 3D robotic dispensing, have previously demonstrated successful patterning of multiple cell populations, but are limited in the range of printable hydrogel matrices and in processing reproducible cell numbers at high cell concentrations. Recently laser-based systems have also successfully been used to print multiple skeletal cell populations in 3D,[100] attaining microscale organization of deposited cells without compromising cell survival or inducing damage to pheno- or genotype.
When applying the 3DF system for design of tissue-engineered bone grafts, we demonstrate that osteogenic progenitors survive the 3DF deposition process and retain the ability to differentiate towards the osteogenic lineage. Our finding that human and goat primary stem cells survive the shear stresses imposed on them during the deposition process is in line with other studies demonstrating high survival of printed cells (80-95%),[114,116] although sometimes cell death was noted. Due to the shear-thinning of the hydrogel, an increased cell survival at higher dispensing pressures (explained by the associated drop in shear stress) is seen in the measured range. This phenomenon of shear-thinning is common behavior for natural and synthetic polymers[615] and is often used for minimal invasive material delivery.[616] The retention of differentiation after printing is in line with findings by others.[100,625]

Tailoring diffusion of oxygen

Arguably the biggest challenge in the field of bone tissue engineering remains efficient diffusion of oxygen and nutrients to the cells. Restricted diffusion of nutrients is a limiting factor in the development of large, clinically relevant-sized grafts. As a result of the inadequate supply of oxygen, hypoxia is common within deeper regions of TE constructs.[469] Upon *in vivo* implantation, survival of transplanted cells is dependent on the degree of vascularization of TE graft.[457]Approaches to tackle this challenge include: 1) the use of channeled scaffolds,[477] 2) the use

of micro-electro-mechanical systems and microfluidic technologies to recapitulate the development of branching networks of the microvasculature[106] and 3) prevascularization of TE constructs with endothelial (progenitor) cells.[552] In this thesis we addressed this pervasive problem by a combination of 1) and 3): design of porous, cell-laden constructs containing endothelial progenitors.

We were the first to design and print porous, cell-laden hydrogels with 3DF. The porosity of hydrogel scaffolds is tailored in 3DF system by changing the distance between the deposited fibers, their orientation and thickness. Porous cell-laden hydrogel constructs have previously been used for adipose tissue engineering, but in that case they were punched out instead of printed.[507] Porous printed constructs promote oxygenation of embedded MSCs and support the survival and differentiation of embedded cells *in vitro* and tissue ingrowth *in vivo*, as demonstrated in our studies. Previously, it has been shown that by providing a certain degree of porosity in a construct, diffusion of oxygen and nutrients through the construct will increase.[477,478] This will in turn promote cell viability and can stimulate differentiation potential of progenitor cells[463] as well as ingrowth of capillaries,[21] vital for adequate bone development. It is demonstrated in other studies that the reduction of cell viability in hydrogels and the corresponding drop in oxygen tension varies between hydrogel matrices.[496]

Prevascularization using EPCs

Cell-based therapies using endothelial cells (ECs) or their progenitors aim at accelerating vascularization of tissue-engineered implants by creating a blood vessel network in the graft prior to implantation that connects to the host vasculature. Endothelial progenitors (EPCs) isolated from peripheral blood are a potent source of the endothelial cells, and can form blood-vessel networks that connect to the host circulation upon implantation *in vivo*.[564,626] In our studies we describe for the first time the isolation and characterization of endothelial progenitor cells from peripheral blood and bone marrow of goats, an important animal model in orthopedic surgery. We demonstrate that MSCs support the proliferation of EPCs and stabilize the formed cellular networks. *In vivo*, PB-EPCs assemble into early blood vessels, which are more pronounced in the presence of MSCs. This is especially important for the development of large, clinically relevant-sized bone grafts. Functional anastomosis of EPC-networks with host vessels is an important result. We show that at least some, if not all of these networks connect to the host circulation, as confirmed by the presence of erythrocytes in the lumina,. In our studies we ascribe the newly formed and perfused tubular networks to the transplanted cells and not to host cells, as no network formation was observed in empty hydrogel constructs or samples seeded with dead EPCs. We could not positively identify the vessel forming cells by transplanted cell-specific staining and therefore don't claim that the seeded cells actually form the blood vessels. Other studies have shown that transplanted late outgrowth EPCs are able to integrate into the newly formed vessels, however the degree of integration is very limited. Often neovascularisation of TE grafts is derived from the host tissue and not accounted for by delivered cells.[627,628] Genetic labeling of transplanted cells and the use of fluorescent *in situ* hybridization techniques or species-specific antibodies in future studies will help determine the origin of the endothelial cells in our constructs.

Heterogeneous grafts

Current cell-based bone tissue engineering strategies often rely on the use of a single cell and matrix type for production of mineralized bone matrix. In contrast, most natural tissues including bone comprise from multiple cell types, profiting from the ability of the cells to interact with

each other. These interactions, either by direct cell-to-cell contacts or through humoral responses, can in some cases synergistically contribute to elaborate ECM formation. In TE, biomimicking approach aims to recapitulate temporo-spatial presentation of cells, matrix and growth factors in native tissues. Organ printing by 3DF is a potent cell-deposition tool in this approach. An attractive feature of 3DF system is the combined printing of cell-laden hydrogel scaffolds by using multiple printing heads. Using this, distinct cell populations are printed at defined locations within one construct, resulting in heterogeneous constructs. Specifically, by combining osteoprogenitors with endothelial progenitors or with chondrocytes, we set out to fabricate bone grafts with vascular bed structures suitable for integration with the systemic circulation, while osteochondral constructs are interesting for treatment of deep osteochondral defects.

We validated the ability of 3DF system to design viable, 3D-structured printed constructs, by demonstrating heterogeneous ECM formation in printed ostochondral grafts *in vitro* and *in vivo*, as well as heterogeneous tissue formation in printed vascularized bone grafts after implantation. None of the currently used 3D organ printing techniques have surpassed 3D arrangement of multiple cell populations and addressed extracellular matrix and tissue formation by the printed populations upon extensive *in vitro* culture and *in vivo* implantation like we did in our studies. Cells remained restricted to their compartment of the heterogeneous scaffold and produced extracellular matrix corresponding to the deposited cell type. Maintenance of the required phenotype in printed constructs *in vitro* is an important challenge for successful skeletal tissue engineering, as chondrocytes can easily dedifferentiate during inadequate *in vitro* culture,[255] while it is very difficult to achieve osteogenic differentiation as osteogenic cells that are embedded in hydrogel matrices tend to undergo chondrogenic differentiation.[261] Heterogeneous constructs manufactured by a 3D fiber deposition technique yielded viable and functional tissue equivalents with elaborate tissue formation upon *in vivo* implantation. Erythrocyte-filled blood vessels formed in EPC-laden part of the construct, demonstrated formation of functional printed tissue, surpassing currently available *in vitro* data on printed endothelial cells and cell-aggregates.[122] Limited osteogenic differentiation by printed MSCs in alginate and elaborate bone tissue formation in Matrigel demonstrating osteoblasts lining the newly formed bone is in line with previous findings demonstrating low bone formation in alginates and superior bone formation in gelatinious protein mixtures like Matrigel.[209,502] Comparison of printed heterogeneous tissues to randomly mixed controls in future studies will help elucidate whether anatomical tissue design is necessary to achieve more functional grafts.

Future directions

Materials

Initially, a hydrogel must provide a stable matrix for survival of embedded osteogenic progenitors. Current hydrogel materials can hardly meet the requirement of bone tissue biomechanics, although it is important to consider that for many tissue defects the original biomechanical properties of the used scaffold material do not have to match those of regenerated tissue, because the scaffold is meant to be completely remodeled. Synthetic hydrogels allow modification with photoliable groups for covalent UV-crosslinking. Photoliable chemistries can be tuned to spatially and temporally regulate the gel's elastic modulus to obtain the desired viscoelasticity,[129] and can be additionally modified with adhesive sequences to support survival of

adhesion-sensitive osteoprogenitors.[629] Furthermore, these materials can be tailored with sequences and side groups (e.g. heparin-binding domains, covalently bound GF peptides and phosphate groups) that would accelerate the formation of mineralized matrix and bone tissue, with corresponding rise in mechanical properties. Supramolecular gels consisting of water-swollen self-assembled peptide amphiphils are another potentially promising approach to design cytocompatible hydrogels reminiscent of extracellular matrix with defined biomechanics and tailored with bioactive cues.[630,631] Combining printing of stiff materials with mechanically weak hydrogels, is expected to profit from increased elasticity of the resultant scaffolds for implantation and cell-supportive properties of gel matrices, respectively. A recent example includes combining two-photon polymerization to fabricate stiff porous PEGDA scaffolds with LIFT organ printing technology depositing multiple cell types on the inside of the scaffold.[102] Another potential application of organ printing involves combining anisotropically stiff materials with permeability coefficients. Resulting poroelastic structure reacts to mechanical loads thereby directing fluid flow within the material via convective transport. The application of such mechanoactive materials is expected to lead to better nutrient exchange in engineered bone tissue.[632]

Formation of the newly formed bone and subsequent remodeling of the newly formed tissue, should ideally coincide with degradation and resorption of the printed biomaterial. Degradation of the printed matrix is vital as the permanence of biomaterial on long follow-up could compromise the biomechanics of the new bone. Hydrogels modified with MMP-sensitive sites[129] combined with composite scaffolds made of synthetic polymers and ceramics are expected to meet the (cell-driven) degradation requirements.

Oxygen levels

Clinical application of cell-based tissue engineering has so far been limited by loss of function or death of the transplanted cells after transplantation.[457] The substantial cells loss that occurs within several days after delivery to the recipient is likely to result from inadequate availability of oxygen and nutrients for the cells in the interior of the hybrid implant due to delayed vascularization.[633] Pore size and porosity are key scaffold design parameters affecting vascularization ingrowth and new tissue formation and can be easily tailored by 3D printing approach, easily achieving pore size of ≥300 micrometer necessary for bone formation.[21] Further sophistication in design of anisotropically porous scaffolds is expected to contribute to complex tissue formation *in vivo*, in for example engineered osteochondral grafts. In printed bone grafts, built-in tubes seeded in the lumina with angiogenic growth factors or cells are attractive features to promote inosculation with host vascular network.

Next to methods focused on acceleration of blood vessel ingrowth, techniques to promote the ability of the graft to survive in conditions of limited oxygen supply are expected to result in more successful tissue repair. Several animal species and various cell types, particularly vascular endothelial cells,[634] show hypoxia tolerance that enables them to survive in environment that is deprived of oxygen by inducing a hypometabolic state characterized by reduced oxygen consumption.[635] Induction of hypoxia tolerance can be of therapeutic value to protect the cells against severe hypoxia after transplantation.[635] Pharmacological inhibition of enzymes that negatively regulate the stability of hypoxia induced factor, hereby inducing hypoxia tolerance, may be used to protect the transplanted cells from ischemic injury.[635,636] Priming of cultured multipotent stromal cells by hypoxic preconditioning might contribute to their survival upon *in*

vivo implantation.[637] Furthermore, it would be attractive to use varying oxygen tension during construct development *in vitro* to direct stem cell differentiation,[461] for example yielding anisotropically oxygenized scaffolds for engineered osteochondral grafts. These strategies will depend on the precise knowledge of the effects of oxygen levels on cell function. Printed constructs with graded oxygen tensions, that function as *in vitro* model systems, may help pinpointing relevant oxygen tensions.

Cells

By incorporating different cell types at predefined locations, cell-seeded graft mimicking cell distribution in native tissues can be printed. It remains to be validated whether printed tissues reminiscent of native tissue geometry, spatial organization, and the microenvironment of the cells will accelerate and improve the formation of skeletal tissues. Apart from the obvious benefit of printed bone- and cartilage tissue separately, it would be interesting to study osteochondral constructs to promote integration of TE grafts with the surrounding tissue. Potentially, such constructs may help to overcome current drawbacks of osteochondral grafts such as compromised cartilage tissue formation[49] and fibrous capsule formation between and around the tissue layers.[49,610,638]

A novel development is to print grafts directly *in vivo*.[113,540] Laser-printed acellular HA nanoparticles with glycerol hydrogel for treatment of calvarial defects *in situ* demonstrated bone formation in the samples.[540] However the resultant implants printed with biological laser printing were solid without interconnected pores and the composition of the printed mixtures requires optimization as no significant effect of this mixture on bone repair was found. *In vivo* ink-jet printing of cells combined with gene transfection is a promising new approach[113] to promote tissue formation.

Currently, the organized deposition of cells by 3DF and formation of cm-scaled tissues *in vitro* lies a considerable distance away from actual printing of tissues for clinical application. *In vivo* implantation of heterogeneous printed grafts, at ectopic as well as orthotopic locations, will provide an answer on the quality and quantity of tissue formation within the printed grafts. Important issues to investigate are the necessary cell densities and proportions and whether the imposed cell organization is actually necessary for obtaining fully functional newly formed tissues upon *in vivo* implantation. Also of interest is the nature of tissue formation in the transition zone between different tissues as seen in the osteochondral design. Controlled delivery of biological factors in printed constructs is expected to lead to further functionalisation of complex tissue grafts.

Chapter 13

Samenvatting in het Nederlands

Samenvatting

Botweefsel vermalen tot botchips wordt in de orthopaedische chirurgie gebruikt bij rugchirurgie en om grote botdefecten na trauma op te vullen. Een mogelijk alternatief voor autoloog botweefsel is regeneratie van botweefsel in het lab, door hybride implantaten te maken die bestaan uit lichaamseigen botvormende (stam)cellen, ondersteunende biomatrices en groeifactoren die botvorming bevorderen. Hoewel kleine botfragmenten van millimeter-schaal op deze manier gemaakt kunnen worden, is de toepassing van cellulaire kunstbotimplantaten van centimeter-schaal in de operatiekamer nog geen klinische realiteit. Dit komt voornamelijk door het optreden van celdood in de kern van de grote botimplantaten. Reden voor deze celdood is de tijd die nodig is voor het ontwikkelen van een adequate doorbloeding van de implantaten. Daarnaast zijn de huidige hybride implantaten veelal gevormd door één type cellen gezaaid op of in een bepaalde biomatrix, eventueel aangevuld door één type groeifactor. In het lichaam heeft botweefsel een aanmerkelijk complexere samenstelling en bestaat uit multipele celtypen (onder andere mesenchymale en hematopoietische stamcellen, osteoblasten en endotheelcellen), verscheidene extracellulaire matrixmoleculen en multipele groeifactoren. Al deze componenten hebben een bepaalde driedimensionale rangschikking en temporospatieel patroon van presentatie. Uit eerder onderzoek blijkt dat het combineren van verschillende cellen of groeifactoren positieve of synergistische effecten kan hebben op botvorming en vascularisatie van de hybride implantaten *in vivo*. Het zou daarom aantrekkelijk kunnen zijn om voor de regeneratie van klinisch toepasbare grote stukken botweefsel gebruik te maken van technieken die de anatomische organisatie van natuurlijk botweefsel nabootsen. De zogenaamde weefselprinttechniek is een nieuwe benadering in de regeneratieve geneeskunde die cellen, vermengd met een hydrogelmatrix, laag voor laag opbouwt tot een 3D-structuur waarbij multipele celtypen met verscheidene matrices geprint kunnen worden in één construct. Met behulp van deze technologie kan getest worden of de georganiseerde (anatomische) opbouw van een hybride construct een positieve bijdrage kan leveren aan het ontwikkelen van functionele centimeter-schaal botimplantaten. Door de structuren met poriën te printen worden de ingebedde cellen sneller voorzien van nutriënten *in vitro* en kunnen bloedvaten *in vivo* makkelijker ingroeien. Door botvormende (stam)cellen te combineren met bloedvatvormende (stam)cellen kunnen de constructen vóór de implantatie gevasculariseerd worden waarmee de tijd die nodig is voor de ingroei van de bloedvaten verminderd wordt.

In dit proefschrift hebben we het gebruik van '3D fiber deposition', een bepaald soort weefselprinttechniek, voor het ontwikkelen van (gevascularisseerde) bot implantaten geanalyseerd. In **hoofdstuk 2** beschrijven wij de rationale voor het toepassen van weefselprinttechniek en bespreken we studies die illustreren dat het nabootsen van de anatomische opbouw in bot en kraakbeen tissue engineering de functionaliteit van hybride constructen bevordert. We bespreken tevens het zelforganiserend potentieel van de cellen, en stellen dat het vinden van een balans tussen zelforganisatie van de cellen en opgelegde organisatie door weefselprint techniek functionele 3D weefselstructuren voor *in vitro* testen en *in vivo* implantatie zal helpen ontwikkelen.

In het eerste deel van het proefschrift worden de belangrijkste parameters en componenten van het printproces beschreven. **Hoofdstuk 3** is een literatuurstudie naar het gebruik van hydrogelmatrices in tissue engineering van bot en kraakbeen in het algemeen, en het gebruik van verschillende hydrogels in weefselprinttechniek in het bijzonder. Hydrogels zijn rijk gehydreerde polymeerketens waartussen cellen ingekapseld kunnen worden, en deze polymeren worden naar origine ingedeeld. Over het algemeen ondersteunen natuurlijke matrices de celhechting, -migratie

en -differentiatie, maar zijn het veelal zwakke gels met variabele chemische samenstelling en snelle en onvoorspelbare degradatie. Synthetische hydrogels zijn betrouwbare matrices met voorspelbare chemische samenstelling en mechanische eigenschappen, maar bieden de ingekapselde cellen weinig houvast en geven geen ondersteuning voor de differentiatie. Daarom is het voor de succesvolle toepassing in botregeneratie noodzakelijk dat deze polymeerketens gemodificeerd worden, bijvoorbeeld met adhesiesequenties en extracellulaire matrixcomponenten.
Een ander hoofdcomponent van het printproces is de printmachine. In **hoofdstuk 4** laten we zien hoe 3D fiber deposition gebruikt kan worden voor het printen van vitale 3D hydrogelconstructen. Botvormende stamcellen overleven het printproces en behouden hun differentiatiepotentieel. Verdere overleving van de cellen is afhankelijk van het type hydrogel.
Van alle synthetische hydrogels zijn UV-gevoelige polymeren dankzij hun mechanische stabiliteit het meest veelbelovende materiaal voor bot en kraakbeen tissue engineering. In **hoofdstuk 5** worden de effecten van UV blootstelling op overleving, delingsactiviteit en osteogene differentiatie van botvormende stamcellen bepaald. Wij hebben laten zien dat overleving van de cellen in hydrogels niet negatief wordt beïnvloed door photopolymerisatie, dit in tegenstelling tot cellen die in monolaag groeien. Waarschijnlijk komt dit doordat de vrije radicalen die DNA- en celschade kunnen aanrichten in de gel gebruikt worden voor propagatie van de polymerisatie. Voor het printen van 3D-constructen gebruikten wij een nieuwe UV- en temperatuurgevoelige polymeer, Lutrol F127 AlaL (**hoofdstuk 6**).
Bij het maken van constructen is het 3D-ontwerp belangrijk, omdat hiermee de hoeveelheid en de rangschikking van de cellen, de mate van porositeit en de poriegrootte bepaald worden, welke op hun beurt de celdifferentiatie, de nutriëntentoevoer en mate van vascularisatie sturen. In **hoofdstuk 11** demonstreren wij dat door het aanpassen van printparameters (celdichtheid, afstand tussen de geprinte hydrogelfilamenten en oriëntatie daarvan, printdruk en -snelheid) de porositeit, mechanische eigenschappen en cellulariteit van het construct gevarieerd kunnen worden. In **hoofdstuk 7** wordt beschreven hoe de porositeit van het construct de zuurstofvoorziening van ingekapselde cellen *in vitro en in vivo* beinvloedt, en hoe dit resulteert in de verandering van metabolisme en differentiatie van ingebedde botvormende stamcellen. In constructen zonder poriën lieten de cellen verhoogde expressie van hypoxiemarkers zien en produceerden ze meer lactaat. Er waren minder levende cellen en er werden meer apoptotische cellen gezien in vergelijking met poreuze constructen. Porositeit van de constructen ondersteunde osteogene differentiatie van botvormende stamcellen *in vitro* en oxygenatie van ingebedde cellen en vascularisatie van de constructen *in vivo*.
Veelal zijn ongemodificeerde hydrogels niet in staat om de ingebedde botvormende (stam)cellen te stimuleren om (veel) botmatrix te maken. Het toevoegen van calciumfosfaatpartikels aan de hydrogels kan gebruikt worden om botvorming *in vivo* te induceren. Daarom hebben we het osteoinductief potentieel van twee verschillende printbare cellulaire hydrogel-calciumfosfaat-matrices getest: Matrigels met gesinterde bicalciumfostaat-micropartikels en Matrigels met toegevoegde apatitische nanodeeltjes. Zoals wij laten zien in **hoofdstuk 8** leidt het toevoegen van bicalciumfostaat-micropartikels aan Matrigel tot uitgebreide botvorming, terwijl er geen botvorming optreedt in ongemodificeerde Matrigels, en het toevoegen van apatitische nanopartikels slechts een osteoclastische reactie induceert.
Het ontwikkelen van heterogene implantaten met multipele soorten cellen komt aan bod in het tweede deel van het proefschrift. Hierbij illustreren we in **hoofdstuk 9** dat endotheelstamcellen,

geïsoleerd uit perifeer bloed, capillaire netwerken kunnen vormen *in vitro* en dat deze cellen na implantatie in combinatie met botvormende stamcellen stabiele bloedvaten vormen en een positieve bijdrage leveren aan botvorming. In **hoofdstukken 10 en 11** laten we het ontwikkelen van geprinte heterogene constructen zien, bestaande uit twee verschillende celtypen, en valideren wij heterogene weefselvorming in deze constructen na implantatie. In **hoofdstuk 10** hebben we geprinte implantaten ontworpen met in één compartiment botvormende stamcellen en in het andere compartiment geprinte endotheelstamcellen. In **hoofdstuk 11** wordt voor het ontwikkelen van osteochondrale implantaten gekozen voor een construct waarin een compartiment met chondrocyten naast een compartiment met botvormende stamcellen is geprint. Tijdens de implantatie bleven de cellen beperkt tot het geprinte compartiment van het implantaat en maakten ze hun eigen celspecifieke matrix.

De studies in dit proefschrift illustreren de mogelijkheid om met een weefselprinter vitale en functionele heterogene implantaten te maken die in de toekomst mogelijk bij de orthopedische behandeling van grote botdefecten kunnen worden toegepast.

References

References

1. Boden SD. Overview of the biology of lumbar spine fusion and principles for selecting a bone graft substitute. *Spine (Phila Pa 1976)* 2002;27(16 Suppl 1):S26-31.
2. Arrington ED, Smith WJ, Chambers HG, Bucknell AL, Davino NA. Complications of iliac crest bone graft harvesting. *Clin Orthop Relat Res* 1996(329):300-309.
3. Silber JS, Anderson DG, Daffner SD, et al. Donor site morbidity after anterior iliac crest bone harvest for single-level anterior cervical discectomy and fusion. *Spine (Phila Pa 1976)* 2003;28(2):134-139.
4. Delawi D, Dhert WJ, Castelein RM, Verbout AJ, Oner FC. The incidence of donor site pain after bone graft harvesting from the posterior iliac crest may be overestimated: a study on spine fracture patients. *Spine (Phila Pa 1976)* 2007;32(17):1865-1868.
5. Sandhu HS, Grewal HS, Parvataneni H. Bone grafting for spinal fusion. *Orthop Clin North Am* 1999;30(4):685-698.
6. Marcacci M, Kon E, Moukhachev V, et al. Stem cells associated with macroporous bioceramics for long bone repair: 6- to 7-year outcome of a pilot clinical study. *Tissue Eng* 2007;13(5):947-955.
7. Gupta MC, Maitra S. Bone grafts and bone morphogenetic proteins in spine fusion. *Cell Tissue Bank* 2002;3(4):255-267.
8. Cancedda R, Bianchi G, Derubeis A, Quarto R. Cell therapy for bone disease: a review of current status. *Stem Cells* 2003;21(5):610-619.
9. Cancedda R, Giannoni P, Mastrogiacomo M. A tissue engineering approach to bone repair in large animal models and in clinical practice. *Biomaterials* 2007;28(29):4240-4250.
10. Giannoudis PV, Dinopoulos H, Tsiridis E. Bone substitutes: an update. *Injury* 2005;36 Suppl 3:S20-27.
11. Kruyt M, De Bruijn J, Rouwkema J, et al. Analysis of the dynamics of bone formation, effect of cell seeding density, and potential of allogeneic cells in cell-based bone tissue engineering in goats. *Tissue Eng Part A* 2008;14(6):1081-1088.
12. Hutmacher DW, Schantz JT, Lam CX, Tan KC, Lim TC. State of the art and future directions of scaffold-based bone engineering from a biomaterials perspective. *J Tissue Eng Regen Med* 2007;1(4):245-260.
13. Jansen JA, Vehof JW, Ruhe PQ, et al. Growth factor-loaded scaffolds for bone engineering. *J Control Release* 2005;101(1-3):127-136.
14. Kempen DH, Lu L, Heijink A, et al. Effect of local sequential VEGF and BMP-2 delivery on ectopic and orthotopic bone regeneration. *Biomaterials* 2009;30(14):2816-2825.
15. Delawi D, Dhert WJ, Rillardon L, et al. A prospective, randomized, controlled, multicenter study of osteogenic protein-1 in instrumented posterolateral fusions: report on safety and feasibility. *Spine (Phila Pa 1976)* 2010;35(12):1185-1191.
16. Novicoff WM, Manaswi A, Hogan MV, Brubaker SM, Mihalko WM, Saleh KJ. Critical analysis of the evidence for current technologies in bone-healing and repair. *J Bone Joint Surg Am* 2008;90 Suppl 1:85-91.
17. Kruyt MC, Delawi D, Habibovic P, Oner FC, van Blitterswijk CA, Dhert WJ. Relevance of bone graft viability in a goat transverse process model. *J Orthop Res* 2009;27(8):1055-1059.
18. Kruyt MC, de Bruijn JD, Wilson CE, et al. Viable osteogenic cells are obligatory for tissue-engineered ectopic bone formation in goats. *Tissue Eng* 2003;9(2):327-336.
19. Griffith LG, Naughton G. Tissue engineering--current challenges and expanding opportunities. *Science* 2002;295(5557):1009-1014.
20. Tilkorn DJ, Bedogni A, Keramidaris E, et al. Implanted myoblast survival is dependent on the degree of vascularization in a novel delayed implantation/prevascularization tissue engineering model. *Tissue Eng Part A* 2010;16(1):165-178.
21. Karageorgiou V, Kaplan D. Porosity of 3D biomaterial scaffolds and osteogenesis. *Biomaterials* 2005;26(27):5474-5491.
22. Kruyt MC, Stijns MM, Fedorovich NE, et al. Genetic marking with the DeltaLNGFR-gene for tracing goat cells in bone tissue engineering. *J Orthop Res* 2004;22(4):697-702.
23. Olivo C, Alblas J, Verweij V, Van Zonneveld AJ, Dhert WJ, Martens AC. In vivo bioluminescence imaging study to monitor ectopic bone formation by luciferase gene marked mesenchymal stem cells. *J Orthop Res* 2008;26(7):901-909.
24. Tortelli F, Tasso R, Loiacono F, Cancedda R. The development of tissue-engineered bone of different origin through endochondral and intramembranous ossification following the implantation of mesenchymal stem cells and osteoblasts in a murine model. *Biomaterials* 2010;31(2):242-249.
25. Kruyt MC, Dhert WJ, Oner FC, van Blitterswijk CA, Verbout AJ, de Bruijn JD. Analysis of ectopic and orthotopic bone formation in cell-based tissue-engineered constructs in goats. *Biomaterials* 2007;28(10):1798-1805.
26. Kaigler D, Krebsbach PH, Wang Z, West ER, Horger K, Mooney DJ. Transplanted endothelial cells enhance orthotopic bone regeneration. *J Dent Res* 2006;85(7):633-637.
27. Kim TK, Sharma B, Williams CG, et al. Experimental model for cartilage tissue engineering to regenerate the zonal organization of articular cartilage. *Osteoarthritis Cartilage* 2003;11(9):653-664.
28. Mironov V, Boland T, Trusk T, Forgacs G, Markwald RR. Organ printing: computer-aided jet-based 3D tissue engineering. *Trends Biotechnol* 2003;21(4):157-161.
29. Yeong WY, Chua CK, Leong KF, Chandrasekaran M. Rapid prototyping in tissue engineering: challenges and potential. *Trends Biotechnol* 2004;22(12):643-652.
30. Woodfield TB, Malda J, de Wijn J, Peters F, Riesle J, van Blitterswijk CA. Design of porous scaffolds for cartilage tissue engineering using a three-dimensional fiber-deposition technique. *Biomaterials* 2004;25(18):4149-4161.
31. Chawla K, Klein TJ, Schumacher BL, et al. Short-term retention of labeled chondrocyte subpopulations in stratified tissue-engineered cartilaginous constructs implanted in vivo in mini-pigs. *Tissue Eng* 2007;13(7):1525-1537.
32. Ng KW, Ateshian GA, Hung CT. Zonal chondrocytes seeded in a layered agarose hydrogel create engineered cartilage with depth-dependent cellular and mechanical inhomogeneity. *Tissue Eng Part A* 2009;15(9):2315-2324.
33. Gawlitta D, Farrell E, Malda J, Creemers LB, Alblas J, Dhert WJ. Modulating endochondral ossification of multipotent stromal cells for bone regeneration. *Tissue Eng Part B Rev* 2010;16(4):385-395.
34. Sharma B, Elisseeff JH. Engineering structurally organized cartilage and bone tissues. *Ann Biomed Eng* 2004;32(1):148-159.
35. Kojima K, Bonassar LJ, Roy AK, Mizuno H, Cortiella J, Vacanti CA. A composite tissue-engineered trachea using sheep nasal chondrocyte and epithelial cells. *FASEB J* 2003;17(8):823-828.

36. Ibarra C, Jannetta C, Vacanti CA, et al. Tissue engineered meniscus: a potential new alternative to allogeneic meniscus transplantation. *Transplant Proc* 1997;29(1-2):986-988.
37. Kamil SH, Kojima K, Vacanti MP, Bonassar LJ, Vacanti CA, Eavey RD. In vitro tissue engineering to generate a human-sized auricle and nasal tip. *Laryngoscope* 2003;113(1):90-94.
38. Mizuno H, Roy AK, Vacanti CA, Kojima K, Ueda M, Bonassar LJ. Tissue-engineered composites of anulus fibrosus and nucleus pulposus for intervertebral disc replacement. *Spine (Phila Pa 1976)* 2004;29(12):1290-1297; discussion 1297-1298.
39. Martin I, Miot S, Barbero A, Jakob M, Wendt D. Osteochondral tissue engineering. *J Biomech* 2007;40(4):750-765.
40. Hung CT, Lima EG, Mauck RL, et al. Anatomically shaped osteochondral constructs for articular cartilage repair. *J Biomech* 2003;36(12):1853-1864.
41. Puelacher WC, Vacanti JP, Ferraro NF, Schloo B, Vacanti CA. Femoral shaft reconstruction using tissue-engineered growth of bone. *Int J Oral Maxillofac Surg* 1996;25(3):223-228.
42. Weng Y, Cao Y, Silva CA, Vacanti MP, Vacanti CA. Tissue-engineered composites of bone and cartilage for mandible condylar reconstruction. *J Oral Maxillofac Surg* 2001;59(2):185-190.
43. Lee SH, Shin H. Matrices and scaffolds for delivery of bioactive molecules in bone and cartilage tissue engineering. *Adv Drug Deliv Rev* 2007;59(4-5):339-359.
44. Richardson TP, Peters MC, Ennett AB, Mooney DJ. Polymeric system for dual growth factor delivery. *Nat Biotechnol* 2001;19(11):1029-1034.
45. Yancopoulos GD, Davis S, Gale NW, Rudge JS, Wiegand SJ, Holash J. Vascular-specific growth factors and blood vessel formation. *Nature* 2000;407(6801):242-248.
46. Klein TJ, Schumacher BL, Schmidt TA, et al. Tissue engineering of stratified articular cartilage from chondrocyte subpopulations. *Osteoarthritis Cartilage* 2003;11(8):595-602.
47. Sharma B, Williams CG, Kim TK, et al. Designing zonal organization into tissue-engineered cartilage. *Tissue Eng* 2007;13(2):405-414.
48. Sherwood JK, Riley SL, Palazzolo R, et al. A three-dimensional osteochondral composite scaffold for articular cartilage repair. *Biomaterials* 2002;23(24):4739-4751.
49. Gao J, Dennis JE, Solchaga LA, Awadallah AS, Goldberg VM, Caplan AI. Tissue-engineered fabrication of an osteochondral composite graft using rat bone marrow-derived mesenchymal stem cells. *Tissue Eng* 2001;7(4):363-371.
50. Schaefer D, Martin I, Jundt G, et al. Tissue-engineered composites for the repair of large osteochondral defects. *Arthritis Rheum* 2002;46(9):2524-2534.
51. Byrne DP, Lacroix D, Planell JA, Kelly DJ, Prendergast PJ. Simulation of tissue differentiation in a scaffold as a function of porosity, Young's modulus and dissolution rate: application of mechanobiological models in tissue engineering. *Biomaterials* 2007;28(36):5544-5554.
52. Kelly DJ, Prendergast PJ. Prediction of the optimal mechanical properties for a scaffold used in osteochondral defect repair. *Tissue Eng* 2006;12(9):2509-2519.
53. Perez-Pomares JM, Foty RA. Tissue fusion and cell sorting in embryonic development and disease: biomedical implications. *Bioessays* 2006;28(8):809-821.
54. Rago AP, Dean DM, Morgan JR. Controlling cell position in complex heterotypic 3D microtissues by tissue fusion. *Biotechnol Bioeng* 2009;102(4):1231-1241.
55. Jakab K, Neagu A, Mironov V, Markwald RR, Forgacs G. Engineering biological structures of prescribed shape using self-assembling multicellular systems. *Proc Natl Acad Sci U S A* 2004;101(9):2864-2869.
56. Jakab K, Norotte C, Damon B, et al. Tissue engineering by self-assembly of cells printed into topologically defined structures. *Tissue Eng Part A* 2008;14(3):413-421.
57. Boland T, Mironov V, Gutowska A, Roth EA, Markwald RR. Cell and organ printing 2: fusion of cell aggregates in three-dimensional gels. *Anat Rec A Discov Mol Cell Evol Biol* 2003;272(2):497-502.
58. Foty RA, Steinberg MS. The differential adhesion hypothesis: a direct evaluation. *Dev Biol* 2005;278(1):255-263.
59. Dean DM, Morgan JR. Cytoskeletal-mediated tension modulates the directed self-assembly of microtissues. *Tissue Eng Part A* 2008;14(12):1989-1997.
60. Jakab K, Damon B, Marga F, et al. Relating cell and tissue mechanics: implications and applications. *Dev Dyn* 2008;237(9):2438-2449.
61. Lin RZ, Chang HY. Recent advances in three-dimensional multicellular spheroid culture for biomedical research. *Biotechnol J* 2008;3(9-10):1172-1184.
62. DeLise AM, Fischer L, Tuan RS. Cellular interactions and signaling in cartilage development. *Osteoarthritis Cartilage* 2000;8(5):309-334.
63. Armstrong PB, Armstrong MT. Intercellular invasion and the organizational stability of tissues: a role for fibronectin. *Biochim Biophys Acta* 2000;1470(2):O9-20.
64. Boyan BD, Schwartz Z. Response of musculoskeletal cells to biomaterials. *J Am Acad Orthop Surg* 2006;14(10 Spec No.):S157-162.
65. Lin CY, Schek RM, Mistry AS, et al. Functional bone engineering using ex vivo gene therapy and topology-optimized, biodegradable polymer composite scaffolds. *Tissue Eng* 2005;11(9-10):1589-1598.
66. Stahl A, Wenger A, Weber H, Stark GB, Augustin HG, Finkenzeller G. Bi-directional cell contact-dependent regulation of gene expression between endothelial cells and osteoblasts in a three-dimensional spheroidal coculture model. *Biochem Biophys Res Commun* 2004;322(2):684-692.
67. Wenger A, Stahl A, Weber H, et al. Modulation of in vitro angiogenesis in a three-dimensional spheroidal coculture model for bone tissue engineering. *Tissue Eng* 2004;10(9-10):1536-1547.
68. Korff T, Kimmina S, Martiny-Baron G, Augustin HG. Blood vessel maturation in a 3-dimensional spheroidal coculture model: direct contact with smooth muscle cells regulates endothelial cell quiescence and abrogates VEGF responsiveness. *Faseb J* 2001;15(2):447-457.
69. Hayes AJ, Hall A, Brown L, Tubo R, Caterson B. Macromolecular organization and in vitro growth characteristics of scaffold-free neocartilage grafts. *J Histochem Cytochem* 2007;55(8):853-866.

70. Alsberg E, Anderson KW, Albeiruti A, Rowley JA, Mooney DJ. Engineering growing tissues. *Proc Natl Acad Sci U S A* 2002;99(19):12025-12030.
71. Kaigler D, Krebsbach PH, West ER, Horger K, Huang YC, Mooney DJ. Endothelial cell modulation of bone marrow stromal cell osteogenic potential. *Faseb J* 2005;19(6):665-667.
72. Potier E, Ferreira E, Andriamanalijaona R, et al. Hypoxia affects mesenchymal stromal cell osteogenic differentiation and angiogenic factor expression. *Bone* 2007;40(4):1078-1087.
73. Isogai N, Landis W, Kim TH, Gerstenfeld LC, Upton J, Vacanti JP. Formation of phalanges and small joints by tissue-engineering. *J Bone Joint Surg Am* 1999;81(3):306-316.
74. Unger RE, Ghanaati S, Orth C, et al. The rapid anastomosis between prevascularized networks on silk fibroin scaffolds generated in vitro with cocultures of human microvascular endothelial and osteoblast cells and the host vasculature. *Biomaterials* 2010;31(27):6959-6967.
75. Hutmacher DW, Sittinger M, Risbud MV. Scaffold-based tissue engineering: rationale for computer-aided design and solid free-form fabrication systems. *Trends Biotechnol* 2004;22(7):354-362.
76. Tsang VL, Bhatia SN. Three-dimensional tissue fabrication. *Adv Drug Deliv Rev* 2004;56(11):1635-1647.
77. Sachlos E, Czernuszka JT. Making tissue engineering scaffolds work. Review: the application of solid freeform fabrication technology to the production of tissue engineering scaffolds. *Eur Cell Mater* 2003;5:29-39; discussion 39-40.
78. Dalton PD, Woodfield T, Hutmacher DW. Snapshot: Polymer scaffolds for tissue engineering. *Biomaterials* 2009;30(4):701-702.
79. Lin CY, Kikuchi N, Hollister SJ. A novel method for biomaterial scaffold internal architecture design to match bone elastic properties with desired porosity. *J Biomech* 2004;37(5):623-636.
80. Alhadlaq A, Elisseeff JH, Hong L, et al. Adult stem cell driven genesis of human-shaped articular condyle. *Ann Biomed Eng* 2004;32(7):911-923.
81. Hollister SJ. Porous scaffold design for tissue engineering. *Nat Mater* 2005;4(7):518-524.
82. Moroni L, de Wijn JR, van Blitterswijk CA. 3D fiber-deposited scaffolds for tissue engineering: influence of pores geometry and architecture on dynamic mechanical properties. *Biomaterials* 2006;27(7):974-985.
83. Moroni L, de Wijn JR, van Blitterswijk CA. Three-dimensional fiber-deposited PEOT/PBT copolymer scaffolds for tissue engineering: influence of porosity, molecular network mesh size, and swelling in aqueous media on dynamic mechanical properties. *J Biomed Mater Res A* 2005;75(4):957-965.
84. Woodfield TB, Van Blitterswijk CA, De Wijn J, Sims TJ, Hollander AP, Riesle J. Polymer scaffolds fabricated with pore-size gradients as a model for studying the zonal organization within tissue-engineered cartilage constructs. *Tissue Eng* 2005;11(9-10):1297-1311.
85. Chen YM, Shiraishi N, Satokawa H, et al. Cultivation of endothelial cells on adhesive protein-free synthetic polymer gels. *Biomaterials* 2005;26(22):4588-4596.
86. Hahn MS, Taite LJ, Moon JJ, Rowland MC, Ruffino KA, West JL. Photolithographic patterning of polyethylene glycol hydrogels. *Biomaterials* 2006;27(12):2519-2524.
87. Harris BP, Kutty JK, Fritz EW, Webb CK, Burg KJ, Metters AT. Photopatterned polymer brushes promoting cell adhesion gradients. *Langmuir* 2006;22(10):4467-4471.
88. Sarkar S, Dadhania M, Rourke P, Desai TA, Wong JY. Vascular tissue engineering: microtextured scaffold templates to control organization of vascular smooth muscle cells and extracellular matrix. *Acta Biomater* 2005;1(1):93-100.
89. Brock A, Chang E, Ho CC, et al. Geometric determinants of directional cell motility revealed using microcontact printing. *Langmuir* 2003;19(5):1611-1617.
90. Chen CS, Mrksich M, Huang S, Whitesides GM, Ingber DE. Geometric control of cell life and death. *Science* 1997;276(5317):1425-1428.
91. McBeath R, Pirone DM, Nelson CM, Bhadriraju K, Chen CS. Cell shape, cytoskeletal tension, and RhoA regulate stem cell lineage commitment. *Dev Cell* 2004;6(4):483-495.
92. Dalby MJ, Gadegaard N, Curtis AS, Oreffo RO. Nanotopographical control of human osteoprogenitor differentiation. *Curr Stem Cell Res Ther* 2007;2(2):129-138.
93. Miller ED, Fisher GW, Weiss LE, Walker LM, Campbell PG. Dose-dependent cell growth in response to concentration modulated patterns of FGF-2 printed on fibrin. *Biomaterials* 2006;27(10):2213-2221.
94. Phillippi JA, Miller E, Weiss L, Huard J, Waggoner A, Campbell P. Microenvironments engineered by inkjet bioprinting spatially direct adult stem cells toward muscle- and bone-like subpopulations. *Stem Cells* 2008;26(1):127-134.
95. Cooper GM, Miller ED, Decesare GE, et al. Inkjet-based biopatterning of bone morphogenetic protein-2 to spatially control calvarial bone formation. *Tissue Eng Part A* 2010;16(5):1749-1759.
96. Tsugawa J, Komaki M, Yoshida T, Nakahama KI, Amagasa T, Morita I. Cell-printing and transfer technology applications for bone defects in mice. *J Tissue Eng Regen Med* 2011;DOI: 10.1002/term.366.
97. Melchels F, Malda J, Fedorovich NE, Alblas J, Woodfield TB. Cell and Organ printing. *Comprehensive BIomaterials*: Elsevier; 2010.
98. Odde DJ, Renn MJ. Laser-guided direct writing for applications in biotechnology. *Trends Biotechnol* 1999;17(10):385-389.
99. Barron JA, Wu P, Ladouceur HD, Ringeisen BR. Biological laser printing: a novel technique for creating heterogeneous 3-dimensional cell patterns. *Biomed Microdevices* 2004;6(2):139-147.
100. Gruene M, Deiwick A, Koch L, et al. Laser Printing of Stem Cells for Biofabrication of Scaffold-Free Autologous Grafts. *Tissue Eng Part C Methods* 2010.
101. Koch L, Kuhn S, Sorg H, et al. Laser printing of skin cells and human stem cells. *Tissue Eng Part C Methods* 2010;16(5):847-854.
102. Ovsianikov A, Gruene M, Pflaum M, et al. Laser printing of cells into 3D scaffolds. *Biofabrication* 2010;2(1):014104.
103. Choi NW, Cabodi M, Held B, Gleghorn JP, Bonassar LJ, Stroock AD. Microfluidic scaffolds for tissue engineering. *Nat Mater* 2007;6(11):908-915.
104. Chiu DT, Jeon NL, Huang S, et al. Patterned deposition of cells and proteins onto surfaces by using three-dimensional microfluidic systems. *Proc Natl Acad Sci U S A* 2000;97(6):2408-2413.

105. Hui EE, Bhatia SN. Microscale control of cell contact and spacing via three-component surface patterning. *Langmuir* 2007;23(8):4103-4107.
106. Khademhosseini A, Langer R, Borenstein J, Vacanti JP. Microscale technologies for tissue engineering and biology. *Proc Natl Acad Sci U S A* 2006;103(8):2480-2487.
107. Yeh J, Ling Y, Karp JM, et al. Micromolding of shape-controlled, harvestable cell-laden hydrogels. *Biomaterials* 2006;27(31):5391-5398.
108. Albrecht DR, Tsang VL, Sah RL, Bhatia SN. Photo- and electropatterning of hydrogel-encapsulated living cell arrays. *Lab Chip* 2005;5(1):111-118.
109. Albrecht DR, Underhill GH, Wassermann TB, Sah RL, Bhatia SN. Probing the role of multicellular organization in three-dimensional microenvironments. *Nat Methods* 2006;3(5):369-375.
110. Guillotin B, Souquet A, Catros S, et al. Laser assisted bioprinting of engineered tissue with high cell density and microscale organization. *Biomaterials* 2010;31(28):7250-7256.
111. Xu T, Jin J, Gregory C, Hickman JJ, Boland T. Inkjet printing of viable mammalian cells. *Biomaterials* 2005;26(1):93-99.
112. Varghese D, Deshpande M, Xu T, Kesari P, Ohri S, Boland T. Advances in tissue engineering: cell printing. *J Thorac Cardiovasc Surg* 2005;129(2):470-472.
113. Xu T, Rohozinski J, Zhao W, Moorefield EC, Atala A, Yoo JJ. Inkjet-mediated gene transfection into living cells combined with targeted delivery. *Tissue Eng Part A* 2009;15(1):95-101.
114. Smith CM, Christian JJ, Warren WL, Williams SK. Characterizing environmental factors that impact the viability of tissue-engineered constructs fabricated by a direct-write bioassembly tool. *Tissue Eng* 2007;13(2):373-383.
115. Cohen DL, Malone E, Lipson H, Bonassar LJ. Direct freeform fabrication of seeded hydrogels in arbitrary geometries. *Tissue Eng* 2006;12(5):1325-1335.
116. Chang R, Nam J, Sun W. Effects of dispensing pressure and nozzle diameter on cell survival from solid freeform fabrication-based direct cell writing. *Tissue Eng Part A* 2008;14(1):41-48.
117. Fedorovich NE, De Wijn JR, Verbout AJ, Alblas J, Dhert WJ. Three-dimensional fiber deposition of cell-laden, viable, patterned constructs for bone tissue printing. *Tissue Eng Part A* 2008;14(1):127-133.
118. Lee W, Debasitis JC, Lee VK, et al. Multi-layered culture of human skin fibroblasts and keratinocytes through three-dimensional freeform fabrication. *Biomaterials* 2009;30(8):1587-1595.
119. Klein TJ, Malda J, Sah RL, Hutmacher DW. Tissue engineering of articular cartilage with biomimetic zones. *Tissue Eng Part B Rev* 2009;15(2):143-157.
120. Bhatia SN, Balis UJ, Yarmush ML, Toner M. Effect of cell-cell interactions in preservation of cellular phenotype: cocultivation of hepatocytes and nonparenchymal cells. *Faseb J* 1999;13(14):1883-1900.
121. Mironov V, Reis N, Derby B. Review: bioprinting: a beginning. *Tissue Eng* 2006;12(4):631-634.
122. Norotte C, Marga FS, Niklason LE, Forgacs G. Scaffold-free vascular tissue engineering using bioprinting. *Biomaterials* 2009;30(30):5910-5917.
123. Kelm JM, Lorber V, Snedeker JG, et al. A novel concept for scaffold-free vessel tissue engineering: self-assembly of microtissue building blocks. *J Biotechnol* 2010;148(1):46-55.
124. Pampaloni F, Reynaud EG, Stelzer EH. The third dimension bridges the gap between cell culture and live tissue. *Nat Rev Mol Cell Biol* 2007;8(10):839-845.
125. Smalley KS, Lioni M, Herlyn M. Life isn't flat: taking cancer biology to the next dimension. *In Vitro Cell Dev Biol Anim* 2006;42(8-9):242-247.
126. Griffith LG, Swartz MA. Capturing complex 3D tissue physiology in vitro. *Nat Rev Mol Cell Biol* 2006;7(3):211-224.
127. Rouwkema J, Gibbs S, Lutolf MP, Martin I, Vunjak-Novakovic G, Malda J. In vitro platforms for tissue engineering: implications to basic research and clinical translation. *Journal of Tissue Engineering and Regenerative Medicine* 2011;accepted.
128. Hollister SJ. Scaffold engineering: a bridge to where? *Biofabrication* 2009;1(1):012001.
129. Lutolf MP, Hubbell JA. Synthetic biomaterials as instructive extracellular microenvironments for morphogenesis in tissue engineering. *Nat Biotechnol* 2005;23(1):47-55.
130. Waldman SD, Spiteri CG, Grynpas MD, Pilliar RM, Hong J, Kandel RA. Effect of biomechanical conditioning on cartilaginous tissue formation in vitro. *J Bone Joint Surg Am* 2003;85-A Suppl 2:101-105.
131. Waldman SD, Spiteri CG, Grynpas MD, Pilliar RM, Kandel RA. Long-term intermittent compressive stimulation improves the composition and mechanical properties of tissue-engineered cartilage. *Tissue Eng* 2004;10(9-10):1323-1331.
132. Waldman SD, Couto DC, Grynpas MD, Pilliar RM, Kandel RA. A single application of cyclic loading can accelerate matrix deposition and enhance the properties of tissue-engineered cartilage. *Osteoarthritis Cartilage* 2006;14(4):323-330.
133. Wang X, Yan Y, Pan Y, et al. Generation of three-dimensional hepatocyte/gelatin structures with rapid prototyping system. *Tissue Eng* 2006;12(1):83-90.
134. Levenberg S, Rouwkema J, Macdonald M, et al. Engineering vascularized skeletal muscle tissue. *Nat Biotechnol* 2005;23(7):879-884.
135. Auerbach R, Lewis R, Shinners B, Kubai L, Akhtar N. Angiogenesis assays: a critical overview. *Clin Chem* 2003;49(1):32-40.
136. Olszta MJ, Cheng X, Jee AS, et al. Bone structure and formation: a new perspective. *Materials Science and Engineering* 2007;R 58:77-116.
137. Sikavitsas VI, Temenoff JS, Mikos AG. Biomaterials and bone mechanotransduction. *Biomaterials* 2001;22(19):2581-2593.
138. Weiner S, Traub W, Wagner HD. Lamellar bone: structure-function relations. *J Struct Biol* 1999;126(3):241-255.
139. Calvi LM, Adams GB, Weibrecht KW, et al. Osteoblastic cells regulate the haematopoietic stem cell niche. *Nature* 2003;425(6960):841-846.
140. Carano RA, Filvaroff EH. Angiogenesis and bone repair. *Drug Discov Today* 2003;8(21):980-989.
141. Hausman MR, Schaffler MB, Majeska RJ. Prevention of fracture healing in rats by an inhibitor of angiogenesis. *Bone* 2001;29(6):560-564.
142. Gerber HP, Vu TH, Ryan AM, Kowalski J, Werb Z, Ferrara N. VEGF couples hypertrophic cartilage remodeling, ossification and angiogenesis during endochondral bone formation. *Nat Med* 1999;5(6):623-628.
143. Hsiong SX, Mooney DJ. Regeneration of vascularized bone. *Periodontol 2000* 2006;41:109-122.

144. Gerstenfeld LC, Cullinane DM, Barnes GL, Graves DT, Einhorn TA. Fracture healing as a post-natal developmental process: molecular, spatial, and temporal aspects of its regulation. *J Cell Biochem* 2003;88(5):873-884.

145. Huang Z, Nelson ER, Smith RL, Goodman SB. The sequential expression profiles of growth factors from osteoprogenitors [correction of osteroprogenitors] to osteoblasts in vitro. *Tissue Eng* 2007;13(9):2311-2320.

146. Ferguson CM, Miclau T, Hu D, Alpern E, Helms JA. Common molecular pathways in skeletal morphogenesis and repair. *Ann N Y Acad Sci* 1998;857:33-42.

147. Yu Y, Yang JL, Chapman-Sheath PJ, Walsh WR. TGF-beta, BMPS, and their signal transducing mediators, Smads, in rat fracture healing. *J Biomed Mater Res* 2002;60(3):392-397.

148. Nilsson O, Parker EA, Hegde A, Chau M, Barnes KM, Baron J. Gradients in bone morphogenetic protein-related gene expression across the growth plate. *J Endocrinol* 2007;193(1):75-84.

149. Vunjak-Novakovic G, Freed LE. Culture of organized cell communities. *Adv Drug Deliv Rev* 1998;33(1-2):15-30.

150. Poole AR, Kojima T, Yasuda T, Mwale F, Kobayashi M, Laverty S. Composition and structure of articular cartilage: a template for tissue repair. *Clin Orthop Relat Res* 2001(391 Suppl):S26-33.

151. Darling EM, Athanasiou KA. Retaining zonal chondrocyte phenotype by means of novel growth environments. *Tissue Eng* 2005;11(3-4):395-403.

152. Mann BK, Gobin AS, Tsai AT, Schmedlen RH, West JL. Smooth muscle cell growth in photopolymerized hydrogels with cell adhesive and proteolytically degradable domains: synthetic ECM analogs for tissue engineering. *Biomaterials* 2001;22(22):3045-3051.

153. Salinas CN, Anseth KS. The enhancement of chondrogenic differentiation of human mesenchymal stem cells by enzymatically regulated RGD functionalities. *Biomaterials* 2008;29(15):2370-2377.

154. Harley BA, Hastings AZ, Yannas IV, Sannino A. Fabricating tubular scaffolds with a radial pore size gradient by a spinning technique. *Biomaterials* 2006;27(6):866-874.

155. Oh SH, Park IK, Kim JM, Lee JH. In vitro and in vivo characteristics of PCL scaffolds with pore size gradient fabricated by a centrifugation method. *Biomaterials* 2007;28(9):1664-1671.

156. Loeser RF, Pacione CA, Chubinskaya S. The combination of insulin-like growth factor 1 and osteogenic protein 1 promotes increased survival of and matrix synthesis by normal and osteoarthritic human articular chondrocytes. *Arthritis Rheum* 2003;48(8):2188-2196.

157. Loeser RF, Chubinskaya S, Pacione C, Im HJ. Basic fibroblast growth factor inhibits the anabolic activity of insulin-like growth factor 1 and osteogenic protein 1 in adult human articular chondrocytes. *Arthritis Rheum* 2005;52(12):3910-3917.

158. Chubinskaya S, Hakimiyan A, Pacione C, et al. Synergistic effect of IGF-1 and OP-1 on matrix formation by normal and OA chondrocytes cultured in alginate beads. *Osteoarthritis Cartilage* 2007;15(4):421-430.

159. Ley CD, Olsen MW, Lund EL, Kristjansen PE. Angiogenic synergy of bFGF and VEGF is antagonized by Angiopoietin-2 in a modified in vivo Matrigel assay. *Microvasc Res* 2004;68(3):161-168.

160. Carmeliet P. Angiogenesis in health and disease. *Nat Med* 2003;9(6):653-660.

161. Raiche AT, Puleo DA. In vitro effects of combined and sequential delivery of two bone growth factors. *Biomaterials* 2004;25(4):677-685.

162. Sumner DR, Turner TM, Urban RM, Virdi AS, Inoue N. Additive enhancement of implant fixation following combined treatment with rhTGF-beta2 and rhBMP-2 in a canine model. *J Bone Joint Surg Am* 2006;88(4):806-817.

163. Simmons CA, Alsberg E, Hsiong S, Kim WJ, Mooney DJ. Dual growth factor delivery and controlled scaffold degradation enhance in vivo bone formation by transplanted bone marrow stromal cells. *Bone* 2004;35(2):562-569.

164. Peng H, Wright V, Usas A, et al. Synergistic enhancement of bone formation and healing by stem cell-expressed VEGF and bone morphogenetic protein-4. *J Clin Invest* 2002;110(6):751-759.

165. Huang YC, Kaigler D, Rice KG, Krebsbach PH, Mooney DJ. Combined angiogenic and osteogenic factor delivery enhances bone marrow stromal cell-driven bone regeneration. *J Bone Miner Res* 2005;20(5):848-857.

166. Rouwkema J, de Boer J, Van Blitterswijk CA. Endothelial cells assemble into a 3-dimensional prevascular network in a bone tissue engineering construct. *Tissue Eng* 2006;12(9):2685-2693.

167. Fedorovich NE, Haverslag RT, Dhert WJ, Alblas J. The role of endothelial progenitor cells in prevascularized bone tissue engineering: development of heterogeneous constructs. *Tissue Eng Part A*;16(7):2355-2367.

168. Guillotin B, Bourget C, Remy-Zolgadri M, et al. Human primary endothelial cells stimulate human osteoprogenitor cell differentiation. *Cell Physiol Biochem* 2004;14(4-6):325-332.

169. Leung BM, Sefton MV. A modular tissue engineering construct containing smooth muscle cells and endothelial cells. *Ann Biomed Eng* 2007;35(12):2039-2049.

170. Koike N, Fukumura D, Gralla O, Au P, Schechner JS, Jain RK. Tissue engineering: creation of long-lasting blood vessels. *Nature* 2004;428(6979):138-139.

171. Elisseeff J, Puleo C, Yang F, Sharma B. Advances in skeletal tissue engineering with hydrogels. *Orthod Craniofac Res* 2005;8(3):150-161.

172. Alhadlaq A, Mao JJ. Tissue-engineered neogenesis of human-shaped mandibular condyle from rat mesenchymal stem cells. *J Dent Res* 2003;82(12):951-956.

173. Alhadlaq A, Mao JJ. Tissue-engineered osteochondral constructs in the shape of an articular condyle. *J Bone Joint Surg Am* 2005;87(5):936-944.

174. Blewis ME, Schumacher BL, Klein TJ, Schmidt TA, Voegtline MS, Sah RL. Microenvironment regulation of PRG4 phenotype of chondrocytes. *J Orthop Res* 2007;25(5):685-695.

175. Odde DJ RM. Laser-guided direct writing of living cells. *Biotechnology and Bioengineering* 2000;67:312-318.

176. Barron JA, Krizman DB, Ringeisen BR. Laser printing of single cells: statistical analysis, cell viability, and stress. *Ann Biomed Eng* 2005;33(2):121-130.

177. Hopp B, Smausz T, Kresz N, et al. Survival and proliferative ability of various living cell types after laser-induced forward transfer. *Tissue Eng* 2005;11(11-12):1817-1823.

178. Ringeisen BR, Kim H, Barron JA, et al. Laser printing of pluripotent embryonal carcinoma cells. *Tissue Eng* 2004;10(3-4):483-491.

179. Chen CS, Mrksich M, Huang S, Whitesides GM, Ingber DE. Micropatterned surfaces for control of cell shape, position, and function. *Biotechnol Prog* 1998;14(3):356-363.
180. Elloumi Hannachi I, Itoga K, Kumashiro Y, Kobayashi J, Yamato M, Okano T. Fabrication of transferable micropatterned-co-cultured cell sheets with microcontact printing. *Biomaterials* 2009;30(29):5427-5432.
181. Elisseeff J, Ferran A, Hwang S, Varghese S, Zhang Z. The role of biomaterials in stem cell differentiation: applications in the musculoskeletal system. *Stem Cells Dev* 2006;15(3):295-303.
182. Kikuchi A, Okano T. Nanostructured designs of biomedical materials: applications of cell sheet engineering to functional regenerative tissues and organs. *J Control Release* 2005;101(1-3):69-84.
183. Shimizu T, Sekine H, Isoi Y, Yamato M, Kikuchi A, Okano T. Long-term survival and growth of pulsatile myocardial tissue grafts engineered by the layering of cardiomyocyte sheets. *Tissue Eng* 2006;12(3):499-507.
184. L'Heureux N, Paquet S, Labbe R, Germain L, Auger FA. A completely biological tissue-engineered human blood vessel. *Faseb J* 1998;12(1):47-56.
185. Yang S, Leong KF, Du Z, Chua CK. The design of scaffolds for use in tissue engineering. Part II. Rapid prototyping techniques. *Tissue Eng* 2002;8(1):1-11.
186. Lam CXF MX, Teoh SH, Hutmacher DW. Scaffold development using 3D printing with a starch-based polymer. *Materials Science and Engineering C* 2002;20:49-56.
187. Landers R, Hubner U, Schmelzeisen R, Mulhaupt R. Rapid prototyping of scaffolds derived from thermoreversible hydrogels and tailored for applications in tissue engineering. *Biomaterials* 2002;23(23):4437-4447.
188. Ang TH, Sultana FSA, Hutmacher DW, et al. Fabrication of 3D chitosan-hydroxyapatitescaffolds using a robotic dispensing system. *Materials Science and Engineering C* 2002;C 20:35-42.
189. Nahmias Y, Schwartz RE, Verfaillie CM, Odde DJ. Laser-guided direct writing for three-dimensional tissue engineering. *Biotechnol Bioeng* 2005;92(2):129-136.
190. Wilson WC, Jr., Boland T. Cell and organ printing 1: protein and cell printers. *Anat Rec A Discov Mol Cell Evol Biol* 2003;272(2):491-496.
191. Stevens MM, Mayer M, Anderson DG, Weibel DB, Whitesides GM, Langer R. Direct patterning of mammalian cells onto porous tissue engineering substrates using agarose stamps. *Biomaterials* 2005;26(36):7636-7641.
192. Karp JM, Yeo Y, Geng W, et al. A photolithographic method to create cellular micropatterns. *Biomaterials* 2006;27(27):4755-4764.
193. Arcaute K, Mann BK, Wicker RB. Stereolithography of three-dimensional bioactive poly(ethylene glycol) constructs with encapsulated cells. *Ann Biomed Eng* 2006;34(9):1429-1441.
194. Dhariwala B, Hunt E, Boland T. Rapid prototyping of tissue-engineering constructs, using photopolymerizable hydrogels and stereolithography. *Tissue Eng* 2004;10(9-10):1316-1322.
195. Mapili G, Lu Y, Chen S, Roy K. Laser-layered microfabrication of spatially patterned functionalized tissue-engineering scaffolds. *J Biomed Mater Res B Appl Biomater* 2005;75(2):414-424.
196. Lu Y, Mapili G, Suhali G, Chen S, Roy K. A digital micro-mirror device-based system for the microfabrication of complex, spatially patterned tissue engineering scaffolds. *J Biomed Mater Res A* 2006;77(2):396-405.
197. Tan W, Desai TA. Layer-by-layer microfluidics for biomimetic three-dimensional structures. *Biomaterials* 2004;25(7-8):1355-1364.
198. Smith CM, Stone AL, Parkhill RL, et al. Three-dimensional bioassembly tool for generating viable tissue-engineered constructs. *Tissue Eng* 2004;10(9-10):1566-1576.
199. Hoffman AS. Hydrogels for biomedical applications. *Adv Drug Deliv Rev* 2002;54(1):3-12.
200. Hennink WE, van Nostrum CF. Novel crosslinking methods to design hydrogels. *Adv Drug Deliv Rev* 2002;54(1):13-36.
201. Nguyen KT, West JL. Photopolymerizable hydrogels for tissue engineering applications. *Biomaterials* 2002;23(22):4307-4314.
202. Jeong B, Kim SW, Bae YH. Thermosensitive sol-gel reversible hydrogels. *Adv Drug Deliv Rev* 2002;54(1):37-51.
203. Lee KY, Mooney DJ. Hydrogels for tissue engineering. *Chem Rev* 2001;101(7):1869-1879.
204. Roberts A, Wyslouzil BE, Bonassar L. Aerosol delivery of mammalian cells for tissue engineering. *Biotechnol Bioeng* 2005;91(7):801-807.
205. Nahmias Y, Arneja A, Tower TT, Renn MJ, Odde DJ. Cell patterning on biological gels via cell spraying through a mask. *Tissue Eng* 2005;11(5-6):701-708.
206. Liu Y, Chen F, Liu W, et al. Repairing large porcine full-thickness defects of articular cartilage using autologous chondrocyte-engineered cartilage. *Tissue Eng* 2002;8(4):709-721.
207. Schantz JT, Hutmacher DW, Lam CX, et al. Repair of calvarial defects with customised tissue-engineered bone grafts II. Evaluation of cellular efficiency and efficacy in vivo. *Tissue Eng* 2003;9 Suppl 1:S127-139.
208. Spitzer RS, Perka C, Lindenhayn K, Zippel H. Matrix engineering for osteogenic differentiation of rabbit periosteal cells using alpha-tricalcium phosphate particles in a three-dimensional fibrin culture. *J Biomed Mater Res* 2002;59(4):690-696.
209. Xu XL, Lou J, Tang T, et al. Evaluation of different scaffolds for BMP-2 genetic orthopedic tissue engineering. *J Biomed Mater Res B Appl Biomater* 2005;75(2):289-303.
210. Drury JL, Mooney DJ. Hydrogels for tissue engineering: scaffold design variables and applications. *Biomaterials* 2003;24(24):4337-4351.
211. Shin H, Jo S, Mikos AG. Biomimetic materials for tissue engineering. *Biomaterials* 2003;24(24):4353-4364.
212. Burdick JA, Anseth KS. Photoencapsulation of osteoblasts in injectable RGD-modified PEG hydrogels for bone tissue engineering. *Biomaterials* 2002;23(22):4315-4323.
213. Yang F, Williams CG, Wang DA, Lee H, Manson PN, Elisseeff J. The effect of incorporating RGD adhesive peptide in polyethylene glycol diacrylate hydrogel on osteogenesis of bone marrow stromal cells. *Biomaterials* 2005;26(30):5991-5998.
214. Rezania A, Healy KE. The effect of peptide surface density on mineralization of a matrix deposited by osteogenic cells. *J Biomed Mater Res* 2000;52(4):595-600.
215. Shin H, Zygourakis K, Farach-Carson MC, Yaszemski MJ, Mikos AG. Modulation of differentiation and mineralization of marrow stromal cells cultured on biomimetic hydrogels modified with Arg-Gly-Asp containing peptides. *J Biomed Mater Res A* 2004;69(3):535-543.

216. Alsberg E, Anderson KW, Albeiruti A, Franceschi RT, Mooney DJ. Cell-interactive alginate hydrogels for bone tissue engineering. *J Dent Res* 2001;80(11):2025-2029.
217. Maheshwari G, Brown G, Lauffenburger DA, Wells A, Griffith LG. Cell adhesion and motility depend on nanoscale RGD clustering. *J Cell Sci* 2000;113 (Pt 10):1677-1686.
218. Palecek SP, Loftus JC, Ginsberg MH, Lauffenburger DA, Horwitz AF. Integrin-ligand binding properties govern cell migration speed through cell-substratum adhesiveness. *Nature* 1997;385(6616):537-540.
219. Eid K, Chen E, Griffith L, Glowacki J. Effect of RGD coating on osteocompatibility of PLGA-polymer disks in a rat tibial wound. *J Biomed Mater Res* 2001;57(2):224-231.
220. Gobin AS, West JL. Cell migration through defined, synthetic ECM analogs. *Faseb J* 2002;16(7):751-753.
221. Nuttelman CR, Mortisen DJ, Henry SM, Anseth KS. Attachment of fibronectin to poly(vinyl alcohol) hydrogels promotes NIH3T3 cell adhesion, proliferation, and migration. *J Biomed Mater Res* 2001;57(2):217-223.
222. Benoit DS, Anseth KS. The effect on osteoblast function of colocalized RGD and PHSRN epitopes on PEG surfaces. *Biomaterials* 2005;26(25):5209-5220.
223. Suh JK, Matthew HW. Application of chitosan-based polysaccharide biomaterials in cartilage tissue engineering: a review. *Biomaterials* 2000;21(24):2589-2598.
224. Dee KC, Anderson TT, Bizios R. Osteoblast population migration characteristics on substrates modified with immobilized adhesive peptides. *Biomaterials* 1999;20(3):221-227.
225. Lee HJ, Lee JS, Chansakul T, Yu C, Elisseeff JH, Yu SM. Collagen mimetic peptide-conjugated photopolymerizable PEG hydrogel. *Biomaterials* 2006;27(30):5268-5276.
226. Benoit DS, Anseth KS. Heparin functionalized PEG gels that modulate protein adsorption for hMSC adhesion and differentiation. *Acta Biomater* 2005;1(4):461-470.
227. Rice MA, Anseth KS. Encapsulating chondrocytes in copolymer gels: bimodal degradation kinetics influence cell phenotype and extracellular matrix development. *J Biomed Mater Res A* 2004;70(4):560-568.
228. Alsberg E, Kong HJ, Hirano Y, Smith MK, Albeiruti A, Mooney DJ. Regulating bone formation via controlled scaffold degradation. *J Dent Res* 2003;82(11):903-908.
229. Benoit DS, Durney AR, Anseth KS. Manipulations in hydrogel degradation behavior enhance osteoblast function and mineralized tissue formation. *Tissue Eng* 2006;12(6):1663-1673.
230. Bryant SJ, Anseth KS. Hydrogel properties influence ECM production by chondrocytes photoencapsulated in poly(ethylene glycol) hydrogels. *J Biomed Mater Res* 2002;59(1):63-72.
231. Park Y, Lutolf MP, Hubbell JA, Hunziker EB, Wong M. Bovine primary chondrocyte culture in synthetic matrix metalloproteinase-sensitive poly(ethylene glycol)-based hydrogels as a scaffold for cartilage repair. *Tissue Eng* 2004;10(3-4):515-522.
232. Nuttelman CR, Tripodi MC, Anseth KS. Synthetic hydrogel niches that promote hMSC viability. *Matrix Biol* 2005;24(3):208-218.
233. Wang DA, Williams CG, Yang F, Cher N, Lee H, Elisseeff JH. Bioresponsive phosphoester hydrogels for bone tissue engineering. *Tissue Eng* 2005;11(1-2):201-213.
234. Dinbergs ID, Brown L, Edelman ER. Cellular response to transforming growth factor-beta1 and basic fibroblast growth factor depends on release kinetics and extracellular matrix interactions. *J Biol Chem* 1996;271(47):29822-29829.
235. Boontheekul T, Mooney DJ. Protein-based signaling systems in tissue engineering. *Curr Opin Biotechnol* 2003;14(5):559-565.
236. Gobin AS, West JL. Effects of epidermal growth factor on fibroblast migration through biomimetic hydrogels. *Biotechnol Prog* 2003;19(6):1781-1785.
237. Suzuki Y, Tanihara M, Suzuki K, Saitou A, Sufan W, Nishimura Y. Alginate hydrogel linked with synthetic oligopeptide derived from BMP-2 allows ectopic osteoinduction in vivo. *J Biomed Mater Res* 2000;50(3):405-409.
238. Zisch AH, Schenk U, Schense JC, Sakiyama-Elbert SE, Hubbell JA. Covalently conjugated VEGF--fibrin matrices for endothelialization. *J Control Release* 2001;72(1-3):101-113.
239. Lee KY, Peters MC, Anderson KW, Mooney DJ. Controlled growth factor release from synthetic extracellular matrices. *Nature* 2000;408(6815):998-1000.
240. Fang J, Zhu YY, Smiley E, et al. Stimulation of new bone formation by direct transfer of osteogenic plasmid genes. *Proc Natl Acad Sci U S A* 1996;93(12):5753-5758.
241. Bonadio J, Smiley E, Patil P, Goldstein S. Localized, direct plasmid gene delivery in vivo: prolonged therapy results in reproducible tissue regeneration. *Nat Med* 1999;5(7):753-759.
242. Hosseinkhani H, Inatsugu Y, Hiraoka Y, Inoue S, Shimokawa H, Tabata Y. Impregnation of plasmid DNA into three-dimensional scaffolds and medium perfusion enhance in vitro DNA expression of mesenchymal stem cells. *Tissue Eng* 2005;11(9-10):1459-1475.
243. Cao R, Brakenhielm E, Pawliuk R, et al. Angiogenic synergism, vascular stability and improvement of hind-limb ischemia by a combination of PDGF-BB and FGF-2. *Nat Med* 2003;9(5):604-613.
244. Elisseeff J, McIntosh W, Fu K, Blunk BT, Langer R. Controlled-release of IGF-I and TGF-beta1 in a photopolymerizing hydrogel for cartilage tissue engineering. *J Orthop Res* 2001;19(6):1098-1104.
245. Lee KY, Peters MC, Mooney DJ. Comparison of vascular endothelial growth factor and basic fibroblast growth factor on angiogenesis in SCID mice. *J Control Release* 2003;87(1-3):49-56.
246. Hwang NS, Varghese S, Theprungsirikul P, Canver A, Elisseeff J. Enhanced chondrogenic differentiation of murine embryonic stem cells in hydrogels with glucosamine. *Biomaterials* 2006;27(36):6015-6024.
247. Varghese S, Theprungsirikul P, Sahani S, Hwang N, Yarema KJ, Elisseeff JH. Glucosamine modulates chondrocyte proliferation, matrix synthesis, and gene expression. *Osteoarthritis Cartilage* 2007;15(1):59-68.
248. Nuttelman CR, Tripodi MC, Anseth KS. Dexamethasone-functionalized gels induce osteogenic differentiation of encapsulated hMSCs. *J Biomed Mater Res A* 2006;76(1):183-195.
249. Hutmacher DW. Scaffolds in tissue engineering bone and cartilage. *Biomaterials* 2000;21(24):2529-2543.
250. Lee KY, Rowley JA, P. E, Moy EM, Bouhadir KH, Mooney DJ. Controlling mechanical and swelling properties of alginate hydrogels independently by cross-linker type and cross-linking density. *Macromolecules* 2000;33:4291-4294.

251. Buschmann MD, Gluzband YA, Grodzinsky AJ, Hunziker EB. Mechanical compression modulates matrix biosynthesis in chondrocyte/agarose culture. *J Cell Sci* 1995;108 (Pt 4):1497-1508.

252. Ma PX, Langer R. Morphology and mechanical function of long-term in vitro engineered cartilage. *J Biomed Mater Res* 1999;44(2):217-221.

253. Martin I, Obradovic B, Treppo S, et al. Modulation of the mechanical properties of tissue engineered cartilage. *Biorheology* 2000;37(1-2):141-147.

254. Anseth KS, Bowman CN, Brannon-Peppas L. Mechanical properties of hydrogels and their experimental determination. *Biomaterials* 1996;17(17):1647-1657.

255. Benya PD, Shaffer JD. Dedifferentiated chondrocytes reexpress the differentiated collagen phenotype when cultured in agarose gels. *Cell* 1982;30(1):215-224.

256. Buschmann MD, Gluzband YA, Grodzinsky AJ, Kimura JH, Hunziker EB. Chondrocytes in agarose culture synthesize a mechanically functional extracellular matrix. *J Orthop Res* 1992;10(6):745-758.

257. Rahfoth B, Weisser J, Sternkopf F, Aigner T, von der Mark K, Brauer R. Transplantation of allograft chondrocytes embedded in agarose gel into cartilage defects of rabbits. *Osteoarthritis Cartilage* 1998;6(1):50-65.

258. Mouw JK, Case ND, Guldberg RE, Plaas AH, Levenston ME. Variations in matrix composition and GAG fine structure among scaffolds for cartilage tissue engineering. *Osteoarthritis Cartilage* 2005;13(9):828-836.

259. Huang CY, Reuben PM, D'Ippolito G, Schiller PC, Cheung HS. Chondrogenesis of human bone marrow-derived mesenchymal stem cells in agarose culture. *Anat Rec A Discov Mol Cell Evol Biol* 2004;278(1):428-436.

260. Awad HA, Wickham MQ, Leddy HA, Gimble JM, Guilak F. Chondrogenic differentiation of adipose-derived adult stem cells in agarose, alginate, and gelatin scaffolds. *Biomaterials* 2004;25(16):3211-3222.

261. Bahrami S, Stratmann U, Wiesmann HP, Mokrys K, Bruckner P, Szuwart T. Periosteally derived osteoblast-like cells differentiate into chondrocytes in suspension culture in agarose. *Anat Rec* 2000;259(2):124-130.

262. Shoichet MS LR, White ML, Winn SR. Stability of hydrogels used in cell encapsulation: an in vitro comparison of alginate and agarose. *Biotechnol Bioeng* 1996;50:374-381.

263. Gruber HE, Leslie K, Ingram J, Hoelscher G, Norton HJ, Hanley EN, Jr. Colony formation and matrix production by human anulus cells: modulation in three-dimensional culture. *Spine* 2004;29(13):E267-274.

264. Gruber HE HG, Leslie K, Ingram JA, Hanley EN. Three-dimensional culture of human disc cells within agarose or a collagen sponge: assessment of proteoglycan production. *Biomaterials* 2006;27:371-376.

265. Landers R, Pfister A, Hubner U, John H, Schmelzeisen R, Mulhaupt R. Fabrication of soft tissue engineering scaffolds by means of rapid prototyping techniques. *Journal of Materials Science* 2002;37:3107-3116.

266. Yoneno K, Ohno S, Tanimoto K, et al. Multidifferentiation potential of mesenchymal stem cells in three-dimensional collagen gel cultures. *J Biomed Mater Res A* 2005;75(3):733-741.

267. Kimura T, Yasui N, Ohsawa S, Ono K. Chondrocytes embedded in collagen gels maintain cartilage phenotype during long-term cultures. *Clin Orthop Relat Res* 1984(186):231-239.

268. van Susante JL, Buma P, van Osch GJ, et al. Culture of chondrocytes in alginate and collagen carrier gels. *Acta Orthop Scand* 1995;66(6):549-556.

269. Schuman L, Buma P, Versleyen D, et al. Chondrocyte behaviour within different types of collagen gel in vitro. *Biomaterials* 1995;16(10):809-814.

270. Nehrer S, Breinan HA, Ramappa A, et al. Chondrocyte-seeded collagen matrices implanted in a chondral defect in a canine model. *Biomaterials* 1998;19(24):2313-2328.

271. Wakitani S, Goto T, Young RG, Mansour JM, Goldberg VM, Caplan AI. Repair of large full-thickness articular cartilage defects with allograft articular chondrocytes embedded in a collagen gel. *Tissue Eng* 1998;4(4):429-444.

272. Dorotka R, Bindreiter U, Vavken P, Nehrer S. Behavior of human articular chondrocytes derived from nonarthritic and osteoarthritic cartilage in a collagen matrix. *Tissue Eng* 2005;11(5-6):877-886.

273. Gruber HE, Leslie K, Ingram J, Norton HJ, Hanley EN. Cell-based tissue engineering for the intervertebral disc: in vitro studies of human disc cell gene expression and matrix production within selected cell carriers. *Spine J* 2004;4(1):44-55.

274. Sakai D, Mochida J, Iwashina T, et al. Regenerative effects of transplanting mesenchymal stem cells embedded in atelocollagen to the degenerated intervertebral disc. *Biomaterials* 2006;27(3):335-345.

275. Riew KD, Wright NM, Cheng S, Avioli LV, Lou J. Induction of bone formation using a recombinant adenoviral vector carrying the human BMP-2 gene in a rabbit spinal fusion model. *Calcif Tissue Int* 1998;63(4):357-360.

276. Winn SR, Schmitt JM, Buck D, Hu Y, Grainger D, Hollinger JO. Tissue-engineered bone biomimetic to regenerate calvarial critical-sized defects in athymic rats. *J Biomed Mater Res* 1999;45(4):414-421.

277. Tsuchida H, Hashimoto J, Crawford E, Manske P, Lou J. Engineered allogeneic mesenchymal stem cells repair femoral segmental defect in rats. *J Orthop Res* 2003;21(1):44-53.

278. Riew KD, Lou J, Wright NM, Cheng SL, Bae KT, Avioli LV. Thoracoscopic intradiscal spine fusion using a minimally invasive gene-therapy technique. *J Bone Joint Surg Am* 2003;85-A(5):866-871.

279. Wiesmann HP, Nazer N, Klatt C, Szuwart T, Meyer U. Bone tissue engineering by primary osteoblast-like cells in a monolayer system and 3-dimensional collagen gel. *J Oral Maxillofac Surg* 2003;61(12):1455-1462.

280. Nehrer S, Breinan HA, Ramappa A, et al. Canine chondrocytes seeded in type I and type II collagen implants investigated in vitro. *J Biomed Mater Res* 1997;38(2):95-104.

281. Nehrer S, Breinan HA, Ramappa A, et al. Matrix collagen type and pore size influence behaviour of seeded canine chondrocytes. *Biomaterials* 1997;18(11):769-776.

282. Veilleux NH, Yannas IV, Spector M. Effect of passage number and collagen type on the proliferative, biosynthetic, and contractile activity of adult canine articular chondrocytes in type I and II collagen-glycosaminoglycan matrices in vitro. *Tissue Eng* 2004;10(1-2):119-127.

283. Bosnakovski D, Mizuno M, Kim G, Takagi S, Okumura M, Fujinaga T. Chondrogenic differentiation of bovine bone marrow mesenchymal stem cells (MSCs) in different hydrogels: influence of collagen type II extracellular matrix on MSC chondrogenesis. *Biotechnol Bioeng* 2006;93(6):1152-1163.

284. Awad HA, Butler DL, Boivin GP, et al. Autologous mesenchymal stem cell-mediated repair of tendon. *Tissue Eng* 1999;5(3):267-277.

285. Diduch DR, Jordan LC, Mierisch CM, Balian G. Marrow stromal cells embedded in alginate for repair of osteochondral defects. *Arthroscopy* 2000;16(6):571-577.

286. Ponticiello MS, Schinagl RM, Kadiyala S, Barry FP. Gelatin-based resorbable sponge as a carrier matrix for human mesenchymal stem cells in cartilage regeneration therapy. *J Biomed Mater Res* 2000;52(2):246-255.

287. Payne RG, Yaszemski MJ, Yasko AW, Mikos AG. Development of an injectable, in situ crosslinkable, degradable polymeric carrier for osteogenic cell populations. Part 1. Encapsulation of marrow stromal osteoblasts in surface crosslinked gelatin microparticles. *Biomaterials* 2002;23(22):4359-4371.

288. Vukicevic S, Luyten FP, Kleinman HK, Reddi AH. Differentiation of canalicular cell processes in bone cells by basement membrane matrix components: regulation by discrete domains of laminin. *Cell* 1990;63(2):437-445.

289. Mikuni-Takagaki Y, Kakai Y, Satoyoshi M, et al. Matrix mineralization and the differentiation of osteocyte-like cells in culture. *J Bone Miner Res* 1995;10(2):231-242.

290. Hara A, Ikeda T, Nomura S, Yagita H, Okumura K, Yamauchi Y. In vivo implantation of human osteosarcoma cells in nude mice induces bones with human-derived osteoblasts and mouse-derived osteocytes. *Lab Invest* 1996;75(5):707-717.

291. Cui Q, Ming Xiao Z, Balian G, Wang GJ. Comparison of lumbar spine fusion using mixed and cloned marrow cells. *Spine* 2001;26(21):2305-2310.

292. Malonne H, Eeckman F, Fontaine D, et al. Preparation of poly(N-isopropylacrylamide) copolymers and preliminary assessment of their acute and subacute toxicity in mice. *Eur J Pharm Biopharm* 2005;61(3):188-194.

293. Shimizu T, Yamato M, Kikuchi A, Okano T. Two-dimensional manipulation of cardiac myocyte sheets utilizing temperature-responsive culture dishes augments the pulsatile amplitude. *Tissue Eng* 2001;7(2):141-151.

294. Ohya S, Nakayama Y, Matsuda T. Thermoresponsive artificial extracellular matrix for tissue engineering: hyaluronic acid bioconjugated with poly(N-isopropylacrylamide) grafts. *Biomacromolecules* 2001;2(3):856-863.

295. Kwon IK, Matsuda T. Photo-iniferter-based thermoresponsive block copolymers composed of poly(ethylene glycol) and poly(N-isopropylacrylamide) and chondrocyte immobilization. *Biomaterials* 2006;27(7):986-995.

296. An YH, Webb D, Gutowska A, Mironov VA, Friedman RJ. Regaining chondrocyte phenotype in thermosensitive gel culture. *Anat Rec* 2001;263(4):336-341.

297. Stile RA BW, Healy KE. Synthesis and characterisation of injectable Poly(N-isopropylacrylamide)-based hydorgels that support tissue formation in vitro. *Macromolecules* 1999;32:7370-7379.

298. Stile RA, Healy KE. Thermo-responsive peptide-modified hydrogels for tissue regeneration. *Biomacromolecules* 2001;2(1):185-194.

299. Park KH, Na K, Chung HM. Enhancement of the adhesion of fibroblasts by peptide containing an Arg-Gly-Asp sequence with poly(ethylene glycol) into a thermo-reversible hydrogel as a synthetic extracellular matrix. *Biotechnol Lett* 2005;27(4):227-231.

300. Ibusuki S, Iwamoto Y, Matsuda T. System-engineered cartilage using poly(N-isopropylacrylamide)-grafted gelatin as in situ-formable scaffold: in vivo performance. *Tissue Eng* 2003;9(6):1133-1142.

301. Kim S, Chung EH, Gilbert M, Healy KE. Synthetic MMP-13 degradable ECMs based on poly(N-isopropylacrylamide-co-acrylic acid) semi-interpenetrating polymer networks. I. Degradation and cell migration. *J Biomed Mater Res A* 2005;75(1):73-88.

302. Kim YS, Lim JY, Donahue HJ, Lowe TL. Thermoresponsive terpolymeric films applicable for osteoblastic cell growth and noninvasive cell sheet harvesting. *Tissue Eng* 2005;11(1-2):30-40.

303. Ron ES, Bromberg LE. Temperature-responsive gels and thermogelling polymer matrices for protein and peptide delivery. *Adv Drug Deliv Rev* 1998;31(3):197-221.

304. Khattak SF, Bhatia SR, Roberts SC. Pluronic F127 as a cell encapsulation material: utilization of membrane-stabilizing agents. *Tissue Eng* 2005;11(5-6):974-983.

305. Cao YL, Lach E, Kim TH, Rodriguez A, Arevalo CA, Vacanti CA. Tissue-engineered nipple reconstruction. *Plast Reconstr Surg* 1998;102(7):2293-2298.

306. Kamil SH, Eavey RD, Vacanti MP, Vacanti CA, Hartnick CJ. Tissue-engineered cartilage as a graft source for laryngotracheal reconstruction: a pig model. *Arch Otolaryngol Head Neck Surg* 2004;130(9):1048-1051.

307. Terada S, Yoshimoto H, Fuchs JR, et al. Hydrogel optimization for cultured elastic chondrocytes seeded onto a polyglycolic acid scaffold*. *J Biomed Mater Res A* 2005;75(4):907-916.

308. Cellesi F, Tirelli N, Hubbell JA. Towards a fully-synthetic substitute of alginate: development of a new process using thermal gelation and chemical cross-linking. *Biomaterials* 2004;25(21):5115-5124.

309. Sims CD, Butler PE, Casanova R, et al. Injectable cartilage using polyethylene oxide polymer substrates. *Plast Reconstr Surg* 1996;98(5):843-850.

310. Chen F, Mao T, Tao K, Chen S, Ding G, Gu X. Injectable bone. *British Journal of Oral and Maxillofacial Surgery* 2003;41:240-243.

311. Jeong B, Gutowska A. Lessons from nature: stimuli-responsive polymers and their biomedical applications. *Trends Biotechnol* 2002;20(7):305-311.

312. Behravesh E, Jo S, Zygourakis K, Mikos AG. Synthesis of in situ cross-linkable macroporous biodegradable poly(propylene fumarate-co-ethylene glycol) hydrogels. *Biomacromolecules* 2002;3(2):374-381.

313. Suggs LJ, Mikos AG. Development of poly(propylene fumarate-co-ethylene glycol) as an injectable carrier for endothelial cells. *Cell Transplant* 1999;8(4):345-350.

314. Fisher JP, Jo S, Mikos AG, Reddi AH. Thermoreversible hydrogel scaffolds for articular cartilage engineering. *J Biomed Mater Res A* 2004;71(2):268-274.

315. Peter SJ, Lu L, Kim DJ, Mikos AG. Marrow stromal osteoblast function on a poly(propylene fumarate)/beta-tricalcium phosphate biodegradable orthopaedic composite. *Biomaterials* 2000;21(12):1207-1213.

316. Behravesh E, Zygourakis K, Mikos AG. Adhesion and migration of marrow-derived osteoblasts on injectable in situ crosslinkable poly(propylene fumarate-co-ethylene glycol)-based hydrogels with a covalently linked RGDS peptide. *J Biomed Mater Res A* 2003;65(2):260-270.

317. Payne RG, McGonigle JS, Yaszemski MJ, Yasko AW, Mikos AG. Development of an injectable, in situ crosslinkable, degradable polymeric carrier for osteogenic cell populations. Part 3. Proliferation and differentiation of encapsulated marrow stromal osteoblasts cultured on crosslinking poly(propylene fumarate). *Biomaterials* 2002;23(22):4381-4387.

318. Molinaro G, Leroux JC, Damas J, Adam A. Biocompatibility of thermosensitive chitosan-based hydrogels: an in vivo experimental approach to injectable biomaterials. *Biomaterials* 2002;23(13):2717-2722.

319. Chenite A, Chaput C, Wang D, et al. Novel injectable neutral solutions of chitosan form biodegradable gels in situ. *Biomaterials* 2000;21(21):2155-2161.

320. Hoemann CD, Sun J, Legare A, McKee MD, Buschmann MD. Tissue engineering of cartilage using an injectable and adhesive chitosan-based cell-delivery vehicle. *Osteoarthritis Cartilage* 2005;13(4):318-329.

321. Klokkevold PR, Vandemark L, Kenney EB, Bernard GW. Osteogenesis enhanced by chitosan (poly-N-acetyl glucosaminoglycan) in vitro. *J Periodontol* 1996;67(11):1170-1175.

322. Roughley P, Hoemann C, DesRosiers E, Mwale F, Antoniou J, Alini M. The potential of chitosan-based gels containing intervertebral disc cells for nucleus pulposus supplementation. *Biomaterials* 2006;27(3):388-396.

323. Dang JM, Sun DD, Shin-Ya Y, Sieber AN, Kostuik JP, Leong KW. Temperature-responsive hydroxybutyl chitosan for the culture of mesenchymal stem cells and intervertebral disk cells. *Biomaterials* 2006;27(3):406-418.

324. Di Martino A, Sittinger M, Risbud MV. Chitosan: a versatile biopolymer for orthopaedic tissue-engineering. *Biomaterials* 2005;26(30):5983-5990.

325. Santa-Comba A, Pereira A, Lemos R, et al. Evaluation of carboxymethylcellulose, hydroxypropylmethylcellulose, and aluminum hydroxide as potential carriers for rhBMP-2. *J Biomed Mater Res* 2001;55(3):396-400.

326. Daculsi G, Weiss P, Bouler JM, Gauthier O, Millot F, Aguado E. Biphasic calcium phosphate/hydrosoluble polymer composites: a new concept for bone and dental substitution biomaterials. *Bone* 1999;25(2 Suppl):59S-61S.

327. Trojani C, Weiss P, Michiels JF, et al. Three-dimensional culture and differentiation of human osteogenic cells in an injectable hydroxypropylmethylcellulose hydrogel. *Biomaterials* 2005;26(27):5509-5517.

328. Vinatier C, Magne D, Weiss P, et al. A silanized hydroxypropyl methylcellulose hydrogel for the three-dimensional culture of chondrocytes. *Biomaterials* 2005;26(33):6643-6651.

329. Trivedi N, Keegan M, Steil GM, et al. Islets in alginate macrobeads reverse diabetes despite minimal acute insulin secretory responses. *Transplantation* 2001;71(2):203-211.

330. Atala A, Kim W, Paige KT, Vacanti CA, Retik AB. Endoscopic treatment of vesicoureteral reflux with a chondrocyte-alginate suspension. *J Urol* 1994;152(2 Pt 2):641-643; discussion 644.

331. Grandolfo M, D'Andrea P, Paoletti S, et al. Culture and differentiation of chondrocytes entrapped in alginate gels. *Calcif Tissue Int* 1993;52(1):42-48.

332. Hauselmann HJ, Fernandes RJ, Mok SS, et al. Phenotypic stability of bovine articular chondrocytes after long-term culture in alginate beads. *J Cell Sci* 1994;107 (Pt 1):17-27.

333. Gagne TA, Chappell-Afonso K, Johnson JL, et al. Enhanced proliferation and differentiation of human articular chondrocytes when seeded at low cell densities in alginate in vitro. *J Orthop Res* 2000;18(6):882-890.

334. Wong M, Siegrist M, Gaschen V, Park Y, Graber W, Studer D. Collagen fibrillogenesis by chondrocytes in alginate. *Tissue Eng* 2002;8(6):979-987.

335. Fragonas E, Valente M, Pozzi-Mucelli M, et al. Articular cartilage repair in rabbits by using suspensions of allogenic chondrocytes in alginate. *Biomaterials* 2000;21(8):795-801.

336. Chang SC, Rowley JA, Tobias G, et al. Injection molding of chondrocyte/alginate constructs in the shape of facial implants. *J Biomed Mater Res* 2001;55(4):503-511.

337. Erickson GR, Gimble JM, Franklin DM, Rice HE, Awad H, Guilak F. Chondrogenic potential of adipose tissue-derived stromal cells in vitro and in vivo. *Biochem Biophys Res Commun* 2002;290(2):763-769.

338. Steinert A, Weber M, Dimmler A, et al. Chondrogenic differentiation of mesenchymal progenitor cells encapsulated in ultrahigh-viscosity alginate. *J Orthop Res* 2003;21(6):1090-1097.

339. Majmudar G, Bole D, Goldstein SA, Bonadio J. Bone cell culture in a three-dimensional polymer bead stabilizes the differentiated phenotype and provides evidence that osteoblastic cells synthesize type III collagen and fibronectin. *J Bone Miner Res* 1991;6(8):869-881.

340. Kuo CK, Ma PX. Ionically crosslinked alginate hydrogels as scaffolds for tissue engineering: part 1. Structure, gelation rate and mechanical properties. *Biomaterials* 2001;22(6):511-521.

341. Shang Q, Wang Z, Liu W, Shi Y, Cui L, Cao Y. Tissue-engineered bone repair of sheep cranial defects with autologous bone marrow stromal cells. *J Craniofac Surg* 2001;12(6):586-593; discussion 594-585.

342. Lee KY, Alsberg E, Mooney DJ. Degradable and injectable poly(aldehyde guluronate) hydrogels for bone tissue engineering. *J Biomed Mater Res* 2001;56(2):228-233.

343. Iwashina T, Mochida J, Miyazaki T, et al. Low-intensity pulsed ultrasound stimulates cell proliferation and proteoglycan production in rabbit intervertebral disc cells cultured in alginate. *Biomaterials* 2006;27(3):354-361.

344. Risbud MV, Albert TJ, Guttapalli A, et al. Differentiation of mesenchymal stem cells towards a nucleus pulposus-like phenotype in vitro: implications for cell-based transplantation therapy. *Spine* 2004;29(23):2627-2632.

345. Wong M, Siegrist M, Wang X, Hunziker E. Development of mechanically stable alginate/chondrocyte constructs: effects of guluronic acid content and matrix synthesis. *J Orthop Res* 2001;19(3):493-499.

346. Wang L, Shelton RM, Cooper PR, Lawson M, Triffitt JT, Barralet JE. Evaluation of sodium alginate for bone marrow cell tissue engineering. *Biomaterials* 2003;24(20):3475-3481.

347. Bouhadir KH, Lee KY, Alsberg E, Damm KL, Anderson KW, Mooney DJ. Degradation of partially oxidized alginate and its potential application for tissue engineering. *Biotechnol Prog* 2001;17(5):945-950.

348. Lawson MA, Barralet JE, Wang L, Shelton RM, Triffitt JT. Adhesion and growth of bone marrow stromal cells on modified alginate hydrogels. *Tissue Eng* 2004;10(9-10):1480-1491.

349. Bryant SJ, Nuttelman CR, Anseth KS. Cytocompatibility of UV and visible light photoinitiating systems on cultured NIH/3T3 fibroblasts in vitro. *J Biomater Sci Polym Ed* 2000;11(5):439-457.

350. Williams CG, Malik AN, Kim TK, Manson PN, Elisseeff JH. Variable cytocompatibility of six cell lines with photoinitiators used for polymerizing hydrogels and cell encapsulation. *Biomaterials* 2005;26(11):1211-1218.

351. Elisseeff J, McIntosh W, Anseth K, Riley S, Ragan P, Langer R. Photoencapsulation of chondrocytes in poly(ethylene oxide)-based semi-interpenetrating networks. *J Biomed Mater Res* 2000;51(2):164-171.

352. Bryant SJ, Anseth KS. The effects of scaffold thickness on tissue engineered cartilage in photocrosslinked poly(ethylene oxide) hydrogels. *Biomaterials* 2001;22(6):619-626.

353. Williams CG, Kim TK, Taboas A, Malik A, Manson P, Elisseeff J. In vitro chondrogenesis of bone marrow-derived mesenchymal stem cells in a photopolymerizing hydrogel. *Tissue Eng* 2003;9(4):679-688.

354. Elisseeff J, Anseth K, Sims D, McIntosh W, Randolph M, Langer R. Transdermal photopolymerization for minimally invasive implantation. *Proc Natl Acad Sci U S A* 1999;96(6):3104-3107.

355. Nuttelman CR, Tripodi MC, Anseth KS. In vitro osteogenic differentiation of human mesenchymal stem cells photoencapsulated in PEG hydrogels. *J Biomed Mater Res A* 2004;68(4):773-782.

356. Paradossi G, Cavalieri F, Chiessi E, Spagnoli C, Cowman MK. Poly(vinyl alcohol) as versatile biomaterial for potential biomedical applications. *J Mater Sci Mater Med* 2003;14(8):687-691.

357. Oka M, Noguchi T, Kumar P, et al. Development of an artificial articular cartilage. *Clin Mater* 1990;6(4):361-381.

358. Kobayashi M, Toguchida J, Oka M. Development of the shields for tendon injury repair using polyvinyl alcohol--hydrogel (PVA-H). *J Biomed Mater Res* 2001;58(4):344-351.

359. Anseth KS, Metters AT, Bryant SJ, Martens PJ, Elisseeff JH, Bowman CN. In situ forming degradable networks and their application in tissue engineering and drug delivery. *J Control Release* 2002;78(1-3):199-209.

360. Schmedlen RH, Masters KS, West JL. Photocrosslinkable polyvinyl alcohol hydrogels that can be modified with cell adhesion peptides for use in tissue engineering. *Biomaterials* 2002;23(22):4325-4332.

361. Martens PJ, Bryant SJ, Anseth KS. Tailoring the degradation of hydrogels formed from multivinyl poly(ethylene glycol) and poly(vinyl alcohol) macromers for cartilage tissue engineering. *Biomacromolecules* 2003;4(2):283-292.

362. Nuttelman CR, Henry SM, Anseth KS. Synthesis and characterization of photocrosslinkable, degradable poly(vinyl alcohol)-based tissue engineering scaffolds. *Biomaterials* 2002;23(17):3617-3626.

363. Radice M, Brun P, Cortivo R, Scapinelli R, Battaliard C, Abatangelo G. Hyaluronan-based biopolymers as delivery vehicles for bone-marrow-derived mesenchymal progenitors. *J Biomed Mater Res* 2000;50(2):101-109.

364. Lisignoli G, Fini M, Giavaresi G, Nicoli AN, Toneguzzi S, Facchini A. Osteogenesis of large segmental radius defects enhanced by basic fibroblast growth factor activated bone marrow stromal cells grown on non-woven hyaluronic acid-based polymer scaffold. *Biomaterials* 2002;23(4):1043-1051.

365. Solchaga LA, Gao J, Dennis JE, et al. Treatment of osteochondral defects with autologous bone marrow in a hyaluronan-based delivery vehicle. *Tissue Eng* 2002;8(2):333-347.

366. Cristino S, Grassi F, Toneguzzi S, et al. Analysis of mesenchymal stem cells grown on a three-dimensional HYAFF 11-based prototype ligament scaffold. *J Biomed Mater Res A* 2005;73(3):275-283.

367. Shu XZ, Ghosh K, Liu Y, et al. Attachment and spreading of fibroblasts on an RGD peptide-modified injectable hyaluronan hydrogel. *J Biomed Mater Res A* 2004;68(2):365-375.

368. Masters KS, Shah DN, Leinwand LA, Anseth KS. Crosslinked hyaluronan scaffolds as a biologically active carrier for valvular interstitial cells. *Biomaterials* 2005;26(15):2517-2525.

369. Silverman RP, Passaretti D, Huang W, Randolph MA, Yaremchuk MJ. Injectable tissue-engineered cartilage using a fibrin glue polymer. *Plast Reconstr Surg* 1999;103(7):1809-1818.

370. Peretti GM, Xu JW, Bonassar LJ, Kirchhoff CH, Yaremchuk MJ, Randolph MA. Review of Injectable Cartilage Engineering Using Fibrin Gel in Mice and Swine Models. *Tissue Eng* 2006.

371. Perka C, Spitzer RS, Lindenhayn K, Sittinger M, Schultz O. Matrix-mixed culture: new methodology for chondrocyte culture and preparation of cartilage transplants. *J Biomed Mater Res* 2000;49(3):305-311.

372. Passaretti D, Silverman RP, Huang W, et al. Cultured chondrocytes produce injectable tissue-engineered cartilage in hydrogel polymer. *Tissue Eng* 2001;7(6):805-815.

373. Meinhart J, Fussenegger M, Hobling W. Stabilization of fibrin-chondrocyte constructs for cartilage reconstruction. *Ann Plast Surg* 1999;42(6):673-678.

374. Fussenegger M, Meinhart J, Hobling W, Kullich W, Funk S, Bernatzky G. Stabilized autologous fibrin-chondrocyte constructs for cartilage repair in vivo. *Ann Plast Surg* 2003;51(5):493-498.

375. Yamada Y, Boo JS, Ozawa R, et al. Bone regeneration following injection of mesenchymal stem cells and fibrin glue with a biodegradable scaffold. *J Craniomaxillofac Surg* 2003;31(1):27-33.

376. Temenoff JS, Park H, Jabbari E, et al. Thermally cross-linked oligo(poly(ethylene glycol) fumarate) hydrogels support osteogenic differentiation of encapsulated marrow stromal cells in vitro. *Biomacromolecules* 2004;5(1):5-10.

377. Shin H, Quinten Ruhe P, Mikos AG, Jansen JA. In vivo bone and soft tissue response to injectable, biodegradable oligo(poly(ethylene glycol) fumarate) hydrogels. *Biomaterials* 2003;24(19):3201-3211.

378. Yang J, Xu C, Wang C, Kopecek J. Refolding Hydrogels Self-Assembled from N-(2-Hydroxypropyl)methacrylamide Graft Copolymers by Antiparallel Coiled-Coil Formation. *Biomacromolecules* 2006;7(4):1187-1195.

379. Li J, Li X, Ni X, Wang X, Li H, Leong KW. Self-assembled supramolecular hydrogels formed by biodegradable PEO-PHB-PEO triblock copolymers and alpha-cyclodextrin for controlled drug delivery. *Biomaterials* 2006;27(22):4132-4140.

380. Kisiday J, Jin M, Kurz B, et al. Self-assembling peptide hydrogel fosters chondrocyte extracellular matrix production and cell division: implications for cartilage tissue repair. *Proc Natl Acad Sci U S A* 2002;99(15):9996-10001.

381. Hosseinkhani H, Hosseinkhani M, Tian F, Kobayashi H, Tabata Y. Osteogenic differentiation of mesenchymal stem cells in self-assembled peptide-amphiphile nanofibers. *Biomaterials* 2006;27(22):4079-4086.

382. Van Tomme SR, van Steenbergen MJ, De Smedt SC, van Nostrum CF, Hennink WE. Self-gelling hydrogels based on oppositely charged dextran microspheres. *Biomaterials* 2005;26(14):2129-2135.

383. Hennink WE, De Jong SJ, Bos GW, Veldhuis TF, van Nostrum CF. Biodegradable dextran hydrogels crosslinked by stereocomplex formation for the controlled release of pharmaceutical proteins. *Int J Pharm* 2004;277(1-2):99-104.

384. Yamaoka H, Asato H, Ogasawara T, et al. Cartilage tissue engineering using human auricular chondrocytes embedded in different hydrogel materials. *J Biomed Mater Res A* 2006;78(1):1-11.

385. Weinand C, Pomerantseva I, Neville CM, et al. Hydrogel-beta-TCP scaffolds and stem cells for tissue engineering bone. *Bone* 2006;38(4):555-563.

386. Sittinger M, Bujia J, Rotter N, Reitzel D, Minuth WW, Burmester GR. Tissue engineering and autologous transplant formation: practical approaches with resorbable biomaterials and new cell culture techniques. *Biomaterials* 1996;17(3):237-242.

387. Engler AJ, Sen S, Sweeney HL, Discher DE. Matrix elasticity directs stem cell lineage specification. *Cell* 2006;126(4):677-689.

388. Dhiman HK, Ray AR, Panda AK. Three-dimensional chitosan scaffold-based MCF-7 cell culture for the determination of the cytotoxicity of tamoxifen. *Biomaterials* 2005;26(9):979-986.

389. Park A, Wu B, Griffith LG. Integration of surface modification and 3D fabrication techniques to prepare patterned poly(L-lactide) substrates allowing regionally selective cell adhesion. *J Biomater Sci Polym Ed* 1998;9(2):89-110.

390. Farrell E, O'Brien F J, Doyle P, et al. A Collagen-glycosaminoglycan Scaffold Supports Adult Rat Mesenchymal Stem Cell Differentiation Along Osteogenic and Chondrogenic Routes. *Tissue Eng* 2006;12(3):459-468.

391. Hwang NS, Varghese S, Theprungsirikul P, Canver A, Elisseeff J. Enhanced chondrogenic differentiation of murine embryonic stem cells in hydrogels with glucosamine. *Biomaterials* 2006.

392. Sawhney AS, Pathak CP, Hubbell JA. Bioerodible hydrogels based on photopolymerized poly(ethylene glycol)-co-poly(alpha-hydorxy acid) diacrylate macromers. *Macromolecules* 1993;26:581-587.

393. Halstenberg S, Panitch A, Rizzi S, Hall H, Hubbell JA. Biologically engineered protein-graft-poly(ethylene glycol) hydrogels: a cell adhesive and plasmin-degradable biosynthetic material for tissue repair. *Biomacromolecules* 2002;3(4):710-723.

394. West JL, Hubbell JA. Polymeric biomaterials with degradation sites for proteases involved in cell migration. *Macromolecules* 1999;32:241-244.

395. Bryant SJ, Anseth KS. Controlling the spatial distribution of ECM components in degradable PEG hydrogels for tissue engineering cartilage. *J Biomed Mater Res A* 2003;64(1):70-79.

396. Lutolf MP, Weber FE, Schmoekel HG, et al. Repair of bone defects using synthetic mimetics of collagenous extracellular matrices. *Nat Biotechnol* 2003;21(5):513-518.

397. Shin H, Temenoff JS, Bowden GC, et al. Osteogenic differentiation of rat bone marrow stromal cells cultured on Arg-Gly-Asp modified hydrogels without dexamethasone and beta-glycerol phosphate. *Biomaterials* 2005;26(17):3645-3654.

398. Peretti GM, Xu JW, Bonassar LJ, Kirchhoff CH, Yaremchuk MJ, Randolph MA. Review of injectable cartilage engineering using fibrin gel in mice and swine models. *Tissue Eng* 2006;12(5):1151-1168.

399. van Susante JL, Buma P, Schuman L, Homminga GN, van den Berg WB, Veth RP. Resurfacing potential of heterologous chondrocytes suspended in fibrin glue in large full-thickness defects of femoral articular cartilage: an experimental study in the goat. *Biomaterials* 1999;20(13):1167-1175.

400. Endres M, Hutmacher DW, Salgado AJ, et al. Osteogenic induction of human bone marrow-derived mesenchymal progenitor cells in novel synthetic polymer-hydrogel matrices. *Tissue Eng* 2003;9(4):689-702.

401. Temenoff JS, Park H, Jabbari E, et al. In vitro osteogenic differentiation of marrow stromal cells encapsulated in biodegradable hydrogels. *J Biomed Mater Res A* 2004;70(2):235-244.

402. Stern S, Lindenhayn K, Schultz O, Perka C. Cultivation of porcine cells from the nucleus pulposus in a fibrin/hyaluronic acid matrix. *Acta Orthop Scand* 2000;71(5):496-502.

403. Noth U, Schupp K, Heymer A, et al. Anterior cruciate ligament constructs fabricated from human mesenchymal stem cells in a collagen type I hydrogel. *Cytotherapy* 2005;7(5):447-455.

404. Patel N, Padera R, Sanders GH, et al. Spatially controlled cell engineering on biodegradable polymer surfaces. *Faseb J* 1998;12(14):1447-1454.

405. Malda J, Woodfield TB, van der Vloodt F, et al. The effect of PEGT/PBT scaffold architecture on oxygen gradients in tissue engineered cartilaginous constructs. *Biomaterials* 2004;25(26):5773-5780.

406. Mironov V. Printing technology to produce living tissue. *Expert Opin Biol Ther* 2003;3(5):701-704.

407. Fedorovich NE, Alblas J, de Wijn JR, Hennink WE, Verbout AJ, Dhert WJ. Hydrogels as extracellular matrices for skeletal tissue engineering: state-of-the-art and novel application in organ printing. *Tissue Eng* 2007;13(8):1905-1925.

408. Peppas NA, Hilt, J.Z., Khademhosseini, A., Langer, R. Hydrogels in biology and medicine: from molecular principles to bionanotechnology. *Advanced Materials* 2006;18:1345-1360.

409. Vermonden T, Fedorovich NE, van Geemen D, et al. Photopolymerized thermosensitive hydrogels: synthesis, degradation, and cytocompatibility. *Biomacromolecules* 2008;9(3):919-926.

410. Lu S, Ramirez WF, Anseth KS. Photopolymerized, multilaminated matrix devices with optimized nonuniform initial concentration profiles to control drug release. *J Pharm Sci* 2000;89(1):45-51.

411. Sharma B, Williams CG, Khan M, Manson P, Elisseeff JH. In vivo chondrogenesis of mesenchymal stem cells in a photopolymerized hydrogel. *Plast Reconstr Surg* 2007;119(1):112-120.

412. Mann BK, Schmedlen RH, West JL. Tethered-TGF-beta increases extracellular matrix production of vascular smooth muscle cells. *Biomaterials* 2001;22(5):439-444.

413. Chun KW, Lee JB, Kim SH, Park TG. Controlled release of plasmid DNA from photo-cross-linked pluronic hydrogels. *Biomaterials* 2005;26(16):3319-3326.

414. Lu S, Anseth KS. Photopolymerization of multilaminated poly(HEMA) hydrogels for controlled release. *J Control Release* 1999;57(3):291-300.

415. Anseth KS, Shastri VR, Langer R. Photopolymerizable degradable polyanhydrides with osteocompatibility. *Nat Biotechnol* 1999;17(2):156-159.

416. Li Q, Wang J, Shahani S, et al. Biodegradable and photocrosslinkable polyphosphoester hydrogel. *Biomaterials* 2006;27(7):1027-1034.

417. Lisby S, Gniadecki R, Wulf HC. UV-induced DNA damage in human keratinocytes: quantitation and correlation with long-term survival. *Exp Dermatol* 2005;14(5):349-355.

418. Henriksen EK, Moan J, Kaalhus O, Brunborg G. Induction and repair of DNA damage in UV-irradiated human lymphocytes. Spectral differences and repair kinetics. *J Photochem Photobiol B* 1996;32(1-2):39-48.

419. Wang B, Matsuoka S, Carpenter PB, Elledge SJ. 53BP1, a mediator of the DNA damage checkpoint. *Science* 2002;298(5597):1435-1438.

420. Abraham RT. Checkpoint signalling: focusing on 53BP1. *Nat Cell Biol* 2002;4(12):E277-279.

421. Hanks CT, Strawn SE, Wataha JC, Craig RG. Cytotoxic effects of resin components on cultured mammalian fibroblasts. *J Dent Res* 1991;70(11):1450-1455.

422. Cruise GM, Hegre OD, Scharp DS, Hubbell JA. A sensitivity study of the key parameters in the interfacial photopolymerization of poly(ethylene glycol) diacrylate upon porcine islets. *Biotechnol Bioeng* 1998;57(6):655-665.

423. Oudshoorn MH, Rissman, R., Bouwstra, J.A., Hennink, W.E,. Synthesis of methacrylated hyaluronic acid with tailored degree of substitution. *Polymer* 2007;48:1915-1920.

424. Oudshoorn MH, Rissmann R, Bouwstra JA, Hennink WE. Synthesis and characterization of hyperbranched polyglycerol hydrogels. *Biomaterials* 2006;27(32):5471-5479.

425. Scholzen T, Gerdes J. The Ki-67 protein: from the known and the unknown. *J Cell Physiol* 2000;182(3):311-322.

426. Dimri GP, Lee X, Basile G, et al. A biomarker that identifies senescent human cells in culture and in aging skin in vivo. *Proc Natl Acad Sci U S A* 1995;92(20):9363-9367.

427. Cristofalo VJ. SA beta Gal staining: biomarker or delusion. *Exp Gerontol* 2005;40(10):836-838.

428. Elisseeff J, Anseth K, Sims D, et al. Transdermal photopolymerization of poly(ethylene oxide)-based injectable hydrogels for tissue-engineered cartilage. *Plast Reconstr Surg* 1999;104(4):1014-1022.

429. Atsumi T, Murata J, Kamiyanagi I, Fujisawa S, Ueha T. Cytotoxicity of photosensitizers camphorquinone and 9-fluorenone with visible light irradiation on a human submandibular-duct cell line in vitro. *Arch Oral Biol* 1998;43(1):73-81.

430. Lee SY, Tae G. Formulation and in vitro characterization of an in situ gelable, photo-polymerizable Pluronic hydrogel suitable for injection. *J Control Release* 2007;119(3):313-319.

431. Morley N, Curnow A, Salter L, Campbell S, Gould D. N-acetyl-L-cysteine prevents DNA damage induced by UVA, UVB and visible radiation in human fibroblasts. *J Photochem Photobiol B* 2003;72(1-3):55-60.

432. Emonet N, Leccia MT, Favier A, Beani JC, Richard MJ. Thiols and selenium: protective effect on human skin fibroblasts exposed to UVA radiation. *J Photochem Photobiol B* 1997;40(1):84-90.

433. Rickard DJ, Wang FL, Rodriguez-Rojas AM, et al. Intermittent treatment with parathyroid hormone (PTH) as well as a non-peptide small molecule agonist of the PTH1 receptor inhibits adipocyte differentiation in human bone marrow stromal cells. *Bone* 2006;39(6):1361-1372.

434. Peiffer I, Eid P, Barbet R, et al. A sub-population of high proliferative potential-quiescent human mesenchymal stem cells is under the reversible control of interferon alpha/beta. *Leukemia* 2007;21(4):714-724.

435. Farre J, Roura S, Prat-Vidal C, et al. FGF-4 increases in vitro expansion rate of human adult bone marrow-derived mesenchymal stem cells. *Growth Factors* 2007;25(2):71-76.

436. Benoit DS, Durney AR, Anseth KS. The effect of heparin-functionalized PEG hydrogels on three-dimensional human mesenchymal stem cell osteogenic differentiation. *Biomaterials* 2007;28(1):66-77.

437. Bryant SJ, Anseth KS, Lee DA, Bader DL. Crosslinking density influences the morphology of chondrocytes photoencapsulated in PEG hydrogels during the application of compressive strain. *J Orthop Res* 2004;22(5):1143-1149.

438. Fukuda J, Khademhosseini A, Yeo Y, et al. Micromolding of photocrosslinkable chitosan hydrogel for spheroid microarray and co-cultures. *Biomaterials* 2006;27(30):5259-5267.

439. Cohn D, Sosnik A, Levy A. Improved reverse thermo-responsive polymeric systems. *Biomaterials* 2003;24(21):3707-3714.

440. Fedorovich NE, Oudshoorn MH, van Geemen D, Hennink WE, Alblas J, Dhert WJ. The effect of photopolymerization on stem cells embedded in hydrogels. *Biomaterials* 2009;30(3):344-353.

441. Swennen I. *Polymerizable, thermosensitive hydrogels as potential drug release systems and matrices for tissue regeneration.* . Ghent: Ph.D. Thesis, Department of Organic Chemistry, Faculty of Sciences, Ghent University 2008.

442. Swennen I, Vermeersch V, Hornhoff M, Schacht E. In situ cross-linkable thermo-responsive hydrogels for drug delivery. *Journal of Controlled Release* 2006(116):e21-e24.

443. Meyvis TK, Stubbe BG, Van Steenbergen MJ, Hennink WE, De Smedt SC, Demeester J. A comparison between the use of dynamic mechanical analysis and oscillatory shear rheometry for the characterisation of hydrogels. *Int J Pharm* 2002;244(1-2):163-168.

444. Na K, Kim SW, Sun BK, et al. Osteogenic differentiation of rabbit mesenchymal stem cells in thermo-reversible hydrogel constructs containing hydroxyapatite and bone morphogenic protein-2 (BMP-2). *Biomaterials* 2007;28(16):2631-2637.

445. Stupack DG, Cheresh DA. Get a ligand, get a life: integrins, signaling and cell survival. *J Cell Sci* 2002;115(Pt 19):3729-3738.

446. Crompton KE, Goud JD, Bellamkonda RV, et al. Polylysine-functionalised thermoresponsive chitosan hydrogel for neural tissue engineering. *Biomaterials* 2007;28(3):441-449.

447. Gurdon JB. A community effect in animal development. *Nature* 1988;336(6201):772-774.

448. Wang DA, Williams CG, Li Q, Sharma B, Elisseeff JH. Synthesis and characterization of a novel degradable phosphate-containing hydrogel. *Biomaterials* 2003;24(22):3969-3980.

449. Bryant SJ, Bender RJ, Durand KL, Anseth KS. Encapsulating chondrocytes in degrading PEG hydrogels with high modulus: engineering gel structural changes to facilitate cartilaginous tissue production. *Biotechnol Bioeng* 2004;86(7):747-755.

450. Engler AJ, Griffin MA, Sen S, Bonnemann CG, Sweeney HL, Discher DE. Myotubes differentiate optimally on substrates with tissue-like stiffness: pathological implications for soft or stiff microenvironments. *J Cell Biol* 2004;166(6):877-887.

451. Carrier RL, Rupnick M, Langer R, Schoen FJ, Freed LE, Vunjak-Novakovic G. Perfusion improves tissue architecture of engineered cardiac muscle. *Tissue Eng* 2002;8(2):175-188.

452. Jain RK. Molecular regulation of vessel maturation. *Nat Med* 2003;9(6):685-693.

453. Radisic M, Deen W, Langer R, Vunjak-Novakovic G. Mathematical model of oxygen distribution in engineered cardiac tissue with parallel channel array perfused with culture medium containing oxygen carriers. *Am J Physiol Heart Circ Physiol* 2005;288(3):H1278-1289.

454. Obradovic B, Carrier RL, Vunjak-Novakovic G, Freed LE. Gas exchange is essential for bioreactor cultivation of tissue engineered cartilage. *Biotechnol Bioeng* 1999;63(2):197-205.

455. Grimshaw MJ, Mason RM. Bovine articular chondrocyte function in vitro depends upon oxygen tension. *Osteoarthritis Cartilage* 2000;8(5):386-392.

456. Lewis MC, Macarthur BD, Malda J, Pettet G, Please CP. Heterogeneous proliferation within engineered cartilaginous tissue: the role of oxygen tension. *Biotechnol Bioeng* 2005;91(5):607-615.

457. Tilkorn D, Messina A, Bedogni A, et al. Implanted myoblast survival is dependent on the degree of vascularization in a novel delayed implantation/prevascularization tissue engineering model. *Tissue Eng Part A* 2010;16(1):165-178.

458. Nemoto S, Fergusson MM, Finkel T. Nutrient availability regulates SIRT1 through a forkhead-dependent pathway. *Science* 2004;306(5704):2105-2108.

459. Mobasheri A, Richardson S, Mobasheri R, Shakibaei M, Hoyland JA. Hypoxia inducible factor-1 and facilitative glucose transporters GLUT1 and GLUT3: putative molecular components of the oxygen and glucose sensing apparatus in articular chondrocytes. *Histol Histopathol* 2005;20(4):1327-1338.

460. Martens G, Cai Y, Hinke S, Stange G, Van de Casteele M, Pipeleers D. Nutrient sensing in pancreatic beta cells suppresses mitochondrial superoxide generation and its contribution to apoptosis. *Biochem Soc Trans* 2005;33(Pt 1):300-301.

461. Ma T, Grayson WL, Frohlich M, Vunjak-Novakovic G. Hypoxia and stem cell-based engineering of mesenchymal tissues. *Biotechnol Prog* 2009;25(1):32-42.

462. Lennon DP, Edmison JM, Caplan AI. Cultivation of rat marrow-derived mesenchymal stem cells in reduced oxygen tension: effects on in vitro and in vivo osteochondrogenesis. *J Cell Physiol* 2001;187(3):345-355.

463. D'Ippolito G, Diabira S, Howard GA, Roos BA, Schiller PC. Low oxygen tension inhibits osteogenic differentiation and enhances stemness of human MIAMI cells. *Bone* 2006;39(3):513-522.

464. Grayson WL, Zhao F, Izadpanah R, Bunnell B, Ma T. Effects of hypoxia on human mesenchymal stem cell expansion and plasticity in 3D constructs. *J Cell Physiol* 2006;207(2):331-339.

465. Grayson WL, Zhao F, Bunnell B, Ma T. Hypoxia enhances proliferation and tissue formation of human mesenchymal stem cells. *Biochem Biophys Res Commun* 2007;358(3):948-953.

466. Carrancio S, Lopez-Holgado N, Sanchez-Guijo FM, et al. Optimization of mesenchymal stem cell expansion procedures by cell separation and culture conditions modification. *Exp Hematol* 2008;36(8):1014-1021.

467. Olmsted-Davis E, Gannon FH, Ozen M, et al. Hypoxic adipocytes pattern early heterotopic bone formation. *Am J Pathol* 2007;170(2):620-632.

468. Kanichai M, Ferguson D, Prendergast PJ, Campbell VA. Hypoxia promotes chondrogenesis in rat mesenchymal stem cells: a role for AKT and hypoxia-inducible factor (HIF)-1alpha. *J Cell Physiol* 2008;216(3):708-715.

469. Malda J, Rouwkema J, Martens DE, et al. Oxygen gradients in tissue-engineered PEGT/PBT cartilaginous constructs: measurement and modeling. *Biotechnol Bioeng* 2004;86(1):9-18.

470. Robins JC, Akeno N, Mukherjee A, et al. Hypoxia induces chondrocyte-specific gene expression in mesenchymal cells in association with transcriptional activation of Sox9. *Bone* 2005;37(3):313-322.

471. Hirao M, Tamai N, Tsumaki N, Yoshikawa H, Myoui A. Oxygen tension regulates chondrocyte differentiation and function during endochondral ossification. *J Biol Chem* 2006;281(41):31079-31092.

472. Muller I, Vaegler M, Holzwarth C, et al. Secretion of angiogenic proteins by human multipotent mesenchymal stromal cells and their clinical potential in the treatment of avascular osteonecrosis. *Leukemia* 2008;22(11):2054-2061.

473. Malladi P, Xu Y, Chiou M, Giaccia AJ, Longaker MT. Effect of reduced oxygen tension on chondrogenesis and osteogenesis in adipose-derived mesenchymal cells. *Am J Physiol Cell Physiol* 2006;290(4):C1139-1146.

474. Utting JC, Robins SP, Brandao-Burch A, Orriss IR, Behar J, Arnett TR. Hypoxia inhibits the growth, differentiation and bone-forming capacity of rat osteoblasts. *Exp Cell Res* 2006;312(10):1693-1702.

475. Hung SC, Pochampally RR, Hsu SC, et al. Short-term exposure of multipotent stromal cells to low oxygen increases their expression of CX3CR1 and CXCR4 and their engraftment in vivo. *PLoS One* 2007;2(5):e416.

476. Kellner K, Liebsch G, Klimant I, et al. Determination of oxygen gradients in engineered tissue using a fluorescent sensor. *Biotechnol Bioeng* 2002;80(1):73-83.

477. Radisic M, Malda J, Epping E, Geng W, Langer R, Vunjak-Novakovic G. Oxygen gradients correlate with cell density and cell viability in engineered cardiac tissue. *Biotechnol Bioeng* 2006;93(2):332-343.

478. Malda J, Klein TJ, Upton Z. The roles of hypoxia in the in vitro engineering of tissues. *Tissue Eng* 2007;13(9):2153-2162.

479. Volkmer E, Drosse I, Otto S, et al. Hypoxia in static and dynamic 3D culture systems for tissue engineering of bone. *Tissue Eng Part A* 2008;14(8):1331-1340.

480. Malda J, Martens DE, Tramper J, van Blitterswijk CA, Riesle J. Cartilage tissue engineering: controversy in the effect of oxygen. *Crit Rev Biotechnol* 2003;23(3):175-194.

481. Dimicco MA, and Sah, R.L. Dependence of cartilage matrix composition on biosynthesis, diffusion, and reaction. *Transport in Porous Media* 2003(50):57-73.

482. Du D, Furukawa K, Ushida T. Oscillatory perfusion seeding and culturing of osteoblast-like cells on porous beta-tricalcium phosphate scaffolds. *J Biomed Mater Res A* 2008;86(3):796-803.

483. Vunjak-Novakovic G, Martin I, Obradovic B, et al. Bioreactor cultivation conditions modulate the composition and mechanical properties of tissue-engineered cartilage. *J Orthop Res* 1999;17(1):130-138.

484. Kelly DJ, Prendergast PJ. Effect of a degraded core on the mechanical behaviour of tissue-engineered cartilage constructs: a poro-elastic finite element analysis. *Med Biol Eng Comput* 2004;42(1):9-13.

485. van den Dolder J, Spauwen PH, Jansen JA. Evaluation of various seeding techniques for culturing osteogenic cells on titanium fiber mesh. *Tissue Eng* 2003;9(2):315-325.

486. Wan Y, Wang Y, Liu Z, et al. Adhesion and proliferation of OCT-1 osteoblast-like cells on micro- and nano-scale topography structured poly(L-lactide). *Biomaterials* 2005;26(21):4453-4459.

487. Mironov V, Kasyanov V, Drake C, Markwald RR. Organ printing: promises and challenges. *Regen Med* 2008;3(1):93-103.
488. Pittenger MF, Mackay AM, Beck SC, et al. Multilineage potential of adult human mesenchymal stem cells. *Science* 1999;284(5411):143-147.
489. Nijkamp MW, Borren A, Govaert KM, et al. Radiofrequency ablation of colorectal liver metastases induces an inflammatory response in distant hepatic metastases but not in local accelerated outgrowth. *J Surg Oncol*;101(7):551-556.
490. Turk T, Leeuwis JW, Gray J, et al. BMP signaling and podocyte markers are decreased in human diabetic nephropathy in association with CTGF overexpression. *J Histochem Cytochem* 2009;57(7):623-631.
491. Sengers BG, Please CP, Oreffo RO. Experimental characterization and computational modelling of two-dimensional cell spreading for skeletal regeneration. *J R Soc Interface* 2007;4(17):1107-1117.
492. Sengers BG, Taylor M, Please CP, Oreffo RO. Computational modelling of cell spreading and tissue regeneration in porous scaffolds. *Biomaterials* 2007;28(10):1926-1940.
493. Hui TY, Cheung KM, Cheung WL, Chan D, Chan BP. In vitro chondrogenic differentiation of human mesenchymal stem cells in collagen microspheres: influence of cell seeding density and collagen concentration. *Biomaterials* 2008;29(22):3201-3212.
494. Takagi M, Umetsu Y, Fujiwara M, Wakitani S. High inoculation cell density could accelerate the differentiation of human bone marrow mesenchymal stem cells to chondrocyte cells. *J Biosci Bioeng* 2007;103(1):98-100.
495. Fink T, Abildtrup L, Fogd K, et al. Induction of adipocyte-like phenotype in human mesenchymal stem cells by hypoxia. *Stem Cells* 2004;22(7):1346-1355.
496. Guaccio A, Borselli C, Oliviero O, Netti PA. Oxygen consumption of chondrocytes in agarose and collagen gels: a comparative analysis. *Biomaterials* 2008;29(10):1484-1493.
497. Jukes JM, Moroni L, van Blitterswijk CA, de Boer J. Critical Steps toward a tissue-engineered cartilage implant using embryonic stem cells. *Tissue Eng Part A* 2008;14(1):135-147.
498. Lee RB, Urban JP. Functional replacement of oxygen by other oxidants in articular cartilage. *Arthritis Rheum* 2002;46(12):3190-3200.
499. Grassl ED, Oegema TR, Tranquillo RT. A fibrin-based arterial media equivalent. *J Biomed Mater Res A* 2003;66(3):550-561.
500. Wiesener MS, Turley H, Allen WE, et al. Induction of endothelial PAS domain protein-1 by hypoxia: characterization and comparison with hypoxia-inducible factor-1alpha. *Blood* 1998;92(7):2260-2268.
501. Sadat S, Gehmert S, Song YH, et al. The cardioprotective effect of mesenchymal stem cells is mediated by IGF-I and VEGF. *Biochem Biophys Res Commun* 2007;363(3):674-679.
502. Weinand C, Gupta R, Huang AY, et al. Comparison of hydrogels in the in vivo formation of tissue-engineered bone using mesenchymal stem cells and beta-tricalcium phosphate. *Tissue Eng* 2007;13(4):757-765.
503. Jankovic B, Aquino-Parsons C, Raleigh JA, et al. Comparison between pimonidazole binding, oxygen electrode measurements, and expression of endogenous hypoxia markers in cancer of the uterine cervix. *Cytometry B Clin Cytom* 2006;70(2):45-55.
504. Hutchison GJ, Valentine HR, Loncaster JA, et al. Hypoxia-inducible factor 1alpha expression as an intrinsic marker of hypoxia: correlation with tumor oxygen, pimonidazole measurements, and outcome in locally advanced carcinoma of the cervix. *Clin Cancer Res* 2004;10(24):8405-8412.
505. Hofer SO, Mitchell GM, Penington AJ, et al. The use of pimonidazole to characterise hypoxia in the internal environment of an in vivo tissue engineering chamber. *Br J Plast Surg* 2005;58(8):1104-1114.
506. Atkin G, Daley FM, Bourne S, Glynne-Jones R, Northover J, Wilson GD. The effect of surgically induced ischaemia on gene expression in a colorectal cancer xenograft model. *Br J Cancer* 2006;94(1):121-127.
507. Stosich MS, Bastian B, Marion NW, Clark PA, Reilly G, Mao JJ. Vascularized adipose tissue grafts from human mesenchymal stem cells with bioactive cues and microchannel conduits. *Tissue Eng* 2007;13(12):2881-2890.
508. Lokmic Z, Stillaert F, Morrison WA, Thompson EW, Mitchell GM. An arteriovenous loop in a protected space generates a permanent, highly vascular, tissue-engineered construct. *FASEB J* 2007;21(2):511-522.
509. Tuli R, Nandi S, Li WJ, et al. Human mesenchymal progenitor cell-based tissue engineering of a single-unit osteochondral construct. *Tissue Eng* 2004;10(7-8):1169-1179.
510. Oh SH, Ward CL, Atala A, Yoo JJ, Harrison BS. Oxygen generating scaffolds for enhancing engineered tissue survival. *Biomaterials* 2009;30(5):757-762.
511. Harrison BS, Eberli D, Lee SJ, Atala A, Yoo JJ. Oxygen producing biomaterials for tissue regeneration. *Biomaterials* 2007;28(31):4628-4634.
512. Mankani MH, Kuznetsov SA, Fowler B, Kingman A, Robey PG. In vivo bone formation by human bone marrow stromal cells: effect of carrier particle size and shape. *Biotechnol Bioeng* 2001;72(1):96-107.
513. Mironov V, Visconti RP, Kasyanov V, Forgacs G, Drake CJ, Markwald RR. Organ printing: tissue spheroids as building blocks. *Biomaterials* 2009;30(12):2164-2174.
514. Michna S, Wu W, Lewis JA. Concentrated hydroxyapatite inks for direct-write assembly of 3-D periodic scaffolds. *Biomaterials* 2005;26(28):5632-5639.
515. Barralet J, Gbureck U, Habibovic P, Vorndran E, Gerard C, Doillon CJ. Angiogenesis in calcium phosphate scaffolds by inorganic copper ion release. *Tissue Eng Part A* 2009;15(7):1601-1609.
516. Chu TM, Orton DG, Hollister SJ, Feinberg SE, Halloran JW. Mechanical and in vivo performance of hydroxyapatite implants with controlled architectures. *Biomaterials* 2002;23(5):1283-1293.
517. Dellinger JG, Cesarano J, 3rd, Jamison RD. Robotic deposition of model hydroxyapatite scaffolds with multiple architectures and multiscale porosity for bone tissue engineering. *J Biomed Mater Res A* 2007;82(2):383-394.
518. Mankani MH, Kuznetsov SA, Marshall GW, Robey PG. Creation of new bone by the percutaneous injection of human bone marrow stromal cell and HA/TCP suspensions. *Tissue Eng Part A* 2008;14(12):1949-1958.
519. Trojani C, Boukhechba F, Scimeca JC, et al. Ectopic bone formation using an injectable biphasic calcium phosphate/Si-HPMC hydrogel composite loaded with undifferentiated bone marrow stromal cells. *Biomaterials* 2006;27(17):3256-3264.
520. Burg KJ, Porter S, Kellam JF. Biomaterial developments for bone tissue engineering. *Biomaterials* 2000;21(23):2347-2359.

521. Ripamonti U. Osteoinduction in porous hydroxyapatite implanted in heterotopic sites of different animal models. *Biomaterials* 1996;17(1):31-35.
522. Navarro M, Michiardi A, Castano O, Planell JA. Biomaterials in orthopaedics. *J R Soc Interface* 2008;5(27):1137-1158.
523. Yuan H, Fernandes H, Habibovic P, et al. Osteoinductive ceramics as a synthetic alternative to autologous bone grafting. *Proc Natl Acad Sci U S A* 2010;107(31):13614-13619.
524. Krebsbach PH, Kuznetsov SA, Satomura K, Emmons RV, Rowe DW, Robey PG. Bone formation in vivo: comparison of osteogenesis by transplanted mouse and human marrow stromal fibroblasts. *Transplantation* 1997;63(8):1059-1069.
525. Bohner M, Baroud G. Injectability of calcium phosphate pastes. *Biomaterials* 2005;26(13):1553-1563.
526. Sachlos E, Gotora D, Czernuszka JT. Collagen scaffolds reinforced with biomimetic composite nano-sized carbonate-substituted hydroxyapatite crystals and shaped by rapid prototyping to contain internal microchannels. *Tissue Eng* 2006;12(9):2479-2487.
527. Lee KW, Wang S, Yaszemski MJ, Lu L. Physical properties and cellular responses to crosslinkable poly(propylene fumarate)/hydroxyapatite nanocomposites. *Biomaterials* 2008;29(19):2839-2848.
528. Hong Z, Zhang P, He C, et al. Nano-composite of poly(L-lactide) and surface grafted hydroxyapatite: mechanical properties and biocompatibility. *Biomaterials* 2005;26(32):6296-6304.
529. Liao SS, Cui FZ, Zhang W, Feng QL. Hierarchically biomimetic bone scaffold materials: nano-HA/collagen/PLA composite. *J Biomed Mater Res B Appl Biomater* 2004;69(2):158-165.
530. Kim JU, O'Shaughnessy B. Morphology selection of nanoparticle dispersions by polymer media. *Phys Rev Lett* 2002;89(23):238301.
531. Yuan H, van Blitterswijk CA, de Groot K, de Bruijn JD. A comparison of bone formation in biphasic calcium phosphate (BCP) and hydroxyapatite (HA) implanted in muscle and bone of dogs at different time periods. *J Biomed Mater Res A* 2006;78(1):139-147.
532. Kumar R, Prakash KH, Cheang P, Khor KA. Temperature driven morphological changes of chemically precipitated hydroxyapatite nanoparticles. *Langmuir* 2004;20(13):5196-5200.
533. Gibson IR, Bonfield W. Novel synthesis and characterization of an AB-type carbonate-substituted hydroxyapatite. *J Biomed Mater Res* 2002;59(4):697-708.
534. Leeuwenburgh SC, Jansen JA, Mikos AG. Functionalization of oligo(poly(ethylene glycol)fumarate) hydrogels with finely dispersed calcium phosphate nanocrystals for bone-substituting purposes. *J Biomater Sci Polym Ed* 2007;18(12):1547-1564.
535. Erlebacher A, Derynck R. Increased expression of TGF-beta 2 in osteoblasts results in an osteoporosis-like phenotype. *J Cell Biol* 1996;132(1-2):195-210.
536. Dominici M, Rasini V, Bussolari R, et al. Restoration and reversible expansion of the osteoblastic hematopoietic stem cell niche after marrow radioablation. *Blood* 2009;114(11):2333-2343.
537. Carvalho AL, Faria PE, Grisi MF, et al. Effects of granule size on the osteoconductivity of bovine and synthetic hydroxyapatite: a histologic and histometric study in dogs. *J Oral Implantol* 2007;33(5):267-276.
538. Jung UW, Choi SY, Pang EK, Kim CS, Choi SH, Cho KS. The effect of varying the particle size of beta tricalcium phosphate carrier of recombinant human bone morphogenetic protein-4 on bone formation in rat calvarial defects. *J Periodontol* 2006;77(5):765-772.
539. Yuan H, Barbieri D, Zhou H, Bao C., Wang R, de Bruijn J. Osteoinductive injectable bone. *Advanced Functional Materials* under review.
540. Keriquel V, Guillemot F, Arnault I, et al. In vivo bioprinting for computer- and robotic-assisted medical intervention: preliminary study in mice. *Biofabrication* 2010;2(1):014101.
541. Higashi T, Okamoto H. Influence of particle size of hydroxyapatite as a capping agent on cell proliferation of cultured fibroblasts. *J Endod* 1996;22(5):236-239.
542. Higashi T, Okamoto H. Influence of particle size of calcium phosphate ceramics as a capping agent on the formation of a hard tissue barrier in amputated dental pulp. *J Endod* 1996;22(6):281-283.
543. Zaidi M, Moonga BS, Huang CL. Calcium sensing and cell signaling processes in the local regulation of osteoclastic bone resorption. *Biol Rev Camb Philos Soc* 2004;79(1):79-100.
544. Gauthier O, Boix D, Grimandi G, et al. A new injectable calcium phosphate biomaterial for immediate bone filling of extraction sockets: a preliminary study in dogs. *J Periodontol* 1999;70(4):375-383.
545. Gauthier O, Bouler JM, Weiss P, Bosco J, Aguado E, Daculsi G. Short-term effects of mineral particle sizes on cellular degradation activity after implantation of injectable calcium phosphate biomaterials and the consequences for bone substitution. *Bone* 1999;25(2 Suppl):71S-74S.
546. Kondo N, Ogose A, Tokunaga K, et al. Osteoinduction with highly purified beta-tricalcium phosphate in dog dorsal muscles and the proliferation of osteoclasts before heterotopic bone formation. *Biomaterials* 2006;27(25):4419-4427.
547. Patel M, Patel KJ, Caccamese JF, Coletti DP, Sauk JJ, Fisher JP. Characterization of cyclic acetal hydroxyapatite nanocomposites for craniofacial tissue engineering. *J Biomed Mater Res A* 2010;94(2):408-418.
548. Griffith CK, Miller C, Sainson RC, et al. Diffusion limits of an in vitro thick prevascularized tissue. *Tissue Eng* 2005;11(1-2):257-266.
549. Akita S, Tamai N, Myoui A, et al. Capillary vessel network integration by inserting a vascular pedicle enhances bone formation in tissue-engineered bone using interconnected porous hydroxyapatite ceramics. *Tissue Eng* 2004;10(5-6):789-795.
550. Mori S, Yoshikawa H, Hashimoto J, et al. Antiangiogenic agent (TNP-470) inhibition of ectopic bone formation induced by bone morphogenetic protein-2. *Bone* 1998;22(2):99-105.
551. Kannan RY, Salacinski HJ, Sales K, Butler P, Seifalian AM. The roles of tissue engineering and vascularisation in the development of micro-vascular networks: a review. *Biomaterials* 2005;26(14):1857-1875.
552. Rouwkema J, Rivron NC, van Blitterswijk CA. Vascularization in tissue engineering. *Trends Biotechnol* 2008;26(8):434-441.
553. Yu H, Vandevord PJ, Gong W, et al. Promotion of osteogenesis in tissue-engineered bone by pre-seeding endothelial progenitor cells-derived endothelial cells. *J Orthop Res* 2008;26(8):1147-1152.
554. Black AF, Berthod F, L'Heureux N, Germain L, Auger FA. In vitro reconstruction of a human capillary-like network in a tissue-engineered skin equivalent. *Faseb J* 1998;12(13):1331-1340.

555. Nor JE, Peters MC, Christensen JB, et al. Engineering and characterization of functional human microvessels in immunodeficient mice. *Lab Invest* 2001;81(4):453-463.

556. Schechner JS, Nath AK, Zheng L, et al. In vivo formation of complex microvessels lined by human endothelial cells in an immunodeficient mouse. *Proc Natl Acad Sci U S A* 2000;97(16):9191-9196.

557. Wang DS, Miura M, Demura H, Sato K. Anabolic effects of 1,25-dihydroxyvitamin D3 on osteoblasts are enhanced by vascular endothelial growth factor produced by osteoblasts and by growth factors produced by endothelial cells. *Endocrinology* 1997;138(7):2953-2962.

558. Deckers MM, van Bezooijen RL, van der Horst G, et al. Bone morphogenetic proteins stimulate angiogenesis through osteoblast-derived vascular endothelial growth factor A. *Endocrinology* 2002;143(4):1545-1553.

559. Bouletreau PJ, Warren SM, Spector JA, et al. Hypoxia and VEGF up-regulate BMP-2 mRNA and protein expression in microvascular endothelial cells: implications for fracture healing. *Plast Reconstr Surg* 2002;109(7):2384-2397.

560. Kaigler D, Krebsbach PH, Polverini PJ, Mooney DJ. Role of vascular endothelial growth factor in bone marrow stromal cell modulation of endothelial cells. *Tissue Eng* 2003;9(1):95-103.

561. Villars F, Bordenave L, Bareille R, Amedee J. Effect of human endothelial cells on human bone marrow stromal cell phenotype: role of VEGF? *J Cell Biochem* 2000;79(4):672-685.

562. Finkenzeller G, Arabatzis G, Geyer M, Wenger A, Bannasch H, Stark GB. Gene expression profiling reveals platelet-derived growth factor receptor alpha as a target of cell contact-dependent gene regulation in an endothelial cell-osteoblast co-culture model. *Tissue Eng* 2006;12(10):2889-2903.

563. Lin Y, Weisdorf DJ, Solovey A, Hebbel RP. Origins of circulating endothelial cells and endothelial outgrowth from blood. *J Clin Invest* 2000;105(1):71-77.

564. Rafii S, Lyden D. Therapeutic stem and progenitor cell transplantation for organ vascularization and regeneration. *Nat Med* 2003;9(6):702-712.

565. Fuchs S, Hofmann A, Kirkpatrick CJ. Microvessel-like structures from outgrowth endothelial cells from human peripheral blood in 2-dimensional and 3-dimensional co-cultures with osteoblastic lineage cells. *Tissue Eng* 2007;13(10):2577-2588.

566. Matsumoto T, Kuroda R, Mifune Y, et al. Circulating endothelial/skeletal progenitor cells for bone regeneration and healing. *Bone* 2008;43(3):434-439.

567. Reyes M, Dudek A, Jahagirdar B, Koodie L, Marker PH, Verfaillie CM. Origin of endothelial progenitors in human postnatal bone marrow. *J Clin Invest* 2002;109(3):337-346.

568. Asahara T, Murohara T, Sullivan A, et al. Isolation of putative progenitor endothelial cells for angiogenesis. *Science* 1997;275(5302):964-967.

569. Murohara T, Ikeda H, Duan J, et al. Transplanted cord blood-derived endothelial precursor cells augment postnatal neovascularization. *J Clin Invest* 2000;105(11):1527-1536.

570. Ishikawa M, Asahara T. Endothelial progenitor cell culture for vascular regeneration. *Stem Cells Dev* 2004;13(4):344-349.

571. Fuchs S, Hermanns MI, Kirkpatrick CJ. Retention of a differentiated endothelial phenotype by outgrowth endothelial cells isolated from human peripheral blood and expanded in long-term cultures. *Cell Tissue Res* 2006;326(1):79-92.

572. Kalka C, Masuda H, Takahashi T, et al. Transplantation of ex vivo expanded endothelial progenitor cells for therapeutic neovascularization. *Proc Natl Acad Sci U S A* 2000;97(7):3422-3427.

573. Kawamoto A, Tkebuchava T, Yamaguchi J, et al. Intramyocardial transplantation of autologous endothelial progenitor cells for therapeutic neovascularization of myocardial ischemia. *Circulation* 2003;107(3):461-468.

574. Sieminski AL, Hebbel RP, Gooch KJ. Improved microvascular network in vitro by human blood outgrowth endothelial cells relative to vessel-derived endothelial cells. *Tissue Eng* 2005;11(9-10):1332-1345.

575. Gulati R, Jevremovic D, Peterson TE, et al. Diverse origin and function of cells with endothelial phenotype obtained from adult human blood. *Circ Res* 2003;93(11):1023-1025.

576. Hur J, Yoon CH, Kim HS, et al. Characterization of two types of endothelial progenitor cells and their different contributions to neovasculogenesis. *Arterioscler Thromb Vasc Biol* 2004;24(2):288-293.

577. Ingram DA, Mead LE, Tanaka H, et al. Identification of a novel hierarchy of endothelial progenitor cells using human peripheral and umbilical cord blood. *Blood* 2004;104(9):2752-2760.

578. Shi Q, Rafii S, Wu MH, et al. Evidence for circulating bone marrow-derived endothelial cells. *Blood* 1998;92(2):362-367.

579. Yoder MC, Mead LE, Prater D, et al. Redefining endothelial progenitor cells via clonal analysis and hematopoietic stem/progenitor cell principals. *Blood* 2007;109(5):1801-1809.

580. Stahl A, Wu X, Wenger A, Klagsbrun M, Kurschat P. Endothelial progenitor cell sprouting in spheroid cultures is resistant to inhibition by osteoblasts: a model for bone replacement grafts. *FEBS Lett* 2005;579(24):5338-5342.

581. Finkenzeller G, Torio-Padron N, Momeni A, Mehlhorn AT, Stark GB. In vitro angiogenesis properties of endothelial progenitor cells: a promising tool for vascularization of ex vivo engineered tissues. *Tissue Eng* 2007;13(7):1413-1420.

582. Yuan H, Van Den Doel M, Li S, Van Blitterswijk CA, De Groot K, De Bruijn JD. A comparison of the osteoinductive potential of two calcium phosphate ceramics implanted intramuscularly in goats. *J Mater Sci Mater Med* 2002;13(12):1271-1275.

583. Niederauer GG, Slivka MA, Leatherbury NC, et al. Evaluation of multiphase implants for repair of focal osteochondral defects in goats. *Biomaterials* 2000;21(24):2561-2574.

584. Darling EM, Athanasiou KA. Growth factor impact on articular cartilage subpopulations. *Cell Tissue Res* 2005;322(3):463-473.

585. Dell'Accio F, Vanlauwe J, Bellemans J, Neys J, De Bari C, Luyten FP. Expanded phenotypically stable chondrocytes persist in the repair tissue and contribute to cartilage matrix formation and structural integration in a goat model of autologous chondrocyte implantation. *J Orthop Res* 2003;21(1):123-131.

586. Kruyt MC, Dhert WJ, Yuan H, et al. Bone tissue engineering in a critical size defect compared to ectopic implantations in the goat. *J Orthop Res* 2004;22(3):544-551.

587. Liu J, Wang XB, Park DS, Lisanti MP. Caveolin-1 expression enhances endothelial capillary tubule formation. *J Biol Chem* 2002;277(12):10661-10668.

588. Geuze RE, Wegman F, Oner FC, Dhert WJ, Alblas J. Influence of endothelial progenitor cells and platelet gel on tissue-engineered bone ectopically in goats. *Tissue Eng Part A* 2009;15(11):3669-3677.

589. Rehman J, Li J, Orschell CM, March KL. Peripheral blood "endothelial progenitor cells" are derived from monocyte/macrophages and secrete angiogenic growth factors. *Circulation* 2003;107(8):1164-1169.

590. Rouwkema J, Westerweel PE, de Boer J, Verhaar MC, van Blitterswijk CA. The use of endothelial progenitor cells for prevascularized bone tissue engineering. *Tissue Eng Part A* 2009;15(8):2015-2027.

591. Melero-Martin JM, De Obaldia ME, Kang SY, et al. Engineering robust and functional vascular networks in vivo with human adult and cord blood-derived progenitor cells. *Circ Res* 2008;103(2):194-202.

592. Sieminski AL, Padera RF, Blunk T, Gooch KJ. Systemic delivery of human growth hormone using genetically modified tissue-engineered microvascular networks: prolonged delivery and endothelial survival with inclusion of nonendothelial cells. *Tissue Eng* 2002;8(6):1057-1069.

593. Wu X, Rabkin-Aikawa E, Guleserian KJ, et al. Tissue-engineered microvessels on three-dimensional biodegradable scaffolds using human endothelial progenitor cells. *Am J Physiol Heart Circ Physiol* 2004;287(2):H480-487.

594. Unger RE, Sartoris A, Peters K, et al. Tissue-like self-assembly in cocultures of endothelial cells and osteoblasts and the formation of microcapillary-like structures on three-dimensional porous biomaterials. *Biomaterials* 2007;28(27):3965-3976.

595. Ko HC, Milthorpe BK, McFarland CD. Engineering thick tissues--the vascularisation problem. *Eur Cell Mater* 2007;14:1-18; discussion 18-19.

596. Villars F, Guillotin B, Amedee T, et al. Effect of HUVEC on human osteoprogenitor cell differentiation needs heterotypic gap junction communication. *Am J Physiol Cell Physiol* 2002;282(4):C775-785.

597. Chen FM, Zhang M, Wu ZF. Toward delivery of multiple growth factors in tissue engineering. *Biomaterials* 2010;31(24):6279-6308.

598. Phillips JE, Burns KL, Le Doux JM, Guldberg RE, Garcia AJ. Engineering graded tissue interfaces. *Proc Natl Acad Sci U S A* 2008;105(34):12170-12175.

599. Grellier M, Bordenave L, Amedee J. Cell-to-cell communication between osteogenic and endothelial lineages: implications for tissue engineering. *Trends Biotechnol* 2009;27(10):562-571.

600. Guillemot F, Souquet A, Catros S, et al. High-throughput laser printing of cells and biomaterials for tissue engineering. *Acta Biomater* 2010;6(7):2494-2500.

601. Santos MI, Unger RE, Sousa RA, Reis RL, Kirkpatrick CJ. Crosstalk between osteoblasts and endothelial cells co-cultured on a polycaprolactone-starch scaffold and the in vitro development of vascularization. *Biomaterials* 2009;30(26):4407-4415.

602. Lee SA, Chung SE, Park W, Lee SH, Kwon S. Three-dimensional fabrication of heterogeneous microstructures using soft membrane deformation and optofluidic maskless lithography. *Lab Chip* 2009;9(12):1670-1675.

603. Fuchs S, Ghanaati S, Orth C, et al. Contribution of outgrowth endothelial cells from human peripheral blood on in vivo vascularization of bone tissue engineered constructs based on starch polycaprolactone scaffolds. *Biomaterials* 2009;30(4):526-534.

604. Zhu XD, Zhang HJ, Fan HS, Li W, Zhang XD. Effect of phase composition and microstructure of calcium phosphate ceramic particles on protein adsorption. *Acta Biomater* 2010;6(4):1536-1541.

605. Daculsi G, Uzel AP, Weiss P, Goyenvalle E, Aguado E. Developments in injectable multiphasic biomaterials. The performance of microporous biphasic calcium phosphate granules and hydrogels. *J Mater Sci Mater Med* 2010;21(3):855-861.

606. Prakash D, Learmonth D. Natural progression of osteo-chondral defect in the femoral condyle. *Knee* 2002;9(1):7-10.

607. Marcacci M, Kon E, Delcogliano M, Filardo G, Busacca M, Zaffagnini S. Arthroscopic autologous osteochondral grafting for cartilage defects of the knee: prospective study results at a minimum 7-year follow-up. *Am J Sports Med* 2007;35(12):2014-2021.

608. Hangody L, Vasarhelyi G, Hangody LR, et al. Autologous osteochondral grafting--technique and long-term results. *Injury* 2008;39 Suppl 1:S32-39.

609. Kon E, Gobbi A, Filardo G, Delcogliano M, Zaffagnini S, Marcacci M. Arthroscopic second-generation autologous chondrocyte implantation compared with microfracture for chondral lesions of the knee: prospective nonrandomized study at 5 years. *Am J Sports Med* 2009;37(1):33-41.

610. Schaefer D, Martin I, Shastri P, et al. In vitro generation of osteochondral composites. *Biomaterials* 2000;21(24):2599-2606.

611. Klein TJ, Malda J, Sah RL, Hutmacher DW. Tissue Engineering of Articular Cartilage with Biomimetic Zones. *Tissue Eng Part B Rev* 2009.

612. Siddappa R, Martens A, Doorn J, et al. cAMP/PKA pathway activation in human mesenchymal stem cells in vitro results in robust bone formation in vivo. *Proc Natl Acad Sci U S A* 2008;105(20):7281-7286.

613. Guo JF, Jourdian GW, MacCallum DK. Culture and growth characteristics of chondrocytes encapsulated in alginate beads. *Connect Tissue Res* 1989;19(2-4):277-297.

614. Moroni L, de Wijn JR, van Blitterswijk CA. Integrating novel technologies to fabricate smart scaffolds. *J Biomater Sci Polym Ed* 2008;19(5):543-572.

615. Song F, Zhang LM, Li NN, Shi JF. In situ crosslinkable hydrogel formed from a polysaccharide-based hydrogelator. *Biomacromolecules* 2009;10(4):959-965.

616. Haines-Butterick L, Rajagopal K, Branco M, et al. Controlling hydrogelation kinetics by peptide design for three-dimensional encapsulation and injectable delivery of cells. *Proc Natl Acad Sci U S A* 2007;104(19):7791-7796.

617. Lee MG, Choi S, Park JK. Three-dimensional hydrodynamic focusing with a single sheath flow in a single-layer microfluidic device. *Lab Chip* 2009;9(21):3155-3160.

618. Williams DF. On the mechanisms of biocompatibility. *Biomaterials* 2008;29(20):2941-2953.

619. Thonhoff JR, Lou DI, Jordan PM, Zhao X, Wu P. Compatibility of human fetal neural stem cells with hydrogel biomaterials in vitro. *Brain Res* 2008;1187:42-51.

620. Fedorovich NE, Swennen I, Girones J, et al. Evaluation of photocrosslinked Lutrol hydrogel for tissue printing applications. *Biomacromolecules* 2009;10(7):1689-1696.

621. Kellner K, Liebsch, G., Klimant, I., Wolfbeis, O.S., Blunk, T., Schulz, M.B, and Gopferich, A. Determination of oxygen gradients in engineered tissue using a fluorescent sensor. *Biotechnol Bioeng* 2002;80(1):73-83.

622. Drosse I, Volkmer E, Capanna R, De Biase P, Mutschler W, Schieker M. Tissue engineering for bone defect healing: an update on a multi-component approach. *Injury* 2008;39 Suppl 2:S9-20.
623. Schimming R, Schmelzeisen R. Tissue-engineered bone for maxillary sinus augmentation. *J Oral Maxillofac Surg* 2004;62(6):724-729.
624. Cushing MC, Anseth KS. Materials science. Hydrogel cell cultures. *Science* 2007;316(5828):1133-1134.
625. Yan Y, Wang X, Pan Y, et al. Fabrication of viable tissue-engineered constructs with 3D cell-assembly technique. *Biomaterials* 2005;26(29):5864-5871.
626. Asahara T, Kawamoto A. Endothelial progenitor cells for postnatal vasculogenesis. *Am J Physiol Cell Physiol* 2004;287(3):C572-579.
627. Neels JG, Thinnes T, Loskutoff DJ. Angiogenesis in an in vivo model of adipose tissue development. *Faseb J* 2004;18(9):983-985.
628. Krenning G, van Luyn MJ, Harmsen MC. Endothelial progenitor cell-based neovascularization: implications for therapy. *Trends Mol Med* 2009;15(4):180-189.
629. Kloxin AM, Kasko AM, Salinas CN, Anseth KS. Photodegradable hydrogels for dynamic tuning of physical and chemical properties. *Science* 2009;324(5923):59-63.
630. Hartgerink JD, Beniash E, Stupp SI. Peptide-amphiphile nanofibers: a versatile scaffold for the preparation of self-assembling materials. *Proc Natl Acad Sci U S A* 2002;99(8):5133-5138.
631. Hosseinkhani H, Hosseinkhani M, Tian F, Kobayashi H, Tabata Y. Ectopic bone formation in collagen sponge self-assembled peptide-amphiphile nanofibers hybrid scaffold in a perfusion culture bioreactor. *Biomaterials* 2006;27(29):5089-5098.
632. Knothe Tate ML, Steck R, Anderson EJ. Bone as an inspiration for a novel class of mechanoactive materials. *Biomaterials* 2009;30(2):133-140.
633. Smith MK, Peters MC, Richardson TP, Garbern JC, Mooney DJ. Locally enhanced angiogenesis promotes transplanted cell survival. *Tissue Eng* 2004;10(1-2):63-71.
634. Tretyakov AV, Farber HW. Endothelial cell tolerance to hypoxia. Potential role of purine nucleotide phosphates. *J Clin Invest* 1995;95(2):738-744.
635. Aragones J, Schneider M, Van Geyte K, et al. Deficiency or inhibition of oxygen sensor Phd1 induces hypoxia tolerance by reprogramming basal metabolism. *Nat Genet* 2008;40(2):170-180.
636. Hill P, Shukla D, Tran MG, et al. Inhibition of hypoxia inducible factor hydroxylases protects against renal ischemia-reperfusion injury. *J Am Soc Nephrol* 2008;19(1):39-46.
637. Theus MH, Wei L, Cui L, et al. In vitro hypoxic preconditioning of embryonic stem cells as a strategy of promoting cell survival and functional benefits after transplantation into the ischemic rat brain. *Exp Neurol* 2008;210(2):656-670.
638. van Susante JL, Buma P, Homminga GN, van den Berg WB, Veth RP. Chondrocyte-seeded hydroxyapatite for repair of large articular cartilage defects. A pilot study in the goat. *Biomaterials* 1998;19(24):2367-2374.

Acknowledgement

I would like to express my gratitude to the following people and institutions for their contribution to the work described in this thesis and their support.

Wouter Dhert
Clemens van Blitterswijk
Jacqueline Alblas
Jos Malda
Debby Gawlitta
Ab Verbout
Moyo Kruijt
Laura Creemers
Daniël Saris
Cumhur Öner
Yvonne van der Helm
Mattie van Rijen
Herma Roestenburg
Leontine Schuijff
Antoinette Zielman
Sylvia Visser
Angelina Bentvelzen-Peek
Jacqueline Manné

Group of prof. Wim Hennink
Group of prof. Etienne Schacht
People from Xpand Biotech
People at the GDL
Department of Pathology
Department of Vascular Medicine

Stichting Anna Fonds
Stichting de Drie Lichten

My fellow research residents
Clayton Wilson
Henk-Jan Prins
Lorenzo Moroni
Joost de Wijn
Hendrik John
Huipin Yuan
Hugo Andre Alves
Eric Epping
Peter Sodaar
Paul Westers

René Haverslag
Daphne van Geemen
Esmeralda Bosman
Tijmen van Blijswijk
Elske Kuipers
Hans Wijnberg
Frank Assen

Roel Custers
Wouter Schuurman

Wil en Els Leeuwis
My parents

Jan Willem

Curriculum vitae and list of publications

Personally I'm always ready to learn, although I do not always like being taught.
Sir Winston Churchill

Curriculum vitae

Natalja Evgenjevna Fedorovich was born July 5th, 1979 in Leningrad (presently St. Petersburg), in Sovjet Union. At the age of 14 she moved to De Bilt together with her mother who was invited for a post-doc position at KNMI. Natalja graduated in 1997 from College Blaucapel (Gerrit Rietveld College, Utrecht) *cum laude*, and enrolled to study Medical Biology at Utrecht University. Joint classes with medical students have proven fascinating, and in 1999 she started medical school combing medical biology and medicine curricula. In 2002 she initiated her scientific career at the department of orthopaedics in the UMC Utrecht, as a master student contributing to studies of, then PhD students, and presently doctors in philosophy and orthopaedic surgeons, dr. Moyo C. Kruyt and dr. Floor van Eijk. In 2003 she spent half-a-year in St. Petersburg, doing rotations in Military Medical Academy at the department of prof. dr. Andrei Novik, a position generously negotiated by prof. dr. Ton Hagenbeek. In 2005 she started as a PhD student on the project "3D tissue printing for bone tissue engineering", financed by the Mosaic program. This program is founded by The Netherlands Organisation for Scientific Research (NWO) and the Ministry of Education, Culture and Science and stimulates PhD research by the talented students from an ethnic minority. The prototype of 3D fiber deposition machine, described in this thesis, was available though close collaboration with University of Twente, and initial research with this machine was conducted in 2006 in Bilthoven under invaluable supervision by dr. Lorenzo Moroni and dr. Joost de Wijn from the Institute for Biomedical Technology. Polymers used for printing were provided in collaboration with the group of prof. dr Wim E. Hennink, the department of Biopharmaceutics, Utrecht University, and also Polymer Chemistry and Biomaterials Research Group, Ghent University, Belgium. The work was performed under inspirational guidance of prof. dr. Wouter Dhert, and supervised by dr. Jacqueline Alblas. In 2008 dr. Wouter Dhert was promoted to professor and became the promoter of this thesis, alongside prof. dr. Clemens A. van Blitterswijk. In 2010 Natalja worked for eight months as a surgery resident in Diakonessenhuis Hospital in Utrecht, where after she switched her career to commence pathology training at the Academic Medical Center Amsterdam (prof. dr. Marc van de Vijver) in January 2011.

Natalja Leeuwis Fedorovich is married since 2007 to Jan Willem Leeuwis whom she indeed met during joint classes with medical students in 1999.

Manuscripts

Fedorovich NE, Wijnberg H, Dhert WJA, Alblas J. *Distinct tissue formation by heterogeneous printing of osteo- and endothelial progenitor cells.* Tissue Engineering Part A. 2011, doi: 10.1089/ten.TEA.2011.0019.

Fedorovich NE, Haverslag RT, Dhert WJ, Alblas J. *The Role of Endothelial Progenitor Cells in Prevascularized Bone Tissue Engineering: Development of Heterogeneous Constructs.* Tissue Engineering Part A. 2010, 16(7):2355-67.

Seyednejad H, Vermonden T, **Fedorovich NE**, van Eijk R, van Steenbergen MJ, Dhert WJ, van Nostrum CF, Hennink WE. *Synthesis and characterization of hydroxyl-functionalized caprolactone copolymers and their effect on adhesion, proliferation, and differentiation of human mesenchymal stem cells.* Biomacromolecules. 2009, 10(11):3048-54.

Fedorovich NE, Swennen I, Girones J, Moroni L, van Blitterswijk CA, Schacht E, Alblas J, Dhert WJ. *Evaluation of Photocrosslinked Lutrol Hydrogel for Tissue Printing Applications.* Biomacromolecules. 2009, 10(7):1689–96.

van Eijk F, Saris DB, **Fedorovich NE**, Kruyt MC, Willems WJ, Verbout AJ, Martens AC, Dhert WJ, Creemers L. *In vivo matrix production by bone marrow stromal cells seeded on PLGA scaffolds for ligament tissue engineering.* Tissue Eng Part A. 2009; 15(10):3109-17.

Fedorovich NE, Oudshoorn MM, van Geemen D, Hennink WE, Alblas J, Dhert WJA. *The effect of photopolymerization on stem cells embedded in hydrogels.* Biomaterials 2008; 30(3):344-53.

Fedorovich NE, De Wijn JR, Verbout AJ, Alblas J, Dhert WJ. *Three-dimensional fiber deposition of cell-laden, viable, patterned constructs for bone tissue printing.* Tissue Engineering Part A. 2008;14(1):127-33.

Vermonden T, **Fedorovich NE**, van Geemen D, Alblas J, van Nostrum CF, Dhert WJ, Hennink WE. *Photopolymerized thermosensitive hydrogels: synthesis, degradation, and cytocompatibility.* Biomacromolecules. 2008; 9(3):919-26.

Fedorovich NE, Alblas J, de Wijn JR, Hennink WE, Verbout AJ, Dhert WJA. *Hydrogels as extracellular matrices for skeletal tissue engineering: state-of-the-art and novel application in organ printing.* Tissue Engineering. 2007; 13(8):1905-25.

Kruyt MC, Stijns MM, **Fedorovich NE**, De Bruijn JD, Van Blitterswijk CA, Verbout AJ, Rozemuller H, Hagenbeek A, Dhert WJ, Martens AC. *Genetic marking with the DeltaLNGFR-gene for tracing goat cells in bone tissue engineering.* J Orthop Res. 2004; 22(4):697-702.

Book chapters

Fedorovich NE, Moroni L, Malda J, Alblas J, van Blitterswijk CA, Dhert WJA. *3D-fiber deposition for tissue engineering and organ printing applications.*
In: Ringeisen B, Spargo BJ, Wu PK (eds.) Cell and Organ printing, Dordrecht, Springer Science + Business Media BV, 2010; chapter 13, p.225-239

Melchels F, Malda J, **Fedorovich NE**, Alblas J, Woodfield T. *Organ printing.*
In: Kirkpatrick J, Hutmacher D, Healy K, Grainger D, Ducheyne P (eds.) Comprehensive Biomaterials, Six-Volume Set. Elsevier Science 2011, chapter 195, (in press)